QUANTUM LIQUIDS AND QUANTUM CRYSTALS

Mechanism of "rigid-body" rotation of the superfluid and normal components during phase separation of a supersaturated ^{3}He–^{4}He solution

É. A. Pashitskiĭ[a)]

Institute of Physics, pr. Nauki 46, Kiev 03028, Ukraine

V. N. Mal'nev[b)] and R. A. Naryshkin[c)]

Taras Shevchenko Kiev National University, Physics Department, pr. Glushkova 6, Kiev 03022, Ukraine

(Submitted February 18, 2005; resubmitted March 11, 2005)
Fiz. Nizk. Temp. **31**, 1095–1099 (October 2005)

It is shown that unstable hydrodynamic vortices can form inside subcritical domains in the normal component of a supersaturated decomposing ^{3}He–^{4}He solution. A mechanism for the entrainment of the superfluid component by the normal component of the ^{3}He–^{4}He solution into "rigid-body" rotation due to Hall–Vinen–Bekarevich–Khalatnikov forces in the equations of two-fluid hydrodynamics, which leads to the creation of quantized vortices, is considered. An increase of the average density of quantized vortices can increase the rate of heterogeneous decomposition of the ^{3}He–^{4}He solution. © *2005 American Institute of Physics*.
[DOI: 10.1063/1.2126941]

I. INTRODUCTION

It was shown in Ref. 1 that in the process of decomposition of a supersaturated superfluid solution of the quantum fluids ^{3}He and ^{4}He, classical hydrodynamic vortices can be nucleated inside subcritical nuclei (domains of decomposition) in the normal component, with an azimuthal velocity component distributed linearly with respect to the radius of the vortex, $v_{n\varphi}(r,t)=\omega_n(t)r$, which corresponds to "rigid-body" rotation of the liquid with an angular velocity $\omega_n(t)$ that increases with time. Such vortices develop under the influence of convective and Coriolis forces arising because of convergent radial flows with a velocity $v_n(r,t)=-\beta_n(t)r$. These flows compensate the efflux of the light fraction of the separated solution (the isotope ^{3}He) from the volume under conditions of chemical and dynamic equilibrium of the domains of decomposition with the surrounding supersaturated (metastable) solution ^{3}He–^{4}He. The process of decomposition of the solution can be described with the aid of a volume sink $-q(t)$ and a vertical flow of ^{3}He atoms with a velocity v_z. Therefore, an effective equation of continuity with a volume sink holds within a cylindrical domain:[1,2]

$$\frac{\partial(\rho_n+\rho_s)}{\partial t}+\mathrm{div}(\rho_n\mathbf{v}_n+\rho_s\mathbf{v}_s)=-q(t). \tag{1}$$

Here ρ_n,ρ_s and $\mathbf{v}_n,\mathbf{v}_s$ are the densities and hydrodynamic velocities of the normal and superfluid components, respectively. The liquid will henceforth be assumed incompressible.

In Ref. 1 it was assumed that there is complete entrainment of the superfluid component by the normal component, i.e., the hydrodynamic velocity of the superfluid component $\mathbf{v}_s=\mathbf{v}_n$, and, in particular, for "rigid-body" rotation of the liquid $v_{s\varphi}=v_{n\varphi}=\omega_n r$.

At first glance this contradicts the quantum nature of the superfluid velocity, which is described by the gradient of the phase $\nabla\theta_s$ of the macroscopic superfluid order parameter $\mathbf{v}_s=(\hbar/m_4)|\Psi_s|^2\nabla\theta_s$ (where m_4 is the mass of a ^{4}He atom, and $|\Psi_s|$ is the modulus of the order parameter). In that case curl $\mathbf{v}_s\equiv 0$, so that the "rigid-body" rotation of the superfluid component as a whole is impossible. However, if the angular velocity of rotation of the superfluid liquid ω_s exceeds a minimum critical value $\omega_{c1}=(\hbar/m^2R_0^2)\ln(R_0/a_0)$ (where R_0 is the radius of the vessel and a_0 is the radius of the normal core of a quantized vortex), then quantized vortices will be created in the volume, the normal cores of which have a finite vorticity curl $\mathbf{v}_s\neq 0$. For a sufficiently large number of quantized vortices the mean value of this vorticity $\omega_0=2\omega_s$. In this case the quantized vortices form a regular triangular lattice with a mean vortex density $n_v=\omega_0/\kappa$ (where $\kappa=2\pi\hbar/m_4$ is the quantum of circulation of the velocity).

In the present paper we consider in more detail the mechanism of entrainment of the superfluid component by the rotating normal component due to the Hall–Vinen–Bekarevic–Khalatnikov (HVBK) tensor forces at a nonzero initial vorticity. It is shown that the superfluid component is entrained into an accelerated "rigid-body" rotation, which in turn can lead to growth of the rate of decomposition of the supersaturated ^{3}He–^{4}He solution.

II. FORCES OF ENTRAINMENT OF THE SUPERFLUID COMPONENT OF A ^{3}He–^{4}He SOLUTION

We consider the equations of two-fluid hydrodynamics[3] including the macroscopic coupling forces, calculated in Refs. 4–6, that arise in the presence of quantized vortices in a superfluid component with a certain spatially uniform mean vorticity $\omega_0\neq 0$:

$$\frac{\partial \mathbf{v}_s}{\partial t}+(\mathbf{v}_s\cdot\nabla)\mathbf{v}_s=-\frac{1}{\rho_s}\nabla p_s+\mathbf{g}+\frac{\rho_n}{2\rho}\nabla(\mathbf{v}_n-\mathbf{v}_s)^2-\frac{1}{2}B'\frac{\rho_n}{\rho}[\omega_0\times(\mathbf{v}_n-\mathbf{v}_s)]-\frac{1}{2}B\frac{\rho_n}{\rho}\left[\frac{\omega_0}{|\omega_0|}\times[\omega_0\times(\mathbf{v}_n-\mathbf{v}_s)]\right], \quad (2)$$

$$\frac{\partial \mathbf{v}_n}{\partial t}+(\mathbf{v}_n\nabla)\mathbf{v}_n=-\frac{1}{\rho_n}\nabla p_n+\mathbf{g}-\frac{\rho_s}{2\rho}\nabla(\mathbf{v}_n-\mathbf{v}_s)^2+\nu_n\Delta\mathbf{v}_n-\frac{1}{2}B'\frac{\rho_s}{\rho}[\omega_0\times(\mathbf{v}_n-\mathbf{v}_s)]-\frac{1}{2}B\frac{\rho_s}{\rho}\left[\frac{\omega_0}{|\omega_0|}\times[\omega_0\times(\mathbf{v}_n-\mathbf{v}_s)]\right]. \quad (3)$$

Here B and B' are the Vinen–Hall coefficients, ρ_s and ρ_n are the densities of the superfluid and normal components, $\rho=\rho_n+\rho_s$, $p_s=P\rho_s/\rho$ and $p_n=P\rho_n/\rho$ are the partial pressures, P is the total pressure, $\mathbf{g}$ is the acceleration of gravity, and ν_n is the coefficient of kinematic viscosity of the normal component.

We note that the system of equations (2) and (3) was obtained for describing the motion of the normal and superfluid components of the quantum liquid ^{4}He. We consider a temperature region in which the normal component consists mainly of the ^{3}He impurity and the superfluid component is exclusively ^{4}He (see Ref. 1), and we assume that the HVBK equations are applicable.

In a supersaturated ^{3}He–^{4}He solution the process of spontaneous nucleation of the domains of decomposition begins with the formation of ^{3}He microdrops, which float to the surface of the solution in the field of gravity. Thus the presence of the ^{3}He impurity gives rise to a volume sink [see the continuity equation (1)] and to vertically ascending flows in the domain of decomposition, making possible a hydrodynamic instability of the "rigid-body" rotation within the domains of decomposition.

We consider the process of decomposition of the ^{3}He–^{4}He electron within a subcritical nucleus (domain of decomposition) in the form of a cylinder of radius R_0. For an axially symmetric flow under the condition that ω_0 is parallel to the z axis, Eqs. (2) and (3) take the following form in cylindrical coordinates:

$$\frac{\partial v_{sr}}{\partial t}+v_{sr}\frac{\partial v_{sr}}{\partial r}-\frac{v_{s\varphi}^2}{r}=-\frac{1}{\rho}\frac{\partial P}{\partial r}+\frac{\rho_n}{2\rho}\frac{\partial}{\partial r}(\mathbf{v}_n-\mathbf{v}_s)^2+\frac{1}{2}B'\frac{\rho_n}{\rho}\omega_0(v_{n\varphi}-v_{s\varphi})+\frac{1}{2}B\frac{\rho_n}{\rho}\omega_0(v_{nr}-v_{sr}), \quad (4)$$

$$\frac{\partial v_{s\varphi}}{\partial t}+v_{sr}\frac{\partial v_{s\varphi}}{\partial r}+\frac{v_{sr}v_{s\varphi}}{r}=-\frac{1}{2}B'\frac{\rho_n}{\rho}\omega_0(v_{nr}-v_{sr})+\frac{1}{2}B\frac{\rho_n}{\rho}\omega_0(v_{n\varphi}-v_{s\varphi}), \quad (5)$$

$$\frac{\partial v_{sz}}{\partial t}+v_{sz}\frac{\partial v_{sz}}{\partial z}=-\frac{1}{\rho}\frac{\partial P}{\partial z}-g+\frac{\rho_n}{2\rho}\frac{\partial}{\partial z}(\mathbf{v}_n-\mathbf{v}_s)^2, \quad (6)$$

$$\frac{\partial v_{nr}}{\partial t}+v_{nr}\frac{\partial v_{nr}}{\partial r}-\frac{v_{n\varphi}^2}{r}=-\frac{1}{\rho}\frac{\partial P}{\partial r}+\nu_n\left(\frac{\partial^2 v_{nr}}{\partial r^2}+\frac{1}{r}\frac{\partial v_{nr}}{\partial r}-\frac{v_{nr}}{r^2}\right)-\frac{\rho_s}{2\rho}\frac{\partial}{\partial r}(\mathbf{v}_n-\mathbf{v}_s)^2+\frac{1}{2}B'\frac{\rho_s}{\rho}\omega_0(v_{n\varphi}-v_{s\varphi})+\frac{1}{2}B\frac{\rho_s}{\rho}\omega_0(v_{nr}-v_{sr}), \quad (7)$$

$$\frac{\partial v_{n\varphi}}{\partial t}+v_{nr}\frac{\partial v_{n\varphi}}{\partial r}+\frac{v_{nr}v_{n\varphi}}{r}=\nu_n\left(\frac{\partial^2 v_{n\varphi}}{\partial r^2}+\frac{1}{r}\frac{\partial v_{n\varphi}}{\partial r}-\frac{v_{n\varphi}}{r^2}\right)-\frac{1}{2}B'\frac{\rho_s}{\rho}\omega_0(v_{nr}-v_{sr})+\frac{1}{2}B\frac{\rho_s}{\rho}\omega_0(v_{n\varphi}-v_{s\varphi}), \quad (8)$$

$$\frac{\partial v_{nz}}{\partial t}+v_{nz}\frac{\partial v_{nz}}{\partial z}=-\frac{1}{\rho}\frac{\partial P}{\partial z}-g+\nu_n\frac{\partial^2 v_{nz}}{\partial z^2}-\frac{\rho_s}{2\rho}\frac{\partial}{\partial z}(\mathbf{v}_n-\mathbf{v}_s)^2. \quad (9)$$

Here it is assumed that inside a domain of decomposition one can neglect the dependences of the azimuthal and radial velocities on z and of the axial velocity on r. Here the effects of the convective and Coriolis forces due to the existence of radial flows of the normal and superfluid components and the influence of a downward directed force of gravity are taken into account.

If the coordinate dependence of the hydrodynamic velocities of the normal component is chosen in the form of functions linear in r and z:

$$v_{nr}(r,t)=-\beta_n(t)r,\quad v_{n\varphi}(r,t)=\omega_n(t)r,\quad v_{nz}(z,t)=\alpha_n(t)z, \quad (10)$$

then on the right-hand sides of Eqs. (7)–(9) the terms with the coefficient ν_n, which describe the effect of the bulk viscosity (for an incompressible fluid), are identically equal to zero.

The radial, azimuthal, and axial velocities of the superfluid component will also be sought in the form

$$v_{sr}(r,t)=-\beta_s(t)r,\quad v_{s\varphi}(r,t)=\omega_s(t)r,\quad v_{sz}(z,t)=\alpha_s(t)z. \quad (11)$$

Here, as we have said, the parameter ω_0 has the meaning of the mean vorticity of the superfluid component $\operatorname{curl}\mathbf{v}_s$, which is equal to twice the angular velocity ω_s. The latter is related to the mean vortex density n_v in a regular triangular vortex lattice by the relation $n_v=2\omega_s/\kappa$.

As a result, with relations (10) and (11) taken into account, we obtain the following system of first-order nonlinear differential equations for determination of the functions $\alpha_{n,s}(t)$, $\beta_{n,s}(t)$, $\omega_{n,s}(t)$ and the pressure $P(r,z,t)$:

$$(\dot{\alpha}_s+\alpha_s^2)z=-\frac{1}{\rho}\frac{\partial P}{\partial z}-g+\frac{\rho_n}{\rho}(\alpha_n-\alpha_s)^2 z, \quad (12)$$

$$(\dot{\alpha}_n + \alpha_n^2)z = -\frac{1}{\rho}\frac{\partial P}{\partial z} - g - \frac{\rho_s}{\rho}(\alpha_n - \alpha_s)^2 z, \tag{13}$$

$$-\dot{\beta}_s + \beta_s^2 - \omega_s^2 = -\frac{1}{\rho r}\frac{\partial P}{\partial r} + \frac{\rho_n}{\rho}[(\beta_n - \beta_s)^2 + (\omega_n - \omega_s)^2] - \frac{\rho_n}{\rho}\omega_s[B(\beta_n - \beta_s) - B'(\omega_n - \omega_s)], \tag{14}$$

$$-\dot{\beta}_n + \beta_n^2 - \omega_n^2 = -\frac{1}{\rho r}\frac{\partial P}{\partial r} - \frac{\rho_s}{\rho}[(\beta_n - \beta_s)^2 + (\omega_n - \omega_s)^2] - \frac{\rho_s}{\rho}\omega_s[B(\beta_n - \beta_s) - B'(\omega_n - \omega_s)], \tag{15}$$

$$\dot{\omega}_s - 2\beta_s\omega_s = \frac{\rho_n}{\rho}\omega_s[B(\omega_n - \omega_s) + B'(\beta_n - \beta_s)], \tag{16}$$

$$\dot{\omega}_n - 2\beta_n\omega_n = \frac{\rho_s}{\rho}\omega_s[B(\omega_n - \omega_s) + B'(\beta_n - \beta_s)], \tag{17}$$

In Eqs. (14)–(17) a time-dependent mean macroscopic angular velocity $\omega_s(t)$ is used in the expressions for the HVBK forces instead of the mean initial vorticity ω_0. Furthermore, it is necessary to satisfy the continuity equation (1), which for the given velocity profiles can be written in the form

$$\rho_n(\alpha_n - 2\beta_n) + \rho_s(\alpha_s - 2\beta_s) = -q. \tag{18}$$

Knowing the time dependence of $\alpha_{n,s}$, $\beta_{n,s}$, $\omega_{n,s}$, q, we can use equations (13) and (14) to find the dependence of the pressure P on the coordinates r, z and time t. With this in mind, we eliminate the pressure from the system of equations (12)–(18), which then takes the form

$$\dot{\alpha}_s = \dot{\alpha}_n + 2\alpha_n(\alpha_n - \alpha_s), \tag{19}$$

$$\dot{\beta}_n - \dot{\beta}_s = \omega_s(\omega_n - \omega_s)\left[B'\frac{\rho_n - \rho_s}{\rho} - 2\right] + (\beta_n - \beta_s)\left[2\beta_n - B\frac{\rho_n - \rho_s}{\rho}\omega_s\right], \tag{20}$$

$$\dot{\omega}_s = 2\beta_s\omega_s + \frac{\rho_n}{\rho}\omega_s[B(\omega_n - \omega_s) + B'(\beta_n - \beta_s)], \tag{21}$$

$$\dot{\omega}_n = 2\beta_n\omega_n + \frac{\rho_s}{\rho}\omega_s[B(\omega_n - \omega_s) + B'(\beta_n - \beta_s)], \tag{22}$$

$$\rho_n\alpha_n + \rho_s\alpha_s + q = 2\rho_n\beta_n + 2\rho_s\beta_s. \tag{23}$$

III. ACCELERATION OF THE "RIGID-BODY" ROTATION OF THE SUPERFLUID AND NORMAL COMPONENTS IN A REGIME OF "EXPLOSIVE" INSTABILITY

We shall show that for $q=0$ the system of equations (12)–(18) has an exact self-consistent solution of the nonlinear "explosive" instability type, when all the velocity components vary in time by the law $\sim(t_0-t)^{-1}$ and reach formally infinite values after a finite time interval.

With allowance for the continuity equation, we shall seek the time dependence of the parameters that determine the profiles of the hydrodynamic velocities of the normal and superfluid components in the form

$$\alpha_{n,s} = 2\beta_{n,s} = \frac{2b_{n,s}}{t_0 - t}, \quad \omega_{n,s} = \frac{a_{n,s}}{t_0 - t}. \tag{24}$$

As a result, we obtain a system of nonlinear algebraic equations for finding the unknown constants $b_{n,s}$, $a_{n,s}$ and the pressure $P(r,z,t)$:

$$-b_s + b_s^2 - a_s^2 = -\frac{1}{\rho r}\frac{\partial P}{\partial r}(t_0 - t)^2 + \frac{\rho_n}{\rho}[(b_n - b_s)^2 + (a_n - a_s)^2] + \frac{\rho_n B' a_s}{\rho}(a_n - a_s) - \frac{\rho_n B a_s}{\rho}(b_n - b_s), \tag{25}$$

$$a_s(1 - 2b_s) = \frac{\rho_n B' a_s}{\rho}(b_n - b_s) + \frac{\rho_n B a_s}{\rho}(a_n - a_s), \tag{26}$$

$$2b_s(2b_s + 1) = -\frac{1}{\rho z}\frac{\partial P}{\partial z}(t_0 - t)^2 - \frac{g}{z}(t_0 - t)^2 + \frac{4\rho_n}{\rho}(b_n - b_s)^2, \tag{27}$$

$$-b_n + b_n^2 - a_n^2 = -\frac{1}{\rho r}\frac{\partial P}{\partial r}(t_0 - t)^2 - \frac{\rho_s}{\rho}[(b_n - b_s)^2 + (a_n - a_s)^2] + \frac{\rho_s B' a_s}{\rho}(a_n - a_s) - \frac{\rho_s B a_s}{\rho}(b_n - b_s), \tag{28}$$

$$a_n(1 - 2b_n) = \frac{\rho_s B' a_s}{\rho}(b_n - b_s) - \frac{\rho_s B a_s}{\rho}(a_n - a_s), \tag{29}$$

$$2b_n(2b_n + 1) = -\frac{1}{\rho z}\frac{\partial P}{\partial z}(t_0 - t)^2 - \frac{g}{z}(t_0 - t)^2 + \frac{4\rho_s}{\rho}(b_n - b_s)^2. \tag{30}$$

Solving the system of equations (25)–(30), we find a solution corresponding to the regime of complete entrainment of the superfluid component by the normal component:

$$b_s = b_n = \frac{1}{2}, \quad a_n = a_s = 1, \quad t_0 = \omega^{-1}(0), \tag{31}$$

$$P(r,z,t) = P(0,0,t) - \rho g z - \frac{\rho z^2}{(t_0 - t)^2} + \frac{5}{8}\frac{\rho r^2}{(t_0 - t)^2}. \tag{32}$$

Thus the development of hydrodynamic classical vortices inside the subcritical domains of the decomposing ^{3}He–^{4}He solution leads to complete entrainment of the superfluid component by the normal component on account of an increase of the density of quantized vortices, which bring about a coupling of these components. However, this regime

of "explosive" acceleration of the "rigid-body" rotation is realized only when the initial vorticities of the superfluid and normal components are equal.

In the case when the superfluid component is initially motionless and does not contain quantized vortices, so that $\omega_s(0)=\beta_s(0)=0$, the system of equations (12)–(17) in the absence of vertical flows ($\alpha_n=\alpha_s=0$) for $q=2\rho_n\beta_n\neq 0$ reduces to

$$-\frac{1}{\rho r}\frac{\partial P}{\partial r}+\frac{\rho_n}{\rho}(\beta_n^2+\omega_n^2)=0, \tag{33}$$

$$-\frac{d\beta_n}{dt}+\beta_n^2-\omega_n^2=-\frac{1}{\rho r}\frac{\partial P}{\partial r}-\frac{\rho_s}{\rho}(\beta_n^2+\omega_n^2), \tag{34}$$

$$\frac{d\omega_n}{dt}-2\beta_n\omega_n=0. \tag{35}$$

Equation (34) with (33) taken into account, under the condition $\rho=\rho_n+\rho_s$ takes the form

$$\frac{d\beta_n(t)}{dt}-2\beta_n^2(t)=0 \tag{36}$$

and coincides with Eq. (35) if one sets $\beta_n(t)=\omega_n(t)$. Then the solution of the nonlinear equations (35) and (36) takes the form

$$\beta_n(t)=\omega_n(t)=\frac{\omega_n(0)}{1-2\omega_n(0)t}, \tag{37}$$

which corresponds to an "explosive" instability with a singularity in time at $t=[2\omega_n(0)]^{-1}$ under the condition that the volume sink strength $q(t)=2\rho_n\beta_n(t)$ also grows according to the law $\sim[1-2\omega_n(0)t]^{-1}$.

However, at a certain time $t=t_1$, where t_1 is determined by the condition

$$\omega_n(t_1)=\frac{\omega_n(0)}{1-2\omega_n(0)t_1}=\omega_{c1}, \tag{38}$$

quantized vortices begin to be created in the superfluid component. As a result, coupling of the superfluid and normal components arises on account of the HVBK forces, so that in the approximation linear in ω_s and β_s Eqs. (20) and (21) assume the form

$$\frac{d\beta_s}{dt}=\left[\frac{\rho_n-\rho_s}{\rho}(B-B')+2\right]\beta_n\omega_s+2\beta_n\beta_s, \tag{39}$$

$$\frac{d\omega_s}{dt}=\frac{\rho_n}{\rho}(B+B')\beta_n\omega_s. \tag{40}$$

From Eq. (40) we find the averaged time dependence of the angular velocity of the superfluid component:

$$\omega_s(t)=\omega_{c1}\left(\frac{1-2\omega_n(0)t_1}{1-2\omega_n(0)t}\right)^{(B+B')\rho_n/2\rho}. \tag{41}$$

Then Eq. (39) has a general solution of the form (for $t>t_1$

$$\beta_s(t)=\omega_{c1}\frac{(\rho_n-\rho_s)(B-B')+2\rho}{\rho_n(B+B')-2\rho}\times\left[\left(\frac{1-2\omega_n(0)t_1}{1-2\omega_n(0)t}\right)^{(B+B')\rho_n/2\rho}-\frac{1-2\omega_n(0)t_1}{1-2\omega_n(0)t}\right]. \tag{42}$$

As we see, $\beta_s(t_1)=0$, and for $t\to[2\omega_n(0)]^{-1}$ both components of the superfluid velocity (41) and (42) are also increasing functions in the regime of the "explosive" instability. Hence it follows that the superfluid component is entrained into an accelerated "rigid-body" rotation of the normal component. Here a sharp growth of the mean velocity of the quantized vortices occurs, which should lead to growth of the rate of heterogeneous decomposition of the supersaturated ^{3}He–^{4}He solution as a result of the trapping of ^{3}He atoms by the normal cores of the quantized vortices.[7]

In accordance with what we have said above, the characteristic time for development of the "explosive" instability is equal in order of magnitude to $[\omega_n(0)]^{-1}$, where $\omega_n(0)$ is the initial angular velocity of rotation. Thus there should exist a relation between the rate of heterogeneous decomposition of the solution and the angular velocity of rotation of the vessel in which it is found. We stress that the volume sink strength $q(t)=2\rho_n\beta_n(t)$ should depend on time in an "explosive" manner, which corresponds to an increase of the rate of formation of ^{3}He microdrops and, hence, to acceleration of the rate of decomposition.

Estimates show that in a vessel of radius $R_0\sim 1-5$ cm the comparatively slow rotation of the Earth ($\omega\sim 10^{-4}$ rad/s) will be sufficient for practically instantaneous [$t_1=0$; see Eq. (38)] attainment of the critical angular velocity $\omega_{c1}=(\hbar/m_4R_0^2)\ln(R_0/a_0)$. For a quantitative analysis to determine the characteristic rates of heterogeneous decomposition of a supersaturated ^{3}He–^{4}He solution in the general case it will be necessary to have numerical values of the coefficients B and B' and the initial vorticity $2\omega_n(0)$.

In closing, the authors thank E. Ya. Rudavskii for helpful discussions.

[a]E-mail: pashitsk@iop.kiev.ua
[b]E-mail: malnev@i.com.ua
[c]E-mail: naryshkin@univ.kiev.ua

[1]É. A. Pashitskiĭ, V. N. Mal'nev, and R. A. Naryshkin, Fiz. Nizk. Temp. **31**, 141 (2005) [Low Temp. Phys. **31**, 171 (2005)].
[2]É. A. Pashitskiĭ, Prikl. Gidrodin. **4**(76), 50 (2002).
[3]I. M. Khalatnikov, *Theory of Superconductivity* [in Russian] (Fizmatgiz, Moscow 1971).
[4]H. E. Hall, Proc. R. Soc. London, Ser. A **245**, 546 (1958); Adv. Phys. **9**, 89 (1960).
[5]W. F. Vinen, Proc. R. Soc. London, Ser. A **260**, 218 (1961).
[6]I. L. Bekarevich and I. M. Khalatnikov, Zh. Eksp. Teor. Fiz. **40**, 920 (1961) [Sov. Phys. JETP **13**, 643 (1961)].
[7]V. A. Mikheev, É. Ya. Rudavskii, V. K. Chagovets, and G. A. Sheshin, Fiz. Nizk. Temp. **17**, 444 (1991) [Sov. J. Low Temp. Phys. **17**, 233 (1991)].

Translated by Steve Torstveit

Dynamic electrostriction of a Bose condensate and of a system of neutral atoms

A. M. Kosevich[a)]

B. Verkin Institute for Low Temperature Physics and Engineering, National Academy of Sciences of Ukraine, pr. Lenina 47, Kharkov 61103, Ukraine

(Submitted May 30, 2005; resubmitted July 25, 2005)
Fiz. Nizk. Temp. **31**, 1100–1103 (October 2005)

It is shown that the condensate of a Bose gas of neutral atoms has electrical properties that are reflected in the dynamics of the condensate and do not reduce to a trivial polarization of the atomic gases in an external electric field. The concept of an isotropic atomic quadrupole moment whose distribution creates a distribution of the macroscopic electric potential $\langle\varphi\rangle$ in a system of neutral atoms is used. The nonuniform distribution of atoms that arises in a sound wave, for example, will produce an electric field whose behavior is determined by the dynamics of $\langle\varphi\rangle$.
 [DOI: 10.1063/1.2126942]

We consider the Bose condensate of a neutral gas whose atoms are found in a ground state of the S type and therefore have no intrinsic dipole moments. The electric potential outside such an atom is zero. Inside the atom, however, there exists an intra-atomic electric potential produced mainly by the positively charged nucleus. Its value is not hard to find, and the macroscopic sense is easily understood in the conceptual framework of classical electrodynamics. To estimate this potential we investigate a model distribution of the electric potential inside the atom. In the long-wavelength approximation such a potential is characterized by its mean value. We use a simple model of an atom in an S state, assuming the electrons are distributed uniformly on a sphere of radius a with a total charge $-Z|e|$. The mean electrostatic potential inside such an atomic sphere of volume $V_0 = 4\pi a^3/3$ is equal to $\varphi_0 = 3Z|e|/(2a)$. Consequently, the atom produces a potential which in the macroscopic description is equal to

$$\varphi(\mathbf{x}) = \varphi_0 V_0 \delta(\mathbf{x} - \mathbf{x}_0), \tag{1}$$

where $\mathbf{x}_0$ is the coordinate of the center of mass of the atom.

A rigorous derivation of relation (1) is easily given for a specified degree of approximation. Let φ be the electric potential of the atom according to Poisson's equation $\Delta\varphi = -4\pi\rho_{\text{el}}$ (Δ is the Laplacian operator), where ρ_{el} is the charge density in the atom:

$$\rho_{\text{el}}(\mathbf{x}) = |e|[Z\delta(\mathbf{x} - \mathbf{x}_0) - \eta(\mathbf{x} - \mathbf{x}_0)]; \tag{2}$$

and $\eta(\mathbf{x})$ is the density of the electron distribution in the atom.

The calculation is conveniently done in the $\mathbf{k}$ representation, introducing the Fourier components of the potential and the charge density:

$$\varphi_k = \int \varphi(\mathbf{x}) e^{-i\mathbf{k}\cdot\mathbf{x}} dV, \quad \rho_k = |e|(Z - \eta_k) e^{-i\mathbf{k}\cdot\mathbf{x}_0}.$$

These components are connected by a relation that derives in an obvious way from Poisson's equation, and therefore

$$k^2\varphi_k = 4\pi\rho_k = 4\pi|e|(Z - \eta_k) e^{-i\mathbf{k}\cdot\mathbf{x}_0}. \tag{3}$$

As we want to obtain closed formulas, we shall assume that the distribution of electric charge Z in the atom is described by the square modulus of the wave function of the S state of the electron in the hydrogen atom:

$$\eta(\mathbf{x} - \mathbf{x}_0) = \eta(|\mathbf{x} - \mathbf{x}_0|) = \frac{Z}{\pi a^3} \exp\left(-\frac{2|\mathbf{x} - \mathbf{x}_0|}{a}\right),$$

where a is the Bohr radius. Then the Fourier component will be equal to

$$\eta_k = \frac{Z}{(1 + \kappa^2)^2}, \quad \kappa = \frac{ak}{2}. \tag{4}$$

Substituting Eq. (4) into (3), we obtain

$$\varphi_k = \pi Z|e|a^2 \left(\frac{1}{1 + \kappa^2} + \frac{1}{(1 + \kappa^2)^2}\right) e^{-i\mathbf{k}\cdot\mathbf{x}_0}. \tag{5}$$

The product ea^2 has dimensions of a quadrupole moment, and in Ref. 1 the quantity $q = -Z|e|a^2$ is called the isotropic quadrupole moment (IQM) of the atom. In the long-wavelength approximation ($ak \ll 1$) relation (5) reduces to

$$\varphi_k = 2\pi Z|e|a^2 e^{-i\mathbf{k}\cdot\mathbf{x}_0}. \tag{6}$$

It is clear that the Fourier transform (6) in the coordinate representation corresponds to the Fermi potential[2]

$$\varphi(\mathbf{x}) = -2\pi q \delta(\mathbf{x} - \mathbf{x}_0), \tag{7}$$

which, up to differences of notation, agrees with the potential (1) obtained by qualitative estimates. It can be assumed that this justifies the use of formula (1) or (7) in long-wavelength calculations. However, let us continue the calculation to obtain a more accurate explicit expression for the function $\varphi(\mathbf{x})$.

Using the comparatively simple form of the Fourier transform (5), we calculate the potential itself:

$$\varphi(\mathbf{x}) = \frac{1}{(2\pi)^3} \int \varphi\, e^{i\mathbf{k}\cdot\mathbf{x}}\, d^3k = \frac{Z|e|}{r}\left(1 + \frac{r}{a}\right) e^{-2r/a}, \tag{8}$$

where the coordinate is measured from the nucleus of the atom: $r = |\mathbf{x} - \mathbf{x}_0|$. The trustworthiness of formula (8) is confirmed by the reasonable behavior of the potential in the limiting cases $r \ll a$ and $r \gg a$. It describes a highly localized

distribution of the potential, which in the long-wavelength approximation can be characterized completely as delta-function-like. Indeed, the total potential (8) over the whole volume is equal to

$$\int \varphi(\mathbf{x})dV = 2\pi Z|e|a^2,$$

which allows us to write the potential in the form (7).

Thus, an electric field that decays rapidly with distance arises around a neutral atom:

$$\mathbf{E} = 2\pi q \text{ grad } \delta(\mathbf{x}-\mathbf{x}_0).$$

Each atom creates a localized electric field that resembles a dilatation center in the theory of elasticity, with a total vector $\langle \mathbf{E} \rangle$ equal to zero but with a nonzero "longitudinal moment" $\langle \mathbf{x}\cdot\mathbf{E}\rangle \neq 0$. In the simple atomic model used this field arises on the sphere of radius a where the electric double layer separating the interior part of the atom (having potential φ_0) and the exterior part of the space (where the potential is equal to zero) is concentrated. This field is directed along the radius, i.e., it is normal to the aforementioned sphere, forming an "electric hedgehog." Assuming the thickness of the double layer is equal to a, we obtain the value of the electric field at the atom:

$$E_0 = \varphi_0/a = -3Z|e|/(2a^2) = 2\pi q/(aV_0).$$

The system of atoms creates a distribution of the electric potential

$$\varphi(\mathbf{x}) = 2\pi q\, n(\mathbf{x}), \quad n(\mathbf{x}) = \sum_\alpha \delta(\mathbf{x}-\mathbf{x}_\alpha), \tag{9}$$

where $\mathbf{x}_\alpha$, the coordinate of the αth atom, is summed over all atoms in the system, and $n(\mathbf{x})$ is the microscopically defined atomic density distribution.

It should be noted that the formulas obtained above are not specific to atoms of a Bose condensate; in the long-wavelength approximation they describe the classical electrical properties of any almost ideal gas. Nevertheless, let us calculate the mean values of the electrical characteristics in some given state of the condensate, describing its ground state or some weakly excited stationary state. In a coherent condensate state the atoms form a single ordered structure characterized by the wave function

$$\Psi(\mathbf{x}_\alpha) = \Psi(\mathbf{x}_1, \mathbf{x}_2, \mathbf{x}_3, \dots). \tag{10}$$

The mean density of atoms in the state under consideration is

$$\langle n(\mathbf{x})\rangle = \sum_\alpha \langle \Psi|\delta(\mathbf{x}-\mathbf{x}_\alpha)|\Psi\rangle = \sum_\alpha |\psi_\alpha(\mathbf{x})|^2, \tag{11}$$

where we have introduced a single-particle density

$$|\psi_\alpha(\mathbf{x}_\alpha)|^2 = \int |\Psi(\dots, \mathbf{x}_\beta, \dots)|^2 \prod_{\beta\neq\alpha} dV_\beta.$$

In an almost ideal Bose gas one can describe the weakly excited long-wavelength states using an approximation of the mean field type, assuming that all the atoms are found in the same single-particle quantum state, the wave function of which, $\psi_\alpha(\mathbf{x}_\alpha) = \psi_0(\mathbf{x}_\alpha)$ (for all α), satisfies the Gross–Pitaevskiĭ equation.[3] Such an approximation is usually used in finding the Bogolyubov spectrum for weakly excited states of the condensate.

In writing Eq. (11) it is understood that the density of atoms in the condensate can be a function of the coordinates, but one that varies substantially only over distances large compared to the interatomic distances. It is in such a way that the possibility of describing the excitations of the condensate is treated in the theory of superfluidity.[3]

The mean electric potential is obtained by averaging (9) over the positions of the centers of mass of all the atoms, i.e., over the state described by the function (10):

$$\langle\varphi\rangle = \langle\Psi|\varphi|\Psi\rangle = -2\pi q\sum_\alpha |\psi_\alpha(\mathbf{x})|^2 = -2\pi q\langle n(\mathbf{x})\rangle, \tag{12}$$

and is described by the mean density of atoms.

Since practically all the atoms in the Bose condensate are found in a state with $\mathbf{p}=0$, they feel the averaged potential (12). The potential $\langle\varphi\rangle$ stands as an independent characteristic that determines the distribution of the isotropic quadrupole moment. It can be assumed that the presence of the field $\langle\varphi\rangle$ is a manifestation of the "long-range order" inherent to the condensate state of a Bose gas.

The interaction of a neutral atom with the electric field in the approximation linear in the field has the form $\delta U_{\text{int}} = (1/2)q\Delta\varphi$, where q is the IQM of the atom and Δ is the Laplacian operator. This formula can be used to find the energy of the pairwise electric interaction of two neutral atoms:

$$U(\mathbf{x}_1-\mathbf{x}_2) = -2\pi q^2\Delta\delta(\mathbf{x}_1-\mathbf{x}_2), \tag{13}$$

the Fourier component of which is equal to

$$U_k = \pi q^2 k^2. \tag{14}$$

However, interaction (13), which is the long-wavelength limit of the direct Coulomb interaction, does not exhaust the description of the possible interactions of atoms in the condensate. First, in formula (13) and in all the previous papers it has been assumed that the distribution of electrons is "hard" and is not deformed under a contact interaction. However, there is a strong additional interaction of atoms due to the deformation of the electron shells where the atoms come together and which has a $\mathbf{k}$-independent Fourier component (recall that we are analyzing the case $(ak)^2 \ll 1$); this interaction is taken into account primarily in the calculation of the Bogolyubov spectrum of oscillations of the condensate and in the formulation of the Gross–Pitaevskiĭ equations.[3] Second, an analysis of this atomic contact interaction in Ref. 4 led to the conclusion that the finite size a of the atom should be taken into account in the formula for the pair interaction energy $U(\mathbf{x}) = U_0\delta(\mathbf{x})$. In spherical coordinates this can be done by assuming that $r \gg a$ and taking the interaction energy in the form $U(\mathbf{x}) = U_0/(4\pi a^2)\delta(r-a)$. As a result, the Fourier component U_k, besides the constant part U_0, takes on an additional correction having order of magnitude $(ak)^2$ comparable with expression (14) but with the opposite sign to (14). Therefore the pair interaction energy of neutral atoms in the long-wavelength approximation should be written in the form

$$U(\mathbf{x}) = U_0\delta(\mathbf{x}) + U_1 a^2 \Delta\delta(\mathbf{x}), \tag{15}$$

where the parameter U_1 is of order of magnitude U_0, but its value and the sign can be investigated only as a result of a microscopic calculation. Nevertheless, formulas (7) and (12) are sufficient for description of the electrical phenomena in the condensate, since the electric effect is very small, and the distribution of atoms in the system can be obtained and described without taking this effect into account.

In the spatially nonuniform case, when n_0 depends on the coordinates (to the degree indicated above), there arises a mean electric field

$$\mathbf{E} = 2\pi q \operatorname{grad} n_0. \tag{16}$$

We note that both the electric potential and field and the distribution of electric charge are directly proportional to the mean density of distribution of atomic IQMs in the gas, i.e., the quantity

$$Q = q\langle n(\mathbf{x})\rangle.$$

However, according to the electrodynamics of continuous media, a nonuniform distribution of the density of quadrupole moments even in the absence of electric field gives rise to polarization of the gas with a polarization vector

$$\mathbf{P} = -\frac{1}{2}\operatorname{grad} Q. \tag{17}$$

A formula equivalent to this expression was used in Ref. 5 with reference to Ref. 6 in a discussion of the polarization of a quantum liquid.

We note that the electric field and polarization vector created by the nonuniformity of Q are such that they do not create an electric displacement vector in the gas:

$$\mathbf{D} = \mathbf{E} + 4\pi\mathbf{P} = 0.$$

This result reflects the absence of free external charges in the gas. Consequently, the low-frequency dynamics of the gas under study cannot give rise to long-wavelength transverse oscillations of the electric field. However, it has been shown that the nonuniformity of the distribution of atoms in the gas gives rise to a longitudinal electric field and a longitudinal polarization of the gas.

A controllable nonuniformity of the density in a Bose gas is most easily created in the propagation of first sound, the amplitude of which is determined by oscillations of the pressure p in the gas. In that case, at low temperatures we have

$$\delta\varphi = -\frac{2\pi q}{ms^2}\delta p = \frac{2Z\pi|e|a^2}{ms^2}\delta p, \tag{18}$$

where m is the mass of an atom and s is the speed of sound. The excitation of an electric field by the pressure gradient in the sound wave is naturally called dynamic electrostriction.

It was mentioned above that formulas (7) and (12) are not specific to the atoms of a Bose condensate, and in the long-wavelength approximation they describe the electrical properties of any atoms. In particular, formula (18) should describe the electric field in a dielectric quantum fluid, e.g., He II. However, the meaning, value, and even the sign of the parameter q in Eq. (18) can differ. The point is that in writing the basic formulas it was assumed that the electron distribution $n(\mathbf{x}-\mathbf{x}_0)$ in the atom under study depends only on the intra-atomic electron interactions—the other atoms are far away. In a liquid such an assumption is incorrect—the mutual electric polarization of neighboring atoms substantially deforms the electron shells, and the electron density becomes different. In a first approximation in the polarization effect the mean dipole moment of each atom remains zero. However, in the next approximation, that in which the usual van der Waals forces are calculated (see Ref. 2), a nonzero effect arises which is proportional to the mean square fluctuations of the induced dipole moments, and an additional term proportional to $(ak)^2$ appears in the expansion (4). As a result, relation (16) takes the form

$$\mathbf{E} = -\frac{2Z\pi|e|}{ms^2}\operatorname{grad}(l_0^2 p), \tag{19}$$

where the parameter l_0^2 (which, of course, depends on the state of the system) becomes a phenomenological parameter of the model, the value of which must be determined by a comparison of formula (19) with the experimentally measured electric field in the neutral liquid. Consequently, it is of interest to make an experimental observation of electric oscillations upon the passage of first sound in liquid helium under approximately the same conditions as those for the observation of electric effects in superfluid helium upon the passage of second sound.[7]

The author thanks É. A. Pashitskiĭ for a discussion and V. D. Natsik for critical comments.

[a)]E-mail: kosevich@ilt.kharkov.ua

[1]A. M. Kosevich, Fiz. Nizk. Temp. **31**, 50 (2005) [Low Temp. Phys. **31**, 37 (2005)].
[2]I. O. Vakarchuk, *Quantum Mechanics* [in Ukrainian], LNU, L'viv (2004).
[3]E. M. Lifshitz and L. P. Pitaevskiĭ, *Statistical Physics*, Part 2, Butterworth-Heinemann, London (1980), Nauka, Moscow (1978).
[4]K. A. Brueckner and K. Sawada, Phys. Rev. **106**, 1128 (1957).
[5]L. A. Melnikovsky, arxiv: cond-mat/0505102, V1, 4 May (2005).
[6]J. Prost and J. P. Marceron, J. Phys. **38**, 315 (1977).
[7]A. S. Rybalko, Fiz. Nizk. Temp. **30**, 1321 (2004) [Low Temp. Phys. **30**, 994 (2004)].

Translated by Steve Torstveit

SUPERCONDUCTIVITY, INCLUDING HIGH-TEMPERATURE SUPERCONDUCTIVITY

Low-frequency phonons in the point-contact spectrum of MgB_2

V. V. Fisun,[a] L. Yu. Triputen, and I. K. Yanson

B. Verkin Institute for Low Temperature Physics and Engineering, National Academy of Sciences of Ukraine, pr. Lenina 47, Kharkov 61103, Ukraine

(Submitted February 14, 2005)
Fiz. Nizk. Temp. **31**, 1104–1109 (October 2005)

The second derivatives of the current-voltage characteristics of heterocontacts between a film of MgB_2 and counterelectrodes of pure metals (Cu, Ag, Au, Be) are investigated by the method of point-contact (PC) spectroscopy. The PC spectra are studied in the normal ($T \geqslant T_c$) and superconducting ($T < T_c$) states along the direction of the c axis. In the normal state the spectra have a feature in the energy interval ~20–30 mV in the form of a broad peak or a smeared kink. It is conjectured that the low-frequency modes of the phonon spectrum are also responsible for the high value of the superconducting transition temperature in MgB_2. In the superconducting state the spectral features become N-shaped in the region of the low-frequency peak. © *2005 American Institute of Physics*. [DOI: 10.1063/1.2126943]

INTRODUCTION

The superconducting properties of magnesium dibromide MgB_2 were discovered only a few years ago.[1] MgB_2 has the highest superconducting transition temperature of all the known s–p metals and alloys: $T_c \sim 39$ K. Like the other dibromides, MgB_2 has a hexagonal structure containing graphite-like layers of boron atoms separated by magnesium layers with the hexagonal close-packed (hcp) arrangement. The manganese atoms are positioned at the centers of hexagons formed by boron, so that the bond between the atoms in the boron layers is more significant than that between the atoms in the magnesium layers. The unusual two-band character of the electron structure is of interest for different groups of investigators doing detailed studies of this compound. MgB_2 presents a rare example of a highly anisotropic superconductor with two energy gaps, with values of 2.5 and 7.0 meV. It is important to note that both gaps vanish at the same critical transition temperature ~38–40 K. The existence of two superconducting energy gaps is confirmed by the experimental data obtained using tunneling[2] and point-contact[3,4] (PC) spectroscopy.

The electronic structure of MgB_2 consists of two groups of bands: pairs of anisotropic quasi-two-dimensional (2D) σ bands with a strong electron-phonon interaction and pairs of practically isotropic three-dimensional (3D) π bands with a weak electron-phonon interaction, which are formed by the local p_{xy} and p_z orbitals of boron. In accordance with the theoretical models, the π and σ bands are weakly coupled to each other and have different dynamical and topological properties. The role of the p_{xy} orbitals of boron in the transport and thermodynamic properties of MgB_2 is extremely important. Between the π and σ bands there is weak coupling. The value of the electron-phonon interaction (EPI) parameter λ for the σ band, according to Ref. 5, reaches 2–3. The structure of the σ band is such that in the ΓA direction the Fermi energy of the hole carriers is ~0.5–0.6 eV. It is supposed[6] that the low Fermi velocity leads to a significant nonadiabatic correction to T_c.

The phonon dispersion curves determined[7] by inelastic x-ray scattering indicate a peak at 75 meV in the ΓA direction with E_{2g} symmetry. According to theoretical estimates, the optical phonons corresponding to the E_{2g} vibrational modes of the graphite-like layers of boron atoms play the dominant role in the mechanism of superconductivity. It is assumed that the high value of the critical temperature is due to the interaction of E_{2g} phonon mode, which corresponds to antiparallel vibrations of the atoms in the boron planes, and the conduction electrons of the σ band.

The phonon structure of c-oriented films and single crystals of MgB_2 has been investigated[8–10] by the method of PC spectroscopy. The PC spectra in the superconducting state exhibit structure in the region of phonon energies ~30–100 meV that is in good agreement with the data from inelastic neutron scattering, tunneling spectroscopy, and theoretical calculations. It was noted[9] that this structure vanishes upon transition to the normal state ($T \geqslant T_c$). The intensity of the observed phonon structure increases with increasing value of the small interval Δ_π, which suggests that it can be attributed to the superconducting energy gap in the π band. The asymptotic expressions obtained in Ref. 11 for the nonlinear conduction of tunnel, ballistic, and diffusive contacts in the case $eV \geqslant \Delta$ are in qualitative and quantitative agreement with measurements of the phonon structure in the PC spectra for MgB_2. It is shown that the shape of the $dV/dI(V)$ characteristics of the different forms of point constants (ballistic, tunneling, diffusive) are practically identical at biases below 80 meV. It was noted[10] that if the superconducting gap corresponding to the π band is equal to 2.5 meV, then the PC spectra will have a kink at ~20–30 meV in addition to features in the 60–70 meV region.

As a rule, in investigations of the phonon spectrum of a superconductor by the method of PC spectroscopy the point

contacts are selected for study by the criteria of maximal intensities of the superconducting parameters (such as, e.g., the amplitude of the minima on the first derivative of the current-voltage (I–V) characteristic, $dV/dI(V)$, of the point contact, which reflect the superconducting gap, and the value of the excess current). In that case, however, it becomes hard to separate the observed features into spectral ones, due to backscattering of the electrons with the emission of phonons (as in the normal state) and those caused by nonlinear energy dependence of the superconducting gap, and, hence, of the excess current.[11] The intensity of the features due to the dependence of the superconducting energy gap can be much greater than the phonon spectral features. We also note that the spectral peaks are transformed to N-shaped when the ballistic regime is destroyed and the thermal regime is approached.[12] In addition, there exist features due to the destruction of the superconducting current paths or the appearance of additional scattering centers in the point contacts. The energy position and intensity of these features change upon changes in the temperature of the experiment or in strong magnetic fields. We note that the narrowing of the phonon features will have a different form depending on which of the currents through the point contact is dominant—the direct or tunneling conductance—and also on the regime of electron transport through the contact, and for this reason it is hard to determine. As we have said, in spite of the fact that a number of features whose energy positions are in good agreement with those of the phonon features are present in the superconducting state, upon the transition of the superconductor to the normal state at a temperature above T_c the second derivative of the I–V characteristic of such point contacts often exhibits no spectral nonlinearity.[13] The phonon spectrum at low temperatures in the normal state cannot be studied because high enough magnetic fields are not available (in our experiments the magnetic field was limited to a value of ~4 T).

SPECIFICS OF THE EXPERIMENT

In this paper we report a study of the phonon structure of the superconductor MgB_2 by the method of PC spectroscopy with the use of different counterelectrodes. PC spectroscopy permits obtaining direct experimental data on the EPI of the point contact, which can be used for choosing better-founded theoretical models describing the interaction of the electron and phonon subsystems. The method consists in the study of the nonlinearity of the I–V characteristics of metallic (nontunnel) contacts with a characteristic size smaller than the inelastic mean free path of the electron at temperature T and voltage V: $l_{\text{in}}(T,eV)$. According to the theory,[14] the second derivative of the I–V characteristic, in the case of a ballistic regime of electron transport between electrodes with strongly different Fermi velocities, is directly proportional to the PC spectral function of the EPI of the metal with the lower Fermi velocity v_F. The function $g_{PC}(\omega)=\alpha^2_{PC}(\omega)F(\omega)$ is close in structure to the well-known Eliashberg function, where $\alpha^2_{PC}(\omega)$ is the square of the EPI matrix element averaged over the Fermi surface, and $F(\omega)$ is the phonon density of states. The second derivative of the I–V characteristic, which is proportional to the second harmonic of the modulating voltage $V_2(V)$, at liquid helium temperature is equal to:

$$\frac{d^2V}{dI^2} \propto \frac{d(\ln R)}{dV} = \frac{4ed}{3\hbar v_F}\alpha^2_{PC}(\omega)F(\omega)_{\hbar\omega=eV}.$$

In the model of a clean aperture, the diameter of the contact is related to R_0 [Ω], its normal-state resistance at zero voltage, by the Sharvin formula:

$$d=\left(\frac{16}{3\pi}\frac{\rho\ell}{R_0}\right)^{1/2} \approx \frac{30}{R_0^{1/2}}\ [\text{nm}].$$

In a study of heterocontacts the intensity of the partial contribution of MgB_2 to the PC spectrum of the heterocontact should, according to the theory,[15] be larger, since the value of the Fermi velocity of MgB_2 is lower ($v_F \sim 10^5$ m/s) than the Fermi velocity of the counterelectrode ($v_F \sim 10^6$ m/s). The intensity of the PC spectrum is proportional to $\sim d/(v_F\tau_e)$, where τ_e is the inelastic relaxation time. It should be noted that the relative intensity of the PC spectra is not determined uniquely by the resistance of the contact, since the relation between the elastic mean free path and the process remains unknown to us.

The objects of study were MgB_2 films of thickness ~100 nm, oriented with the c axis perpendicular to the substrate.[8,9,11,16] The resistivity of MgB_2 at 40 K was around 1 $\mu\Omega\cdot$cm, and the ratio of the resistance at room temperature to the residual resistance was 2.2. The measurements consisted in registration of the first $[dV/dI(V)\propto V_1(V)]$ and second $[d^2V/dI^2(V)\propto V_c(V)]$ harmonics of the harmonics of a small modulating signal by the method of synchronous detection.

To eliminate the influence of superconductivity on the spectral features of MgB_2 the point contacts were created in the normal state of MgB_2 at a temperature of 30 K in a magnetic field of 4 T. The absence of any features on the second derivatives of the I–V characteristics of the point contacts at zero voltage (Fig. 1) served as confirmation of the normal state. However, under these conditions the temperature smearing is more than 10 meV, making it hard to estimate the EPI parameter λ:

$$\lambda = 2\int_0^\infty g_{PC}(\omega)\frac{d\omega}{\omega}.$$

As counterelectrodes we used several pure metals with different Debye temperatures (namely Cu, Ag, Au, and Be). The absence of low-frequency phonons in the Be spectrum was a clear indication that the phonon features that we observed were due to MgB_2 (see below).

The selection criterion of the PCs found in the normal state was the presence of a spectral feature on the second derivative of the I–V characteristic of the contact at voltages of 20–30 meV (Fig. 1). It is known that an important factor determining the quality of a point contact in the superconducting state is the presence of gap minima on the first derivative of the I–V characteristic, which we can observe only at low temperatures ($T<T_c$). In spite of the fact that the superconducting characteristics did not figure into the selection of the point contacts, their presence at low temperatures *a posteriori* attested to the high quality of the contacts (see, e.g., Fig. 2). Since MgB_2 has two gaps, which are associated with the different directions of the crystallographic axes, the values of these gaps can be used to assess the orientation of

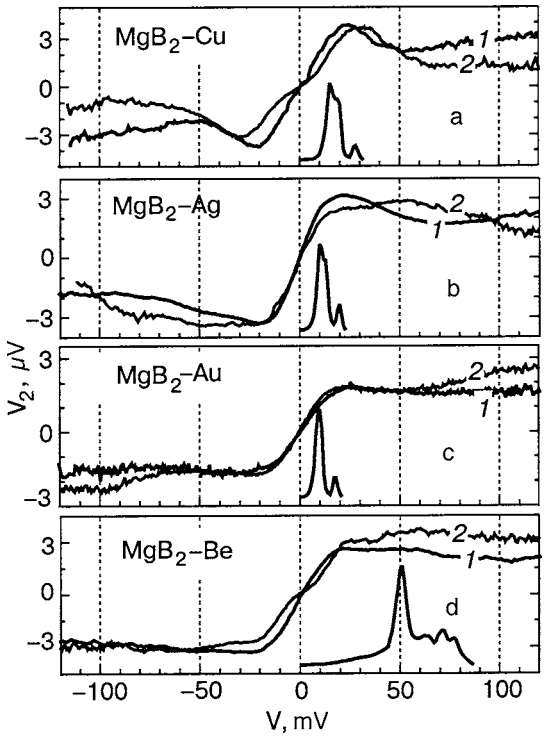

FIG. 1. PC spectrum of the point contacts. MgB_2–Cu; $V_{1,0}$=4.72 mV, T=28 K, R_0=670 m (*1*); $V_{1,0}$=6.2 mV, T=31 K, R_0=53 Ω (*2*) (a). MgB_2–Ag: $V_{1,0}$=7.24 mV, T=28 K, R_0=82 Ω (*1*); $V_{1,0}$=7.02 mV, T=30 K, R_0=105 Ω (*2*) (b). MgB_2–Au: $V_{1,0}$=2.62 mV, T=40 K, R_0=58 Ω (*1*); $V_{1,0}$=2.36 mV, T=40 K, R_0=60 Ω (*2*) (c). MgB_2–Be: $V_{1,0}$=7.93 mV, T=28 K, R_0=32 Ω (*1*); $V_{1,0}$=4.7 mV, T=33 K, R_0=92 Ω (*2*) (d). The magnetic field H=4 T for all the PCs. Shown for comparison at positive bias are the spectra of the counterelectrodes, arbitrarily shifted along the vertical axis.

the axis of the PC. A nominally point contact was created in the direction of the c axis of a MgB_2 film characterized by a small gap Δ_π. As is seen in Fig. 2, the gap minima on the first derivative of the I–V characteristic of the PCs studied corresponds to a small gap. It may be concluded from what

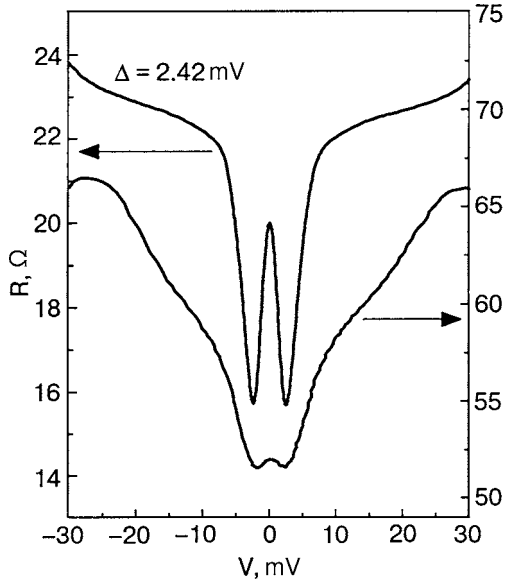

FIG. 2. The first derivatives of the I–V characteristic at T=4.2 K, H=0 T, corresponding to the MgB_2–Ag and MgB_2–Au heterocontacts characterized in Fig. 1.

we have said that the observed spectral feature is associated with the direction of the c axis of close to it.

RESULTS

Figure 1 shows the PC spectra of MgB_2–N heterocontacts (N is a normal metal) which exhibit features in the form a single broad peak or a smeared kink in the energy interval 20–30 meV; the energy positions of these features are independent of the counterelectrodes used. Also shown in Fig. 1 are the PC spectra of these counterelectrodes at helium temperatures, taken from an atlas[17] (for clarity the spectra have been shifted arbitrarily relative to the zero of the vertical axis). It is obvious that it would be more correct to use the spectra of the counterelectrodes at the same temperatures as for the spectra of the heterocontacts. However, the thermal smearing leads to only a slight upward shift of the energies of the main maxima that is unimportant in the present study. It is important to note that even in the case of a nonballistic regime of electron transport the energy position of the main maxima of the counterelectrodes is shifted to higher energies by only 9% in the thermal regime.[18]

The observed low-frequency feature on the PC spectra corresponds to the spectral regime, since the value of the resistance of the contacts lies in an interval of 30–105 Ω [for example, the value of the resistance for a MgB_2–Ag heterocontact (see curve *1* in Fig. 1) is 82 Ω]. For realization of the spectral regime the size of the contact must be less than the electron mean free path, which corresponds to a resistance value of more than 10 Ω. This follows from the estimates of the ratio of the diameter of the contact to the mean free path of the electron in the review.[13] According to the Sharvin formula, for $\rho\ell \cong 4.9\times10^{-12}\ \Omega\cdot\mathrm{cm}^2$ and a resistance $R \sim 10\ \Omega$ both in the direction of the c axis and in the ab plane, the characteristic size d of the contact in the ballistic regime is ~7 nm. Then l_{ab}=70 nm and l_c=18 nm. If the PC contains contaminants and the mean free path is small, then Maxwell's formula $d=\rho/R$ is applicable. In that case the value of d is 0.7 and 2.6 nm for the ab plane and the direction of the c axis, respectively. Further confirmation of the spectral regime also comes from the fact that when the temperature is raised to 70 K, the maximum at ~20–30 meV is smeared out while maintaining its position on the energy axis.

The spectra at T=30 K in a magnetic field of 4 T do not carry any information about the superconducting characteristics of MgB_2. It is important to note, however, that the PC region undergoes a transition to the superconducting state upon a slight decrease in temperature (by 1–2 K), attesting to the superconducting modification of MgB_2 under the contact. Upon further decrease of the temperature a portion of the current passing through the PC is transported through superconducting regions. In that case the features due to superconductivity increase significantly.

Figure 3a shows the PC spectra of MgB_2–Ag in the normal (T=30 K, H=4 T; curve *1*) and superconducting (curves *2, 3*) states. It can be seen that lowering the temperature leads to the appearance of a peak in the PC spectrum near zero voltage which is due to Andreev reflection at the *NS* boundary, and a number of features in the phonon region of frequencies, 30–90 meV. Curve *2* demonstrates the PC

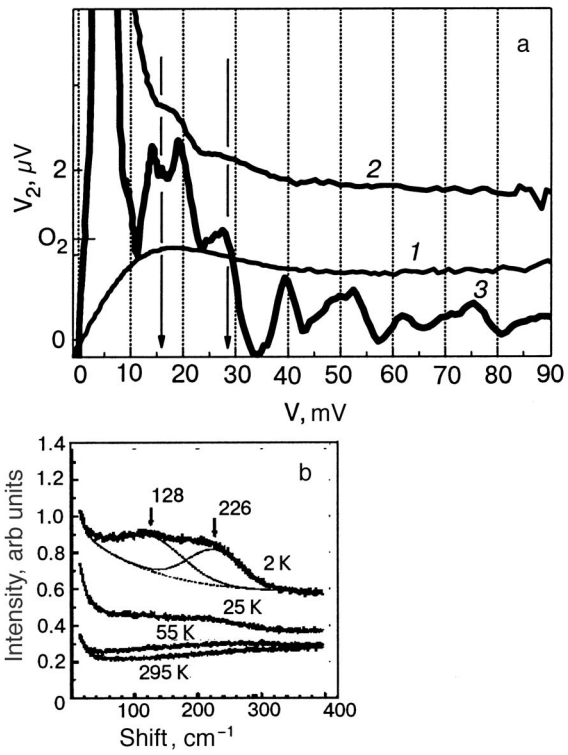

FIG. 3. PC spectra of a MgB_2–Ag heterocontact: normal state, $R=42\ \Omega$ (*1*); $T=20$ K, $V_{1,0}=2.23$ mV, the superconducting state (*2,3*); the zero of curve *2* is shifted upward along the vertical (a). The Raman scattering spectra of MgB_2 (Ref. 19) (b).

spectrum at an intermediate temperature ($T=20$ K, $H=4$ T), on which at $V\rightarrow 0$ one observes a transformation of the low-frequency phonon feature into two smeared downward steps at energies of ~16 and 28 meV (~126 and 228 cm^{-1}) against the background of the nonlinearity due to the superconductivity. Upon further decrease of temperature the phonon features become N-shaped on account of the deviation from the ballistic regime (curve *3*). The energy position of the N-shaped features has only an approximate correspondence with the position of the phonon peaks on the energy axis. In Fig. 3b we show for comparison the Raman scattering spectrum taken from Ref. 19. The relationship between the scales of the abscissas for those spectra and the PC spectrum is 1 meV=8.065 cm^{-1}. It is seen that the energy position of the low-frequency spectral features on curve *3* in Fig. 3a is in good agreement with the experimental data from the Raman spectroscopy (vertical lines in Fig. 3a and 3b). The authors of Ref. 19 mention that the observed features are not due to nonlinearity of the superconducting gap and they are observed to temperatures exceeding the value of T_c for MgB_2 (see the curves for $T=25$, 55, and 295 K in Fig. 3b). In Ref. 20 the PC spectra measured in the normal state ($T=3-$K, $H=7$ T) are presented; on those spectra, together with features in the region 15–35 mV, one observes a pronounced peak at 60 mV and two broadened peaks at 80 and 90 mV.

A comparison with the spectrum of the phonon density of states obtained by inelastic neutron scattering[21] shows that, starting at $eV\sim 20$ mV the spectrum exhibits a rise corresponding to the position of the low-frequency PC peak that we observed. It is possible that the absence of clear low-frequency features in the spectrum of the neutron density of states is due to their low intensity and the strong anisotropy of the EPI in MgB_2, which leads to an increase of the spectral function of the EPI in that energy interval.

It should be noted that the order-of-magnitude more intense peaks in the 60 and 70 meV region are absent on practically all the PC spectra at 4.2 K; this is because the MgB_2 films are oriented with the *c* axis perpendicular to the substrate.[8–10] However, in spite of the fact that the MgB_2 film has a *c* orientation, the PC spectra in the normal state typically have, in addition to the kink, a strongly smeared peak in the energy region 50–70 meV (this peak is not discussed in the present paper). This may be indicative of a possible slight deviation of the direction of the current flow from the *c* axis, since, as was shown in Ref. 10, high-frequency features are characteristic for the *ab* plane.

Because of the complexity of the compound, the small value of the mean free path, and also the significant technical difficulties in making point contacts, it is not possible at present to obtain intensity PC spectra corresponding to the model of a clean aperture for determining the important integrated EPI parameter λ. However, we hope that more-perfect samples will in the future permit one to make point contacts of better quality and to overcome the difficulty of determining λ.

CONCLUSION

We have investigated the PC spectra of MgB_2 with a low-frequency spectral feature whose energy position is independent of the counterelectrodes used. We assume that the spectral peak that we have observed on the PC spectra of MgB_2 in the normal state is due to low-frequency modes of the phonon spectrum in the direction of the *c* axis or close to it. These low-frequency models of the phonon spectrum may play a significant role in the mechanism of superconductivity of magnesium diboride.

This study was supported by the Ministry of Education and Science of Ukraine, Project No. F7/528–2001. The authors are deeply grateful to Prof. Sung-Ik Lee for providing the samples.

[a)]E-mail: fisun@ilt.kharkov.ua

[1]J. Nagamatsu, N. Nakagava, T. Muranaka, Y. Zenitani, and J. Akimitsu, Nature (London) **410**, 63 (2001).
[2]H. Schmidt, J. F. Zasadzinski, K. E. Gray, and D. G. Hinks, Physica C **385**, 221 (2003).
[3]P. Szabo, P. Samuely, J. Kacmarcik, Th. Klein, J. Marcus, D. Furchart, S. Miragila, C. Marcenat, and A. G. M. Jansen, Phys. Rev. Lett. **87**, 137005 (2001).
[4]Yu. G. Naidyuk, I. K. Yanson, L. V. Tyutrina, N. L. Bobrov, P. N. Chubov, W. N. Kang, Hyeong-Jin Kim, Eun-Mi Choi, C. U. Jung, and Sung-Ik Lee, JETP Lett. **75**, 283 (2002).
[5]H. J. Choi, D. Roundy, H. Sun, M. L. Cohen, and S. G. Louie, Phys. Rev. B **66**, 020513(R) (2002).
[6]E. Cappelutti, S. Ciuchi, C. Grimaldi, L. Pietronero, and S. Strassler, Phys. Rev. Lett. **88**, 117003 (2003).
[7]A. Shukla, M. Calandra, M. d'Astuto, M. Lazzeri, F. Mauri, C. Bellin, M. Krisch, J. Karpinski, S. M. Kazakov, J. Jun, D. Daghero, and K. Parlinski, Phys. Rev. Lett. **90**, 095506 (2003).
[8]N. L. Bobrov, P. N. Chubov, Yu. G. Naidyuk, L. V. Tyutrina, I. K. Yanson, W. N. Kang, Hyeong-Jin Kim, Eun-Mi Choi, and Sung-Ik Lee, in *Quan-*

tum Mesoscopic Phenomena and Mesoscopic Devices in Microelectronics, J. F. Annett and S. Kruchinin (eds.), Kluwer Academic (2002), p. 225.
[9]I. K. Yanson, V. V. Fisun, N. L. Bobrov, Yu. G. Naidyuk, W. N. Kang, Eun-Mi Choi, Hyun-Jung Kim, and Sung-Ik Lee, Phys. Rev. B **67**, 024517 (2003).
[10]Yu. G. Naidyuk, I. K. Yanson, O. E. Kvitnitskaya, S. Lee, and S. Tajima, Phys. Rev. Lett. **90**, 197001 (2003).
[11]I. K. Yanson, S. I. Beloborod'ko, Yu. G. Naidyuk, O. V. Dolgov, and A. A. Golubov, Phys. Rev. B **69**, 100501 (2004).
[12]I. K. Yanson, V. V. Fisun, N. L. Bobrov, and L. F. Rybal'chenko, JETP Lett. **45**, 543 russ 425 (1987).
[13]I. K. Yanson and Yu. G. Naidyuk, Fiz. Nizk. Temp. **30**, 355 (2004) [Low Temp. Phys. **30**, 261 (2004)].
[14]I. O. Kulik, A. N. Omel'yanchuk, and R. I. Shekhter, Fiz. Nizk. Temp. **3**, 1543 (1977) [Sov. J. Low Temp. Phys. **3**, 740 (1977)].
[15]R. I. Shekhter and I. O. Kulik, Fiz. Nizk. Temp. **9**, 46 (1983) [Sov. J. Low Temp. Phys. **9**, 22 (1983)].
[16]W. N. Kang, Hyeong-Jin Kim, Eun-Mi Choi, C. U. Jung, and Sung-Ik Lee, Science **292**, 1521 (2001); W. N. Kang, Eun-Mi Choi, Hyeong-Jin Kim, Hyun-Jung Kim, and Sung-Ik Lee, Physica C **385**, 24 (2003).
[17]A. V. Khotkevich and I. K. Yanson, *Atlas of Point-Contact Spectra of Electron-Phonon Interactions in Metals*, Kluver, Dordrecht 1995), Naukova Dumka, Kiev (1986).
[18]I. K. Yanson and O. I. Shklyarevskii, Fiz. Nizk. Temp. **12**, 899 (1986) [Sov. J. Low Temp. Phys. **12**, 509 (1986)].
[19]K. Kunc, I. Loa, K. Syassen, R. K. Kremer, and K. Ahn, J. Phys.: Condens. Matter **13**, 9945 (2001).
[20]P. Szabo, P. Samuely, J. Kacmarcik, Th. Klein, J. Marcus, and A. G. M. Jansen, Physica C **388**, 145 (2003).
[21]R. Osborn, E. A. Goremychkin, A. I. Kolesnikov, and D. G. Hinks, Phys. Rev. Lett. **87**, 017005 (2001).

Translated by Steve Torstveit

Coordinate transformation in the model of long Josephson junctions: geometrically equivalent Josephson junctions

E. G. Semerdzhieva[a)]

Plovdiv University, Plovdiv 4000, Bulgaria

T. L. Boyadzhiev[b)]

Joint Institute for Physical Research, Dubna 141980, Russia

Yu. M. Shukrinov[c)]

Joint Institute for Physical Research, Dubna 141980, Russia; Physical Technical Institute, Dushanbe 734063, Tajikistan

(Submitted March 17, 2005)
Fiz. Nizk. Temp. **31**, 1110–1116 (October 2005)

The transition from the model of a long Josephson junction of variable width to the model of a junction with a coordinate-dependent Josephson current amplitude is effected through a coordinate transformation. This establishes the correspondence between the classes of Josephson junctions of variable width and quasi-one-dimensional junctions with a variable thickness of the barrier layer. It is shown that for a junction of exponentially varying width the barrier layer of the equivalent quasi-one-dimensional junction has a distributed resistive inhomogeneity that acts as an attractor for magnetic flux vortices. The curve of the critical current versus magnetic field for a Josephson junction with a resistive microinhomogeneity is constructed with the aid of a numerical simulation, and a comparison is made with the critical curve of a junction of exponentially varying width. The possibility of replacing a distributed inhomogeneity in a Josephson junction by a local inhomogeneity at the end of the junction is thereby demonstrated; this can have certain advantages from a technological point of view. © *2005 American Institute of Physics*. [DOI: 10.1063/1.2128072]

I. INTRODUCTION

An interesting research topic in the physics of Josephson junctions (JJs) and one that has received intensive development in recent years is the influence of a potential due to an external field or to the geometry on the motion of vortices in long junctions. As examples one can cite the study of the potential created by a spatial variation of the radial component of the magnetic field in an annular junction[1] and of a field-induced saw-tooth potential in the same annular junction[2] and the study of the fluxon qubit in a modified annular (heart-shaped) geometry.[3] Potentials produced by spatial variation of the width of the junction, corresponding to a force acting on the fluxon in the direction of narrowing, were studied in Refs. 4–12. Unidirectional motion of fluxons has a certain advantage in the design of oscillators based on the motion of fluxons.[13–15] In particular, an exponential variation of the junction width provides better impedance matching with an output load[4] and allows one to avoid the chaotic regimes inherent to rectangular junctions. The structure and stability of static magnetic flux vortices and the corresponding critical curves in long JJs of exponentially varying width were investigated in Refs. 4, 8, 11, and 12.

In this paper it is shown that effects arising in a junction of variable width also take place for JJs whose barrier layer contains a resistive inhomogeneity. The critical curves—critical current versus magnetic field—are constructed numerically for long JJs of exponentially varying width and rectangular junctions with a localized resistive inhomogeneity. From a technological standpoint JJs with a resistive inhomogeneity can be preferable in some cases.

II. COORDINATE TRANSFORMATION

We consider a long JJ whose dimension along the y axis (width) is a smooth function $W(x)$ on the interval $x \in [0,L]$. Here L is the length of the junction (all of the quantities used are rendered dimensionless in the standard way[16]). We assume that

$$\max_{x\in[0,L]} W(x) \ll L.$$

We introduce the shape function $\sigma(x)$ of the junction with the aid of the relation

$$\sigma(x) = -\frac{W_x(x)}{W(x)}. \tag{1}$$

Here and below a subscript is used to denote differentiation with respect to the corresponding independent variable. The case $W_x(x) \equiv 0$ corresponds to a rectangular junction. Then the boundary-value problem for the static magnetic flux $\varphi(x)$ in such a JJ is written in the form

$$-\varphi_{xx} + \sigma(x)\varphi_x + \sin\varphi + g(x) = 0, \tag{2a}$$

$$\varphi_x(0) = h_0, \quad \varphi_x(L) = h_L. \tag{2b}$$

The concrete expressions for $q(x)$, h_0, and h_L depend, in particular, on the means of injection of the external current γ. For junctions with an overlapping geometry, as are consid-

ered below, the base current $\gamma(x)$ flows through the whole junction. Consequently, $g(x)=\gamma(x)-\sigma h_B$, $h_0=h_B$, $h_L=h_B$ (h_B is the external magnetic field, which is directed along the y axis in the plane of the barrier layer). The term $-\sigma h_B$ is due to the variable width of the junction. Neglecting surface effects, one can to a first approximation set $\gamma(x)=$const. A derivation of Eq. (2a) in the general case is given in Ref. 5.

Let us consider an ordinary change of spatial coordinate:

$$\xi = v(x), \tag{3}$$

where the variable $\xi \in [0,l]$, and the right-hand side is a solution of the boundary-value problem

$$-v_{xx} + \sigma(x)v_x = 0, \tag{4a}$$

$$v(0) = 0, \quad \min_{x\in[0,L]} v_x(x) = 1. \tag{4b}$$

The parameters L and l are connected by the relation $l=v(L)$. The first boundary condition in (4b) matches up the initial points of the intervals of variation of the variables x and ξ, while the second serves for normalization (see below).

In the new independent variable the boundary condition (2) takes the form

$$-\varphi_{\xi\xi} + j_D(\xi)\sin\varphi + j(\xi) = 0, \tag{5a}$$

$$\varphi_\xi(0) = H_0, \quad \varphi_\xi(l) = H_L. \tag{5b}$$

Here $u(\xi)$ is the inverse function of $v(x)$. Here $j_D(\xi) \equiv u_\xi^2(\xi)$ and $j(\xi)\equiv u_\xi^2(\xi)g(u(\xi))$, and also

$$H_0 \equiv u_\xi(0)h_0, \quad H_L \equiv u_\xi(l)h_L.$$

From a formal standpoint Eq. (5a) describes the magnetic flux distribution in a one-dimensional JJ with a variable amplitude of the Josephson current, $j_D(\xi)$. Such a junction is inhomogeneous[17]—the thickness of its barrier layer varies along the length as $d(\xi)\sim u_\xi^{-2}(\xi)$. The term $j(\xi)$ is a current that varies along the junction, generated by variation of the geometry, external magnetic field, and external current.

Thus the transformation (3) and (4) establishes a relation between a JJ of variable width and a "one-dimensional" junction having a thickness of the insulating layer that varies along the junction. For brevity we shall speak of x junctions and ξ junctions.

For junctions of exponentially diminishing width (referred to below as EJJs), which were considered in Refs. [8–11], we have $\sigma=$const$\geqslant 0$. Then $W(x)=W_0\exp(-\sigma x)$, where W_0 is the width of the JJ at the $x=0$ end. In this case the transformation (3) takes the form

$$\xi = \frac{1}{\sigma}(e^{\sigma x} - 1).$$

Then for the right-hand boundary of the ξ junction we find $l=(e^{\sigma L}-1)/\sigma > L$, i.e., the ξ junction is longer than the corresponding x junction.

In the particular case considered, a change of the normalized amplitude of the Josephson current of the ξ junction

$$j_D(\xi) \equiv u_\xi^2(\xi) \equiv \frac{1}{(1+\sigma\xi)^2} \tag{6}$$

can occur as a result of a barrier-layer thickness that varies smoothly along the junction. Here the amplitude is maximum (and the barrier-layer thickness minimum) at the left end of the junction [see the second condition in Eq. (4b)] and minimum (maximum, respectively) at the right end. Thus a resistive inhomogeneity is an attractor[17] for magnetic flux distributions in the junction, drawing the latter toward the right end, as has been observed experimentally[4] and confirmed by numerical simulation.[4,11,12]

III. MODELS OF A JUNCTION WITH A RESISTIVE INHOMOGENEITY

It is of interest to investigate the possibility of replacing an inhomogeneity distributed over the whole length of the junction by an inhomogeneity localized near the right end. The simplest choice is a point inhomogeneity of "strength" $\mu\geqslant 0$ at the right end of the junction. In that case[17]

$$j_D(x) = 1 - \mu\delta(x-L).$$

Here $\delta(x)$ is the Dirac delta function. A JJ with such an inhomogeneity will be denoted below as δJJ. For $\mu=0$ the junction is homogeneous. The corresponding boundary-value problem in the case of overlapping geometry is described in the form [$x\in(0,L)$]

$$-\varphi_{xx} + \sin\varphi + \gamma = 0, \tag{7a}$$

$$\varphi_x(0) = h_B, \quad \varphi_x(L) + \mu\sin\varphi(L) = h_B. \tag{7b}$$

We note that independently of the junction geometry the presence of a point inhomogeneity at the right end leads to nonlinear boundary conditions.

Another example of an inhomogeneity that will be considered below is the model of a junction (IJJ) in the form of a narrow rectangular well of width $\Delta \ll L$ and depth $1-\kappa$:

$$j_D(x) = 1 - (1-\kappa)\theta(x+\Delta-L).$$

Here $\theta(x)$ is the Heaviside step function. The parameter $\kappa \geqslant 0$ specifies the fraction of the Josephson current through the inhomogeneity. We note that the inhomogeneity of the barrier layer represents a microresistor only for $\kappa<1$. In particular, if $\kappa=0$ the Josephson current is absent on the segment $[L-\Delta,L]$. The choice $\kappa=1$ means that the thickness of the barrier layer of the junction is constant, and the amplitude $j_D(x)=1$ for $\xi\in(0,L]$. For $\kappa>1$ the inhomogeneity is a microshort that repels magnetic flux vortices.[17]

The corresponding boundary-value problem for the magnetic flux $\varphi(x)$ in the case of overlapping geometry is written in the form

$$-\varphi_{xx} + j_D(x)\sin\varphi + \gamma = 0, \tag{8a}$$

$$\varphi_x(0) = h_B, \quad \varphi_x(L) = h_B. \tag{8b}$$

In a numerical simulation of the magnetic-field dependence of the critical current, transitions from the superconducting to the resistive regime are interpreted mathematically as bifurcations of the magnetic flux in the junction upon variation of the parameters.[17] For studying the stability, each

solution $\varphi(x)$ of the boundary-value problems (7) and (8) is associated to a regular Sturm–Liouville (S-L) problem with a potential that depends on the concrete solution (see the details in Refs. 17–19). The S-L eigenvalue problems allow one to assess the stability or instability of $\varphi(x)$. The boundary conditions are determined by the choice of model. In particular, for model (7) with a point inhomogeneity the S-L problem takes the form

$$-\psi_{xx}+q(x)\psi=\lambda\psi, \tag{9a}$$

$$\psi_x(0)=0, \quad \psi_x(L)+\mu\cos\varphi(L)\psi(L)=0, \tag{9b}$$

where the potential is determined by the expression $q(x)=\cos\varphi(x)$.

For model (8) with a rectangular inhomogeneity the S-L problem is

$$-\psi_{xx}+q(x)\psi=\lambda\psi, \tag{10a}$$

$$\psi_x(0)=0, \quad \psi_x(L)=0. \tag{10b}$$

In the case under study the potential $q(x)=j_D(x)\cos\varphi(x)$.

The wave function $\psi(x)$ must satisfy the normalization condition

$$\int_0^L \psi^2(x)dx-1=0. \tag{11}$$

We note that problems (9) and (10) have a discrete nondegenerate spectrum bounded from below. In addition, since the solutions of the boundary-value problems (7) and (9) depend smoothly on the parameters h_B and γ, the eigenvalues and eigenfunctions of equations (9) and (10) also depend on these parameters. Let $\lambda_{\min}(h_B,\gamma)$ be the minimum eigenvalue corresponding to a certain distribution $\varphi(x)$. The point with coordinates h_B and γ on the (h_B,γ) plane is called[17] a bifurcation point of $\varphi(x)$ if the following condition holds:

$$\lambda_{\min}(h_B,\gamma)=0. \tag{12}$$

The bifurcation curve of any magnetic flux distribution in a junction is the geometric locus of bifurcation points of a concrete vortex, corresponding to pairs (h_B,γ) for which Eq. (12) holds.

In view of the fact that for specified h_B and γ the boundary-value problems (7) and (9), as a rule, have more than one solution, the critical curve of the junction as a whole is constructed as the envelope of bifurcation curves for different solutions. In other words, the critical curve of the junction consists of pieces of the bifurcation curves corresponding to different distributions with the highest critical current γ for the given field h_B.

For calculation of relation (12) we used the method proposed in Ref. 18: the system of equations (7) and (10) [respectively Eq. (8) and (10)] at fixed λ and field h_B (and current γ) is solved as a nonlinear eigenvalue problem with the spectral parameter γ (respectively, h_B). This method of seeking bifurcation points and its generalization was used in Ref. 19 for solving a wide class of physical problems.

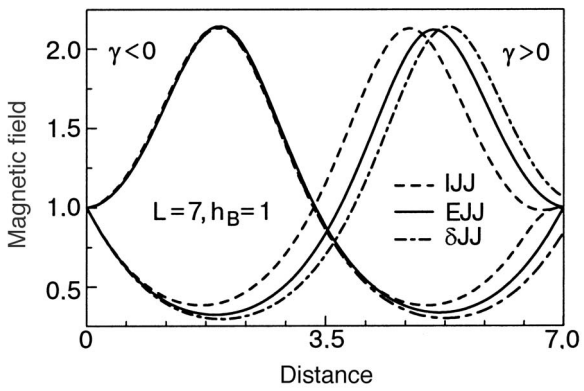

FIG. 1. The magnetic field of the fluxon Φ^1 for three models of the inhomogeneity.

IV. NUMERICAL RESULTS

Let us compare the results of numerical simulations for constructing the critical curves for the model of a JJ in an overlapping geometry with an exponentially varying width and a model with an inhomogeneity on the right end.

Figure 1 shows the "bifurcation" distributions of the magnetic field $\varphi_x(x)$ for the main fluxon Φ^1 along the jucntion for three JJ models (EJJ, IJJ, and δJJ) for $\lambda_{\min}=10^{-4}$, i.e., before the destruction of the fluxon by the current γ. The corresponding distributions of the Josephson current $j_D(x)\sin\varphi$ in the JJ are presented in Fig. 2.

We note the good qualitative agreement of the curves. Their quantitative difference is observed predominantly in the region where the amplitude of the Josephson current is minimum; this is due to the form of the inhomogeneity (attractor).

Figure 3 demonstrates the critical curves of the form (12) corresponding to stable solutions of the boundary-value problems (2) and (8). The solid curves correspond to distributions of the magnetic flux for the model of a JJ with a width that varies by an exponential law (EJJ) with a coefficient $\sigma=0.07$, the dashed curves are for models of an inhomogeneous JJ with a finite rectangular inhomogeneity (IJJ) with parameters $\Delta=0.7$, $\kappa=0.1$. Each critical curve reflects a certain closed figure on the (h_B,γ) plane, the currents $h_B=h_{\min}$ and $h_B=h_{\max}$ are the lower and upper critical magnetic fields for the vortex under study. We note that because of the

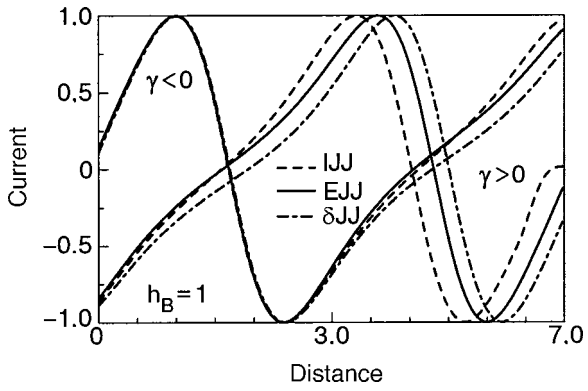

FIG. 2. Distribution of the Josephson current for three models of the inhomogeneity.

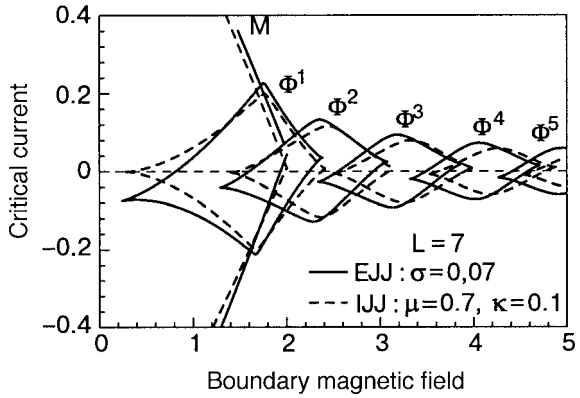

FIG. 3. Bifurcation curves for a JJ of variable width and a JJ with a rectangular inhomogeneity.

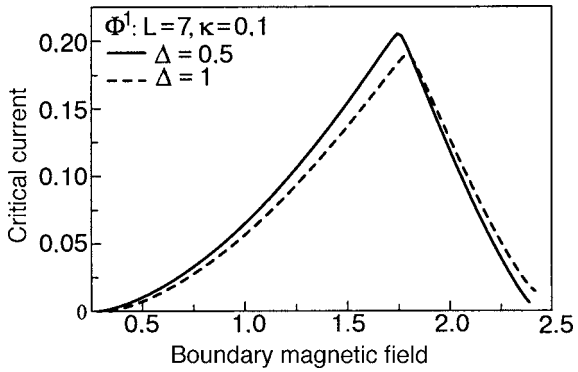

FIG. 5. Influence of the parameter Δ on the bifurcation curve of Φ^1.

presence of an additional "geometric" current $\sigma(\varphi_x(x)-h_B)$ in the EJJ model the critical value of the current γ corresponding to the two indicated values of h_B is nonzero.

A numerical simulation shows that, unlike a JJ with a resistive inhomogeneity within the segment $(0,L)$ (Refs. 18 and 19), in a junction with an inhomogeneity at the end, even for rather large values of h_B (the solutions were checked numerically to $h_B=10$) there are no stable mixed fluxon-antifluxon vortices contributing to the critical curve. Therefore the critical curves of the junction as a whole consist only of segments of the critical curves for a Meissner (M) distribution and "pure" n-fluxon vortices Φ^n, $n=1,2,\ldots$. The maxima of the critical curves fall off monotonically with increasing field h_B (in junctions with an internal inhomogeneity the maxima of the critical curves fall off nonmonotonically because of the stabilizing influence[19] of the inhomogeneity on the mixed fluxon-antifluxon vortex pairs).

Let us illustrate the process of vortex destruction (the transition to an unstable state) upon variation of the current γ for the case of the IJJ model. In a field $h_B=1$ at a current $\gamma\geqslant 0$, two stable distributions of magnetic flux can exist in the model: M and Φ^1. As the current increases, the main fluxon Φ^1 is destroyed first (the critical current for it is $\gamma_{cr}(\Phi^1)\approx 0.062$), and then the Meissner distribution. Thus for $h_B=1$ the critical current of the junction $\gamma_{cr}=\gamma_{cr}(\mathrm{M})\approx 0.597$. For $h_B=1.9$ the boundary-value problem (8) has three stable solutions—M, Φ^1, and Φ^2, which occur in the following succession with increasing γ: $\Phi^2\rightarrow \mathrm{M}\rightarrow\Phi^1$. The critical current of the junction in this case is $\gamma_{cr}=\gamma_{cr}(\Phi^1)\approx 0.157$. Analogously, for $h_B=2.2$ we have $\gamma_{cr}=\gamma_{cr}(\Phi^2)\approx 0.092$.

The critical curves of the current versus magnetic field for the three JJ models discussed above are exhibited in Fig. 4. The dot-and-dash line corresponds to the model of a JJ with a point inhomogeneity ($\mu=0.2$) on the right end (δJJ). Note the good qualitative agreement of the critical curves for the three models. For values of h_B that are not too high, the leftward displacement of the critical curves of the individual vortices by the "geometric" current in the EJJ model has only a weak influence on the behavior of the critical curve of the junction as a whole.

We note that variation of the parameters of a rectangular inhomogeneity (of width Δ and depth κ) has a weak influence on the numerical results, i.e., the boundary-value problem (8) is structurally stable upon variation of those two parameters. This assertion is illustrated in Fig. 5, which shows the dependence (12) for the main fluxon Φ^1 at $\gamma_{cr}\geqslant 0$, $\kappa=0.1$ and values of $\Delta=0.5$ and $\Delta=1$. Analogously, Fig. 6 shows the dependence (12) for the main fluxon Φ^1 for $\gamma_{cr}\geqslant 0$, $\Delta=0.7$ and parameter values $\kappa=0.1$ and $\kappa=0.8$.

V. CONCLUSION

In this paper we have shown that every JJ of variable width can be placed in correspondence with a quasi-one-dimensional junction with a variable thickness of the barrier layer. In the case of junctions whose width varies by an exponential law, the barrier layer of the corresponding quasi-

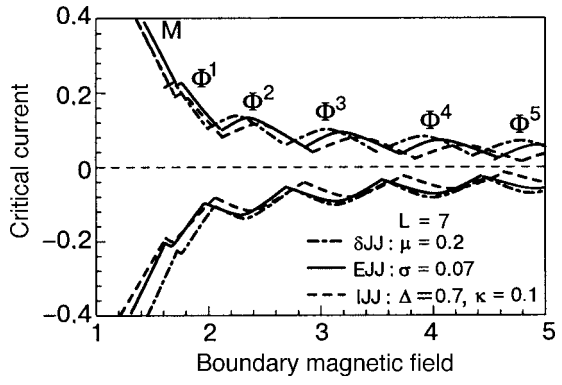

FIG. 4. Critical curves of the current versus magnetic field for three model inhomogeneities.

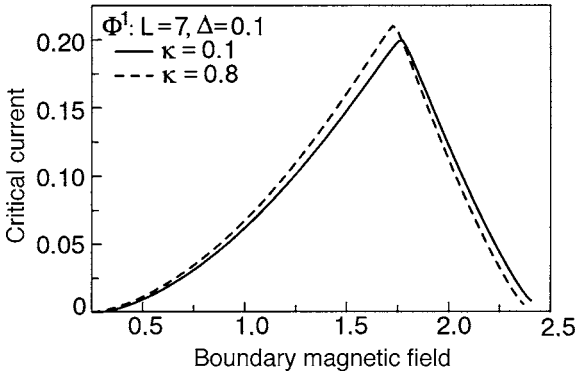

FIG. 6. Influence of the parameter κ on the bifurcation curve of Φ^1.

one-dimensional JJ contains a resistive inhomogeneity distributed along the junction and acting as an attractor for magnetic flux vortices.

The curves of the critical current versus magnetic field obtained from the numerical simulation demonstrate that such an inhomogeneity can be replaced by a local inhomogeneity at the end of the JJ, which may have certain advantages from a technological point of view.

The authors thank Prof. Yu. Kolesnichenko (B. Verkin Institute for Low Temperature Physics and Engineering, Kharkov) for helpful discussions.

[a)]E-mail: elis@jinr.ru
[b)]E-mail: todorlb@jinr.ru
[c)]E-mail: shukrinv@thsun1.jinr.ru

[1]N. Gronbech-Jensen, P. S. Lomdahl, and M. R. Samuelsen, Phys. Rev. B **43**, 12799 (1991).
[2]G. Carapella, Phys. Rev. B **63**, 054515 (2001); G. Carapella and G. Costabile, Phys. Rev. Lett. **87**, 077002 (2001).
[3]A. Wallraff, Y. Koval, M. Levitchev, M. V. Fistul, and A. V. Ustinov, J. Low Temp. Phys. **118**, 543 (2000).
[4]G. Carapella, N. Martucciello, and G. Costabile, Phys. Rev. B **66**, 134531 (2002).
[5]E. Goldobin, A. Sterck, and D. Koelle, e-print: cond-mat/0008237.
[6]S. Sakai, M. R. Samuelsen, and O. H. Olsen, Phys. Rev. B **36**, 217 (1987).
[7]S. Pagano *et al.*, in *Nonlinear Superconducting Devices and High Tc Materials*, R. D. Parmentier and N. F. Pedersen (eds.), World Scientific, Singapore (1995).
[8]A. Benabdallah, J. G. Caputo, and A. C. Scott, Phys. Rev. B **54**, 16139 (1996).
[9]A. Benabdallah, J. G. Caputo, and A. C. Scott, J. Appl. Phys. **88**, 3527 (2000).
[10]E. Goldobin, A. Sterck, and D. Koelle, Phys. Rev. E **63**, 031111 (2001).
[11]E. G. Semerdjieva, T. L. Boyadjiev, and Yu. M. Shukrinov, Fiz. Nizk. Temp. **30**, 610 (2004) [Low Temp. Phys. **30**, 456 (2004)].
[12]Yu. M. Shukrinov, E. G. Semerdjieva, and T. L. Boyadjiev, e-print: cond-mat/0410048 (Accepted for J. Low Temp. Phys.).
[13]V. P. Koshelets *et al.*, Physica C **372–376**, 316 (2001).
[14]T. Nagatsuma *et al.*, J. Appl. Phys. **58**, 4412 (1985).
[15]V. P. Koshelets *et al.*, Phys. Rev. B **56**, 5572 (1997).
[16]K. K. Licharev, *Dynamics of Josephson Junctions and Circuits*, (Gordon and Breach, New York 1986).
[17]Yu. S. Gal'pern and A. T. Filippov, Zh. Éksp. Teor. Fiz. **86**, 1527 (1984) [Sov. Phys. JETP **59**, 894 (1984)], Sov. Phys. JETP **59**, 894 (1984).
[18]T. L. Boyadzhiev, D. V. Pavlov, I. V. Puzynin, Soobshchenie OIYaI R11-88-409, JINR, Dubna (1988); T. L. Boyadzhiev, D. V. Pavlov, and I. V. Puzynin, in *Numerical Methods and Applications, in Proceedings of the International Conference on Numumerical Mathematics and Applications, Sofia (1988)*.
[19]T. L. Boyadzhiev, Doctoral Dissertation [in Russian], OIYaI, Dubna (2002).

Translated by Steve Torstveit

LOW-TEMPERATURE MAGNETISM

Magnetotransport properties of Er/Sc artificial multilayer structures

Yu. N. Chiang,[a] O. G. Shevchenko, and R. N. Kolenov

B. Verkin Institute for Low Temperature Physics and Engineering, National Academy of Sciences of Ukraine, pr. Lenina 47, Kharkov 61103, Ukraine

(Submitted January 17, 2005; revised manuscript received April 13, 2005)
Fiz. Nizk. Temp. **31**, 1117–1124 (October 2005)

Comparative studies of the transport properties—resistance, magnetoresistance, and Hall effect—of Er/Sc multilayer structures and erbium films prepared by the same deposition technology are carried out for the first time. Those properties of the structures are modified substantially in comparison with those of elemental erbium. The magnetoresistance of the samples is "giant," although it cannot compete in absolute magnitude with the values for superlattices based on *d* ferromagnetic materials. In the region of helium temperatures the Hall coefficient in the multilayer systems is more than an order of magnitude greater than at room temperature. It follows from the data for the Hall coefficient and magnetoresistance in that temperature region that the zero-field magnetization of the *f* structure is greater than the magnetization of the bulk *f* material in the ferromagnetic state. The conductance of the Er/Sc multilayer structure at $T>20$ K is lower than at helium temperatures. The features mentioned are described in terms of a temperature-induced rearrangement of the magnetic ordering of the erbium layers in the Er/Sc structures. © *2005 American Institute of Physics*. [DOI: 10.1063/1.2128073]

Despite many years of effort there is still no complete understanding of how the concept of an exchange interaction due to correlation of the electron spins is compatible with the behavior of the kinetic characteristics of metals, which basically conforms to a description in terms of the simple approximations of band theory. However, progress in the technology of epitaxial film growth,[1] primarily films of transition *d* metals and rare-earth magnetic materials, have permitted a close approach to the experimental study of this problem, in particular, to the investigation of the role of exchange interaction mechanisms in establishing some magnetic structure or other and the manifestation of such an interaction, if it occurs, in the character of the electronic conductivity. Studies of multilayer systems with magnetic layers alternating with spacer layers of various nonmagnetic materials, metallic or nonmetallic,[2,3] grown by the aforementioned technology have revealed the novel possibility of artificially varying the magnetic characteristics of systems and observing the unusual, often contradictory, relationship of these characteristics to the behavior of the electron transport. For example, in multilayer systems of the FM/NM/FM type, where the ferromagnetic (FM) material is a transition *d* metal, a "giant" negative magnetoresistance is observed (up to 150% in Fe/Cr structures),[4–6] which is explained as a manifestation of an oscillatory exchange coupling through the nonmagnetic (NM) spacers. At the same time, a magnetoresistance (MR) of the same sign and of comparable magnitude ($\approx 20\%$) has been observed in a nonlayered magnetically inhomogeneous material,[7] and in multilayers in which the magnetic phases are rare-earth *f* metals (for which, unlike *d* metals, the magnetism and transport can be reasonably attributed to different groups of charge carriers) a positive MR$\approx 30\%$ has been observed.[8] In studying the features of the transport properties of magnetic systems it is customary to rely on the well-tried concept of spin-dependent scattering of conduction electrons in the theory of the Ruderman–Kittel–Kasuya–Yosida (RKKY) indirect exchange interaction,[9–11] the experimental justification of which continues to be extremely topical, especially for rare-earth ferromagnets.

The fact that there are no reasons for the appearance of direct magnetic coupling between atoms in rare-earth metals makes them interesting objects for studying the nature of the magnetic ordering as such and, in particular, as constituents of multilayer superlattices. At the same time, there have been very few studies of superlattices based on rare earths, and those have been mainly devoted to their magnetic properties without reference to their transport characteristics (exceptions are Refs. 8 and 12, for systems with Dy, Gd, and Nd).

In this paper we present the results of the first investigation of the magnetotransport properties of Er/Sc multilayer structures in combination with the results for Er prepared by the same deposition technology as the multilayers by the method of magnetron sputtering in an Ar atmosphere.

Figure 1 shows a diagram of the arrangement and nominal thicknesses of the deposited layers in the structures studied. The number of Er/Sc bilayers in each structure is also indicated. Mica was used as the substrates for the multistructures, while the polycrystalline Er sample, 920 Å thick, was deposited on sitall (pyroceramic). In sample No. 2 the bilayers in the growth direction *c* consisted of one Sc monolayer and three Er monolayers. Sample No. 3 contained two blocks—an upper block of 19 bilayers (two monolayers of Sc and five monolayers of Er) and a lower block of 20 bilayers (two monolayers of Sc and three monolayers of Er). The total volume of Er in the systems studied was not less than twice that of Sc, so that it was possible to compare the

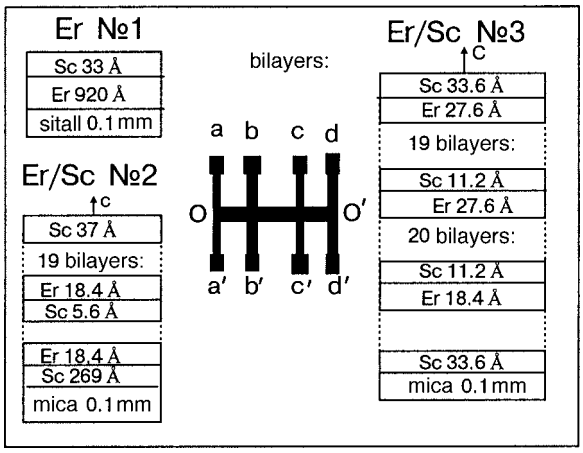

FIG. 1. Arrangement and thickness of the layers in the structures investigated.

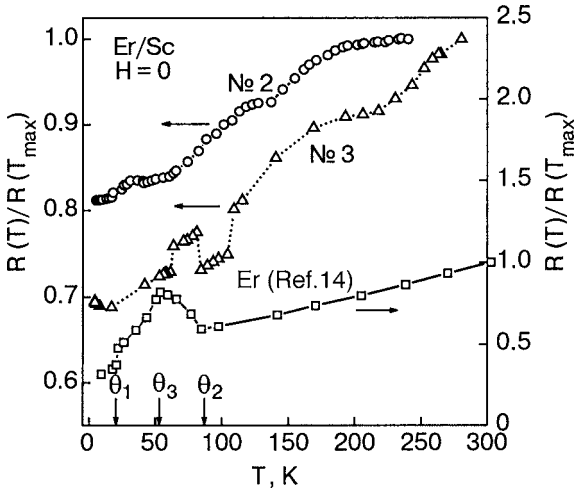

FIG. 2. Temperature dependence of the resistance of the O–O' region of samples Nos. 2 and 3, relative to the resistance at $T=240$ K (No. 2) and 280 K (No. 3). The arrows indicate the characteristic temperatures of the magnetic phase transitions in elemental Er: $\theta_1 \approx 20$ K; $\theta_2 \approx 84$ K; $\theta_3 \approx 54$ K.

transport properties of bulk erbium (sample No. 1) and the systems with discrete layers of nonmagnetic scandium intercalated in the matrix of magnetic erbium (samples Nos. 2 and 3).

The samples were deposited in the branched configuration shown in Fig. 1 for measurements of the resistance and Hall emf in the region O–O' by the standard 4-probe technique. A dc measuring current I from 10^{-2} to 1 mA was passed in the film plane along O–O'. Electrical connection to the samples was achieved by clamping plates of platinum foil to contact areas a-d, a'-d'.

It is known that the lattice constants of Er and Sc differ by 6% along the c axis and by 8% along the a axis, which obviously precludes obtaining superlattices with a single-crystal character over the whole volume of the sample, although in the samples studied the layers of magnetic Er and nonmagnetic Sc form a quasiperiodic structure. The values of the room-temperature resistivity ρ_{Er} and ρ_{Sc} obtained for a parallel connection scheme turned out, in the case of sample No. 2, to be comparable to the known values for polycrystalline materials[13] ($\simeq 100\ \mu\Omega\cdot$cm and $\simeq 60\ \mu\Omega\cdot$cm, respectively), while for sample No. 3 they were several times smaller ($\leqslant 20\ \mu\Omega\cdot$cm and $\simeq 10\ \mu\Omega\cdot$cm, respectively), as for very pure materials.[14] The resistivity ρ_{Er} estimated from the measurements for sample No. 1 was close to the value indicated above for the high-resistivity sample No. 2. Since the growth of these artificial superlattices can be regarded as the insertion of a foreign material (Sc) into an initially homogeneous material (Er), and the creation of such a defect structure generally speaking cannot in itself *improve* the conductivity of the system, the difference in the conductance of two samples obtained by the same technology already points to causes other than simple scattering on defects for the change in character of the transport in the structures studied, even in zero magnetic field.

Figure 2 shows the temperature behavior of the resistance relative to its value at room temperature for samples Nos. 2 and 3. The character of the anomalies of this behavior in the structures studied and the temperature regions where they are manifested correlate with the known features of the temperature dependence of the resistance of elemental erbium. It has been established that such features are due to a rearrangement of the magnetic structure of erbium, i.e., to transitions from the paramagnetic state to an antiferromagnetic state (temperature θ_2) and further to a ferromagnetic state (at θ_1) as the temperature is lowered.[14–18] The temperature θ_3 corresponds to a rearrangement of the structure in the antiferromagnetic region from a sinusoidal to a cycloidal phase.[16,17]

The connection between the changes in character of the transport and the changes of the magnetic structure should be manifested most clearly when an external magnetic field, even a very weak one, is applied, since the magnetic energy required for the formation of a nonzero magnetization is low, and in certain materials there is even a partial spontaneous magnetization in the absence of external field. Figures 3–8 show the results of measurements of the MR and Hall effect in our samples at fields up to 7 kOe.

Figure 3 shows a three-dimensional projection of the temperature dependence of the transverse MR of erbium (sample No. 1), i.e., the relative change of the resistance

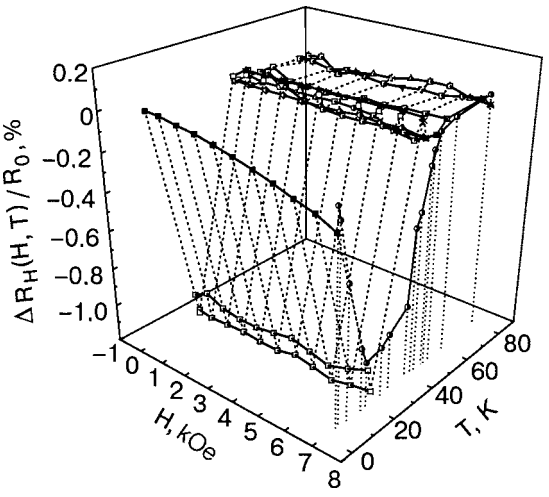

FIG. 3. Temperature-field curves of the magnetoresistance of the erbium film.

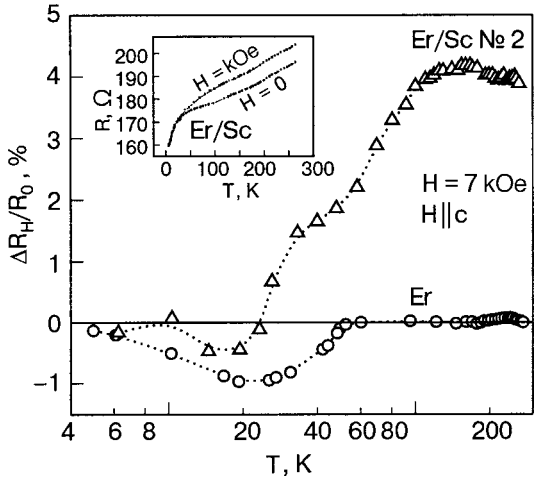

FIG. 4. Temperature dependence of the magnetoresistance of erbium and of an Er/Sc multilayer system. The inset shows the resistance of the system as a function of temperature in the absence of magnetic field and in a field of 7 kOe.

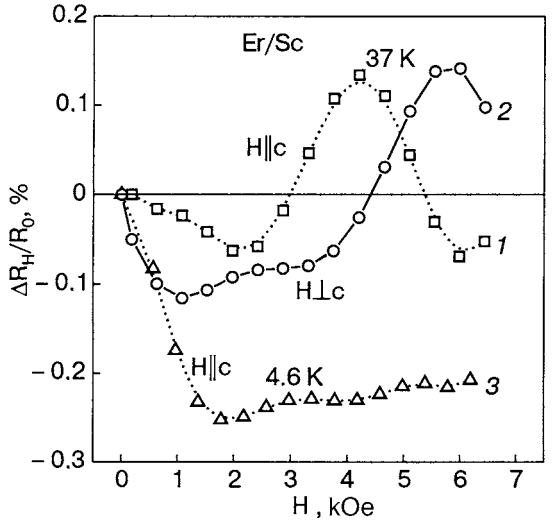

FIG. 6. Transverse (curves *1,3*) and longitudinal (curve *2*) MR of the Er/Sc system versus magnetic field at temperatures above and below θ_1.

$\Delta R_H(H,T)/R_0(T)=(R_H(T)-R_0(T))/R_0(T)$, for external magnetic fields varying from 500 Oe to 7 kOe and temperatures from 4.6 to 80 K in comparison to the resistance at zero field (in the geometry $\mathbf{H}\|\mathbf{c}$). It is seen immediately that the change of the MR first, is intimately related to the characteristic temperatures of magnetic ordering in erbium (indicated in Fig. 2), and, second, in the region below θ_3 it is negative, corresponding to an increase of the conductance. In the temperature region 10–50 K the MR undergoes a strong change at fields of only about 1 kOe $[(\Delta R/R(T=23.5\text{ K}) \approx -1\%]$, after which it varies weakly with magnetic field. We note that this accords with the small value given in Ref. 19 for the magnetization saturation field corresponding the to ferromagnetic ordering of erbium.

Figure 4 shows the temperature dependence of the MR of erbium over a wider temperature interval—from helium to room temperatures—for a field value of 7 kOe; the character of this curve is typical for other fields in the interval 0.4–7 kOe. From a comparison of this curve with the temperature behavior of the MR of a multilayer sample, also shown in the figure, it follows that the character of this behavior in the Er/Sc structures is substantially different: the MR is positive and decreases with decreasing temperature from a value of +4% at 300 K down to 0 at ≈23.5 K, where it changes sign. The values of the parameter $\omega\tau$, which determines the efficiency of the magnetic field, did not exceed 10^{-4}–10^{-3} in the whole range of temperatures and fields both in the case of erbium and for multilayer structures. Such values correspond to the low-field regime, in which the variation of the usual MR ($\Delta\rho_{xx}/\rho_0$) cannot exceed a fraction of a percent. Thus we can consider the value of the positive MR of the Er/Sc structure observed in the interval 50–250 K to be "giant." Attempts to explain the appearance of a positive MR, e.g., by the possibility that the degree of specularity of the reflection at the interfaces is decreased by a transverse magnetic field, as was proposed in Ref. 8, are unfounded, especially in our case, when the MR does not increase with decreasing temperature, as in the Dy/Sc superlattice,[8] but rather decreases. We shall show that there are no other reasons for such unusual behavior of the MR

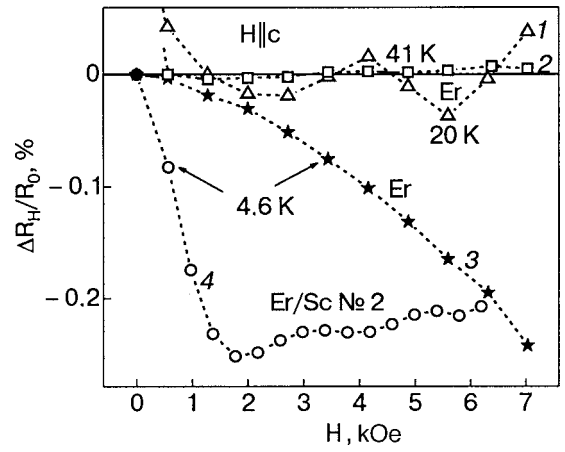

FIG. 5. Transverse magnetoresistance of erbium and of an Er/Sc system versus the magnetic field: *1,2,3*—MR of erbium at 20, 41, and 4.6 K, respectively; *4*—MR of the Er/Sc system at 4.6 K. Curves *1* and *2* are displaced along the vertical by +1%.

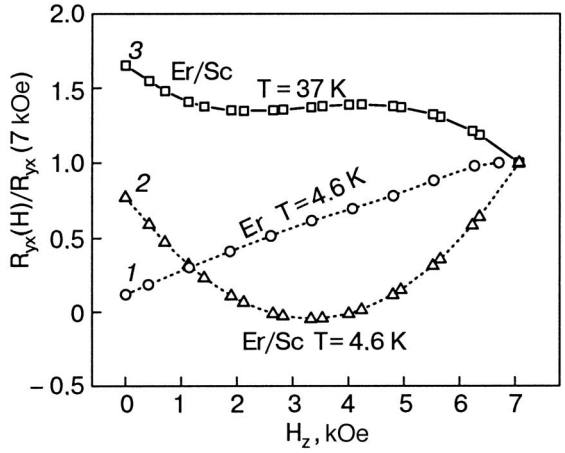

FIG. 7. Hall resistance of erbium (*1*) and of the Er/Sc multilayer structure (*2,3*) as a function of magnetic field in comparison with its value for H =7 kOe.

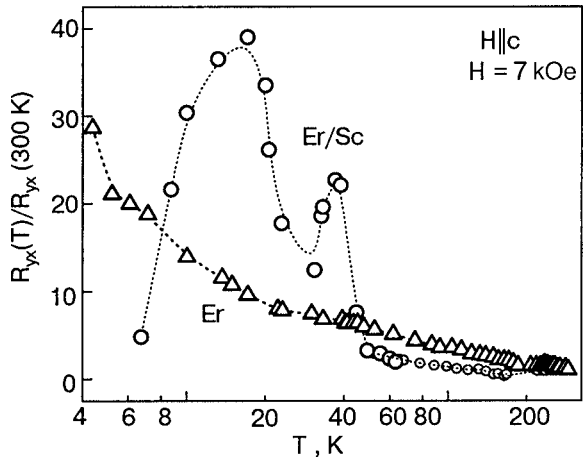

FIG. 8. Temperature dependence of the Hall resistance of the Er film and of an Er/Sc structure.

except for changes of the magnetic structure of the Er/Sc multilayer system in comparison with the magnetic structure of bulk erbium.

Despite the fact that the influence of magnetic field on the behavior of the transport properties of the systems under study is substantially weaker than the influence of temperature, which brings about a rearrangement of the magnetic structure, such a rearrangement should be reflected most fully in the character of the field dependences, and that is what our experiment shows.

Figure 5 shows the dependence of the MR on the magnetic field H for Er at 41, 20, and 4.6 K and for the Er/Sc structure at 4.6 K, and Fig. 6 shows the dependence on H of the transverse MR of the structure at temperatures of 37 and 4.6 K and of the longitudinal MR of the structure at $T=37$ K (curves *1*, *2* in Fig. 6). Furthermore, at helium temperatures 4.2–4.6 K the dependence of the MR of the system on H has a inflection point at around 1.5 kOe (curve *4* in Fig. 5), which is absent on the curve for erbium (curve *3*). This last curve also shows no tendency toward saturation, as does the dependence of the Hall coefficient of Er in the whole field interval investigated at these same temperatures (Fig. 7, curve *1*). In other words, the inflection point on the field curve MR(H) for the multilayer structure arises at a lower field than the field of complete saturation of the magnetic moment in the erbium layers.[19] A similar situation was encountered, in particular, in a study of the Co/Au system, where anomalies in the behavior of the MR were also observed at fields much less than the saturation field.[20]

It is natural to suppose that this disagreement may be due to the spin-dependent nature of the scattering of conduction electrons by magnetically ordered layers. In that case the contribution to the resistance from scattering by a pair of magnetic layers separated by a nonmagnetic spacer becomes dependent on the mutual orientation (parallel or antiparallel) of the magnetization vectors at the boundaries of the spacer.[4,21,22] In particular, under otherwise equal conditions for all the interfaces and under the usual assumption that the orientation of the spin of a conduction electron antiparallel to the moment of the magnetic layer [the so-called "minority" (↓) orientation] corresponds to more efficient electron scattering than the parallel ["majority" (↑)] orientation, the value of the conductivity and the corresponding sign of the MR in the multilayer structure will depend on the ratio of the number of pairs of boundaries (the number of nonmagnetic layers) with the same or with a different mutual orientation of the moments of the adjacent magnetic layers.

Most likely this ratio cannot in principle be equal to unity, either by virtue of the smallness of the phase coherence length of the moments with respect to the thickness of the structure, as is apparently the case for our high-resistivity samples, or because of the presence of more than one period of the oscillatory exchange coupling,[23] if such a case is realized at all in systems with rare-earth magnetic metals.

We shall therefore assume that the negative sign of the MR of the Er/Sc structure and the inflection point on its H dependence in the region of helium temperatures reflect a change of the orientation of the moments of a number of magnetic layers of erbium at a rather low field in the direction toward establishment of a ferromagnetic orientation, which in the case of a spin-dependent character of the scattering of conduction electrons can lead to an increase of the conductance of the multilayer structure as a whole. Here the behavior of the Hall resistance with change in magnetic field and the presence of a minimum on the $R_{yx}(H)$ curve (Fig. 7) attests to the existence of a remanent magnetization M_0 of the system in zero field and, accordingly, of a magnetization component M_{0z} perpendicular to the film ($\|c$), which varies with temperature because of the temperature-dependent rearrangement of the magnetic structure, including in the region of helium temperatures. The data in Fig. 7 can be used to estimate the ratio of the remanent magnetizations of the multilayer system Er/Sc in the "quasiferromagnetic" and "quasiantiferromagnetic" temperature regimes from the values of the measured Hall voltage at $H=0$.

The measured Hall resistance for a magnetic system is customarily written in the form

$$R_H = R_{yx} = \frac{U_{yx}}{I_x} = \frac{1}{d}[R_0 H_z + R_s 4\pi M_z],$$

$$R_0 = \omega\tau\frac{\rho}{H_z}, \quad R_s = C_1\rho + C_2\rho^2, \tag{1}$$

where d is the thickness of the sample, R_0 and R_s are the normal and anomalous Hall constants, respectively, M_z is the transverse component of the magnetization, ρ is the resistivity, and C_1 and C_2 are constants. At low fields M_z depends linearly on the field, and one can therefore write $M_z=\chi_z H_z + C_3\chi_{0z}$ (χ_0 is the susceptibility in the absence of magnetic field). It follows from Fig. 2 that the variation of ρ for erbium in the interval from 4.2 to 37 K does not exceed 2%. Ultimately, the corresponding ratios of the Hall resistance at $H=0$ from curves *1* (37 K) and *2* (4.6 K) for the multilayer structure and curve *3* (4.6 K) for Er (Fig. 7), according to (1), is

$$\left.\frac{R_{H=0}(T>\theta_1)}{R_{H=0}(T<\theta_1)}\right|^{\mathrm{Er/Sc}} = \frac{\chi_0(T>\theta_1)}{\chi_0(T<\theta_1)} \simeq 2;$$

$$\left.\frac{R_{H=0}^{\mathrm{Er/Sc}}}{R_{H=0}^{\mathrm{Er}}}\right|_{T<\theta_1} = \left.\frac{\chi_0^{\mathrm{Er/Sc}}}{\chi_0^{\mathrm{Er}}}\right|_{T<\theta_1} = 6-14.$$

Thus our data indicate that the conductance of the Er/Sc system studied is extremely sensitive to rearrangement of the magnetic structure even at comparatively low magnetic fields of around 1 kOe, which is suggestive of incomplete ordering of the magnetic moments of the layer in all the temperature regions characteristic for the magnetic structures of elemental Er and of small values of the magnetic energy required for reorientation of the moments in the erbium layers in the multilayer samples. It is possible that this last circumstance explains the positive MR of the structure (up to 4% at 300 K; Fig. 4): in the paramagnetic region of uncorrelated erbium layers in the multilayer samples a magnetic field, by ordering the moments in the Er layers and turning on the contribution from scattering on the pair of interfaces of the nonmagnetic layer, with antiparallel (though asymmetric in value) moments of the Er layers adjacent to these interfaces, causes an increase of the resistance of the multilayer system as a whole. With decreasing temperature and the transition to a more ordered distribution of moments in the Er layers and at the interfaces, the conductance of the Er/Sc structure grows (see the inset in Fig. 4), and that leads to vanishing of the positive MR. That the observed temperature dependence of the MR is unrelated to the dependence on the parameter $\omega\tau$ attests both to the estimate of that parameter given above and the identical nature of the slopes of the $R(T)$ curves for $H=0$ and $H\neq 0$ (inset to Fig. 4).

The causes of the negative MR in the Er film $(\Delta R/R)_{\max}\approx -1\%$ in a certain region of the nonferromagnetic state (Fig. 4) is apparently due to inhomogeneity of the structure of our film, in particular, to a specific distribution and interaction of local magnetic moments in a magnetic field.

The comparative data on the behavior of the conductance of the investigated Er/Sc structures and of a continuous erbium film in the absence and presence of magnetic field allows one to judge the following circumstances.

First, according to the Hall coefficient measurements the magnetization of a multilayer system in the absence of field is substantially nonzero and differs from the magnetization of a continuous erbium film under the same conditions; this must indicate that the very fact that interfaces are present plays a role in the change of the transport characteristics of the system in comparison with those of an nonlayered rare-earth material. Second, in certain temperature regions these changes are manifested anomalously, which indicates that they are related to both the type of magnetic structure of the f layers, which is temperature dependent, and to the character of the distribution of the directions of the moments of these layers in the system, which determines the value of the total magnetic moment of the system as a whole. This means, in particular, that in the case of a uniform distribution of moments in each individual magnetic layer a change of the total magnetic moment is possible only upon the establishment of a distribution of orientations of the moments of the magnetic f layers at the interfaces with the nonmagnetic layers of the multilayer system which does not average out.

In turn, because of the weak (or completely absent) direct exchange interaction of the $4f$ layers in rare-earth metals, the orientation of the moments at the interfaces can be reflected in the character of the conductance of the Er/Sc structure through a spin-dependent coupling with the conduction electrons of the nonmagnetic scandium spacers, whereas in elemental erbium such a coupling can be realized only through the f–s spin-orbit interaction at the ions. The idea of a spin-dependent mechanism of interaction of the magnetic layers of the system leads immediately to dependence of the scattering efficiency at the interface on the mutual orientation of the electron spin in the nonmagnetic layer and the moment in the f layer. Under otherwise equal conditions a large change of conductance is given by the antiparallel and not by the parallel orientation of the moments on opposite interfaces of the nonmagnetic layer: the value of the MR is larger in the antiferromagnetic region than in the ferromagnetic region.

The overall trend of the Hall resistance R_{yx} in the multilayer system with temperature in the ingerval 4.2–300 K (Fig. 8) demonstrates anomalously large changes of this characteristic in the region where the rearrangement of the magnetic structure from antiferromagnetic to ferromagnetic occurs. The character of these changes corresponds to second-order phase transitions.

Thus we have made the first comparative studies of the transport properties—the resistance, MR, and Hall effect—of Er/Sc multilayer structures and elemental erbium, prepared by the same deposition technology. The indicated properties of the multilayer systems are modified substantially in comparison with those same properties of elemental erbium. The MR becomes "giant," although in absolute magnitude it cannot compete with the values realized in superlattices based on the d ferromagnetic materials Fe and Co.

In the region of helium temperatures the Hall coefficient in the Er/Sc system reaches values more than an order of magnitude greater than the value at room temperature. It is found that the features of the transport and Hall coefficient in the investigated multilayer systems are correlated with the concepts of a temperature-dependent rearrangement of the magnetic ordering of the erbium layers and a spin-dependent mechanism of scattering of the conduction electrons.

Without invoking the magnetic measurements it is shown that the magnetization of the f structure in zero field is higher than the remanent magnetization of the f material in the ferromagnetic state, while the conductance of the Er/Sc structure in the proposed region of the antiferromagnetic state of the erbium layers is lower than the conductance in the ferromagnetic state of the same layers.

We are grateful to Prof. S. Oseroff (San Diego State University) for providing the rare-earth metal targets and to A. N. Stetsenko and V. V. Zorchenko (National Technical University "KPI") for preparing the Er films and Er/Sc multilayer systems.

[a)]E-mail: chiang@ilt.kharkov.ua

[1]J. Kwo, D. B. McWhan, M. Hong, E. M. Gyorgy, L. C. Feldman, and J. E. Cunningham, in *Layered Structures, Epitaxy and Interface*, J. H. Gibson and L. R. Dawson (eds.), Materials Research Society, Pittsburg (1985), Mater. Res. Soc. Symp. Proc., Vol. 37, p. 509.
[2]P. Grunberg, R. Schreiber, Y. Pang, M. B. Brodsky, and H. Sowers, Phys. Rev. Lett. **57**, 2442 (1986).

[3]A. Fert and P. Bruno, in *Ultrathin Magnetic Structures*, B. Heinrich and J. A. C. Bland (eds.), Springer-Verlag, Berlin (1994), Vol. 2, Chap. 2.2, p. 82.
[4]M. N. Baibich, J. M. Broto, A. Fert, F. Nguyen van Dau, F. Petroff, P. Eitenne, G. Creuzet, A. Friederich, and J. Chazelas, Phys. Rev. Lett. **61**, 2472 (1988).
[5]S. S. P. Parkin, R. F. Marks, R. F. C. Farrow, G. R. Harp, Q. H. Lam, and R. J. Savoy, Phys. Rev. B **46**, 9262 (1992); E. E. Fullerton, M. J. Conover, J. E. Mattson, C. H. Sowers, and S. D. Bader, Appl. Phys. Lett. **63**, 1699 (1993).
[6]L. A. Chebotkevich, Yu. D. Vorob'ev, A. S. Samardak, and A. V. Ognev, Fiz. Tverd. Tela (Leningrad) **45**, 863 (2003) [Phys. Solid State **45**, 907 (2003)].
[7]A. E. Berkowitz, J. R. Mitchell, M. J. Carey, A. P. Young, S. Zhang, F. E. Spada, F. T. Parker, A. Hutten, and G. Thomas, Phys. Rev. Lett. **68**, 3745 (1992); J. Q. Xiao, J. S. Jiang, and C. L. Chien, *ibid.* **68**, 3749 (1992).
[8]F. Tsui, C. Uher, and C. P. Flynn, Phys. Rev. Lett. **72**, 3084 (1994).
[9]M. A. Ruderman and C. Kittel, Phys. Rev. **96**, 99 (1954).
[10]T. Kasuya, Prog. Theor. Phys. **16**, 45 (1956).
[11]K. Yosida, Phys. Rev. **106**, 893 (1957).
[12]A. T. Hindmarch and B. J. Hickey, Phys. Rev. Lett. **91**, 116601 (2003).
[13]K. A. Gschneider, *Rare Earth Alloys*, Van Nostrand, Princeton (1961), Mir, Moscow (1965).
[14]R. W. Green, S. Legvold, and F. H. Spedding, Phys. Rev. **122**, 827 (1961).
[15]R. V. Colvin, S. Legvold, and F. H. Spedding, Phys. Rev. **120**, 741 (1960).
[16]M. Habenschuss, C. Stassis, S. K. Sinha, and H. W. Deckman and F. H. Sredding, Phys. Rev. B **10**, 1020 (1974).
[17]D. Gibbs, J. Bohr, J. D. Axe, D. E. Moncton, and K. L. D'Amico, Phys. Rev. B **34**, 8182 (1986).
[18]J. A. Borchers, M. B. Salamon, R. Du, C. P. Flynn, J. J. Rhyne, and R. W. Erwin, J. Appl. Phys. **63**, 3458 (1988).
[19]J. R. Banister, S. Legvold, and F. H. Spedding, Phys. Rev. **94**, 1140 (1954).
[20]W. Vavra, C. H. Lee, F. G. Lamelas, Hui He, R. Clark, and C. Uher, Phys. Rev. B **42**, 4889 (1990).
[21]G. Binasch, P. Grunberg, F. Saurenbach, and W. Zinn, Phys. Rev. B **39**, 4828 (1989).
[22]R. E. Camley and J. Barnaoe, Phys. Rev. Lett. **63**, 664 (1989).
[23]P. Bruno and C. Chappert, Phys. Rev. B **46**, 261 (1992).

Translated by Steve Torstveit

Phenomenological treatment of the giant magnetoelectric effect in some ferroelectromagnets

I. E. Chupis[a)]

B. Verkin Institute for Low Temperature Physics and Engineering, National Academy of Sciences of Ukraine, pr. Lenina 47, Kharkov 61103, Ukraine

(Submitted February 10, 2005)
Fiz. Nizk. Temp. **31**, 1125–1129 (October 2005)

It is shown that the colossal changes of the dielectric constant and electric polarization observed in $DyMn_2O_5$ and $TbMnO_3$ in magnetic fields of the order of a few tesla can occur in ferroelectromagnets in which the temperatures of the ferroelectric and magnetic transitions are close and the values of the electric polarization are small. The appearance of electric polarization in the commensurate magnetic phase of $TbMnO_3$ and the change of its orientation in a magnetic field are interpreted as being the result of a renormalization of the ferroelectric energy by the magnetoelectric interaction. The existence of a weak ferromagnetic moment along the c axis in the commensurate phase of $TbMnO_3$ is predicted. © *2005 American Institute of Physics*.
[DOI: 10.1063/1.2128074]

The magnetoelectric (ME) effect, i.e., the inducing of an electric polarization by a magnetic field and of a magnetic moment by an electric field, is usually weak on account of the weakness of the ME interactions. Appreciable values of the ME effect can be expected only in magnetically ordered (anti)ferroelectrics (ferroelectromagnets) with close temperatures of the magnetic and ferroelectric transitions.[1] For example, in nickel-iodine boracite, where the temperatures of the magnetic and ferroelectric (FE) transitions coincide, a change of the dielectric constant of the order of 30% in a magnetic field has been observed.[2] This change is small, however, in compounds with very different transition temperatures, such as $BiMnO_3$.[3] A giant change of the dielectric constant in a magnetic field of the order of a few tesla has recently been observed in certain rhombic ferroelectric ferromagnets.[4,5] In antiferromagnetic $DyMn_2O_5$ the change of the dielectric constant in a magnetic field $H=7$ T was of the order of 100%. A giant change of the electric polarization in a magnetic field of the order of a several tesla was observed[5] in $TbMnO_3$. This effect was also accompanied by a slight ($\sim 10\%$) change of the dielectric constant. No theoretical interpretation of the experimental results was offered in those papers. The discovery of giant changes of the dielectric constant and electric polarization in comparatively low magnetic fields in the ferroelectromagnets $TbMnO_3$ and $DyMn_2O_5$ means that there is a real possibility of effective magnetic control of the FE state.

In this paper an interpretation of the possibility of giant changes of the dielectric constant and electric polarization in a magnetic field is proposed on the basis of general phenomenological concepts. The FE phase transitions observed in $TbMnO_3$ are considered to be the result of a renormalization of the FE constants by the magnetoelectric interaction.

The possibility of colossal changes of the dielectric constant in a magnetic field (the magnetodielectric effect[4]) can be easily understood from general considerations. We write the thermodynamic potential of an isotropic FE–AF with close temperatures of the ferroelectric FE and antiferromagnetic AF transitions in the form of an expansion to terms no higher than fourth order in the antiferromagnetic vector **L**, polarization **P**, and magnetization **M**:

$$\Phi = \frac{a_0}{2}L^2 + \frac{u}{4}L^4 + \frac{\kappa}{2}M^2 - MH + \frac{\lambda}{2}L^2M^2 + \frac{b_0}{2}P^2 + \frac{c}{4}P^4 - PE + \frac{\gamma_0}{2}L^2P^2 + \frac{\gamma}{2}M^2P^2. \quad (1)$$

Here $E(H)$ is the electric (magnetic) field, and the terms with coefficients γ and γ_0 are the ME energy. The fourth-order term in the magnetization is dropped, since we are considering an AF transition. By minimizing Φ (1) with respect to L, M, and P and keeping terms not higher than first order in the ME interaction, we find that the dielectric susceptibility $X = \partial P/\partial E \approx (\partial^2\Phi/\partial P^2)^{-1}$.

For the FE state we have the expression

$$X^{-1} = 2cP^2 = 2(b + \Gamma M^2),\ b = -b_0 + \gamma_0 a_0 u^{-1},$$

$$\Gamma = -\gamma + \lambda\gamma_0 u^{-1},$$

$$M = H(\kappa + \lambda L^2)^{-1},\ b + \Gamma M^2 > 0,\ \beta > 0,\ c > 0,\ u > 0,$$

$$b = \beta(\Theta_0 - T) > 0, \quad (2)$$

where Θ_0 is the Curie temperature in the absence of magnetic field.

In the paraelectric phase we have

$$X^{-1} = -b - \Gamma M^2, \quad b + \Gamma M^2 < 0. \quad (3)$$

The Curie temperature is shifted in a magnetic field:

$$\Theta = \Theta_0 + \Gamma\beta^{-1}M^2. \quad (4)$$

The sign of the shift depends on the sign of the ME constant Γ. Usually the shift of the Curie temperature in magnetic field is small, $|\Theta - \Theta_0| = |\Gamma|M^2/cP_0^2(0) \ll \Theta_0$, where $P_0(0)$ is the spontaneous electric polarization at $T=0$.

However, the spontaneous electric polarization not only can grow with decreasing temperature but can also be a nonmonotonic function as a result of the interaction with other

subsystems of the crystal. These interactions renormalize the FE constant b_0 (2), and, as a result of the renormalization, the constant b, i.e., P_0, can be a nonmonotonic function of temperature. If the constant b is small (i.e., the electric polarization is small) and the constants b and Γ are of different sign, then the condition $b+\Gamma M^2=0$ can be satisfied at not very high magnetic fields. In that case the ME interaction induces a FE phase transition and the dielectric constant $\varepsilon=1+4\pi\mathrm{X}$ undergoes a giant (of the order of 100%) change in the magnetic field, as at a proper FE transition. Indeed, the two crystals studied[4,5] both have a small electric polarization $P \sim 10^{-4}\ \mathrm{C\cdot m^{-2}}$ (in comparison, e.g., $P\sim 10^{-1}\ \mathrm{C\cdot m^{-2}}$ in $BaTiO_3$).

In orthorhombic $DyMn_2O_5$ a series of phase transitions which are close in temperature is observed: an AF transition at $T=T_N$, a FE transition at $\Theta<T_N$, and an AF transition from the commensurate to an incommensurate magnetic state at $T_N'<\Theta$. Below Θ the spontaneous polarization initially grows and then decreases significantly, changing sign near T_N' (Ref. 4). The Curie temperature Θ in a magnetic field directed along the **a** axis decreases ($\Gamma<0$), while for the field direction along the **b** axis it increases ($\Gamma>0$) (see Fig. 2 of Ref. 4). Consequently, the effect of magnetic field on the electric polarization depends on its direction: P increases for the direction of **H** along the **a** axis and decreases if **H** is parallel to the **b** axis. In sum, near T_N' a giant change of the dielectric constant $\varepsilon=1+4\pi\mathrm{X}$ occurs in a magnetic field directed along the **a** axis. A magnetic field directed along the **b** axis, on the contrary, suppresses the dielectric anomaly.[4]

It follows from Eq. (2) that an anomalous value of ε can occur in a magnetic field H_c,

$$H_c=\sqrt{\frac{-b}{\Gamma}}\mathrm{X}_m^{-1}, \tag{5}$$

where X_m is the magnetic susceptibility. The value of the critical field H_c decreases with increasing X_m. That is why the colossal ME effect is observed in not too high magnetic fields in those crystals where the FE and AF transition temperatures are close.[4,5]

Thus the observation of a giant ME effect in experimentally accessible magnetic fields is possible in crystals for which: 1) the spontaneous electric polarization is small; 2) the temperatures of the magnetic and ferro(antiferro)electric transitions are close; 3) the constants b and Γ are of opposite sign.

In the orthorhombic manganate $TbMnO_3$ (space group *Pbnm*) an electric polarization arises along the **c** axis at the transition from the sinusoidally modulated AF phase to the commensurate one.[5] In the commensurate AF phase a magnetic field of a few tesla induces a switching of the electric polarization from the **c** axis to the **a** axis. The authors of Ref. 5 assumed that the reorientation of the polarization is a consequence of a reorientation of the magnetic moments of the Tb^{3+} ions.[5] The giant change of the electric polarization ($\Delta P\approx 6\times 10^{-4}\ \mathrm{C\cdot m^{-2}}\sim P$) is accompanied by only a slight (10%) change of ε_c.

An interpretation of the observed FE transitions in $TbMnO_3$ in a magnetic field is proposed below in which the terbium ions are found in the paramagnetic state and the magnetic ordering is created by the Mn^{3+} ions.

According to Ref. 6, the long-period sinusoidal AF ordering at $T<41$ K is the result of distortion and orbital ordering. The Mn^{3+} spins are directed along the **b** axis.[7] The observed magnetic anomalies near the temperatures $\sim$7 K and $\sim$27 K are due to ordering of the terbium and manganese spins, respectively. The anomaly at $T_l\approx 27$ K corresponds to the transition between the commensurate and incommensurate AF phases. Simultaneously with the AF ordering below T_l an electric polarization appears along the $Z(\mathbf{c})$ axis. The dielectric constant ε_c has a distinct anomaly near T_l.[5] The maximum value of the electric polarization is small, $P_z\approx 8\times 10^{-4}\ \mathrm{C\cdot m^{-2}}$. The authors of Ref. 5 consider the FE transition to be an improper transition, the primary order parameter of which is a distortion mode.

The unit cell of $TbMnO_3$ contains four Mn^{3+} ions and four Tb^3 ions in the following positions:

$$\mathrm{Mn^{3+}}\text{: } 1(1/2,0,0),\quad 2(1/2,0,1/2),\quad 3(0,1/2,1/2),\quad 4(0,1/2,0),$$

$$\mathrm{Tb^{3+}}\text{: } 5(x,y,1/4),\quad 6(\bar{x},\bar{y},3/4),\quad 7(x+1/2,-y+1/2,3/4),8(-x+1/2,y+1/2,1/4).$$

The magnetic state is denoted by the symbols $G(g)$, $C(c)$, and $M(m)$ for the the Mn ions (capital letters) and Tb ions (lower-case letters),[8] where

$$\mathbf{A}=\mathbf{M}_1-\mathbf{M}_2-\mathbf{M}_3+\mathbf{M}_4,$$

$$\mathbf{G}=\mathbf{M}_1-\mathbf{M}_2+\mathbf{M}_3-\mathbf{M}_4,$$

$$\mathbf{C}=\mathbf{M}_1+\mathbf{M}_2-\mathbf{M}_3-\mathbf{M}_4,$$

$$\mathbf{g}=\mathbf{M}_5-\mathbf{M}_6-\mathbf{M}_7+\mathbf{M}_8,$$

$$\mathbf{a}=\mathbf{M}_5-\mathbf{M}_6+\mathbf{M}_7-\mathbf{M}_8,$$

$$\mathbf{c}=\mathbf{M}_5+\mathbf{M}_6-\mathbf{M}_7-\mathbf{M}_8,$$

$$\mathbf{M}=\sum_1^4\mathbf{M}_n,\quad \mathbf{m}=\sum_5^8\mathbf{M}_n. \tag{6}$$

The transformations of the magnetic vectors (6), of **P**, and of the strain tensor u_{ik} under the operations of the symmetry elements of the space group *Pbnm* are presented in Table I.

Let us consider the states in the temperature interval $T'<T<T_l$ (T' is the temperature of the magnetic ordering of the terbium ions), where the terbium subsystem is paramagnetic. The spins of the Mn^{3+} ions are directed along the **b** axis, i.e., A_y is nonzero. Simultaneously with A_y an electric polarization P_z appears. It can be supposed that the magnetic ordering of the Mn^{3+} ions induces a ferroelectric transition on account of the Jahn-Teller distortion, by analogy with RMn_2O_5.[4,9] Since the value of P_z is small, the FE transition is improper. In this case, for example, the energy of the crystal can contain a term in the first power of the electric polarization. It is seen from Table I that invariants containing the first power of the polarization and the distortion tensor do not appear in the energy. The terms of the first power in P_z and quadratic in the magnetic moments in the absence of magnetic field in the state A_y are the following: $P_zA_yg_y$,

TABLE I. Irreducible representations of the group *Pbnm*.

Γ_i	I	2_{1x}	2_{1y}	Components
Γ_1	+1	+1	+1	$A_x, G_y, C_z, c_z, u_{xx}, u_{yy}, u_{zz}$
Γ_2	+1	+1	−1	$M_x, C_y, G_z, m_x, c_y, u_{yz}$
Γ_3	+1	−1	+1	$A_z, C_x, M_y, m_y, c_x, u_{xz}$
Γ_4	+1	−1	−1	$A_y, G_x, M_z, m_z, u_{xy}$
Γ_5	−1	+1	+1	a_x, g_y
Γ_6	−1	−1	−1	a_y, g_x, P_z
Γ_7	−1	−1	+1	a_z, P_y
Γ_8	−1	+1	−1	g_z, P_x

$P_zA_ya_x$. Since $g_y=a_x=0$ (the terbium subsystem is not ordered), there must be some other mechanism for the appearance of P_z below the temperature T_l. In this paper it is proposed that an electric polarization $P_z=P_c\neq 0$ arises below T_l as a consequence of the magnetoelectric renormalization of the FE constant b_0 by the ME interaction term $\gamma_0 P_z^2 A_y^2$ (1). This term contains an interaction of the electric polarization with the magnetic moments both through the exchange and anisotropic magnetic forces and through the distortion $u_{ii}\sim A_y^2$. We then have [see Eq. (2)]: $b_0=b_{0c}>0$, $b=b_c=-b_0-\gamma_{0c}A_y^2>0$, $\gamma_{0c}<0$. Satisfaction of the condition $b_c>0$ means that the ME and FE energies should be quantities of the same order.

The presence of the invariant M_zA_y in the energy (see Table I) means that the commensurate magnetic phase below T_l is a weak ferromagnet. This conclusion is confirmed by the absence of any noticeable anomalies of the magnetization at high fields in the temperature region under study (Fig. 3e of Ref. 5). In the exchange approximation, with only nearest neighbors (NN) taken into account one can set

$$\mathbf{A}\neq 0,\quad \mathbf{g}\neq 0,\quad \mathbf{G}=\mathbf{C}=\mathbf{c}=\mathbf{a}=0,$$

$$\mathbf{M}_1=\mathbf{M}_4,\quad \mathbf{M}_2=\mathbf{M}_3,\quad \mathbf{M}_5=\mathbf{M}_8,$$

$$\mathbf{M}_6=\mathbf{M}_7,\quad A_y=2(\mathbf{M}_1-\mathbf{M}_2)_y.$$

The presence of the invariants $P_zA_yg_y$, m_zA_y, and m_zM_z in the energy indicates that the subsystem of Mn ions magnetically biases the subsystem of Tb ions and that the appearance of P_z induces the appearance of antiferromagnetic ordering of the terbium spins along the Y axis. The presence of the anisotropic relativistic invariants A_yG_x and M_zG_x in the energy indicates that the spin structure is actually slightly noncollinear (the so-called "three-dimensional cross"). In the following qualitative treatment we shall limit consideration to the NN approximation. The FM–FE state, in which A_y, M_z, P_z, and g_y are nonzero in the absence of magnetic field, will be referred to below as state I.

A magnetic field alters the electric polarization P_z and the dielectric constant ε_c [see Eqs. (2) and (3)]. In the paraelectric phase ($T>T_l$) the constants $-b_c=b_{0c}>0$, $-\Gamma_c=\gamma_c$. The constant $\gamma_c>0$, since ε_c decreases with magnetic field (Fig. 2a of Ref. 5). The temperature of the FE transition decreases in magnetic field (Fig. 2a of Ref. 5), i.e., the constant $\Gamma_c=\gamma_{0c}u^{-1}\lambda-\gamma_c<0$. The negative sign of Γ_c means that P_z decreases with increasing magnetic field, as is observed experimentally (Fig. 2c of Ref. 5).

In state I the dielectric constant ε_c grows in a magnetic field (Fig. 3a of Ref. 5). Indeed, from Eq. (2) we have

$$\Delta\varepsilon_c=\varepsilon_c(H)-\varepsilon_c(0)=-\frac{\Gamma_cM^2}{2b_c(b_c+\Gamma_cM^2)}>0. \tag{7}$$

The change of ε_c in low fields is small.

The dielectric constant $\varepsilon_{xx}=\varepsilon_a$ along the **a** axis does not have anomalies at T_l, i.e., $P_x=0(b_a<0)$. The value of ε_a increases in magnetic field (Fig. 3b of Ref. 5), i.e., the ME constant $\Gamma_a>0$. It follows from Eq. (3) that

$$\Delta\varepsilon_a=\varepsilon_a(H)-\varepsilon_a(0)=\frac{\Gamma_aM^2}{b_a(b_a+\Gamma_aM^2)}>0,$$

$$M<M_a=(-b_a/\Gamma_a)^{1/2}. \tag{8}$$

The quantities $\varepsilon(\Delta\varepsilon)$ have an anomaly (a sharp peak) if $b+\Gamma M^2=0$ [see Eqs. (7) and (8)]. This condition means that the ME and FE energies are equal. If the constant Γ is independent of temperature, then $b^{-1}M^2$ is also unchanging with temperature. The quantity b^{-1} is proportional to the dielectric constant, which, according to the experimental data (Fig. 1d of Ref. 5), is indeed independent of temperature along the **a** and **c** directions below T_l. Thus the values of $M_{a,c}$ corresponding to the maxima of $\varepsilon_{a,c}$ in fields $H_{a,c}=M_{a,c}\chi_m^{-1}$ (5) should also be unchanging with temperature. The experimental data (Figs. 3a,b in Ref. 5) are as follows: 1) $T=9$ K, $H_a\approx H_c\approx 5$ T; 2) $T=12$ K, $H_a\approx H_c\approx 6$ T; 3) $T=15$ K, $H_a\approx H_c\approx 7$ T; 4) $T=18$ K, $H_a\approx H_c\approx 8$ T. Indeed, according to the experimental data (Fig. 3e of Ref. 5) the magnetic moment is the same in all these cases, $M_k\cong 3.2\mu_B$ per formula unit. This confirms the idea of an effective renormalization of the FE energy by the ME interaction. The value of M_k is the same for ε_a and ε_c, i.e., M_k is that value of the magnetic moment upon the reaching of which a phase transition occurs in the crystal. The unit cell of $TbMnO_3$, with a volume $V_c=2.3\times 10^{-22}$ cm^3, contains four formula units, i.e., the critical magnetic moment density $M_{0k}=4M_kV_c^{-1}$. The values of the constants b_a and b_c can be found from the permittivity data (Fig. 1d of Ref. 5), $b_c=0.2$, $b_a=-0.5$. Thus we have the relations

$$\frac{b_c}{b_a}=\frac{\Gamma_c}{\Gamma_a},\quad |\Gamma_c|=\frac{b_c}{M_{0k}^2}\approx 6.10^{-7}\ \text{c.g.s e.s.u.},$$

$$\Gamma_a\approx 1.5\cdot 10^{-6}\ \text{c.g.s e.s.u.}. \tag{9}$$

In a magnetic field directed along the Y axis additional invariants quadratic in the magnetic moments appear in the energy:

$$M_yA_z, m_yA_z, P_zM_yg_z, P_zm_yg_z, P_xM_yg_x, P_xm_yg_x.$$

The appearance of the invariant M_yA_z means that a state in which **A** is perpendicular to **H** can exist (state II). The transition from state I to state II under the influence of magnetic field is a rotation of **A** from the Y axis toward the Z axis. After the spin reorientation at the field $H=H_{sf}$ the electric

polarization along the Z axis produced by A_y vanishes. However, since the ME constant $\Gamma_a > 0$, an electric polarization along the X axis appears if the magnetic field $H > H_a$:

$$P_x = \mathrm{X}_m(\Gamma_a/c_a)^{1/2}\sqrt{H^2 - H_a^2}. \quad (10)$$

State II has nonzero $A = A_z$, $M = M_y$, and $P = P_x$ ($A_y = M_z = P_z = 0$). The dielectric susceptibility along the **a** axis is determined by expression (2), where $b = b_a < 0$, $\Gamma = \Gamma_a > 0$. If $H = 0$, then $\mathrm{X}_a(0) = (-b_a)^{-1}$. Consequently, the value of $f = [\varepsilon_a(H) - \varepsilon_a(0)]/\varepsilon_a(0)$ is

$$f = \frac{2M^2 - 3M_a^2}{2(b_a - 4\pi)(M^2 - M_a^2)}, \quad H > H_a. \quad (11)$$

The function (11) is positive for $H_a < H < (3/2)^{1/2}H_a$ and negative for $H > (3/2)^{1/2}H_a$. This behavioral tendency of the function f and also the quadratic dependence of $\Delta\varepsilon_a$ (8) on H at low magnetic field is seen on the experimental curves (Fig. 3d of Ref. 5). However, a quantitative comparison with the experimental data is complicated by the hysteresis of the field curves of ε and P. The phase transition from state I to state II is a first-order transition. Apparently the spin reorientation field H_{sf}, the field H_c at which P_z vanishes, and the field H_a at which P_x appears are not very different. The temperature dependence of the fields H_a and H_c is determined by the magnetic susceptibility X_m, which increases significantly below 18 K as the ordering temperature of the Tb^{3+} spins is approached (Fig. 1b of Ref. 5). Therefore, the value of the transition field increases with increasing temperature, as is observed experimentally (Fig. 4 of Ref. 5). Although the first-order character of the phase transition is clearly observed in the FE subsystem, the magnetic moment does not have visible anomalies far from T_N' (Fig. 3e of Ref. 5), since the FE energy is small compared to the magnetic energy. In the case considered, the ME and FE energies are of the same order. Therefore the ME interaction has a significant effect on the FE state and a weak effect on the magnetic state. The appearance of $P_x \neq 0$, because of the existence of the invariants $P_x M_y g_x$ and $P_x m_y g_x$, gives rise to a component g_x, i.e., the antiferromagnetic vector of the terbium ions is reoriented toward the X axis.

Thus the phenomenological treatment presented has shown the possibility of colossal changes of the electric polarization and dielectric constant at not very high magnetic fields as a result of a renormalization mechanism in the case when the electric polarization is small and the FE and ME energies are of the same order. The renormalization hypothesis is qualitatively confirmed by the experimental data in the ferroelectromagnets $TbMnO_3$ and $DyMn_2O_5$. The existence of a weak ferromagnetic moment along the Z axis in $TbMnO_3$ in the commensurate magnetic phase is predicted. It is assumed (contrary to the hypothesis made by the authors of Ref. 5) that at high magnetic field the spin reorientation of the Mn^{3+} ions (and not the Tb^{3+} ions) occurs first, and then an electric polarization appears along the X axis and the reorientation of the magnetic moments of Tb^{3+} occurs.

[a)]E-mail: chupis@ilt.kharkov.ua

[1]G. A. Smolenskiĭ and I. E. Chupis, Usp. Fiz. Nauk **137**, 415 (1982) [Sov. Phys. Usp. **25**, 475 (1982)].
[2]L. N. Baturov, B. I. Al'shin, and Yu. N. Yarmukhamedov, Fiz. Tverd. Tela (Leningrad) **20**, 2254 (1978) [Sov. Phys. Solid State **20**, 1300 (1978)].
[3]T. Kimura, S. Kawamoto, I. Ymada, M. Azuma, M. Takano, and Y. Tokura, Phys. Rev. B **67**, 180401 (2003).
[4]N. Hur, S. Park, P. A. Sharma, S. Guha, and S.-W. Cheong, Phys. Rev. Lett. **93**, 107207 (2004).
[5]T. Kimura, T. Goto, H. Shintani, K. Ishizaka, T. Arima, and Y. Tokura, Nature (London) **426**, 55 (2003).
[6]T. Kimura *et al.*, Phys. Rev. B **68**, 060403(R) (2003).
[7]S. Quezel, F. Tcheou, J. Rossat-Mignot, G. Quezel, and E. Roudaut, Physica B **86–88**, 916 (1977).
[8]E. A. Turov, A. V. Kolchanov, V. V. Men'shenin, I. F. Mirsaev, and V. V. Nikolaev, *Symmetry and the Physical Properties of Antiferromagnets* [in Russian], Fizmatgiz, Moscow (2001).
[9]E. I. Golovenchits, N. V. Morozov, V. A. Sanina, and L. M. Sapozhnikova, Fiz. Tverd. Tela (St. Petersburg) **34**, 108 (1992) [Sov. Phys. Solid State **34**, 56 (1992)].
[10]J. Blasco, C. Ritter, J. Garsia, J. M. de Teresa, J. Pérez-Cacho, and M. R. Ibarra, Phys. Rev. B **62**, 5609 (2000).

Translated by Steve Torstveit

Electron paramagnetic resonance study of the singlet magnet $KTb(WO_4)_2$

K. G. Dergachev, M. I. Kobets, A. A. Loginov, and E. N. Khatsko[a)]

B. Verkin Institute for Low Temperature Physics and Engineering, National Academy of Sciences of Ukraine, pr. Lenina 47, Kharkov 61103, Ukraine

(Submitted February 25, 2005; resubmitted April 13, 2005)
Fiz. Nizk. Temp. **31**, 1130–1142 (October 2005)

The electron paramagnetic resonance (EPR) spectrum of $KTb(WO_4)_2$ is investigated in the frequency range 14–120 GHz and magnetic field range 0–70 kOe at helium temperature. The observed triplet structure of the spectrum is interpreted as a manifestation of resonance in three-site clusters. On this basis a value of the g factor ($g \approx 13.3$) and an estimate of the gap ($\delta \approx 1$ K) are obtained for the quasi-doublet ion Tb^{3+} in the crystalline field of $KTb(WO_4)_2$, and the parameters of the dipole ($I_d \approx 1.6$ K) and exchange ($I_{ex} \approx 0.9$ K) AFM interactions of the nearest neighbors in the chains are determined for the corresponding singlet magnet model. A first-order structural phase transition, induced by an external magnetic field lying in the basal plane of the crystal, is observed. © *2005 American Institute of Physics*. [DOI: 10.1063/1.2128075]

I. INTRODUCTION

Alkali-rare-earth double molybdates and tungstates have been actively studied for a long time. Many compounds of this class are characterized by a strong magnetic anisotropy of the rare-earth ions, a low local symmetry, and a pronounced chain structure of the positions occupied by them. The electronic spectrum of rare-earth ions in the crystalline field usually has low-lying excited levels, and that leads to the possibility of reorganization of the corresponding electronic states both by an external magnetic field and by displacements of the ions. This is responsible, in particular, for the magnetic-field-induced structural phase transitions observed in various compounds of this class.[1–7] In the case of non-Kramers rare-earth ions the lowest electronic levels often form a quasi-doublet with a gap δ of the order of 1 K, well separated from the rest of the spectrum. The magnetic dipole and exchange interactions in these compounds are of this same order of magnitude. Therefore, singlet and excitonic types of magnets can be realized in these compounds (in the second case the interactions are insufficient to induce magnetic order suppressed by the gap δ; Refs. 8 and 9). In the non-Kramers case the contribution to the magnetic properties of the crystal from the higher-lying excitations of the rare-earth ions are also unusual.[8] All of these circumstances lend great interest to the study of such systems. Here it is possible to study a number of topical questions in solid state physics in a comparatively simple situation. Among such topics are the interaction of electronic excitations with lattice vibrations (the Jahn–Teller effect, polaron effects, etc.), structural phase transitions taking place by unusual scenarios (incommensurability, strong fluctuations), and nonlinear regimes of microwave energy absorption, which are comparatively easy to achieve here because of the long relaxation times of the elementary excitations.[10,11]

One member of this family of compounds that has practically escaped study is $KTb(WO_4)_2$, which contains the rare-earth ion Tb^{3+} ($^7F_6$) with an odd number of electrons. The goal of the present study was to investigate its magnetic properties by the EPR method over a wide range of frequencies and magnetic fields: to determine the main parameters of the EPR absorption spectrum and to obtain information about the crystalline field and the character and values of the interactions between low-lying electronic excitations. It is of interest to explore the possibilities of inducing a structural phase transition in this compound by an external magnetic field, as has been observed in the molybdates.[1–7]

II. DESCRIPTION OF THE EXPERIMENT

The $KTb(WO_4)_2$ single crystals were grown by spontaneous crystallization from the flux.[12] The samples grown were bulk crystals with good natural faceting. There have been no results reported on x-ray analysis of this crystal, although the isostructural compound $KY(WO_4)_2$ was studied in Ref. 13. We have used the data obtained by V. H. Baumer (Institute of Single Crystals of the National Academy of Sciences of Ukraine) for $KTb(WO_4)_2$, which will be published in a separate paper along with the results on the static magnetic properties of this crystal. For the resonance measurements we used a standard direct-gain radio spectrometer with a set of cavities for different frequencies.

To understand the geometric aspects of the experiment we use the main structural data (obtained at room temperature). The symmetry of the $KTb(WO_4)_2$ crystal is monoclinic, with space group $C2/c$ (C_{2h}^6). The parameters of its unit cell are $a=10.653$ Å, $b=10.402$ Å, $c=7.573$ Å, $\beta=130.76°$. It contains 4 formula units and consists of two primitive cells. The Tb ions are located on the C_2 rotation axes, parallel to the b axis of the crystal. They form a chain extending along the (101) direction perpendicular to that axis, with a nearest distance between ions $r \approx 4.07$ Å and small opposed displacements of neighboring ions from that straight line in the direction of the b axis by $\pm 0.0216b$ (corresponding to a deviation of the chain links from the direction of the chain by an angle $\xi \approx \pm 6.3°$). Adjacent ions of the chains belong to one primitive cell and are connected by a center of inversion. An orthogonal coordinate system (x,y,z) tied to the crystal is chosen so that $z \| b$, $y \| (101)$; then the angle between the c axis of the crystal and the x axis is

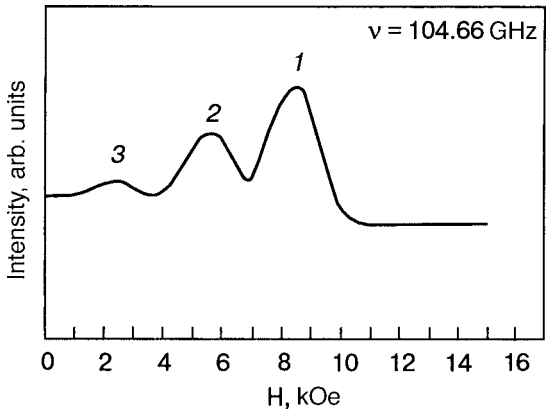

FIG. 1. Form of the EPR absorption spectrum of the Tb^{3+} ion in $KTb(WO_4)_2$ at T=4.2 K.

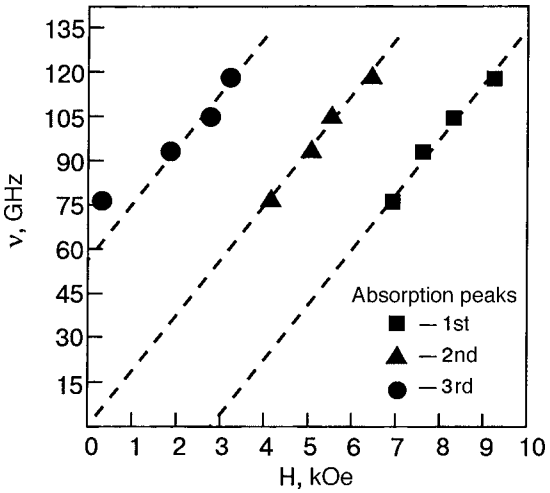

FIG. 2. Frequency-field curves of the absorption spectrum of the Tb^{3+} ion in $KTb(WO_4)_2$ along the direction of the maximum g factor (the b axis). The straight lines are the asymptotes of these plots at large values of the field. The size of the symbols corresponds approximately to the error in the determination of the position of the maximum of the absorption line.

≈4.4°. The samples placed in the cavity had an irregular shape, elongated predominantly in the direction perpendicular to the C_2 axis, with typical dimensions $\approx 1\times 1\times 2$ mm.

Measurements of the resonance absorption of the Tb^{3+} ion in $KTb(WO_4)_2$ were carried out in the frequency range 14–120 GHz at helium temperature. Cylindrical and rectangular cavities of the appropriate frequency range were used, with a device for rotating the sample about an axis perpendicular to the direction of the static external magnetic field **H** (the angle was measured to an accuracy of ±1°). The polarization of the high-frequency magnetic field **h** at the sample was predominantly parallel to the axis of rotation. The magnetic field was produced by a superconducting solenoid with a maximum field of 75 kOe.

Preliminary measurements revealed the presence of resonance absorption in the frequency range used. A typical spectrum is shown in Fig. 1. The first problem was to establish the value and direction of the maximum spectroscopic splitting. In accordance with the local symmetry of the Tb^{3+} ion, this direction should either coincide with the C_2 axis or lie in the basal plane (if structural phase transitions have not occurred on cooling the sample to helium temperature). With this goal a sample oriented beforehand by an x-ray method was placed in the cavity in such a way that the field **H** was parallel to the C_2 axis. The absorption spectrum observed in this field direction in the frequency range 75–120 GHz (Fig. 1) contains three intense absorption peaks, which were situated approximately equidistantly with a mean distance between resonance fields of ≈2.8±0.3 kOe. The widths of the peaks were approximately equal and lay in the range 2–2.5 kOe, varying slightly with frequency. The ratio of their intensities can be roughly estimated as 4:2:1 in order of decreasing resonance field. We shall number these components in that same order (the 1st, 2nd, and 3rd peaks). Figure 2 shows the corresponding frequency-field curves. To within the accuracy of determination of the resonance fields they lie along three straight lines with a g factor of ≈13.3±0.2. For the third line (corresponding to the 3rd peak) the slope of the linear part at the higher fields, from which the g factor for the non-Kramers doublets must be determined, cannot be estimated reliably; however, in connection with the interpretation offered below we adopted the value given above for it also.

The frequency-field curves in a wider frequency interval were also obtained for other directions of **H**, making an angle φ with the C_2 axis in the interval $45° < \varphi < 60°$. Such orientations are the most likely to reveal possible additional resonances. The results showed that in all cases the shape of the lines and their behavior in the frequency interval 75–120 GHz are similar to the case $\mathbf{H} \| C_2$, and no new absorption peaks were detected (Fig. 3). Figure 4 shows typical frequency-field curves over a wide range of frequencies for the angle φ=45°. It is seen that in the low field region the distances between components of the spectrum begin to vary in a complex manner. Upon extrapolation to zero field the presence of two initial splittings for the 2nd and 3rd peaks can be seen, which can be estimated roughly as 20±4 GHz and 75±4 GHz and 1±0.2 K and 3.6±0.2 K, respectively. The behavior of the 1st peak at low fields is more complicated. Its frequency-field curve probably has a minimum at a frequency below 14 GHz (≈0.7 K), at which a weak doubling of the corresponding maximum was observed.

We did not make special measurements of the intensity of the resonance absorption peaks in this study, but their ratio for the three components of the spectrum can be discerned qualitatively. The ratio 4:2:1 holds for all of the directions of the field **H** discussed above for frequencies $\nu \geqslant 50$ GHz. At lower frequencies, however, the intensities of the 1st and 2nd maxima begin to equalize, and at $\nu \leqslant 41$ GHz the 2nd peak becomes the more intense (Fig. 3). On the other hand, increasing the temperature from 4.2 to 36 K also leads to a change of the ratio of the absorption intensity in favor of the 2nd peak. Further increasing the temperature to 58 K causes a broadening of the peaks, so that a single broad maximum is observed at a position corresponding to the central component of the spectrum (Fig. 5). Of course, on the whole the integrated intensity of the absorption falls off with increasing temperature.

In the third series of measurements we investigated the dependence of the resonance field on its orientation in a specified plane at a fixed frequency of 76.33 GHz (optimal for the cavity used). The dependences obtained in different

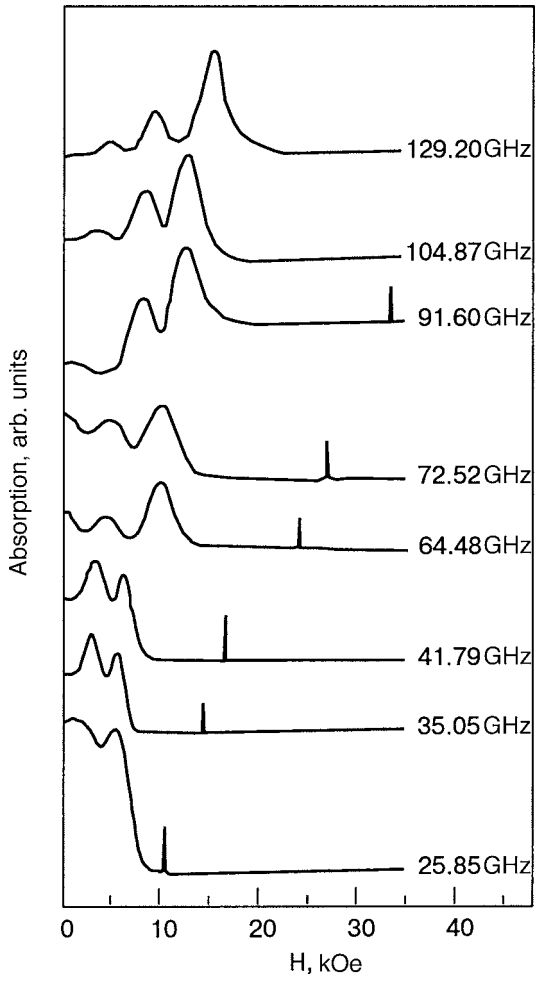

FIG. 3. Form of the EPR absorption spectrum of the Tb^{3+} ion at $T=4.2$ K at different frequencies. The external magnetic field was oriented at an angle of 45° to the magnetic axis of the crystal in the *bc* plane. The narrow line is the DPPH reference signal.

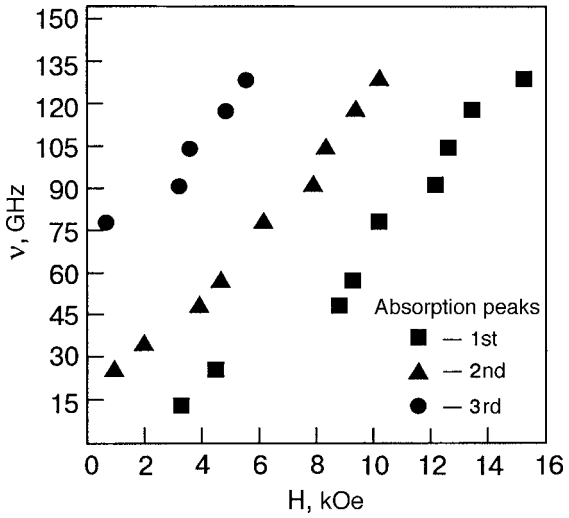

FIG. 4. Frequency-field curves of the absorption spectrum of the Tb^{3+} ion in $KTb(WO_4)_2$ at an angle of 45° to the magnetic axis of the crystal in the *bc* plane. The size of the symbols corresponds approximately to the value of the error of determination of the position of the maxima of the absorption lines.

planes had a similar form in the whole angular interval except in the very close vicinity of the basal plane. Figure 6 shows the dependence of the spectrum on the field direction in a plane lying at an angle $\varphi_0 \approx 45°$ to the C_2 axis and intersecting the basal plane approximately along the *c* axis of the crystal. The maximum *g* factor in that plane is equal to $g'=9.5$. Upon a deviation from the direction b' corresponding to this *g* factor by an angle θ in the interval $0° < \theta < 75°$ a broadening of the maxima and an increase in the distance between them is observed (at the given frequency only the two high-field peaks, the 1st and 2nd, can be seen; they are presented in the figure). At $\theta=75°$ the width of the peaks reaches values $\Delta H=3.5$ kOe, and the distance between them is $\Delta H \approx 4$ kOe. However, upon further increase in the angle θ from 75° to 87°, these values decrease substantially and become noticeably smaller than for $\mathbf{H} \| b'$. It is also seen in Fig. 6 that the isolated structure of each peak is preserved in the whole interval of angle from 0° to 87°, and no signs of their "crossing" are observed, as could occur in the case of two misoriented centers. Figure 7 shows the dependence of the resonance field on the angle in this interval for the 1st and 2nd absorption peaks. We note that on each curve taken at the higher frequency (104.87 GHz) the 3rd absorption peak is also observed; at angles $>75°$ it also begins to rapidly approach the central peak while strongly narrowing in width.

Further increase of the angle above 87° was done with a smaller step (from 1° to approximately 0.2°). In this region of angles, which corresponds to the minimum value of the *g* factor, the following feature is observed in the absorption spectrum. In the interval $87° < \theta < 89.5°$ (the upper boundary is tentative on account of the low accuracy of the angle setting) the lines rapidly come together, and their width becomes less than 300 Oe. At the upper limit of this angular interval in a field $H_c \approx 40$ kOe a jump in intensity occurs at

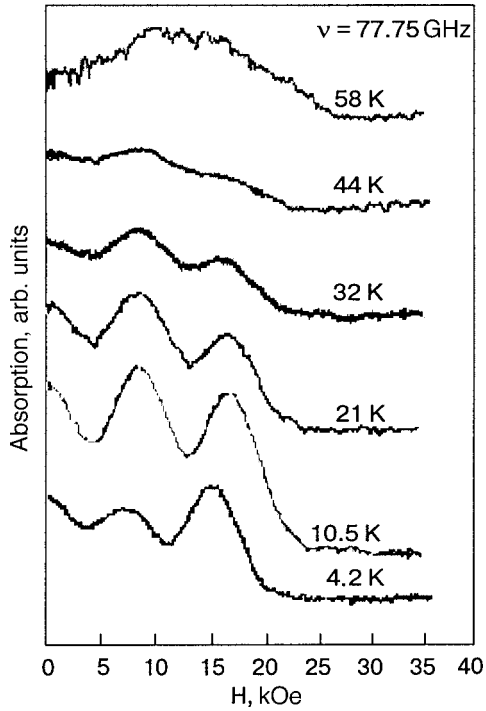

FIG. 5. Form of the EPR absorption spectrum in $KTb(WO_4)_2$ for different temperatures at a frequency $\nu=77.7$ GHz. (The integrated intensities of the lines decrease with increasing temperature. The lines have been plotted with different magnifications in the figure.)

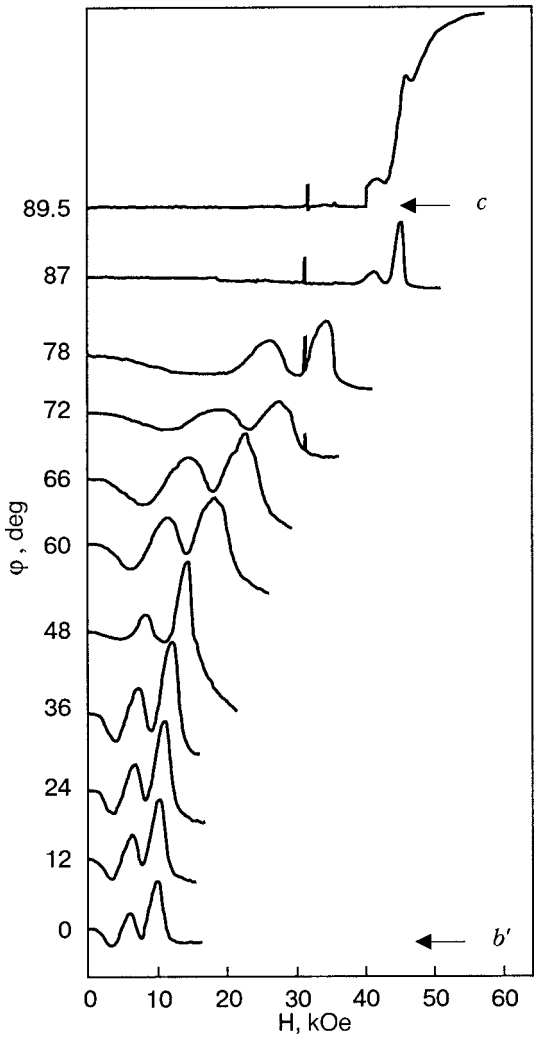

FIG. 6. Transformation of the form of the EPR absorption spectrum in $KTb(WO_4)_2$ in the range of angles 0°–89.5°. The plane of rotation of the magnetic field lies at an angle of ≈45° to the b axis and intersects the basal plane along the c axis of the crystal; b' is the direction of the maximum g factor in that plane; ν=76.33 GHz, T=4.2 K. The narrow line is the DPPH reference signal.

the high-field edge of the 1st absorption peak. As the field is increased further, the intensity, as a rule, continues to grow strongly. However, the line shape of this absorption at high fields could not be investigated because of possible damage to the shaft of the rotating device or destruction of the sample as a result of the large torque (this sometimes occurs together with or immediately after the jump of the absorption intensity). When the field was decreased a small hysteresis of the absorption was observed, with $\Delta H \approx 250$ Oe. Such behavior of the spectrum most likely indicates the presence of a first-order phase transition. Indeed, the absorption line shape at fields corresponding to the phase transition and nearby regions is very sensitive to the angle between the field and the basal plane (which we could not control to a sufficient degree of accuracy) and to the orientation of the field **H** in the basal plane. Apparently there is substantial influence of the defect structure of the sample and the degree of its "clamping" when glued. Further studies are needed to investigate the complex dependence of the phase transition picture on these factors. Figure 8 shows examples of the spectra recorded in the phase transition region, taken at different temperatures at a deviation of the field from the basal plane of less than 20′ (such an accuracy was achieved by rotating the field in a plane making an angle of ≈20° with the basal plane).

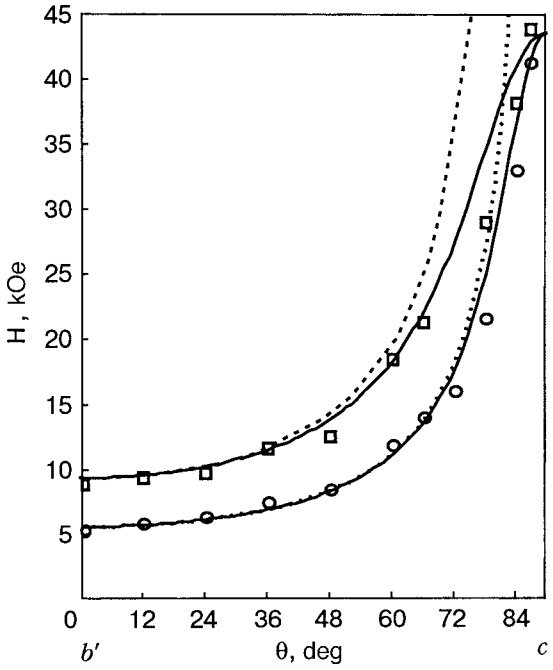

FIG. 7. Angular dependence of the EPR absorption spectrum corresponding to Fig. 6. The solid and dashed curves are theoretical calculations; the points are experimental results.

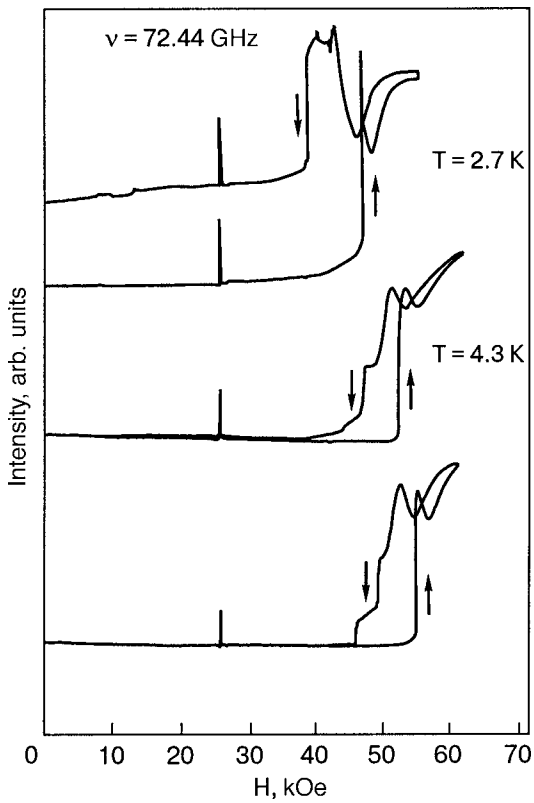

FIG. 8. EPR absorption line shape in the region of the first-order phase transition for different temperatures (the deviation of the field from the basal plane is less than 20′). The narrow line is the DPPH reference signal.

III. DISCUSSION

Let us discuss some questions pertaining the experimental results obtained: the nature of the triplet structure of the spectrum, the possibility of its model description, and estimation of the corresponding parameters; the low-frequency features of the spectrum; the features of the spectrum near the basal plane; the field-induced phase transition. We shall address these questions in that order.

Triplet structure of the spectrum. Model

An isolated quasi-doublet of a non-Kramers magnetic ion in the crystalline field gives one resonance absorption peak in the EPR spectrum, and the dependence of the resonance frequency ν on the value and direction of the external static magnetic field $\mathbf{H}$ is determined by the formula[8]

$$2\pi\hbar\nu = \omega = \sqrt{\delta^2 + \mu_B^2(\mathbf{g}\cdot\mathbf{H})^2} = \sqrt{\delta^2 + \mu_B^2 g^2 H^2 \cos^2\varphi}. \tag{1}$$

Here δ is the value of the energy gap between states Φ_0 and Φ_1 of the quasi-doublet (without loss of generality we assume that upon time inversion $\Phi_0 \to \Phi_0$, $\Phi_1 \to \Phi_1$), and the vector $\mathbf{g}$ (equal to twice the magnetic dipole moment of the transition in Bohr magnetons) is equal to

$$\mathbf{g} \equiv \mathbf{g}_{01} = -2ig_J(\Phi_0, \mathbf{J}\Phi_1), \tag{2}$$

where $\mathbf{J}$ is the total angular momentum operator of the f electrons of the rare-earth ion, $(*,*)$ is the scalar product, g_J is the Lande factor (in the given case $g_J = 3/2$), φ is the angle between directions of the vectors $\mathbf{H}$ and $\mathbf{g}$, and $i = \sqrt{-1}$.

Let us discuss the possible causes of the observation of the triplet structure of the EPR line in the experiments described above. It cannot be explained by the presence of ions with different directions of the $\mathbf{g}$ vectors, since the primitive cell contains two Tb^{3+} ions connected by a center of inversion. The symmetry could be broken if one admits the possibility that a structural phase transition occurs as the temperature is lowered from room to helium temperature. However, the behavior of the absorption maxima on rotation of the crystal in different planes does not reveal the characteristic signs of the presence of different centers. We therefore rule out that possibility. It is important to note that the linear part of the frequency-field curve of the 1st (high-field) absorption peak(Fig. 2) clearly does not extrapolate to the origin of coordinates, as it should according to formula (1). This fact cannot be explained in the model of a magnetic center in the crystalline field with one quasi-doublet of electronic states. It is necessary either to invoke a larger number of electronic levels of the rare-earth ion or to take into account the influence of the interaction of the electronic excitations with each other or with displacements of the ions. Similarly, we have been unable to explain the triplet shape of the absorption line by assuming a quasi-degeneracy greater than two for the ground state of the magnetic ions. Even if a number of improbable assumptions are made as to the structure of the corresponding states in order to achieve the right absorption line shape in a field directed along the C_2 axis, then when the field deviates from that direction the behavior of the absorption peaks will no longer correspond to that observed in experiment (in particular, additional absorption peaks should appear). Nevertheless, we cannot rule out the possible presence of low-lying states that for some reason are not manifested in observable absorption.

In the presence of a single isolated doublet of electronic states the possibility of formation of a triplet structure of the EPR spectrum by magnetic dipole and exchange interactions of the ions has been discussed by various authors.[3,14–17] There the Ising character and quasi-one-dimensionality of the interactions have been used. To apply that treatment to our crystal requires a more accurate description of the situation that exists in this case, taking into account the structural data and the results of our present measurements. To what we have said about the structure of $KTb(WO_4)_2$ above we add that the shortest distances between nearest Tb^{3+} ions of different chains are 7.57 and 6.07 Å for the same and adjacent basal planes, respectively, while the shortest distance within a chain is 4.07 Å. Therefore the interaction of each ion with its nearest neighbors in the chain should be much stronger than the other interactions, which corresponds to one of the conditions necessary for the interpretation considered. As to the second condition, the magnetic moment of the non-Kramers ions with one quasi-doublet of states is always parallel to the vector $\mathbf{g}$ from Eq. (2) (Ising ions). In a sufficiently high external field $[(\delta/\mu_B\mathbf{g}\cdot\mathbf{H})^2 \ll 1]$ a system of such ions becomes practically Ising. Consequently, the prerequisites for interpreting the absorption line shape in analogy with the discussion of Refs. 3 and 14–17 are met. The corresponding arguments are made below in a schematic form sufficient for understanding their application to the given crystal; the finer details can be found in the papers cited above.

First of all, it should be noted that if $\mu_B(\mathbf{g}\cdot\mathbf{H}) \gg \delta$, then Eq. (1) implies a linear dependence of the spectroscopic splitting on the field, with a g factor $g\cos\varphi$. This corresponds to the behavior of the middle absorption peak in Fig. 2 if it is assumed that the corresponding $\mathbf{g}$ vector is directed along the C_2 axis of the crystal, which is a local axis of symmetry for the Tb^{3+} ion (this, in particular, means that the states Φ_0 and Φ_1 of the doublet in Eq. (2) have the same parity with respect to C_2 rotations). The magnitude of this vector, which in this case determines the g factor of the spectral splitting at high field, can be estimated as $|\mathbf{g}| \approx 13.3 \pm 0.2$ (see Fig. 2). We assume that there are no other relevant electronic states of the rare-earth ion in this absorption. Let $\mathbf{m}$, with a single nonzero component m_z, be the restriction of the magnetic moment operator $-\mu_B g_J \mathbf{J}$ of the ion to the space generated by the doublet Φ_0, Φ_1,. The eigenstates of the operator m_z in this space have the form

$$\Phi_{00} = \frac{1}{\sqrt{2}}(\Phi_0 + i\Phi_1), \quad \Phi_{01} = -\frac{1}{\sqrt{2}}(\Phi_0 - i\Phi_1), \tag{3}$$

with eigenvalues $-\mu, \mu$ respectively, where

$$\mu = \frac{1}{2}\mu_B g \quad \left(\boldsymbol{\mu} \equiv \frac{1}{2}\mu_B \mathbf{g}\right), \quad \mu = 6.65\mu_B (g = 13.3); \tag{4}$$

and μ is the maximum possible value of the magnetic moment of the ion, the "saturation moment," if one is taking into account only the states of the given doublet. As usual,[8,9] we introduce for each ion f the "pseudospin" operators $S_{f,x}, S_{f,y}, S_{f,z}$, defining them in the basis (3) by the standard matrix elements of the angular momentum operators with S

$=1/2$, assuming S_z is diagonal and that $(\Phi_{00}, S_z\Phi_{00})=-1/2$. Then the Hamiltonian H_f of the crystalline field and Zeeman interaction with the magnetic field and the magnetic moment operator $\mathbf{m}_f$ for the fth ion will have the form

$$\hat{H}_f = \delta S_{f,x} - \mathbf{H}\cdot\mathbf{m} = \delta S_{f,x} + \mu_B \mathbf{H}\cdot\mathbf{g} S_{f,z},$$

$$\mathbf{m}_f = -\mu_B \mathbf{g} S_{f,z} = -2\boldsymbol{\mu} S_{f,z}. \quad (5)$$

We emphasize that the operators $S_{x,y,z}$ are not components of a vector, and the indices x, y, z in their notation do not refer to the spatial axes—they serve only to indicate the form of the matrix elements of these operators in the basis (3). A magnetic field leads to hybridization of the states Φ_0, Φ_1, so that the eigenstates of the Hamiltonian (5) will be

$$\Phi_0' = \Phi_0 \cos\frac{\eta}{2} + i\Phi_1 \sin\frac{\eta}{2},$$

$$\Phi_1' = -\Phi_0 \sin\frac{\eta}{2} + i\Phi_1 \cos\frac{\eta}{2}, \quad \tan\eta = \mu_B(\mathbf{g}\cdot\mathbf{H})/\delta \quad (6)$$

with the eigenvalues $\pm\omega/2$ (1). In fields $\mu_B \mathbf{g}\cdot\mathbf{H} \gg \delta$ the parameter $\eta \approx \pi/2$, and the wave functions (6) are close to eigenstates (3) of the commuting operators of the magnetic moment, Zeeman interaction, and S_z. It is in fields $\mu_B \mathbf{g}\cdot\mathbf{H} \gg \delta$ that the frequency-field curves in Fig. 2 pertain, and it is for such values of the field that the following discussion mainly relates (except for the low-frequency region of the spectrum).

The magnetic dipole and exchange interactions between ions are expressed in terms of the operators $m_{f,z}$ of the magnetic moment and are also diagonal in the basis of states (3). The total Hamiltonian of the system has the form

$$\hat{H} = \sum \hat{H}_f + V, \quad V = \frac{1}{2}\sum I_{f,g} S_{f,z} S_{g,z},$$

$$I = I_d + I_{\text{ex}}, \quad (7)$$

where the summation is over independently varying site indices f, g. Here the spin-spin interaction parameters I contain dipole I_d and exchange I_{ex} contributions, and the values of I_d can be obtained from the interaction energy W_d of two magnetic moments:

$$W_d = \frac{(\mathbf{m}_1\cdot\mathbf{m}_2)}{r^3} - 3\frac{(\mathbf{m}_1\cdot\mathbf{r})(\mathbf{m}_2\cdot\mathbf{r})}{r^5}, \quad (8)$$

using the expression for $\mathbf{m}$ from (5); $\mathbf{r}$ is the radius vector connecting the moments. For nearest neighbors in the chain $\mathbf{r}$ is almost orthogonal to the direction of the moments, making an angle of $\pi/2-\xi$ with them (see Sec. II), and therefore (8) leads to an antiferromagnetic (AFM) interaction, which for $r=4$ Å corresponds to a value of I_d equal to

$$I_d = \frac{4\mu^2}{r^3}(1 - 3\sin^2\xi), \quad I_d/k_B \approx 1.6 \text{ K}, \quad (9)$$

where k_B is Boltzmann's constant. The energy parameter in compounds of this type is usually of the same order. One can therefore assume that for frequencies 75–120 GHz (corresponding to excitation energies 3.8–6 K) the value of the magnetic field is sufficient for the ground configuration of the moments to be ferromagnetic, despite the AFM character of the nearest-neighbor interaction.

At the measurement temperatures part of the magnetic moments will be oriented counter to the field direction. An ion that absorbs a quantum of the rf field is found in a state with $\langle m_z\rangle = \mu > 0$ ($H_z > 0$). In this case there are three different types of states of the two neighbors nearest to it in the chain.

In the first case both ions are in the ground state and produce at the excited ion a localized dipole field H_d:

$$H_d = \frac{I_d}{2\mu} \approx 1.8 \text{ kOe}. \quad (10)$$

Because of the AFM character, this interaction partially compensates the external field; this corresponds to the highest-lying and most intense maximum on the absorption line at helium temperature.

In the second case both neighboring ions are excited and produce a field of the same magnitude but in the opposite direction, and that adds to the external field. This corresponds to the 3rd maximum of the low-field resonance absorption of the lowest intensity because of the low probability of such configurations at low temperatures (the mean density of flipped magnetic moments is small). In the third case only one neighbor is excited, and the local fields from neighboring ions therefore compensate each other. The frequency-field curve of the corresponding maximum for high fields is described by formula (1) and extrapolates to the origin of coordinates (the 2nd peak, Fig. 2). Since there are two such configurations (the left or right neighbor is excited), this mechanism is weaker than the first only at low temperatures. At high temperatures the probabilities of the different states equalize, and the fact that the number of configurations with zero local field at the absorbing ion is twice as large becomes important. Therefore the 2nd peak should become more intense. Such a transformation of the intensities of the peaks was observed qualitatively in the experiment (Fig. 5). We note that with decreasing frequency, when the Zeeman energy becomes less than the temperature, one again has many excited states, and again the 2nd line becomes the more intense (Fig. 3). However, at low frequencies the presence of a gap does not permit one to use the simple arguments and estimates given above, since in this magnetic field region the difference from the Ising model becomes substantial. Therefore the causes of the variation of the intensity ratio here can be different.

The observed difference of the resonance fields for the 1st and 2nd peaks in the direction $\mathbf{H}\|b$ (Fig. 2) is approximately $H_l = 2.8$ kOe. The greater part of this quantity, according to what we have said, can be attributed to the local dipole field in the ground configuration of the neighboring moments along the chain, $H_d \approx 1.8$ kOe [Eq. (10)]. The remaining part can be ascribed to the AFM exchange interaction, assuming $H_{\text{ex}} \approx 1.0$ kOe. This interaction is naturally assumed to be nonzero only for nearest neighbors along the chain. The given interpretation of the interval H_l between resonance fields allows us to estimate the interaction parameter I of the nearest ions in the chain:

$$I/k_B = 2H_l\mu/k_B \approx 2.5 \text{ K}, \tag{11}$$

which is made up of the dipole parameter (9) and the exchange parameter

$$I_{ex}/k_B \approx 0.9 \text{ K}. \tag{12}$$

The possible local dipole fields from the remaining ions correspond to the observed width of the peaks, and the demagnetizing and Lorenz–Lorentz fields have no effect on the interval between components. Furthermore, they are to a large degree compensated in the samples used in the measurements, so that the corresponding corrections lie within the error limits of the measurements of the positions of the absorption peaks.

Low-frequency dynamics. Estimate of the gap

In the low field region, where a reorganization of the magnetic state occurs, as we have said, the interpretation of the results is complicated considerably. The two initial splittings observed in the experiment are most likely due to the existence of short-range order at $H=0$. It can be assumed that this short-range order appears at least in clusters consisting of the triples of neighboring magnetic ions of the chains which were discussed above. The agreement of the frequency-field curve of the 2nd absorption peak with formula (1) to frequencies $\approx$30 GHz suggests that, because of the rather high temperature, a high probability of configurations of magnetic moments with zero local field at the absorbing ion is preserved even at $H \to 0$. One can then use formula (1) all the way to zero field and make an estimate of the value of the gap from the initial splitting of the 2nd peak, which gives

$$\delta/k_B \approx (1 \pm 0.2)\text{K}. \tag{13}$$

In the spectrum of the cluster indicated above, there is always a transition with an energy exactly equal to the gap energy δ, even when the dipole interaction of the end ions of the cluster is taken into account. Importantly, the presence of the gap leads to an additional repulsion of the energy levels in comparison with the pure Ising model. A numerical calculation of the spectrum of the three-site cluster of the chain for the parameters determined above and $H=0$ gives the following energy levels (with the dipole interaction of the end ions taken into account):

$$1.90,\ 1.56;\ 0.45,\ 0.13;\ -0.15,\ -0.55;\ -1.48,\ -1.86(\text{K}). \tag{14}$$

It is natural to assume that in reality in the paramagnetic state of a singlet magnet only transitions genetically related to a flip of the central moment of the cluster in the corresponding Ising model are observed upon the adiabatic turning on of the gap. It can be shown that they agree with the initial splittings observed. The highest-frequency transitions in the interval 3.76–3.04 K fall in the vicinity of the initial splitting of the 3rd absorption peak, the mean velocity corresponds to the initial splitting for the second peak (δ=1K), and the 1st maximum of the absorption line can presumably be extrapolated into the third group of low-frequency transitions (0.28–0.68 K). Of course, the true resonance frequencies should be found with the environment of the clusters at the given temperature taken into account in a self-consistent manner, with a determination of the relaxation times and oscillator strengths of the corresponding excitations (for example, in the Green's function method for calculating the dynamic susceptibility). It would also be desirable to do a more complete experimental study of the low-frequency dynamics of this crystal in the paramagnetic temperature region, since there the nontrivial properties inherent to a singlet magnet[8,9]—collective states of the cluster—can be realized.

Resonance absorption near the basal plane

Let us discuss the dependence of the positions of the absorption peaks on the direction of the field. For the 2nd peak formula (1) gives the dependence of the resonance field on the angle at a fixed frequency:

$$H = \frac{\sqrt{\omega^2 - \delta^2}}{\mu_B g \cos\varphi}. \tag{16}$$

For the 1st peak the local field $\mathbf{H}_l \| z$ shifts the resonance field by an amount

$$\Delta H = \frac{H_l}{\cos\varphi}. \tag{17}$$

Both relations describe the behavior of the lines poorly for angle $\varphi > 80°$, since they lead to unbounded growth of the resonance fields and of the interval between them for $\varphi \to \pi/2$ (the dashed curves in Fig. 7). This indicates the necessity of taking into account the transverse magnetic moment, which arises on account of high-lying excited states Φ_α of the odd type in second-order perturbation theory. Here the Hamiltonian (5) acquires additional terms, some of which commute with the Hamiltonian of the crystalline field and others with the Zeeman energy.[8] The energy levels of the ion take the form

$$E_0 = \varepsilon_0 - \frac{\omega}{2}, \quad E_1 = \varepsilon_0 + \frac{\omega}{2}, \quad \varepsilon_0 = -\frac{1}{4\Delta} G^s_{i,j} h_i h_j,$$

$$\omega = \sqrt{\delta^2 + (\mathbf{g}\cdot\mathbf{h})^2 + \frac{\delta}{2\Delta} G^a_{i,j} h_i h_j + \frac{1}{16\Delta^2}(G^a_{i,j} h_i h_j)^2 + \frac{1}{4\Delta^2}(G_{i,j} h_i h_j)^2}, \quad \mathbf{h} \equiv \mu_B \mathbf{H}. \tag{18}$$

Here a summation over repeated indices i,j is understood. The three tensors appearing in this expression, G^s, G^a, and G, are expressed by the formulas

$$G^{s,a}_{i,j} = \sum_\alpha \frac{1}{\delta_\alpha}(g^i_{0\alpha}g^i_{0\alpha} \pm g^i_{1\alpha}g^j_{1\alpha}),$$

$$G_{i,j} = \sum_\alpha \frac{1}{\delta_\alpha} g^i_{0\alpha}g^j_{1\alpha}, \quad \delta_\alpha = \frac{\Delta_\alpha}{\Delta}, \tag{19}$$

where Δ_α is the energy separating the ground doublet from the state α (we assume that $\Delta_{1\alpha} \approx \Delta_{0\alpha} = \Delta_\alpha$), and Δ is the minimum distance to the group of states being taken into account and is introduced for convenience in making estimates (here $\delta_\alpha \geqslant 1$). The vectors $\mathbf{g}_{k\alpha}$ ($k=0,1$ numbers the states of the ground doublet) are determined by formula (2) for the corresponding pairs of states.

In expression (18) the term of second order in the field under the square-root sign corresponds to the appearance of a transverse Van Vleck susceptibility. Analysis of the possible magnitudes of the transverse **g** vectors shows that they essentially cannot exceed six at a value of the g factor of the given quasi-doublet equal to 13.3. The spectrum (18) can be substantially anisotropic near the basal plane. For further estimates we restrict consideration to a certain direction. We shall assume in accordance with the experimental situation corresponding to Fig. 6 that the plane of rotation of the field intersects the basal plane along the x axis, which practically coincides with the c axis. In that case the components of the G tensors are conveniently represented in the form (we drop the index x)

$$|G^s| = 2g_s^2, \quad |G^\alpha| = g_a^2, \quad |G| = g_1^2. \tag{20}$$

where g_s, g_a, and g_1 have the typical values of transverse **g** vectors. In this notation formula (18) for the chosen plane of rotation of the field **H** takes the form (we assume for definiteness that $G^a \geqslant 0$)

$$E_0 = \varepsilon_0 - \frac{\omega}{2}, \quad E_1 = \varepsilon_0 + \frac{\omega}{2}, \quad \varepsilon_0 = -\frac{g_s^2}{4\Delta}h_x^2,$$

$$\omega = \sqrt{\delta^2 + g^2h_z^2 + \frac{\delta g_a^2}{2\Delta}h_x^2 + \frac{1}{4\Delta^2}\left(\frac{g_a^4}{4} + g_1^4\right)h_x^4},$$

$$\mathbf{h} = \mu_B\mathbf{H}. \tag{21}$$

Here we have dropped terms corresponding to the y components of the field **H**, since all of the transverse contributions are substantial only in the close vicinity of the basal plane, where the field is directed practically along the x axis. The system of notation adopted for the parameters allows us to stay within physically justified intervals of their values when approximating the experimental data by these formulas.

From Eq. (21) we obtain the dependence of the resonance field on the angle at a fixed frequency:

$$h = \sqrt{\frac{2(\omega^2 - \delta^2)}{q(\varphi) + \sqrt{q^2(\varphi) + p\sin^4\varphi}}},$$

$$q(\varphi) = g^2\cos^2\varphi + \frac{\delta}{2\Delta}g_a^2\sin^2\varphi,$$

$$p = \frac{\omega^2 - \delta^2}{\Delta^2}\left(\frac{g_a^4}{4} + g_1^4\right). \tag{22}$$

This relation describes the behavior of the 2nd peak (Fig. 7), which corresponds to the absence of local field at the absorbing ion (the angle φ_0 between the z axis and the plane of rotation of the field is taken into account by the substitution $\cos\varphi = \cos\varphi_0\cos\theta$; see Sec. II). For estimating the position of the 1st peak we replace the external field **H** in Eq. (21) by $\mathbf{H}+\mathbf{H}_l$, after which the local field $\mathbf{H}_l$ is determined self-consistently by the relations

$$H_{l,z} = \frac{I}{2\mu^2}\langle m_z\rangle, \quad \langle m_z\rangle = -\frac{\partial E_0}{\partial H_z} = \frac{1}{2\omega}\mu_B^2 g^2(H_z - H_{l,z}); \tag{23}$$

$$H_{l,x} = \frac{I}{2\mu^2}\langle m_x\rangle, \quad \langle m_x\rangle = -\frac{\partial E_0}{\partial H_x} = \frac{1}{2\Delta}\mu_B^2 g_s^2(H_x - H_{l,x}) + \frac{1}{2\omega}\left[\frac{\mu_B^2\delta g_a^2}{2\Delta}(H_x - H_{l,x}) + \frac{\mu_B^4}{2\Delta^2}\left(\frac{g_a^4}{4} + g_1^4\right)(H_x - H_{l,x})^3\right]. \tag{24}$$

In the first equations of the system (23) and (24) the local field is calculated from the specified average values of the magnetic moments $\langle\mathbf{m}\rangle$ in the ground state, which are determined by the second equation with the use of the expression for E_0 from (21). Taking the transverse magnetization into account leads to the situation that near the basal plane the magnetic moment of the ion begins rapidly to change its orientation and decrease in value. This leads to a sharp decrease of the local field and to the observed drawing together of the lines. The main part of this effect is due to the decrease of the z component of the magnetic moment, which varies from the large value μ to zero. Therefore, for a qualitative estimate we set $H_{l,x}=0$ in the effective field acting on the ion. In this approximation Eqs. (23) give

$$H_{l,z} = H_z I/(I+\omega). \tag{25}$$

Here the resonance field for the first line is expressed by formula (22) with g replaced by $g\omega/(I+\omega)$. The theoretical curves obtained are in qualitative agreement with the experimental dependences (Fig. 7) for the following values of the parameters:

$$\Delta = 35K, \quad g_a = 5, \quad g_1 = 4.7 (g = 13.3,\ I = 2.5\ \text{K},$$

$$\delta = 1\ \text{K},\ \nu = 76.33\ \text{GHz},\ \varphi_0 = 45^\circ.$$

These values of the parameters correspond to the largest value of the gap Δ for which we were able to construct a realization of states with the corresponding **g** vectors. On the side of low values the only limitation is the use of perturbation theory, so that the corresponding results convey only qualitatively the effects of the appearance of a transverse magnetic moment. The transverse component of the local field can be taken into account more exactly by a numerical calculation for concrete values of the parameters, and that will lead to splitting of the theoretical curves at $\varphi = 90^\circ$. We note that the absorption line shape depends strongly on the direction in the basal plane. In particular, such anisotropy can be introduced by a dipole interaction. When the external field is rotated in the direction of the chains, the dipole interaction

of the transverse Van Vleck moments becomes ferromagnetic, which, in a narrow range of angles, leads first to the merging and then to the opposite order of the lines. The difference of the pictures of the absorption observed at angles $\varphi \approx 89° - 90°$ may also be due to the aforementioned anisotropy of the G tensors.

It should be noted that there can be a contribution to the slowing of the growth of the resonance field from the magnetostriction due to the Zeeman interaction. In a certain interval of angle the z component of the magnetic moment remains close to maximal while the magnetic field has already acquired a large x component; this leads to a large torque. This leads to hybridization of the wave functions of the quasi-doublet with excited states of a different parity, altering the direction of the **g** vector and possibly its value by an amount proportional to the small value of the strain. Here the magnetic moment also deviates slightly from the direction of the C_2 axis, but for a given frequency as before it will reach close to the saturation value. Such a mechanism might to some degree explain the observed slowing of the growth of the resonance field, but it will not lead to a decrease of the distance between components of the doublet [see formula (17)]. It is important to emphasize the difference of the Van Vleck mechanism for the appearance of a transverse magnetic moment, considered above, from the magnetostriction effect that we are discussing now. The Van Vleck mechanism (hybridization of the states of the ground quasi-doublet with high-lying states by the magnetic field), by breaking the invariance with respect to time inversion, leads to a fundamentally different change of the wave functions of the ground quasi-doublet (which is also small, as in the case of deformations). From such states a superposition with an arbitrary direction of the magnetic moment can be formed. Of course, here the value of the saturation moment is highly anisotropic and in this case reaches a minimum for $\langle \mathbf{m} \rangle \perp C_2$. Therefore, obviously, it is the Van Vleck mechanism in the region of angles extremely close to the basal plane that explains both the drawing together and narrowing of the lines. These parameters of the spectrum are determined mainly by the magnetic dipole interactions, which become small because of a decrease of the magnetic moment of the ions. It is important to note that the described behavior of the magnetic moment should lead to a sharp decrease of the torque in that range of angles and, hence, of the corresponding magnetostrictive displacements of the ions.

Field-induced phase transition

Turning now to a discussion of the phase transition, we begin by noting that the temperature and Zeeman energy for which the phase transition was observed are substantially higher than the energy of interaction of the magnetic moments, and the latter can therefore be ignored in a discussion of the nature of the phase transition. Apparently the interaction of the electronic excitations in the doublet with the ionic displacements is apparently also unimportant for the phase transition in this case. It can be shown that for non-Kramers ions an appreciable value of such interactions would lead to a substantial transformation of the EPR line shape. Therefore, the observed phase transition can be due only to the Zeeman interaction, the magnetostriction, and the accompanying optical displacements of the ions. It should be noted that they occur only for field directions deviating from the basal plane by less than 1°, which makes it difficult to study their properties. From the foregoing discussion of the angular dependence of the spectrum we can conclude that immediately prior to the phase transition (in lower fields) the crystal has a small magnetic moment oriented in a direction close to the basal plane, and is therefore not subjected to strong mechanical stresses. This fact is due not only to the Van Vleck mechanism for the appearance of transverse magnetization discussed above (which can play the main role at low temperatures) but also to the temperature averaging over fluctuations of the magnetic moment. Meanwhile, it can be asserted that after the phase transition the magnetic moment of the crystal is rotated from the field direction and again becomes large, as was the case at angles $\varphi \approx 80°$, as is indicated by the partial destruction of the mounting of the sample after the phase transition. For brevity we shall call the low-field phase transverse (relative to the C_2 symmetry axis), while the phase arising after the phase transition will be called canted. An important mechanism of stabilization of the transverse phase is the strong dependence of the entropy on the orientation of the magnetic field,[8] which is manifested in the increase of the transition field with increasing temperature seen in Fig. 8. We note that, unlike the similar transition in $KEr(MoO_4)_2$, in the high-temperature region a sharp decrease of the hysteresis with increasing temperature is not observed. Preliminary estimates show that the mechanism of such a first-order transition can be due to the magnetostriction interaction. Here an important role should be played by the softening of some force constants of the lattice upon its deformation. Because of this it becomes possible for a local minimum to appear in the expression for the nonequilibrium free energy corresponding to the canted phase. The suppression of the phase transition by a firm gluing of the sample also points to a substantial role of the external strain in the mechanism of the phase transition. We shall not discuss the many features of this transition, since we are not yet able to reproduce them regularly in order to link them with certain conditions of the experiment. Therefore rather than prematurely proposing a specific model of this phase transition, we shall limit ourselves to a discussion of the main factors that we consider most essential for its nature.

IV. CONCLUSION

A study of the magnetic resonance spectrum of the crystal $KTb(WO_4)_2$ in the frequency interval 14–120 GHz and field range 0–70 kOe at helium temperature has shown that the line shape of the absorption of energy from the microwave field has a triplet structure. An interpretation using the known ideas about the formation of such a structure by dipole and exchange interactions of the closest ions in the chains has led us to the following conclusions.

1. A quasi-doublet is present in the lower part of the spectrum of the Tb^{3+} ion in the crystalline field of this com-

pound. The states of the doublet have the same parity with respect to C_2 rotations, corresponding to an orientation of the magnetic dipole moment of its transition along the C_2 axis of the crystal (which is its Ising axis, magnetic axis, and the direction of its maximum g factor). The maximum value of the g factor is $g=13.3\pm0.2$. The gap δ is estimated as $\delta=1\pm0.2$ K.

2. The magnetic subsystem of the crystal corresponding to the aforementioned doublet can be described by a singlet-singlet model with mainly AFM interactions. In the "pseudospin" representation ($S=1/2$) the Ising AFM interaction parameter of the nearest neighbors in the chain has a value $I\approx2.5$ K, while the "transverse field" is determined by the value of the gap $\delta\approx1$ K.

3. We believe that the spectrum of three-particle clusters (in zero external field) is manifested in the low-frequency dynamics of the system at a temperature several times greater than the nearest-neighbor interaction energy; this is of significant interest for further study.

4. The angular dependence of the spectrum demonstrates a substantial role of the Van Vleck transverse (relative to the C_2 axis) magnetization in the formation of the EPR spectrum in a transverse magnetic field. Hybridization of the states of the ground doublet leads to states of opposite parity. The presence of such states should be expected below 40 K. It is assumed that this hybridization can be important in the mechanism of the field-induced phase transition in the low-temperature region.

5. The observed first-order phase transition depends critically on the field direction, the deviation of which from the basal plane should be less than 1°. We assume that this is due to the magnetostrictive nature of that phase transition. The main factors in the mechanism of the transition should be: the magnetostriction due to the Zeeman interaction, the strong dependence of the entropy on the magnetic field direction, the softening of some of the force constants of the lattice upon the deformation, and also the transverse Van Vleck magnetic moment.

The authors thank V. S. Kurnosov for a helpful discussion of the results of this study.

[a)]E-mail: khatsko@ilt.kharkov.ua

[1]M. J. M. Leask, A. C. Tropper, and M. R. Wells, J. Phys. C: Solid State Phys. **14**, 3481 (1981).
[2]V. I. Kut'ko, M. I. Kobets, V. A. Pashchenko, and E. N. Khats'ko, Fiz. Nizk. Temp. **21**, 441 (1995) [Low Temp. Phys. **21**, 345 (1995)].
[3]E. N. Khats'ko, Yu. V. Pereverzev, M. I. Kobets, V. A. Pashchenko, and V. I. Kut'ko, Fiz. Nizk. Temp. **21**, 1061 (1995) [Low Temp. Phys. **21**, 816 (1995)].
[4]E. N. Khatsko, M. I. Kobets, V. I. Kutko, and V. Pashchenko, Ferroelectrics **175**, 73 (1996).
[5]E. N. Khatsko, M. I. Kobets and Ju. V. Pereverzev, Ferroelectrics **233**, 93 (1999).
[6]E. N. Khatsko, M. I. Kobets and Ju. V. Pereverzev, Bull. Magn. Reson. **19**, 56 (1999).
[7]E. N. Khatsko, M. I. Kobets, and V. A. Bagulja, Ukr. J. Phys. Optics **1**, 46 (2000).
[8]A. K. Zvezdin, V. M. Matveev, A. A. Mukhin, and A. I. Popov, *Rare-Earth Ions in Magnetically Ordered Crystals* [in Russian], Nauka, Moscow (1985).
[9]É. L. Nagaev, *Magnets with Composite Exchange Interactions* [in Russian], Nauka, Moscow (1988).
[10]V. I. Kut'ko and M. I. Kobets, Fiz. Nizk. Temp. **22**, 1447 (1996) [Low Temp. Phys. **22**, 1099 (1996)].
[11]M. I. Kobets, Fiz. Nizk. Temp. **26**, 96 (2000) [Low Temp. Phys. **26**, 72 (2000)].
[12]A. A. Evdokimov, V. A. Efremov, V. K. Trunov, I. A. Kleĭman, and B. F. Dzhurinskikh, *Compounds of Rare-Earth Elements: Molybdates, Tungstates* [in Russian], Nauka, Moscow (1991).
[13]S. V. Borisov and R. F. Klevtsova, Kristallografiya **13**, 517 (1968) [Sov. Phys. Crystallogr. **13**, 420 (1968)].
[14]A. Abragam and B. Bleaney, *Electron Paramagnetic Resonance of Transition Ions*, Clarendon Press, Oxford (1970), Russian transl. Vol. 1, Mir, Moscow (1972).
[15]A. M. Pshisukha, A. I. Zvyagin, and A. S. Chernyi, Fiz. Nizk. Temp. **2**, 339 (1976) [Sov. J. Low Temp. Phys. **2**, 170 (1976)].
[16]A. R. Kessel' and G. O. Berim, *Magnetic Resonance of Ising Magnets* [in Russian], Nauka, Moscow (1982).
[17]I. M. Krygin, A. D. Prokhorov, V. P. Dyakonov, M. T. Borowiec, and H. Szymczak, Fiz. Tverd. Tela (St. Petersburg) **45**, 1982 (2003) [Phys. Solid State **45**, 2083 (2003)].

Translated by Steve Torstveit

QUANTUM EFFECTS IN SEMICONDUCTORS AND INSULATORS

Experimental study of manifestations of resonance scattering of conduction electrons on transition-element impurities in mercury selenide

V. I. Okulov,[a] A. V. Gergert, T. E. Govorkova, A. V. Korolyov, A. T. Lonchakov, and L. D. Sabirzyanova

Institute of Metal Physics, Urals Branch of the Russian Academy of Sciences, ul. S. Kovaleveskoĭ 18, Ekaterinburg 620219, Russia

S. Yu. Paranchich, M. D. Andriyichuk, and V. P. Romanyuk

Chernovtsy National University, ul. Kotrsyubinskogo 2, Chernovtsy 58012, Ukraine
(Submitted December 31, 2004; resubmitted April 23, 2005)
Fiz. Nizk. Temp. **31**, 1143–1152 (October 2005)

An interpretation of the experimental data on the low-temperature conductivity and magnetic susceptibility of mercury selenide containing donor impurities of transition elements is developed on the basis of electron resonance scattering theory in the Friedel approach. Both existing data and results obtained in the present study, for solid solutions of chromium, cobalt, and gadolinium, are considered. The results of a fitting of the measured temperature dependence of the electron mobility in HgSe:Cr crystals and concentration dependence of the Curie constant in the impurity magnetic susceptibility of HgSe:Co crystals are analyzed to obtain quantitative confirmation of the idea that resonance donor levels of the impurities chromium and cobalt are present in the conduction band of the respective crystals. The resonance level widths are determined and are found to be an order of magnitude larger than those of iron. It is shown that the observed concentration maximum of the electron mobility in mercury selenide containing gadolinium impurities can be explained on the basis of resonance scattering theory, although the existing data are insufficient for justification of such an explanation of the origin of that maximum. © *2005 American Institute of Physics*. [DOI: 10.1063/1.2128076]

INTRODUCTION

Impurities of transition elements in narrow-gap and gapless semiconductors can form resonance energy levels in the conduction band of the host crystal. Electronic states with energies near such levels are hybridized, i.e., they have an electron density that contains both the uniform contribution of the conducting states and a nonuniform part reflecting the localization at the impurity centers. In low temperature limit these levels are donor levels in the ground state, since the electrons occupying them are unified with the system of conductivity electrons of the host. A theoretical description of the hybridization of the donor states can be given on the basis of the quantum theory of resonance scattering. If an impurity energy level corresponds to not to a resonance level but to a bound state, then this means the absence of hybridization, and then the donor electrons appear in inelastic processes of thermal ionization, while at low temperatures they remain after the crystal is prepared. In such a case the impurity levels belong to individual impurities and are either vacant or occupied, while the resonance level belongs to the whole crystal and is filled to some fraction that corresponds to the same electron density for all of the impurities.

Among the semiconductor materials in which the effects of donor energy levels in the conduction band have been observed, the gapless semiconductor mercury selenide containing iron impurities is a well-known example. The main effects among those mentioned—stabilization of the density of conduction electrons when the Fermi energy reaches the donor level and a maximum of the electron mobility as a function of the impurity concentration—have been studied in detail. As was recently shown in Refs. 1 and 2, these effects are predicted by resonance scattering theory. The available experimental data are well described by this theory, are as the data on the concentration dependence of the Curie constant in the spin magnetic susceptibility of localized resonance states.[3] Previously other approaches have been used for interpretation of the mobility maximum, in particular, the Anderson model,[4,5] in which the impurity energy levels are also treated as resonance levels. However, there has been especially widespread adoption of the concepts of the iron ions in mercury selenide as donor impurities with bound states. In a model based on those concepts[6] it was assumed that as the donor concentration is increased after the Fermi energy reaches the energy of the impurity level there are both impurities that do and impurities that do not give up an electron to the conduction band (Fe^{3+} and Fe^{2+} ions). Under this assumption the observed growth of the mobility is explained by assuming that the positions of the ionized impurities (the Fe^{3+} ions), in spite of their low concentration, are in some manner ordered. A discussion of the experimental data on the basis of this model has been given in a number of papers, which have been reviewed in Refs. 7 and 8. However, the initial assumptions of this model are hard to justify, since they reduce to the requirement of the complete absence of hybridization of the donor impurity energy level with states of the conduction band. A bound state is fundamentally dif-

ferent from a hybridized state, and even a little (in some respect or other) hybridization with the conduction band is incompatible with the existence in the ground state of ionized and un-ionized levels with the same energy. The choice of the bound-state model by a number of authors for interpreting effects due to the influence of iron impurities on the electron mobility in mercury selenide, one supposes, was a reflection of the existing ideas that the growth of the mobility with increasing impurity concentration cannot be explained on the basis of resonance scattering theory. It was shown in Refs. 1 and 2 on the basis of the approach developed by Friedel[9] for donor states that those ideas are wrong, and the observed regularities can indeed be explained simply with the aid of resonance scattering theory (and thereby with hybridization taken into account). On the other hand, an experiment was recently done to test directly the applicability of the bound-state model for iron ions in mercury selenide.[10] An analysis of the concentration dependence of the x-ray absorption spectra on iron ions established that the observed dependence differs substantially from that predicted by the bound-state model and corresponds to significant hybridization of the impurity states with the conduction band. Thus studies of mercury selenide containing iron impurities have shown the possibility and desirability of applying electron resonance scattering theory for the description of effects in which the energy levels of transition-element donor impurities are manifested in the properties of the electron system.

The present paper is devoted to an analysis of the experimental data on the electron mobility and magnetic susceptibility of mercury selenide containing impurities of chromium, cobalt, and gadolinium. The observed relationships attesting to the existence of resonance donor states in these systems are discussed on the basis of the theory developed in Refs. 1 and 2. It should be noted here that for the systems with chromium and cobalt there is a large body of data that has been published in Refs. 11–19. Together with those data we shall discuss our new results on the temperature dependence of the electron mobility in systems containing chromium and the concentration dependence of the Curie constant in the spin susceptibility of the resonance state on cobalt impurities. As to the mercury selenide with gadolinium impurity, we have apparently obtained the first data on the concentration maximum of the mobility and we shall discuss its nature only tentatively, demonstrating the capabilities of the theory while at the same time keeping in mind that further studies will be needed to reach any justified conclusions.

MAIN RESULTS OF THE THEORY OF RESONANCE SCATTERING EFFECTS

Let us start by listing the theoretical results that we have used for describing the experimental data.

1. Consider the states of electrons with energies ε in the conduction band of a semiconductor crystal. We denote the density of states of the conduction electrons with a given energy by $g_e(\varepsilon)$. Suppose we have donor impurity centers with concentration n_i. If the donor states are bound, then the electrons are found in the energy levels of the impurities and pass into the conduction band in inelastic ionization processes. Consider another situation, when the donor energy level is found in the conduction band above the level of filling of the other donors by electrons and there is a certain narrow energy interval corresponding to it in which the impurity states are hybridized with states of the conduction band. This means that to each state in this energy interval there corresponds both a delocalized part of the electron density, describing the free motion, and a localized part concentrated near the impurity centers. In this case the impurity energy level does not have the same meaning as for a bound state but it represents a resonance energy for the scattering of a conduction electron. A rigorous description of such a situation is given by the quantum theory of resonance scattering. In the framework of that theory one obtains the following expression for the electron density of states $g(\varepsilon)$ in the resonance interval:

$$g(\varepsilon) = g_e(\varepsilon) + n_i g_i(\varepsilon). \tag{1}$$

The second term describes the contribution of the localized electron density and is nonzero only in the interval $\varepsilon_r - \Gamma < \varepsilon < \varepsilon_r + \Gamma$ around the resonance energy ε_r. The parameter Γ and the complete expression for $g_i(\varepsilon)$ are determined in Ref. 1. The integral of the function $g_i(\varepsilon)$ over the whole resonance interval is equal to ν, the number of localized states that can be occupied by electrons at one impurity center:

$$\nu = \int d\varepsilon\, g_i(\varepsilon). \tag{2}$$

The value of ν is assumed equal to the number of donor electrons from each impurity, so that $n_d = \nu n_i$ is the density of donor electrons. By this condition the resonance scattering center is defined as a donor impurity that gives up ν electrons to the general collective, which is distributed over the states of the conduction band and hybridized states. We note that the number ν is specified by Eq. (2), starting from the filling of the states in the impurity atom, and generally speaking does not coincide with the degree of degeneracy of the resonance level which is used in scattering theory. This noncoincidence, which is important in the present study, was ignored in Ref. 1 in order to simplify the theoretical derivations, and a complete formulation is given in Ref. 20. Based on the existing ideas, we assume that the impurities of certain transition elements (e.g., iron and cobalt) can to a first approximation have the same resonance energies and differ specifically by the degree of occupation (valence) ν. For a resonance level of iron impurities, according to the existing data, it is customary to take $\nu = 1$.

One can use formula (1) to find the Fermi energy of the donor electrons. However, it must be taken into account that the crystal can contain not only the electrons from the donors under consideration but also native electrons with a density n_{0e} and Fermi energy ε_0. Then to determine the total Fermi energy ε_F one must find the number of occupied states by integrating the right-hand side of Eq. (1) from ε_0 to ε_F and then equate the expression obtained to the donor electron density n_d determined above. If the Fermi energy is less than $\varepsilon_r - \Gamma$, then it is determined by the simple equation

$$n_e(\varepsilon_F) = n_{0e} + n_d, \quad \varepsilon_F < \varepsilon_r - \Gamma, \tag{3}$$

where $n_e(\varepsilon_f)$ is the density of conduction electrons. With increasing donor concentration, after the resonance interval is reached, Eq. 3 is replaced by the following:

$$n_d z(\varepsilon_F) + n_e(\varepsilon_F) - n_{0e} = n_d, \quad \varepsilon_F > \varepsilon_r - \Gamma, \tag{4}$$

where $z(\varepsilon)$ is the relative occupation of the localized states, determined as the integral of the function $g_i(\varepsilon)/\nu$. Equation (2) reduces to the form $z(\varepsilon_r+\Gamma)=1$, so that it follows from Eq. (4) that the Fermi energy cannot reach the upper boundary of the resonance interval $\varepsilon_r+\Gamma$ at a nonzero density of conduction electrons. This fact is obvious, since complete occupation of the localized states corresponds to the absence of donor electrons. Thus, with increasing impurity concentration the value of the Fermi energy stabilizes in a narrow interval near the resonance energy; this is the well-known "snagging" effect. The conduction electron density also stabilizes in the interval from $n_e(\varepsilon_r-\Gamma)$ to $n_e(\varepsilon_r+\Gamma)$. In calculating the Fermi energy one can take $n_e(\varepsilon_F)\approx n_e(\varepsilon_r)$ and introduce the constant $n_0=n_e(\varepsilon_r)=n_{0e}$, so that Eq. (4) becomes

$$z(\varepsilon_F) = 1 - n_0/n_d. \tag{5}$$

This equation has a simple meaning and requires the coincidence of two expressions for the spectrum occupation of the localized states in the ground state. The resonance value of the density n_d corresponds to equality of the relative occupations of the localized and delocalized states and is equal to $2n_0$. In the vicinity of the resonance one can obtain a simple formula for the Fermi energy using the expression for $z(\varepsilon)$ given in Ref. 1:

$$z(\varepsilon) = \frac{1}{2} + \frac{1}{\pi}\arctan((\varepsilon-\varepsilon_r)/\Delta) + \left[\frac{1}{2} - \frac{1}{\pi}\arctan(\Gamma/\Delta)\right] \times(\varepsilon-\varepsilon_r)/\Gamma, \tag{6}$$

where Δ is the resonance width, which is much less than the width of the resonance interval Γ. This formula has the form

$$\varepsilon_F = \varepsilon_r + \Delta\cot(\pi n_0/n_d). \tag{7}$$

It is valid when the difference $\varepsilon_F-\varepsilon_r$ does not exceed Δ in order of magnitude.

Near the boundary of the resonance interval the difference $\varepsilon_r+\Gamma-\varepsilon_F$ is proportional to $\Gamma(n_0/n_d)$. The dependence of the conduction electron density on n_d corresponding to formula (7) is obtained as follows:

$$n_e(\varepsilon_F) \approx n_0[1+(\varepsilon_F-\varepsilon_r)/\Delta_e] = n_0[1+(\Delta/\Delta_e)\cot(\pi n_0/n_d)]. \tag{8}$$

The first expression here is a series expansion around the resonance energy, the parameter Δ_e being much greater than Δ.

2. Let us now discuss the concentration dependence of the electron mobility in the ground state, first on the basis of perturbation theory (the Born approximation) for scattering on a charged impurity. If the Fermi energy is found in the resonance interval, then a substantial role is played by scattering on charged donor impurities. Its contribution to the mobility in the first Born approximation is inversely proportional to the square of the effective charge of the impurity. It is not hard to see that the value of that charge is proportional to $1-z(\varepsilon_F)=n_0/n_d$, the fraction of the total charge of the conduction electrons due to an individual impurity. With increasing impurity concentration the effective charge of an individual impurity falls off, and scattering on neutral impurities, which can be described by an additive contribution to the scattering probability, becomes important. Thus the concentration dependence of the mobility is described by the formula

$$\mu = \mu_0(\pi n_0/n_d)[\alpha + (\pi n_0/n_d)^2]^{-1}, \tag{9}$$

where μ_0 is independent of concentration, the constant α describes the contribution of scattering on neutral impurities, and the coefficient π is introduced to simplify the form of the subsequential generalization. This formula, which is valid at small n_0/n_d and α, describes the concentration maximum of the mobility. It was for just such an explanation that it was introduced in Ref. 21, where it was demonstrated on the basis of scattering theory that it is possible for the mobility to increase with increasing impurity concentration. According to the widely held belief, resonance scattering actually does lead to a decrease of mobility, but at lower impurity concentrations, when perturbation theory is inapplicable for calculating the scattering probability. In such a case the following formula for the mobility is valid:

$$\mu = \mu_0(\pi n_0/n_d)[\alpha + \sin^2(\pi n_0/n_d)]^{-1}, \tag{10}$$

the derivation of which is given in Ref. 1. It looks like the result of a simple generalization of formula (9) and goes over to it when the argument of the sine is small. The mobility is minimum for the resonance concentration of n_d, equal to $2n_0$. However, the concentration minimum of the mobility is strongly smeared, and under real conditions it is hard to separate out from the nonresonance behavior. With increase impurity concentration above the resonance the mobility increases and then falls, approaching a value $\mu_0 n_0/n_d\alpha$ which corresponds to scattering on nonresonance impurities. The maximum that arises is well manifested by virtue of the smallness of α, which is a natural property of nonresonance impurities.

3. Let us give the formulas describing the temperature dependence of the electron mobility for the case when the Fermi energy is found in the resonance interval. We consider the region of comparatively low temperatures, where the temperature dependence of the Fermi energy (the chemical potential), which is determined on a much larger scale than the resonance parameters, is unimportant. Then the temperature-dependent electron mobility $\mu(T)$ in the presence of resonance scattering is described by the formula

$$\mu(T) = \mu_0(\pi n_0/n_d)\int d\varepsilon[-f'(\varepsilon)]\{\alpha+\sin^2[\pi z(\varepsilon)-\varphi]\}^{-1}, \tag{11}$$

where $f'(\varepsilon)$ is the derivative of the Fermi function, φ is the phase, which reflects the role of the difference of the transport scattering cross section from the total one, the function $z(\varepsilon)$ is given by formula (6), and the limits of integration $\varepsilon_r\pm\Gamma$ are determined by the resonance interval. It is easy to see the simple relationship of formula (11) to formula (10), which for $T=0$ pertains to the case of a small difference $\varepsilon_F-\varepsilon_r$, when Eq. (7) is valid and the phase φ can be neglected. In these same approximations formula (11) can be transformed to

$$\mu(T) = \mu_0(x/\alpha)\int dE[-f'(E)][1-F^{-1}(E,x)], \tag{12}$$

$$x = \frac{\pi n_0}{n_d}; \quad f'(E) = \frac{1}{T}\frac{\exp(E/T)}{[\exp(E/T)+1]^2},$$

$$F(E,x) = 1 + \alpha + \alpha(E/\Delta + \cot x)^2.$$

The limits of integration can be assumed equal to $\pm\Gamma$, but one must bear in mind the restriction that arose in obtaining the integrand under the assumptions that the temperature (measured in energy units) is not large compared to Δ. Expression (12) has a comparatively transparent form and shows that the mobility $\mu(T)$ varies weakly at low temperatures up to a certain boundary value and then falls off with further increase in temperature. The scale of the boundary temperature is determined by the value of Δ and also depends on the relationship between x^2 and α, on account of the concentration maximum of the mobility at $x^2 \approx \alpha$.

4. Localization of the electron density in resonance donor states leads to the existence of a strongly temperature-dependent contribution χ_d to the spin magnetic susceptibility. As a starting point for its description one can use the well-known formula for the electron spin susceptibility which contains the density of states $n_i g_i(\varepsilon) = n_d z'(\varepsilon)$. We consider a region of relatively high temperatures $T \gg \Delta$ but where the condition of strong degeneracy $T \ll \varepsilon_F$ still holds. A simple formula for the susceptibility in this region, in neglect of the contribution of the exchange interaction of the electrons, has the form[1,3]

$$\chi_d = \mu_e^2(n_i - n_0)/T. \tag{13}$$

This formula pertains to the case of a single electron at a donor resonance level ($\nu = 1$) and is valid for small $z(\varepsilon_F)$, i.e., at impurity concentrations close to n_0 if in this formula we take the effective magnetic moment μ_e equal to the Bohr magneton μ_B, we obtain an expression for the spin susceptibility of $(n_i - n_0)$ atoms with a single valence electron in the case of zero spin of the ion core. In Ref. 3 it was proposed to take the spin of the ion core into account phenomenologically with the aid of a suitably formulated expression for μ_e^2. The result of such an approach can be obtained even without the simplifying assumption of small $n_i - n_0$. For this one should generalize Eq. (5) to the case of finite temperatures and find the correction linear in the temperature to the Fermi energy. The expression for the magnetic susceptibility χ_d of resonance donor states obtained with this correction taken into account describes the concentration dependence in the case when the set of resonance states does not have an intrinsic magnetic moment. In this case the contribution of the resonance states to the susceptibility remains constant as the concentration increases, and the contribution of the ion cores is dominant. In the more relevant case the resonance states do have a localized moment, and in the limit of high concentrations its contribution to the susceptibility, together with the contribution χ_{i0} of the ion cores, forms an expression for the susceptibility that corresponds to a set of impurity spins with occupied donor shells. For this case the formula for the total spin susceptibility χ_i of the donor impurities at concentrations substantially higher than the resonance concentration has the form

$$\chi_i = \chi_{i0} + \chi_d = [\mu_{i0}^2 n_0 + \mu_i^2(n_d - n_0)]/T. \tag{14}$$

If we introduce the spins corresponding to the magnetic moments μ_{i0} and μ_i of the ion core and of an impurity ion with an occupied resonance level, respectively, then we obtain from this formula an expression for the Curie constant $C = \chi_i T$:

$$C = a(S_{i0})n_d + a(S_i)(n_d - n_0), \tag{15}$$

where $a(S) = 4\mu_B^2 S(S+1)/3k$, and k is Boltzmann's constant. This expression was used in Refs. 3 and 21. As a resonance scattering effect it reflects the donor character of the magnetic impurity, which leads to dependence on the energy of the resonance level (the value of n_0) and on the degree of its occupation (the differences of the values of the spins S_{i0} and S_i).

Thus the set of resonance effects mentioned above includes four such effects: the approach of the conduction electron density to a constant value with increasing donor concentration, a concentration maximum of the electron mobility, and certain anomalies of the temperature dependence of the electron mobility and concentration dependence of the Curie constant. These theoretical predictions were adopted by us as a basis for interpreting the experimental data on the electron mobility and magnetic susceptibility obtained for mercury selenide containing transition-element impurities.

GENERAL DISCUSSION OF THE EXPERIMENTAL ARRANGEMENTS

The theoretical results presented above were used for interpretation of experimental data on the manifestations of resonance donor impurities of transition elements in the electron mobility and magnetic susceptibility of a semiconductor with an isotropic dispersion relation of the conduction electrons. As we mentioned in the Introduction, our goal was to investigate systems based on mercury selenide, in which the approximation of an isotropic spectrum is applicable. An analysis of the data obtained on crystals containing iron impurities was given in Refs. 2 and 3. For these well-studied systems the applicability of the theory developed could be reliably established, and by approximating the experimental dependences by the theoretical one we were able to determine the parameters characterizing the resonance scattering. In systems containing other impurities the situation is much more complicated. It is scarcely possible to state with complete certainty that for any of them the problems of the very existence and the position of the resonance energy level have been solved. There are practically no quantitative data on the resonance parameters. In connection with this in the initial stage of applying the theory to such systems we have attempted to analyze on a quantitative level only those experimental dependences that appear suitable for such an analysis at the given time. But we must first stress the following. According to the existing ideas, transition-element impurities in gapless semiconductors form *d*-type electron energy levels near the edge of the conduction band. If we regard it as established for the systems under study that such a donor energy level exists in the conduction band, then the experimental data can be explained on a qualitative level without any contradictions by the theory set forth above. This can also be said for the data which we obtained on systems con-

taining chromium and cobalt in experiments carried out as a continuation of previous studies for which the results were published in Refs. 11–13. However, we deem it advisable to focus attention on establishing the very existence of resonances as the main problem that needs to be solved. The conclusions and estimates given in the papers cited are largely of a qualitative character, since they were obtained in the absence of the necessary quantitative information and without comparison to the theoretical predictions. Essentially the available data on the first resonance effect—the transition to stabilization of the donor electron density—are still too indefinite. The data are likewise insufficient to conclude that a concentration maximum of the electron mobility exists in systems containing cobalt and chromium. The concentration dependence of the Curie constant has apparently escaped study. In such a situation it is advisable to adopt the line of attack described above, as we have done.

TEMPERATURE DEPENDENCE OF THE ELECTRON MOBILITY IN MERCURY SELENIDE CONTAINING CHROMIUM IMPURITIES

Relevant data on the properties of mercury selenide containing chromium impurities for the problem addressed here are given in Refs. 11 and 18. We shall not discuss here the existing results on the Shubnikov–de Haas oscillations and the electron paramagnetic resonance, since they require a separate investigation, and we shall also omit a discussion of the structural aspects of the properties of such systems. In considering the results on the electronic properties we should note once again that in crystals containing chromium impurities it has not been possible to observe any dependence of the density of conduction electrons on the impurity concentration. The measured electron density in the samples studied is practically the same within the error limits of its determination, so that the donor character of chromium impurities in it is not directly manifested. The concentration dependence of the electron mobility has shown evidence of the presence of a maximum: an anomalously elevated value of the mobility was observed for one or two compositions, but a set of data sufficient for quantitative approximation has not be obtained. In the temperature dependence of the magnetic susceptibility of systems containing chromium impurities in the relevant concentration interval an impurity contribution has not been reliably distinguished. At the same time, the character of the temperature dependence of the electron mobility is similar to that observed in systems containing iron impurities. Therefore, after an analysis of the existing data we chose to use the temperature dependence of the mobility for quantitative fitting of the theoretical results. The experimental work was essentially a continuation of the research reported in Ref. 11. Here careful measurements were made in a large volume, and therefore certain data have been refined and corrected. The samples were prepared by the same technique. The measurements of the electrical resistance and Hall coefficient were made on a Quantum Design PPMS-9 unit at the Magnetometry Center of the Institute of Metal Physics of the Urals Branch of the Russian Academy of Sciences. The results for the temperature dependence of the Hall mobility in samples of three compositions in the interval from 2 to 140 K are presented in Fig. 1. A comparison of these results

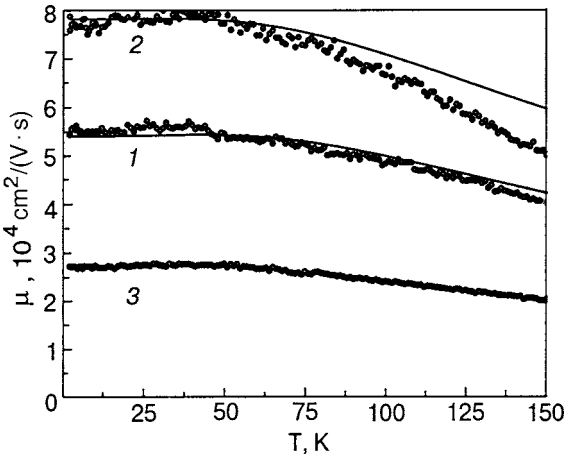

FIG. 1. Temperature dependence of the electron mobility in mercury selenide containing chromium impurities at different concentrations n_i, cm^{-3}: 1×10^{18} (*1*), 1×10^{19} (*2*), 1×10^{20} (*3*). The fitted curves are plotted according to formula (12) with the parameters $\Delta=90$ K, $n_0/\nu=4\times10^{16}$ cm^{-3}, $\alpha=0.001$, $\mu_0=0.7\times10^4$ $cm^2/(V\cdot s)$.

with the data of Ref. 22 on the temperature dependence of the resistivity of mercury selenide suggests that the features observed in this temperature interval are due not to electron–phonon scattering but to effects of electron–impurity scattering. The temperature dependence of the electron mobility obtained in Ref. 22 for crystals with uncontrolled impurities and with a substantially different number of conduction electrons was similar to that obtained by us. We interpret our results on the basis of the assumption that the chromium impurities have a donor character and that a corresponding resonance level exists in the conduction band of mercury selenide. Since the mobility at an impurity concentration of 1×10^{19} cm^{-3} turned out to be higher than at smaller and larger concentrations, that composition can be assumed to correspond to the vicinity of the mobility maximum. In this conjecture we assume that the compositions with impurity concentrations of 1×10^{19} cm^{-3} and 1×10^{18} cm^{-3} belong to the resonance interval and that the combination for these concentrations is described by formula (12). The curves obtained by fitting the two temperature dependences of the Hall mobilities according to this formula are also given in Fig. 1. Such a fitting allowed us to find the values of the resonance parameters rather unambiguously, with an error of not more than 10%.

The value obtained for the width of the resonance energy level of the chromium impurity, $\Delta=90$ K, is an order of magnitude larger than for the iron impurity. Accordingly, the applicability of formula (12) (the fitting curves) is restricted to temperatures not much over 100 K.

We also note that the agreement of the fitted curve with the experimental dependence at a concentration of 1×10^{19} cm^{-3} can be improved with allowance for the temperature correction to the Fermi energy (chemical potential), but for simplicity this was skipped without introducing substantial error in the parameters determined.

The fitting gives a value of the parameter $x=\pi n_0/\nu n_i$ close to 0.1 at a concentration $n_i=1\times10^{18}$ cm^{-3}. Here the measured value of the conduction electron density $n_e(\varepsilon_F)$ is close to 1×10^{18} cm^{-3} in a wide interval of impurity concentrations ($10^{18}-10^{21}$ cm^{-3}), while the concentration n_{0e} ac-

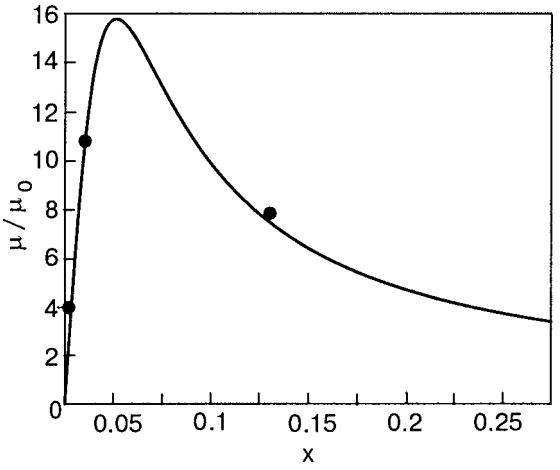

FIG. 2. Relative electron mobility in mercury selenide containing chromium impurities as a function of the relative inverse concentration of impurities (the parameter x), calculated using the parameters obtained by the fitting of the curves in Fig. 1, at a temperature of 4 K. The points denote the values of the mobility belonging to the curves in Fig. 1.

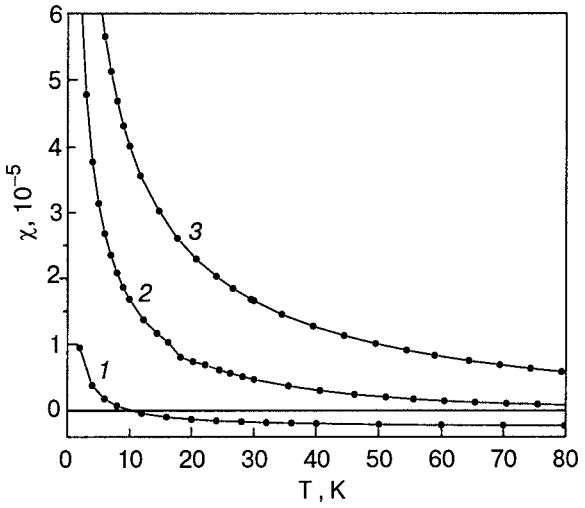

FIG. 3. Temperature dependence of the magnetic susceptibility of mercury selenide containing cobalt for different concentrations n_i, cm^{-3}: 7×10^{18} cm^{-3} (*1*); 5×10^{19} (*2*); 2×10^{20} (*3*).

cording to estimates is several times 10^{17} cm^{-3}. Thus one can assume that in the crystals studied the concentration n_0 is equal in order of magnitude to 10^{17} cm^{-3}, the energy of the donor level is close to the Fermi energy of the native electrons, and, according to an estimate from the concentration $n_e(\varepsilon_F)$, equals 0.07 eV. The ionization state ν of the donors could not be determined reliably but is probably equal to 2 or 3.

The value obtain for the parameter α turned out to be more than an order of magnitude lower than that found for the iron impurities. This is reflected in the wider concentration interval in which resonance scattering of conduction electrons on chromium impurities plays a role, the lower value of the maximum mobility, and the comparatively large values of the nonresonance mobility. Figure 2 shows the curve describing the predicted concentration maximum of the electron mobility as a function for x at the value of α obtained. Besides the values used in the fitting, the point corresponding to the mobility at an impurity concentration of 10^{20} cm^{-3} also falls on this curve.

On the whole, the proposed quantitative interpretation of the temperature dependence of the electron mobility of mercury selenide crystals containing chromium impurities confirmed the possible existence of a resonance energy level of chromium donors and permitted determination of the main resonance parameters.

CONCENTRATION DEPENDENCE OF THE CURIE CONSTANTS IN THE MAGNETIC SUSCEPTIBILITY OF MERCURY SELENIDE CHARACTERIZING COBALT IMPURITIES

The electron mobility in mercury selenide crystals containing cobalt impurities was investigated in Refs. 12, 13, 15, and 19. The temperature dependence of the mobility obtained in Ref. 15 has the same form as in the systems containing iron and chromium, and it could be approximated by a theoretical curve in the same way as described above for the system with chromium if pronounced growth of the mobility with increasing impurity concentration were observed in a certain interval. In the existing data one can discern some evidence of nonmonotonic behavior (presumably a maximum) in the dependence of the mobility on the impurity concentration. However, within the actual error limits for the concentration there is at present scarcely any reliable basis for concluding the observation of a growth of the mobility with increasing concentration in the system containing cobalt. In the systems with chromium data have been obtained for the concentrations between which growth of the mobility is observed within the error limits. Those data were used for the matched fitting and determination of the resonance parameters. For the system with cobalt such a fitting to the existing dependences for systems with cobalt gives value of the parameters that are less justified, since they were obtained in the absence of a matching element for the different dependences which is known to belong to the resonance region. Furthermore, one should note the results of Ref. 19, in which on the basis of an analysis of the data on the dependence of the electron density on pressure at a cobalt concentration of 5×10^{18} cm^{-3} it was shown that such a concentration most likely does not belong to the resonance region. Nevertheless there are insufficient grounds to assert that there is no resonance level of the cobalt impurities. It is therefore advisable to extract the existing information about the resonance from the observed dependences under the assumption that it does exist. Then one can assume that the estimate of the width of a possible resonance level as a quantity of the order of 100 K is valid, and the concentration n_0, according to the data on the Hall coefficient and the concentration of uncontrolled donors can be assumed to lie in the interval $(0.5-1.5)\times10^{18}$ cm^{-3}. Further substantial progress in obtaining data on a possible resonance state in systems containing cobalt can be achieved in an analysis of the temperature dependence of the magnetic susceptibility, which is completely analogous to that observed in systems with iron (Fig. 3). After separating out the paramagnetic impurity contribution we performed a fitting of the obtained concentration dependence of the Curie constant in this distribution according to formula (15). We considered different variants of the singly and doubly ionized donor impurities ($\nu=1$ and $\nu=2$). In the first case it is assumed that the spin of the ion core is

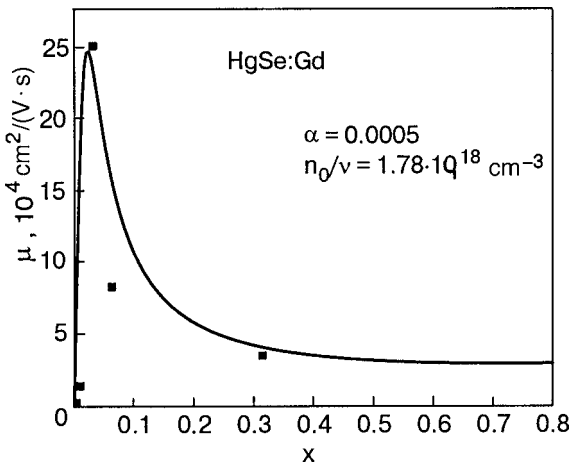

FIG. 4. Dependence of the electron mobility in mercury selenide containing gadolinium impurities on the relative inverse concentration of the impurities (the parameter $x = \pi n_0 / \nu n_i$); experimental (points) and theoretical (solid curve according to formula (9)).

equal to 5/2, and then one would expect that the spin of the un-ionized impurity is close to 2. For double ionization and the same spin of the core the expected spin of the impurity ion is close to 3/2. According to the results obtained, a variant of double ionization at a concentration n_0 close to 1.5×10^{18} cm^{-3} is considerably more probable. This last variant is of interest primarily because it agrees with the data for systems with iron impurities in the framework of the ideas mentioned above, according to which the positions of the energy levels of the iron and cobalt impurity ions in the given host crystal differ little, i.e., the difference of these impurities consists mainly in the degree of occupation of the donor levels. The significantly greater width of the resonant donor level for the cobalt impurities can be explained by the fact that in our treatment it includes the splitting in the crystalline field, since the two donor electrons belong to two nearby resonance levels, and we are treating the set of levels as one. The conclusion that the data for systems with iron and cobalt are in agreement in the given sense, although it is still in need of serious additional confirmation, can serve as an important starting point for subsequent studies.

CONCENTRATION MAXIMUM OF THE ELECTRON MOBILITY IN MERCURY SELENIDE CONTAINING GADOLINIUM IMPURITIES

Experimental data on the concentration dependence of the electron mobility in mercury selenide containing gadolinium impurities are given in Ref. 23, together with some other results of research on the electronic properties and atomic structure of the system mentioned. In the concentration interval of interest to us, the concentration dependence of the mobility shown in Fig. 4 has a pronounced maximum. At the level of study that has now been attained one can seek other mechanisms for such an anomaly. We have adopted an interpretation of the maximum based on the assumption that a resonance level of gadolinium exists in the conduction band of the mercury selenide crystal. The concentration maximum is then described by formula (10). The result of the corresponding fitting is shown by the solid curve in Fig. 4. The parameter values obtained are completely realistic, although of course one cannot state with complete certainty that the resonance level actually exists. Additional serious experimental confirmation of this interpretation and its advantages over other possible interpretations is still needed. Nevertheless, it can be assumed that a concrete argument on the qualitative level has been obtained.

Thus we have shown that the concentration maximum of the mobility observed in mercury selenide containing gadolinium impurities can be described by a formula obtained in the framework of resonance scattering theory. However, the experimental results are as yet insufficient to justify of the possibility of applying this theory to the given system.

RESULTS AND CONCLUSIONS

1. We have shown that the experimental data obtained on mercury selenide crystals containing chromium and cobalt impurities are in agreement with the idea that resonance donor energy levels of the transition-element impurities exist in these crystals. This conclusion is reached on the basis of a quantitative theoretical interpretation of the temperature dependence of the electron mobility and the concentration dependence of the Curie constant.
2. As a result of a detailed fitting of the temperature dependence of the electron mobility predicted by the resonance scattering theory to the experimental data, we have determined the limiting concentration of donor electrons and the parameters that determine the position of the concentration maximum of the mobility in mercury selenide crystals containing chromium impurities.
3. In an analysis of the observed concentration dependence of the Curie constant in the impurity spin magnetic susceptibility of mercury selenide crystals containing cobalt impurities on the basis of the idea that a resonance donor level exists, we have determined the possible limiting values of the concentration of donor electrons and the spin of the impurity. We have established that the experimental data can be explained by assuming that the position of the resonance level of iron and cobalt donor impurities are approximately the same, with allowance for their single and double donor ionization, respectively.
4. We have shown that the observed concentration maximum of the electron mobility in mercury selenide crystals containing gadolinium impurities can be explained on the basis of resonance scattering theory with reasonable values of the resonance parameters.

This study was supported by the Russian Foundation for Basic Research, Grant No. 03-02-16246.

[a]E-mail: okulov@imp.uran.ru

[1]V. I. Okulov, Fiz. Nizk. Temp. **30**, 1194 (2004) [Low Temp. Phys. **30**, 897 (2004)].
[2]V. I. Okulov, L. D. Sabirzyanova, K. S. Sazonova, and S. Yu. Paranchich, Fiz. Nizk. Temp. **30**, 441 (2004) [Low Temp. Phys. **30**, 328 (2004)].
[3]V. I. Okulov, G. A. Alshanskii, V. L. Konstantinov, A. V. Korolyov, E. A. Pamyatnykh,É. A. Neifeld, L. D. Sabirzyanova, and S. Yu. Paranchich, Fiz. Nizk. Temp. **30**, 558 (2004) [Low Temp. Phys. **30**, 417 (2004)].
[4]I. G. Kuleev, I. I. Lyapilin, and V. V. Karyagin, Zh. Eksp. Teor. Fiz. **99**,

172 (1991) [Sov. Phys. JETP **72**, 97 (1991)].
[5]I. G. Kuleev, I. I. Lyapilin, and V. V. Karyagin, Phys. Status Solidi B **163**, 449 (1991).
[6]J. Mycielski, Solid State Commun. **60**, 165 (1986).
[7]Z. Wilamowski, Acta Phys. Pol. A **77**, 133 (1990).
[8]I. M. Tsidil'kovskiĭ, Usp. Fiz. Nauk **162**, 63 (1992) [Sov. Phys. Usp. **35**, 85 (1992)].
[9]J. Friedel, Nuovo Cimento, Suppl. **2**, 287 (1958).
[10]V. I. Okulov, L. D. Sabirzyanova,É. Z. Kurmaev, L. D. Finkel'shteĭn, R. F. Karimov, A. Moewes, and S. Yu. Paranchich, JETP Lett. **81**, 72 (2005).
[11]N. G. Gluzman, N. K. Lerinman, L. D. Sabirzyanova, I. M. Tsidil'kovskiĭ, S. Yu. Paranchich, and Yu. S. Paranchich, Fiz. Tekh. Poluprovodn. **25**, 121 (1991) [Sov. Phys. Semicond. **25**, 71 (1991)].
[12]I. M. Tsidil'kovskiĭ, N. K. Lerinman, L. D. Sabirzyanova, S. Yu. Paranchich, and Yu. S. Paranchich, Fiz. Tekh. Poluprovodn. **26**, 1894 (1992) [Semiconductors **26**, 1062 (1992)].
[13]I. M. Tsidil'kovskiĭ, N. K. Lerinman, L. D. Sabirzyanova, S. Yu. Paranchich, and Yu. S. Paranchich, Phys. Status Solidi B **171**, 153 (1992).
[14]V. D. Prozorovskiĭ, I. Yu. Reshidova, S. Yu. Paranchich, and L. D. Paranchich, Fiz. Tverd. Tela (St. Petersburg) **34**, 882 (1992) Phys. Solid State **34**, 374 (1992)].
[15]M. Averous, C. Fau, S. Charar, M. El Kholdi, V. D. Ribes, and Z. Golacki, Phys. Rev. B **47**, 10261 (1993).
[16]S. K. Misra, J. Peskia, M. Averous, G. Ablart, L. Allam, C. Fau, S. Charar, M. El Kholdi, and M. D. Pace, Solid State Commun. **90**, 273 (1994).
[17]V. D. Prozorovskiĭ, I. Yu. Reshidova, and Yu. S. Paranchich, Fiz. Nizk. Temp. **21**, 576 (1995) [Low Temp. Phys. **21**, 449 (1995)].
[18]V. D. Prozorovskiĭ, I. Yu. Reshidova, A. I. Puzynya, and Yu. S. Paranchich, Fiz. Nizk. Temp. **22**, 1396 (1996) [Low Temp. Phys. **22**, 1058 (1996)].
[19]É. A. Neĭfel'd, K. M. Demchuk, G. I. Kharus, A. É. Bubnova, L. I. Domanskaya, G. L. Shtrapenin, and S. Yu. Paranchich, Fiz. Tekh. Poluprovodn. **31**, 318 (1997) [Semiconductors **31**, 261 (1997)].
[20]V. I. Okulov, Fiz. Met. Metalloved. **100**, No. 2 (2005).
[21]G. A. Alshanskii, V. L. Konstantinov, A. V. Korolyov, E. A. Neifeld, V. I. Okulov, S. U. Paranchich, and L. D. Sabirzyanova, Phys. Met. Metallogr. **93**, Suppl. 1, 142 (2002).
[22]T. Dietl and W. Szymanska, J. Phys. Chem. Solids **39**, 1041 (1978).
[23]M. D. Andriĭchuk, I. V. Gutsul, V. R. Romanyuk, L. D. Paranchich, and S. M. Kalitchuk, Second Ukrainian Scientific Conference on Semiconductor Physics, Chernovtsy–Vizhnitsa, September 20–24, 2004, *Book of Abstracts* [in Russian], Vol. 2, p. 31 (2004).

Translated by Steve Torstveit

Suppression of the differential-tunnelling-conductance peak of a phase-coherent two-layer system by means of thermal fluctuations

A. I. Bezuglyĭ[a)]

Kharkov Physicotechnical Institute National Science Center, ul. Akademicheskaya, 1, Kharkov 61108, Ukraine

(Submitted February 18, 2005; resubmitted April 25, 2005)
Fiz. Nizk. Temp. **31**, 1153–1157 (October 2005)

A high, narrow, interlayer differential-tunnelling-conductance peak is observed at low temperatures in semiconductor heterostructures with two close-lying electron layers. This peak is the consequence of the interlayer phase coherence established in the system by Bose condensation of interlayer excitons, i.e., pairs of an electron and a hole belonging to the different layers. It is shown that increasing the temperature smoothes out the tunnelling-conductance peak by increasing the interlayer-voltage fluctuations. The temperature dependence obtained for the peak height agrees with experiment. © *2005 American Institute of Physics*. [DOI: 10.1063/1.2126944]

I. INTRODUCTION

There has been great interest in recent years in semiconductor heterostructures consisting of close-lying quantum wells each of which contains an almost two-dimensional layer of electrons. When placed in a strong perpendicular magnetic field, these systems demonstrate a number of unusual properties for the total fill factor of the Landau levels, $\nu_T=\nu_1+\nu_2=1$.[1,2] In particular, in low-temperature regions ($T<50$ mK), the dependence of the differential-tunneling conductance on the interlayer voltage, $G_T(V)$, has a high, narrow symmetric peak with a maximum at $V=0$. A temperature increase is accompanied by a rapid decrease of the peak height, and the peak becomes virtually indistinguishable at $T>200$ mK.

The $G_T(V)$ peak is observed only for fairly small distances between the layers, when the Coulomb interaction of the carriers from the different layers becomes substantial. The appearance of the $G_T(V)$ peak is explained by the transition of the two-layer system into a state with interlayer phase coherence. The wave function of a coherent state is antisymmetric relative to exchanges of the electron coordinates (see, for example, Ref. 3 and the literature cited therein). Such a wave function minimizes the interaction energy of the electrons from the different layers, since the configuration probability decreases when two electrons are close to each other. In other words, a correlation hole is located opposite each electron in the other layer. As a consequence, the tunneling of an electron from one layer to another is not blocked by the Coulomb repulsion from the electrons of the other layer, and this in the last analysis results in the $G_T(V)$ peak.

A state with interlayer phase coherence can also be regarded as a state that results from the pairing of electrons from one layer with holes from the other layer.[4,5] A complex order parameter can be introduced for such a phase-coherent n–p system. It was recently shown[6] that the tunneling properties of two-layer systems observed in Refs. 1 and 2 can be explained by the specific dynamics of the phase of the order parameter. In particular, the $G_T(V)$ peak is associated with the transition of the system from a state with fixed phase at low voltages ($V<V_c$) to a state in which the phase monotonically varies with time (for $V>V_c$) (see Section II). The half-width of the V_c peak is proportional to the modulus of the matrix element of the interlayer tunneling, $|T_{12}|$, while its height is independent of $|T_{12}|$. Thus, for weak tunneling, the $G_T(V)$ peak is high and narrow.

In our opinion, it is this small width of the $G_T(V)$ peak that causes its strong suppression by thermal fluctuations of the interlayer voltage even at fairly low temperatures $T\sim eV_c\propto|T_{12}|$, where e is the absolute magnitude of the electronic charge, while the temperature is measured in energy units. Below we give a quantitative description of this effect.

II. EQUATION OF THE DYNAMICS OF A PHASE-COHERENT n–p SYSTEM AND TUNNELING CONDUCTANCE AT $T=0$

We shall describe the behavior of a phase-coherent n–p system by the dynamic equation for the order parameter obtained in Ref. 7 for the gapless case. We believe that this equation, which is analogous to the nonsteady-state Ginzburg–Landau equation, can be used to analyze the dynamics of the experimentally studied[1,2] phase-coherent two-layer systems (see the discussion of this question in Ref. 6).

In a two-layer n–p system, the complex order parameter $\Delta=|\Delta|\exp(i\theta)$ is proportional to the mean $\langle\psi_1(r,t)\psi_2^+(r,t)\rangle$, where ψ_k^+ (ψ_k) is the electron-creation (annihilation) operator in layer k. In the one-dimensional case of interest to us, the dynamic equation has the following form ($\hbar=1$):

$$-\frac{d\Delta}{dt}+ieV\Delta+(A-B|\Delta|^2)\Delta+\frac{T_{12}}{\zeta\tau}=0. \tag{1}$$

The coefficients A and B in this equation are the coefficients of the steady-state Ginzburg–Landau equation. For the gapless case, $A(T)=(2\pi^2/3)\tau_i(T_c^2-T^2)$, $B=4m\tau_i/3M$.[7] Here τ_i is the elastic scattering time of the carriers, T is the temperature, T_c is the critical temperature, $M=m_1+m_2$ is the mass of an electron-hole pair, $m=m_1m_2/M$ is the reduced mass of the pair, and ζ is the dimensionless Coulomb interaction constant.[5] The complex matrix element of the tunneling is $T_{12}=|T_{12}|\exp(i\chi)$.

On the assumption that the tunneling is fairly weak, its influence on the value of the order parameter can be neglected, and it can be assumed that $|\Delta|$ is determined by the steady-state Ginzburg–Landau equation with $T_{12}=0$. In this case, the dynamics of the system are described by the imaginary part of Eq. (1), which constitutes the equation for the phase of the order parameter. It can be written as

$$\dot{\varphi} - eV + eV_c \sin\varphi = 0, \tag{2}$$

where $\varphi=\theta-\chi$, while $V_c=|T_{12}|/(e\zeta\tau|\Delta|)$.

In the approximation for the interlayer tunneling current that is linear in T_{12}, the following expression is obtained in Ref. 7:

$$I = I_c \sin\varphi. \tag{3}$$

Here $I_c=4eN(0)|T_{12}||\Delta|S/\zeta$, where $N(0)=m/\pi$ is the density of states at the Fermi surface, and S is the area of the n–p transition.

When $|V|<V_c$, Eq. (2) has steady-state solution $\varphi=\arcsin V/V_c$, the substitution of which in Eq. (3) gives a tunneling current proportional to the interlayer voltage: $I=G_0V$. We should point out that the characteristic tunneling conductance

$$G_0 = I_c/V_c = 4e^2N(0)\tau|\Delta|^2S \tag{4}$$

is independent of the matrix element of the interlayer tunneling $|T_{12}|$.

When $|V|>V_c$, phase φ monotonically varies with time, while the tunneling current oscillates with frequency $\omega=e\sqrt{V^2-V_c^2}$.[6] The mean value of the tunneling current is given by

$$I = G_0(|V| - \sqrt{V^2 - V_c^2})\operatorname{sign} V. \tag{5}$$

We get from this that, when $|V|>V_c$, the differential tunneling conductance is

$$G_T(V) = -G_0[|V|(V^2 - V_c^2)^{-1/2} - 1]. \tag{6}$$

Equations (4) and (6) determine the $G_T(V)$ dependence at temperature $T=0$. In this limit, $G_T(V)$ has a constant positive value G_0 in the voltage region $|V|<V_c$, discontinuities at $|V|=V_c$, and, being negative, tends to zero when $|V|$ grows without limit.

III. THE EFFECT OF THERMAL FLUCTUATIONS

Conductance $G_T(V)$ already depends on temperature because the temperature-dependent modulus of the order parameter enters into it through G_0. However, we assume that the strong temperature suppression of the $G_T(V)$ peak observed in Refs. 1 and 2 is chiefly caused by the small width of this peak ($\approx 6\ \mu$V), as a consequence of which thermal fluctuations of the voltage substantially smooth out the peak even at the extremely low temperatures of the experiment ($T\sim 0.1$ K).

Under the action of voltage noise, the voltage between the layers of the n–p system has a fluctuational component $V_f(t)$. Provided that $eV\ll T$, the voltage noise is thermal and is determined by the following correlation properties:

$$\langle V_f(t)\rangle = 0, \quad \langle V_f(t)V_f(t')\rangle = 2TG_0^{-1}\delta(t-t'). \tag{7}$$

The Langevin equation for phase $\varphi(t)$ is the equation of motion for a Brownian particle in a viscous medium:

$$\dot{\varphi} - v + \sin\varphi = \xi(t), \tag{8}$$

where this equation describes the situation in which a periodic (in the coordinate) force $\sin\varphi$, a constant force v, and a random force $\xi(t)$ act on a particle with "coordinate" φ. Note that the time in Eq. (8) is measured in units of $(eV_c)^{-1}$, while the voltage and the random force are normalized to V_c: $v=V/V_c$, $\xi(t)=V_f(t)/V_c$. Here the correlator $\langle\xi(t)\xi(t')\rangle=2(T/E_J)\delta(t-t')$, where $E_J=I_c/e$ determines the energy stored in the n–p contact: the given value of phase φ corresponds to the contact energy $E(\varphi)=E_J(1-\cos\varphi)$.

From the Langevin equation, Eq. (8), the Smoluchowski diffusion equation for the probability density $\rho(\varphi,t)$ follows:

$$\frac{\partial\rho}{\partial t} = \frac{\partial}{\partial\varphi}\left[\left(\frac{du}{d\varphi} + \tau\frac{\partial}{\partial\varphi}\right)\rho(\varphi,t)\right], \tag{9}$$

where function $u(\varphi)=-v\varphi+1-\cos\varphi$ determines the "potential relief" of the diffusion problem, while the dimensionless temperature $\tau=T/E_J$ has the meaning of the diffusion coefficient. It is obvious that Eq. (9) is a continuity equation whose right-hand side is (to within the sign) the divergence of the probability flux. For the steady-state random process considered by us, the probability flux

$$w = -\frac{du}{d\varphi}\rho - \tau\frac{d\rho}{d\varphi} \tag{10}$$

is independent of φ. In this case, Eq. (10) with periodic boundary conditions $\rho(0)=\rho(2\pi)$ and normalization condition $\int_0^{2\pi}\rho(\varphi)d\varphi=1$ completely determines the probability distribution $\rho(\varphi)$ and the probability flux w.

It is convenient to write a solution of Eq. (10) that is periodic in φ as follows:[8,9]

$$\rho(\varphi) = \frac{w}{\tau}\frac{\exp(-u(\varphi)/\tau)}{1-\exp(-2\pi v/\tau)}\int_{\varphi}^{2\pi+\varphi} d\varphi'\,\exp(u(\varphi')/\tau). \tag{11}$$

Substituting Eq. (11) into the normalization condition gives for the probability flux the expression

$$w = \frac{\tau}{4\pi}(1-\exp(-2\pi v/\tau))S_0^{-1}(v,\tau). \tag{12}$$

Here we have used the notation

$$S_n(v,\tau) = \int_0^{\pi} d\psi\ \psi''\exp(-2v\psi/\tau)I_0\left(\frac{2}{\tau}\sin\psi\right),$$

where $I_0(x)$ is the modified Bessel function of zeroth order. The averaging of the Langevin equation, Eq. (8), gives $\langle\dot{\varphi}\rangle=-\langle du/d\varphi\rangle$. From this, using the definition of probability flux and the periodicity of $\rho(\varphi)$, we get

$$\langle\dot{\varphi}\rangle = 2\pi w. \tag{13}$$

Substituting Eq. (13) into the Langevin equation averaged over fluctuations leads to the simple expression

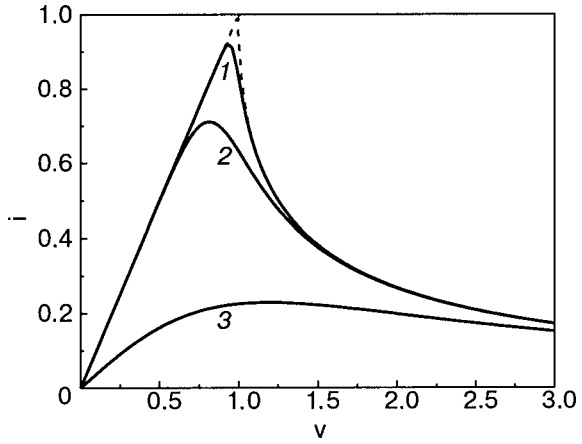

FIG. 1. Family of normalized VARs ($v=V/V_c$, $i=\langle I\rangle/I_c$) of two-layer n–p systems for various values of dimensionless temperature τ: 0.01 (*1*), 0.1 (*2*), 1 (*3*) ($\tau=T/E_J$). The dashed curve shows the VAR at low temperature.

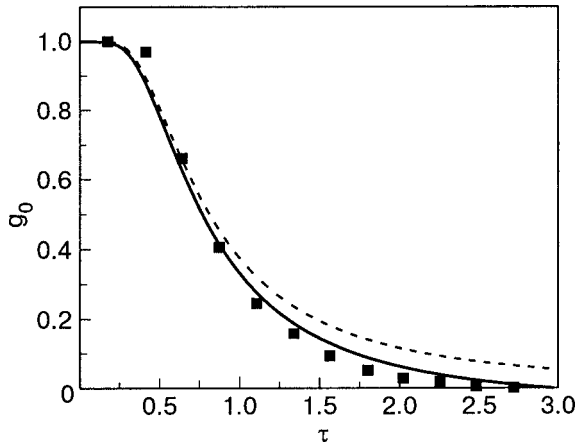

FIG. 3. Normalized peak height of differential-tunnelling conductance g_0 vs dimensionless temperature. The experimental points are taken from Ref. 2. The dashed curve shows the $g_0(\tau)$ dependence, which is given by Eq. (16), while the solid curve is given by Eq. (17).

$$i = v - 2\pi w(v) \tag{14}$$

for the normalized mean tunneling current $i=\langle I\rangle/I_c=\langle\sin\varphi\rangle$. Equation (14) is the volt-ampere response (VAR) of the n–p contact, smoothed by the thermal fluctuations. The family of VARs for various values of parameter τ is shown in Fig. 1.

The normalized differential-tunneling conductance $g_T(v,\tau)\equiv G_T(v,\tau)/G_0$ is given by

$$g_T(v,\tau) = 1 - \pi\exp(-2\pi v/\tau)S_0^{-1}(v,\tau) - (1-\exp(-2\pi v/\tau))S_1(v,\tau)S_0^{-2}(v,\tau). \tag{15}$$

The differential-tunneling-conductance curves smoothed by fluctuations are shown in Fig. 2 as a function of voltage. It can be seen that the fluctuations substantially reduce the height of the tunneling-conductance peak. The temperature dependence of the normalized peak height $g_0(\tau)\equiv g_T(0,\tau)$, which is given by

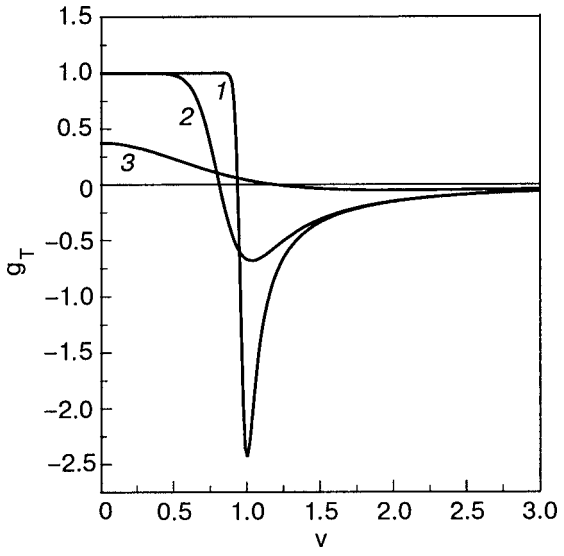

FIG. 2. Family of curves of normalized tunnel conductance g_T [Eq. (15)] as a function of voltage for the following values of dimensionless temperature τ: 0.01 (*1*), 0.1 (*2*), 1 (*3*).

$$g_0(\tau) = 1 - \pi S_0^{-1}(0,\tau), \tag{16}$$

is shown in Fig. 3 by a dashed curve.

IV. DISCUSSION OF THE RESULTS AND COMPARISON WITH EXPERIMENT

Turning to the analogy with a Brownian particle in potential $u(\varphi)$, it can be immediately seen that, at temperatures $\tau\ll 1$ and voltages v not too close to unity, the transition probability of a particle from one potential minimum to another is exponentially small. As a consequence, the mean probability flux w makes a small contribution to the right-hand side of Eq. (14); hence, at low temperatures, the thermal fluctuations have no effect on the VAR all the way to voltages of $v\approx 1$ (see Fig. 1). The ohmic character of the VAR at small τ results in a plateau on the $g_T(v)$ dependence (see Fig. 2). Note that, for $v>1$, potential $u(\varphi)$ has no minima, and the particle (for $v\gg 1$) almost freely slides downward along the contour. In this case, $2\pi w\approx v$ and, according to Eq. (14), the mean current i is small.

In the low-voltage region, when the potential relief is a curve with deep minima, particle-activation output from the minimum has an appreciable probability only at sufficiently high temperatures. As a consequence, all the VARs have the same behavior when $\tau\ll 1$ (see Fig. 1), and this results in a pronounced low-temperature plateau of the differential-tunneling-conductance peak (Fig. 3). Such a plateau is clearly visible on the experimental curves of Refs. 1 and 2.

Proceeding to a quantitative comparison of theory and experiment, we should point out the following: The experiment reported in Refs. 1 and 2 measured the temperature dependence of two quantities, namely, the height and width of the differential-tunneling-conductance peak. To correctly compare the theoretical results obtained in Section III with experiment, it should be kept in mind that their region of applicability is limited by the condition that the fluctuations must be thermal, i.e., $eV\ll T$. Such an inequality is satisfied for all temperatures of the experiment for which the peak height of the tunneling conductance was measured. Conversely, for the measurements of the temperature dependence

of the peak width, the condition that the fluctuations must be thermal breaks down in the entire temperature interval.

The temperature dependence of the differential-tunneling-conductance peak given by Eq. (16) is compared with experiment[2] in Fig. 3. It can be seen in the figure that satisfactory agreement of the theoretical (dashed) curve with experiment is achieved by means of one adjustable parameter E_J (=83 mK). It is assumed in this case that G_0 is independent of temperature. Such an approximation is justified when the value of eV_c that characterizes the peak width is small by comparison with the critical temperature T_c. At the same time, the agreement of theory and experiment can be improved if the $G_0(\Delta(T))$ dependence is taken into consideration. Actually, from the real part of Eq. (1), neglecting the contribution of the small term proportional to T_{12}, it follows that $|\Delta(T)/\Delta(0)|^2 = 1 - T^2/T_c^2$. In this case, for the normalized peak height, we get the expression

$$g_0(\tau) = [1 - \pi S_0^{-1}(0,\tau)][1 - \tau^2 (E_J/T_c)^2]. \quad (17)$$

The curve given by Eq. (17) with $T_c = 0.24$ K is indicated in Fig. 3 by a solid curve. It can be seen that taking the temperature dependence of G_0 into account improves the agreement of theory and experiment.

V. CONCLUSION

The effect of temperature on the differential-tunneling-conductance peak of a two-layer electron-hole n–p system has been considered. This peak is a consequence of the interlayer phase coherence that arises spontaneously in an n–p system as the temperature decreases. The extremely small width of the peak (caused by the proportionality of V_c to the modulus of the matrix element of the interlayer tunneling) results in strong smearing and suppression of the thermal-fluctuation peak even for extremely low temperatures $T \sim eV_c$.

The treatment is based on the dynamic equation obtained earlier[7] for the order parameter of n-p systems. The applicability of this equation to the description of systems consisting of two electron layers in a strong perpendicular magnetic field[1,2] is caused by a single mechanism for both systems—the appearance of phase coherence, namely, Bose condensation of electron-hole pairs with spatially separated components. As a result, the structure of the dynamic equation is completely analogous for both types of systems (see, for example, Ref. 10). The role of the magnetic field in this case mainly consists of strengthening the Coulomb attraction of an electron and a hole.[11]

The author expresses gratitude to S. I. Shevchenko for useful discussions.

[a)]Email: bezugly@ic.kharkov.ua

[1] I. B. Spielman, J. P. Eisenstein, L. N. Pfeiffer, and K. W. West, Phys. Rev. Lett. **84**, 5808 (2000).
[2] I. B. Spielman, J. P. Eisenstein, L. N. Pfeiffer, and K. W. West, Phys. Rev. Lett. **87**, 036803 (2001).
[3] K. Yang, Phys. Rev. Lett. **87**, 056802 (2001).
[4] Yu. E. Lozovik and V. I. Yudson, Zh. Eksp. Teor. Fiz. **71**, 738 (1976) [Sov. Phys. JETP **44**, 389 (1976)].
[5] S. I. Shevchenko, Fiz. Nizk. Temp. **2**, 505 (1976) [Sov. J. Low Temp. Phys. **2**, 251 (1976)].
[6] A. I. Bezuglyĭ and S. I. Shevchenko, Fiz. Nizk. Temp. **30**, 282 (2004) [Low Temp. Phys. **30**, 208 (2004)]; cond-mat/0304103.
[7] A. I. Bezuglyĭ and S. I. Shevchenko, Fiz. Nizk. Temp. **4**, 454 (1978) [Sov. J. Low Temp. Phys. **4**, 222 (1978)].
[8] V. Ambegaokar and B. I. Halperin, Phys. Rev. Lett. **22**, 1364 (1969).
[9] B. Chen and J. Dong, Phys. Rev. B **44**, 10 206 (1991).
[10] A. H. MacDonald, A. A. Burkov, Y. N. Joglekar, and E. Rossi, cond-mat/0310740.
[11] Y. Kuramoto and C. Horie, Solid State Commun. **25**, 713 (1978).

Translated by W. Manthey

PHYSICAL PROPERTIES OF CRYOCRYSTALS

The nuclear-spin conversion effect in the thermal conduction of methane

B. Ya. Gorodilov,[a] A. I. Krivchikov, and O. A. Korolyuk

B. I. Verkin Physicotechnical Institute of Low Temperatures, National Academy of Sciences of Ukraine, pr. Lenina, 47, Kharkov 61103, Ukraine

(Submitted March 14, 2005)
Fiz. Nizk. Temp. **31**, 1158–1162 (October 2005)

This paper discusses the thermal conduction of solid methane at temperatures below the phase-transition temperature. An increase of the thermal conduction of the samples in time is detected at temperatures below 5 K after rapid cooling. The observed effect is associated with the concentration decrease of the *T* modification as a result of conversion. The characteristic time of the nuclear-spin conversion of methane is determined in the 1.8–5-K temperature region. © *2005 American Institute of Physics*. [DOI: 10.1063/1.2126945]

I. INTRODUCTION

The process of nuclear-spin conversion in solid methane establishes the equilibrium distribution between the spin modifications of the molecules (*E*, *T*, and *A*, with total nuclear spins of $I=0$, 1, and 2, respectively). At sufficiently high temperatures, relaxation of the spin subsystem occurs rapidly, and the distribution of the modifications differs little from the equilibrium distribution. As the temperature decreases, the conversion rate slows down, and the distribution of the modifications corresponding to the higher temperature can be maintained in the system for a long time. The conversion rate is determined by the interaction of the proton spins and by the probability of transfer of conversion energy to the methane lattice (to the phonon subsystem). The distribution of the molecules of solid methane over nuclear-spin modifications and the nuclear-spin conversion time at different temperatures have been investigated in a number of experiments using the data of NMR methods (see, for example, Refs. 1–3), magnetic susceptibility,[4] neutron scattering,[5,6] heat-capacity measurements,[7] dilatometric measurements,[8] and also theoretically.[9] The conversion process speeds up when a krypton impurity is introduced into the pure methane.[5,10,11] In the partially ordered phase II of pure methane, where three-fourths of the molecules are orientationally ordered and perform librational vibrations and one-fourth of the molecules rotate almost freely, two characteristic relaxation times are observed, which correspond to nuclear-spin conversion processes in different sublattices. Nijman and Berlinsky[9] estimated the conversion rate at liquid-helium temperatures in the different sublattices. The characteristic nuclear-spin conversion times of almost freely rotating molecules, determined in various experimental papers, have rather large scatter. We should point out that a paramagnetic impurity of O_2, usually present in methane, even in insignificant amounts, has a strong influence on the conversion rate. Despite the rather large amount of work devoted to this problem, the conversion process in methane is still not clear.

The influence of conversion on thermal conductance was detected in Ref. 12, but it was not investigated quantitatively. The thermal conduction of solid methane strongly depends on the character of the orientational motion of the molecules. Anomalous behavior of the thermal conductance is observed in the partially ordered phase of CH_4.[12] The authors of this article assumed that the low value of the thermal-conduction maximum and the loss of the exponential dependence above the temperature of the maximum are the result of the presence of a strong phonon-scattering mechanism, associated with rotational excitation of the methane molecules. The thermal conduction at 4.8 K both after rapid cooling from 25 K and after heating from 1.5 K was also measured for this paper. The resulting thermal conductivities differed by about 10%. The authors explained such behavior by the influence of nuclear-spin conversion on the thermal conduction of methane.

The reason that the treatment of the behavior of the thermal conduction of methane in phase II is so complex is that the phonon scattering can depend on two types of rotational excitations: weakly hindered rotors and librations. In the temperature region below 5 K, the preferred (strongest) phonon-scattering mechanism is phonon-rotation interaction, since the energy spectrum of a CH_4 rotor has several low-lying energy levels, spaced not far from each other, which can participate in resonance scattering of the phonons. The three nuclear-spin modifications of CH_4 can scatter phonons independently of each other. The molecules of the *T* modification of the almost freely rotating rotor are the strongest source of phonon scattering at low temperatures,[10] since they can most efficiently absorb thermal phonons with an energy equal to the energy difference ($\Delta E=12.4$ K) between the ground level and the first excited level of the spectrum of rotational motion. We should point out that the concentration of molecules of the *T* modification of methane decreases as the temperature decreases, since, as a result of conversion, the molecules of the *T* modification transform into the more stable *A* modification. This process affects the thermal conductance, since the number of scattering centers (molecules of the *T* modification of methane) is reduced. Consequently, when the methane sample is rapidly cooled, it is possible to create a nonequilibrium distribution between the nuclear-spin modifications, which will tend to equilibrium as a result of

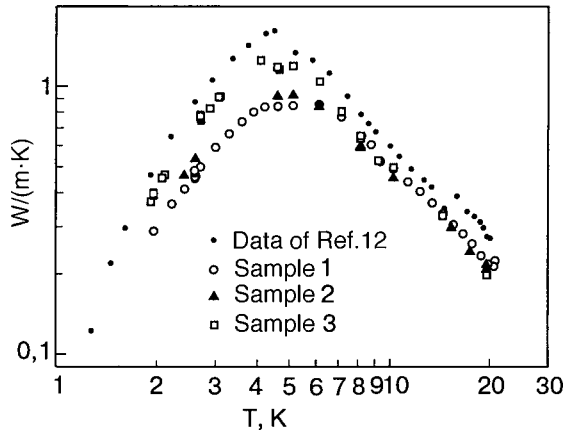

FIG. 1. Thermal conductivity of solid methane vs temperature.

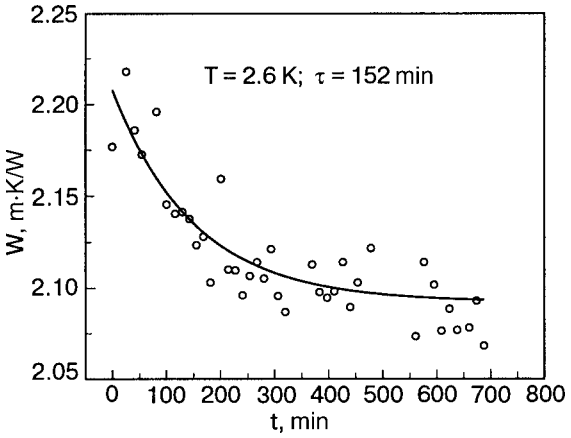

FIG. 2. Thermal resistance of solid methane vs time after rapid cooling.

the nuclear-spin conversion process. In this process, the number of molecules of the T modification will decrease, and this must increase the thermal conductance. The relaxation of the thermal conductance is thus directly associated with relaxation of the molecules of the T modification, tending to thermodynamic equilibrium.

Experiments were carried out for this paper to observe relaxation effects in the thermal conduction of solid methane in the temperature region below 5 K. The relaxation effect must be associated with the nuclear-spin distribution. The investigation of the conversion effect in the thermal conduction of methane can give irrefutable evidence in favor of the concept of the resonance nature of phonon scattering at rotational states dependent on the spin states.[10,13]

II. EXPERIMENT

Measurements of the thermal conduction of four samples of solid methane were made in the temperature interval 1.8–20 K. The chemical purity of the methane was 99.98%, and the concentration of O_2 impurity was below 0.01%. The samples were grown from the liquid phase in a cylindrical stainless steel ampule 38 mm long and 4.5 mm in internal diameter. We should point out that the upper end of the ampule containing the sample has a gradient heater, the middle part of the ampule has two resistance thermometers (upper and lower, the distance between which is 20 mm), while the lower end is attached to a heat sink. The measurement cell is described in Ref. 14. The growth rate of the samples was 0.07 mm/min, with a constant temperature gradient of 0.18 K/mm being maintained along the sample. When the growth was complete, the samples were cooled to 30 K at a rate of 0.15 K/min with the same gradient.

The thermal conduction measurements in the sample at temperatures 1.8–20 K were made by a planar steady-state method (the thermal potentiometer method).

Measurements were first made of the temperature dependence of the thermal conductivity, $K(T)$, corresponding to a distribution of the CH_4 molecules over the spin modifications close to thermodynamic equilibrium. The results of the measurements of the thermal conductivity of methane are shown in Fig. 1. The results of this paper in terms of the position of the maximum and the behavior of the thermal conductivity closely agree with the data of Ref. 12.

Relaxation of the thermal conduction in a methane sample was detected after rapid cooling from 7.1 to 2.6 K. The sample was held for 1.5 h at a temperature of 7.1 K in a state of thermal equilibrium, since the characteristic time of nuclear-spin conversion at this temperature is about half an hour (see below in Fig. 4). The sample was then quickly (in 3 min) cooled to 2.6 K. The time dependence of the thermal conductivity, $K(t)$, was measured at this temperature for 12 h. The mean time between measurements was about 18 min. The thermal conductivity increased with time. Figure 2 shows the time dependence of the thermal resistance of the sample at 2.6 K. The curve in Fig. 2 is an exponential dependence with a relaxation time of $\tau = 152$ min. It is natural to assume that the observed relaxation of the thermal resistance corresponds to a decrease with time of the number of scattering centers.

The concentration variation of each modification with time t (when the conversion rate is independent of the concentration of the modifications) can be written as

$$n(t) = n_{\mathrm{eq}} + \Delta n_0 \exp(-t/\tau),$$

where n_{eq} is the equilibrium concentration of the modification, n_0 is the concentration of the modification at the initial instant, $\Delta n_0 = n_0 - n_{\mathrm{eq}}$ is the difference of the concentrations from the equilibrium value at the initial instant, and τ is the characteristic time of the nuclear-spin conversion. At constant temperature, the thermal resistance of the crystal [when it is determined by only one spin modification (the T modification[13])] depends on time as

$$W(t) = W_{\mathrm{eq}} + W_{\mathrm{ext}} \exp(-t/\tau),$$

where W_{eq} is the total thermal resistance for the equilibrium distribution of the spin modifications (caused both by the phonon-rotational scattering and by other mechanisms), and W_{ext} is the additional resistance, associated with the nonequilibrium concentration of the T modification at the inital instant. Consequently, the characteristic nuclear-spin conversion time can be determined from the time dependence of the thermal resistance obtained after rapid cooling of the sample. However, the measurement of the thermal conduction by the thermal potentiometer method assumes that the sample reaches the steady-state regime in two stages of the temperature measurement in the sample: with the gradient heater turned on and without heating. The steady-state regime can

be completely reached in the methane sample only when the nuclear-spin modifications of the equilibrium state are reached. The thermal conductivity measurements were therefore carried out in the quasi-steady-state regime. The relative variation of the thermal resistance in this case is small: $(W_{ext}-W_{eq})/W_{eq}=6\%$ (Fig. 2). For such an insignificant change of the thermal resistance, the accuracy with which the conversion time is determined is not very high.

To increase the accuracy with which the nuclear-spin conversion time in the sample is determined, a temperature-gradient relaxation method was proposed and implemented. The relaxation of the temperature gradient is directly associated with the relaxation of the thermal conduction in the sample. The essence of the method is as follows: After the sample is quickly cooled to the measurement temperature, the temperature gradient along the sample in time is recorded in the constant-thermal-flux regime. The sample is initially held in a state of thermal equilibrium at a temperature of 10 K for an hour with the gradient heater for the sample switched on. The heater was switched on in order to create a constant heat flux along the sample, directed from above downward. The heater power was chosen so that the temperature difference between the upper and lower thermometers was about 0.3 K. The sample was then quickly cooled (in 3–5 min) to a temperature of $T<5$ K, after which the temperature of the lower thermometer was stabilized at a constant heat flux along the sample. The temperature gradient was measured for 5–6 h, with the temperature of both thermometers being recorded every 0.2 min. An exponential decrease in time of the temperature difference between the thermometers was observed. One of the experimental curves $[\Delta T(t)-\Delta T_{eq}]$ on a semilog scale is shown in Fig. 3 (the temperature of the lower thermometer was $T=2.3$ K). Here $\Delta T(t)$ is the temperature difference between the upper and the lower thermometers at time t, and ΔT_{eq} is the same value when the sample reaches complete thermal equilibrium. The relaxation time of the sample was determined from the slope of the curve. Figure 3 shows two exponential sections. The first of them is associated with the establishment of the quasi-steady-state regime in the sample (thermal relaxation) and is characterized by relaxation time τ_{state}. At $T=2.3$ K, $\tau_{state}=13$ min. In our measurements, τ_{state} varied within the limits 13–30 min. We assume that the second section is characterized by the nuclear-spin conversion time τ, since only thermal relaxation was observed in control measurements carried out on a sample of pure solid Kr similar to those described above. The characteristic time τ_{state} in Kr corresponded to the establishment of the steady-state regime in the sample and was determined by its thermal diffusivity.

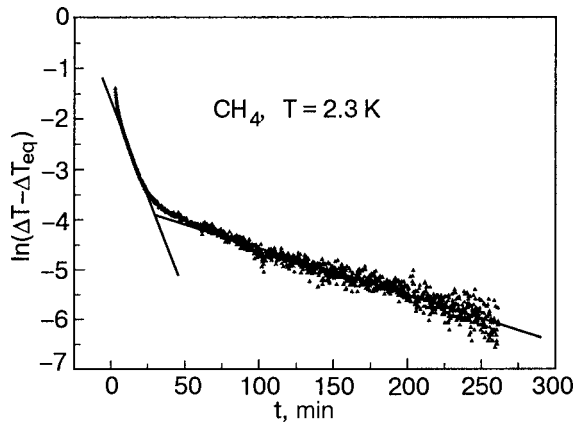

FIG. 3. Value of $\Delta T-\Delta T_{eq}$ vs time for CH_4 at $T=2.3$ K.

TABLE I. Characteristic relaxation times τ obtained after rapid cooling, using the method of relaxation of the temperature gradient in the sample.

T, K	Characteristic spin-conversion time τ, h			
	N1	N2	N3	N4
1.8		1,77		
2			1.18	
2			0.78	
2.05				1.88
2.3		1,76		
2.6	2,53*			
2.7			1.67*	
2.8			1.35	
3.5		2,15		
4				3.4
4.6		1.93		
4.6			1.42	
5		1.73		
5		1.73		

For methane at $T=2.3$ K, $\tau=106$ min. Similar behavior of ΔT is observed in the temperature interval $1.8\text{ K}<T<5$ K. The relative variation of the quantity ΔT observed in experiment is $(\Delta T_{ext}-\Delta T_{eq})/\Delta T_{eq}=1.8$ for $T=2.3$ K, where ΔT_{ext} is the temperature difference at the initial instant. Table I indicates the nuclear-spin conversion times τ obtained in experiment.

The results obtained in this paper qualitatively agree with those that appear in the literature, obtained for the case of a free rotator, although their magnitude is a little larger in

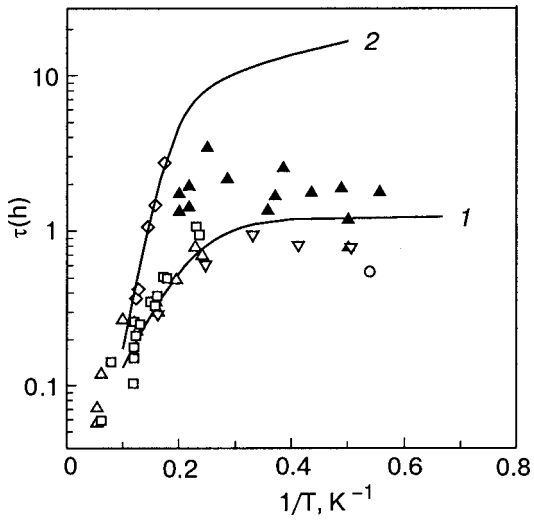

FIG. 4. Dependence of τ on inverse temperature. Comparison with literature data: ▲ our data, △ data of Buchman *et al.*,[3] □ Colwell *et al.*,[7] ○ Code and Higinbotham,[4] ▽ Piott and McCormick,[2] ◇ Aleksandrovskii *et al.*[8] The curves show the theoretical calculations of Ref. 5: for a free rotator (*1*) and for orientationally oriented molecules (*2*).

the given temperature region. In Fig. 4, the curves show the calculation of the conversion rate α from the expression taken from Ref. 5:

$$\alpha = 1/\tau = A(1 + 2\bar{n}_k(E_1)) + B\exp(-C/T),$$

$$\bar{n}_k = (\exp(\omega_k/k_BT) - 1)^{-1},$$

where the first term in the expression is a result of the Bose factor,[9] and the second term includes the thermally activated process; for the free rotator, $E_1 = 12.4$ K is the energy of the $0 \rightarrow 1$ transitions, $A = 0.81$ h^{-1}, $B = 42.6$ h^{-1}, and $C = 19.3$ K; for ordered molecules, $E_1 = 1.7$ K, $A = 0.024$ h^{-1}, $B = 447$ h^{-1}, and $C = 44$ K.[5]

At temperatures close to $T = 5$ K, our data lie between the data for a free rotator and for orientationally ordered molecules.

Relaxation of the temperature gradient was also observed after the sample was rapidly heated from 1.9 to 4–5 K. Unfortunately, the relaxation time could not be determined, since the variation of the gradient was small. An increase of the gradient with time was observed, and this corresponded to an increase of the number of molecules of the T modification of methane as a result of the inverse nuclear-spin conversion process. The fact of inverse conversion serves as an additional argument in favor of the concept of thermal transport in pure methane according to which one of the phonon-scattering mechanisms is resonance scattering by rotational excitations of molecules of the T modification of a weakly hindered rotor of solid CH_4 in phase II.

The thermal conductivity of pure methane has thus been measured in the temperature region 1.8–20 K. Relaxation of the thermal conduction (increase of the thermal conduction) is observed in the temperature region below 5 K after rapid cooling of the sample from 7.1 K. The characteristic relaxation time has been determined in the temperature interval 1.8–5 K. It is concluded that the relaxation of the thermal conduction is associated with a reduction of the number of molecules of the T modification of a hindered rotor as a result of the nuclear-spin conversion process.

The authors express gratitude to V. V. Dudkin for help in making the measurements.

[a]Email: gorodilov@ilt.kharkov.ua

[1]K. P. Wong, J. D. Noble, M. Bloom, and S. Alexander, J. Magn. Reson. (1969-1992) **7**, 55 (1969).
[2]J. E. Piott and W. D. McCormick, Can. J. Phys. **54**, 1784 (1976).
[3]S. Buchman, D. Candela, W. T. Vetterling, and R. V. Pound, Phys. Rev. B **26**, 1459 (1982).
[4]R. F. Code and J. Higinbotham, Can. J. Phys. **54**, 1248 (1976).
[5]S. Grieger, H. Friedrich, B. Asmussen, K. Guckelsberger, D. Nettling, W. Press, and R. Scherm, Z. Phys. B: Condens. Matter **87**, 203 (1992).
[6]K. J. Lushington and J. A. Morrison, Can. J. Phys. **55**, 1580 (1977).
[7]J. H. Colwell, E. K. Gill, and J. A. Morrison, J. Chem. Phys. **39**, 635 (1963).
[8]A. N. Aleksandrovskiĭ, V. B. Kokshenev, V. G. Manzheliĭ, and A. M. Tolkachev, Fiz. Nizk. Temp. **4**, 915 (1978) [Sov. J. Low Temp. Phys. **4**, 435 (1978)].
[9]A. J. Nijman and A. J. Berlinsky, Can. J. Phys. **58**, 1049 (1980).
[10]A. I. Krivchikov, B. Ya. Gorodilov, O. A. Korolyuk, V. G. Manzhelii, and V. V. Dudkin, J. Status Solidi C **1**, 2959 (2004).
[11]M. I. Bagatskii, V. G. Manzhelii, I. Ya. Minchina, D. A. Mashchenko, and I. A. Gospodarev, J. Low Temp. Phys. **130**, 459 (2003).
[12]A. Jezowski, H. Misiorek, V. V. Sumarokov, and B. Ya. Gorodilov, Phys. Rev. B **55**, 5578 (1997).
[13]V. V. Dudkin, B. Ya. Gorodilov, A. I. Krivchikov, and V. G. Manzhelii, Fiz. Nizk. Temp. **26**, 1023 (2000) [Low Temp. Phys. **55**, 5578 (2000)].
[14]O. A. Korolyuk, B. Ya. Gorodilov, A. I. Krivchikov, A. V. Raenko, and A. Ezhovski, Fiz. Nizk. Temp. **27**, 683 (2001) [Low Temp. Phys. **27**, 504 (2001)].

Translated by W. Manthey

CRYSTAL–LATTICE DYNAMICS

Low-temperature thermal conduction and sound damping in a disordered quasi-one-dimensional crystal with a weakly dispersive branch of the vibrations

E. P. Chulkin[a)]

Physicotechnical Institute, Ural Division, Russian Academy of Sciences, Izhevsk 426001, Russia
(Submitted February 9, 2005)
Fiz. Nizk. Temp. **31**, 1163–1170 (October 2005)

This paper discusses the question of how the weak localization of the low-energy acoustic vibrational mode, whose dispersion law has a large flat section, affects the propagation of sound and heat in a nonideal chainlike crystal. Analytical expressions are obtained for the thermal-conduction and sound-damping coefficients for the low-temperature region. The role of specific interference processes of phonon scattering at phonon-density fluctuations close to defects under conditions of weak interaction between the chains is analyzed. It is shown that, in the low-frequency region, where the dispersion law of the vibrational mode under consideration manifests quasi-one-dimensional properties, the renormalization of the thermal-conduction and sound-damping coefficients can be revealed experimentally when the atomic concentration of defects is $c \geqslant 5\%$. The nonstandard temperature dependence of the speed of sound is discussed. © *2005 American Institute of Physics*. [DOI: 10.1063/1.2126946]

I. INTRODUCTION

Investigators have recently devoted significant attention to systems with reduced dimension. References 1–3 discussed the possibility of weak localization of acoustic phonon modes in a nonideal chainlike crystal lattice and its effect on the low-temperature lattice coefficients of thermal conduction and sound damping. Acoustic modes with displacement vectors oriented parallel and perpendicular to weakly bound chains have been specifically considered. Vibrational modes of the first type are longitudinally polarized excitations, while modes of the second type are so-called bending excitations.[4–6] Such modes are detected in experiments on inelastic neutron scattering in quasi-one-dimensional single crystals of $(TaSe_4)_2I$ and $(Ta_{1-x}Nb_xSe_4)_2I$.[7,8] The given crystals are characterized by appreciable anharmonism of the vibrations of the atoms in a direction perpendicular to the chains at a temperature of $T \leqslant 1$ K.

An anomalous low-energy acoustic branch was detected in the same crystals in the $(\zeta,\zeta,0)$ direction and polarized along the direction of the chains. It very rapidly flattens out as wave vector **k** increases and remains in the flat regime in a large part of the Brillouin zone with characteristic frequency ν_0. It should be emphasized that the flat regime of the dispersion curve for acoustic transverse phonons in a large part of the Brillouin zone is insensitive to temperature and is maintained from the lowest temperatures ($T \sim 1$ K) all the way to room temperatures. The presence of such an anomalous vibrational mode has a substantial effect on the propagation of heat and sound in the given compounds.[9,10] We should point out that the nature of the flat dispersion mode has so far not been precisely established. It may simply have a hybridization character (the optical branches corresponding to interchain interaction and polarized along the z axis are anomalously low).

The unusual behavior of the dispersion law of these compounds reflects the fact that, beginning at some characteristic frequency ν_0, the vibrations of the chains are independent. However, the presence of weakly anharmonic interaction between the chains in this case remains in principle. Because of the large phase volume of the one-dimensional dynamic behavior, localization effects (multiple interference on each chain), which are inherent to low-dimension systems, become important.[1–3,11,12] They would occur in a three-dimensional system only for fairly strong disorder and have been analyzed in Refs. 13–16.

The goal of this paper is to investigate the contribution of localization corrections to the thermal conduction and sound damping from an acoustic low-energy dispersion curve with a large flat section. As far as models of disorder are concerned, we shall restrict ourselves to the case of diagonal disorder. It is assumed that the vibrational excitations are elastically scattered at point defects, as well as at each other as a consequence of anharmonism. Moreover, the anharmonic damping is considered to be much less than the impurity damping of the excitations.

II. SETTING UP THE PROBLEM

Let us consider a crystal with isolated impurity atoms. We shall describe its dynamic properties by a standard Hamiltonian, taking into account contributions of third- and fourth-order anharmonism:

$$H = H_0 + H_{\text{imp}} + H_{\text{int}} = H' + H_{\text{int}}, \tag{1}$$

where

$$H_0 = \frac{1}{2M_0}\sum_{n,\alpha}(p_n^\alpha)^2 + \frac{1}{2}\sum_{\substack{n,n'\\ \alpha,\beta}}\Phi_{n,n'}^{(0)\alpha\beta}u_n^\alpha u_{n'}^\beta,$$

$$H_{\rm imp} = \frac{1}{2}\left(\frac{1}{M}-\frac{1}{M_0}\right)\sum_{n,\alpha}c_n(p_n^\alpha)^2 + \frac{1}{2}\sum_{\substack{n,n'\\ \alpha,\beta}}\Delta\Phi_{nn'}^{\alpha\beta}u_n^\alpha u_{n'}^\beta,$$

$$H_{\rm int} = \frac{1}{6}\sum_{\substack{n,n',n''\\ \alpha,\beta,\gamma}}\Phi_{n,n',n''}^{\alpha\beta\gamma}u_n^\alpha u_{n'}^\beta u_{n''}^\gamma + \frac{1}{24}\sum_{\substack{n,n',n'',n'''\\ \alpha,\beta,\gamma,\delta}}\Phi_{n,n'n'',n'''}^{\alpha\beta\gamma\delta}u_n^\alpha u_{n'}^\beta u_{n''}^\gamma u_{n'''}^\delta,$$

$$\Delta\Phi_{nn'}^{\alpha\beta} = \Phi_{nn'}^{\alpha\beta} - \Phi_{nn'}^{(0)\alpha\beta}.$$

Here H_0 is the Hamiltonian of the unperturbed harmonic atomic lattice, $H_{\rm imp}$ is the perturbation caused by impurities in the system, H' is the Hamiltonian of a harmonic nonideal lattice, and $H_{\rm int}$ describes the dynamic anharmonic interionic interaction. As usual, the quantities u_n^α and p_n^α are the Cartesian components of the displacement and momentum operators of the nth atom; M and M_0 are the masses of the atoms of the impurity and ideal lattice, respectively (it is assumed that the impurity is light; i.e., $M<M_0$); and $\Phi_{nn'}$, $\Phi_{nn'n''}$, and $\Phi_{nn'n''n'''}$ are the matrix elements of the second-, third-, and fourth-order force parameters. Index 0 denotes the parameters of the regular system. Factor c_n equals zero if an atom of the matrix is at node n and equals unity if a point defect is at that node. The configuration mean $\langle c_n\rangle_n$ equals the impurity concentration c. For simplicity, we assume in what follows that the matrices of the force parameters are diagonal in the Cartesian indices. To simplify the notation, we replace the combination of nodal subscript n and Cartesian superscript α by n. When carrying out specific calculations, we assume the disorder to be diagonal; i.e., we regard the impurities as isotopic defects. In this case, we draw no distinction between $\Phi_{nn'n''}$ and $\Phi^{(0)}_{nn'n''}$, nor between $\Phi_{nn'n''n'''}$ and $\Phi^{(0)}_{nn'n''n'''}$. We thus consider only the anharmonism of the matrix and assume that it is weak. The results can be generalized to the case of off-diagonal disorder, when $\Delta\Phi_{nn'}\neq 0$.

III. DESCRIPTION OF THE MODEL

We consider a simple dynamic model of a chainlike crystal, whose lattice possesses tetragonal symmetry with parameters a, b of the unit cell. Here b is the parameter that characterizes the distance between the atoms in a chain, and a is the parameter that determines the distance between chains. We assume that the effective force interaction between the atoms along the tetragonal axis $z(\perp)$ is substantially stronger that the interaction in the base plane $xy(\parallel)$.

Using the experimental data from inelastic neutron scattering in Ref. 7 for the transverse flat-dispersion acoustic mode propagating in the base plane and polarized along the z axis, a very simple model dispersion law of the following form was proposed:

$$\omega^2(\mathbf{k}) = \omega^2(\mathbf{k}_\parallel,\mathbf{k}_\perp) = \begin{cases} v_\parallel^2 k_\parallel^2 + v_\perp^2 k_\perp^2, & 0\leqslant k_\parallel\leqslant k_\parallel^0,\\ \omega^2(\mathbf{k}_\parallel) + v_\perp^2 k_\perp^2, & k_\parallel^0 < k_\parallel < k_\parallel^B. \end{cases} \tag{2}$$

Here $\omega(\mathbf{k}_\parallel)=\omega(k_x,k_y)\approx\omega_0$ is the characteristic frequency, whose value $\nu_0=\omega_0/2\pi\approx 0.1$–$0.2$ THz varies as a function of the propagation direction in the base plane and is almost independent of temperature; $v_\parallel$ is the speed of sound in the base plane ($v_\parallel\approx 500$ m/sec); and $v_\perp$ is a speed very close to the longitudinal speed of sound v_{33} in the direction of the chain ($v_\perp\approx v_{33}=4260$ m/sec). The wave vector $k_\parallel^0=\eta k_\parallel^B(\eta\approx 0.3)$ fixes the transition from the "propagating" character of this mode to the "nonpropagating" character for wave vectors $k_\parallel>k_\parallel^0$.

Let us determine the function of the square density of phonon states in the frequency interval $0\leqslant\omega^2\leqslant\omega_0^2$. According to Eq. (2), we have

$$g(\omega)^2 = \frac{1}{\pi N}\sum_{\mathbf{k}}\delta(\omega^2-\omega^2(\mathbf{k})) = \frac{a^2 b\omega}{4\pi^2 v_\parallel^2 v_\perp}; \tag{3}$$

i.e., the dependence has a quasi-three-dimensional character. In the quasi-one-dimensional region of the spectrum $\omega_0^2<\omega^2\leqslant\omega_{\max}^2$, the density of states is expressed by

$$g(\omega) = 2\omega g(\omega^2) = \frac{\sqrt{2}}{\pi\omega_\perp}\frac{1}{\sqrt{1-(\omega_0/\omega)^2}}. \tag{4}$$

Thus, in the frequency interval of interest, the density-of-states function $g(\omega)$ of the transverse flat-dispersion mode weakly depends on frequency. When $\omega_0^2\ll\omega^2$, it coincides with the asymptotic value of the density-of-states function of the longitudinal modes.[1]

We should point out that, by using Eqs. (3) and (4), function $g(\omega)$ is determined in the entire interval of low and intermediate frequencies.

IV. DAMPING OF LOW-FREQUENCY SOUND

Sound propagation depends on the elasticity of the crystal lattice. Its damping is determined by the imaginary part of the polarization operator of a one-particle lattice Green's function. Let us introduce into consideration the one-particle retarded Green's function G^+,[17] assembled on the operators of dynamic atomic displacements u_n:

$$G_{nn'}^+(t-t') = -i\theta(t-t')\langle[u_n(t),u_{n'}(t')]\rangle. \tag{5}$$

Symbol $\langle\ \rangle$ denotes statistical averaging with the Hamiltonian H'. In the momentum representation, the Green's function of the jth polarization mode averaged over impurity configurations is determined by

$$(\tilde{G}_j^+)^{-1}(\mathbf{k},\omega) = (\bar{G}_j^+)^{-1}(\mathbf{k},\omega) - \Pi^j(\mathbf{k},\omega). \tag{6}$$

Here $\bar{G}_j^+(\mathbf{k},\omega)$ is the configuration-averaged retarded single-particle Green's function, corresponding to the total harmonic Hamiltonian H', and $\Pi^j(\mathbf{k},\omega)$ is the polarization operator. In this case,

$$\bar{G}_j^+(\mathbf{k},\omega)=\left(\omega^2-\omega_j^2(\mathbf{k})-i\frac{\omega}{\tau_i^j(\omega)}\right)^{-1}, \tag{7}$$

where the lifetime for elastic processes is

$$\tau_i^j(\omega)=\left[\frac{\pi}{2}c\varepsilon^2\omega^2 g_j(\omega)\right]^{-1}, \tag{8}$$

$g_j(\omega)$ is the spectral partial density-of-states function of the vibrational mode of the jth polarization, $\varepsilon=(M_0-M)/M_0$, and c is the concentration of isotopic defects ($c\ll 1$). Parameter $c\varepsilon^2$ determines the measure of the disorder.

To determine the temperature-dependent part of the damping coefficient of low-frequency sound, it is necessary, taking into account the anharmonic interaction of the phonons, to find the imaginary part of the polarization operator Π^j of the single-frequency lattice Green's function. It can be shown that, in the approximation of cubic anharmonism (see Refs. 2 and 19),

$$\operatorname{Im}\Pi^j=\operatorname{Im}\Pi_1^j+\operatorname{Im}\Pi_2^j, \tag{9}$$

where

$$\operatorname{Im}\Pi_1^j(\mathbf{k},\omega)=\frac{\omega}{T}\sum_{\mathbf{k}_1}\Phi_{\mathbf{k},\mathbf{k}_1+\mathbf{k}/2,\mathbf{k}_1-\mathbf{k}/2}\Phi_{\mathbf{k},\mathbf{k}_1+\mathbf{k}/2,\mathbf{k}_1-\mathbf{k}/2}\int_0^\infty\frac{d\omega_1}{2\pi}n(\omega_1)[n(\omega_1)+1]\operatorname{Re}[\bar{G}^+_{\mathbf{k}_1+\mathbf{k}/2}(\omega_1-\omega)\bar{G}^-_{\mathbf{k}_1-\mathbf{k}/2}(\omega_1)],$$

$$\operatorname{Im}\Pi_2^j(\mathbf{k},\omega)=\frac{\omega}{T}\sum_{\mathbf{k}_1,\mathbf{k}_2}\Phi_{\mathbf{k},\mathbf{k}_1+\mathbf{k}/2,\mathbf{k}_1-\mathbf{k}/2}\Phi_{\mathbf{k},\mathbf{k}_1+\mathbf{k}/2,\mathbf{k}_1-\mathbf{k}/2}\int_0^\infty\frac{d\omega_1}{2\pi}n(\omega_1)[n(\omega_1)+1]$$
$$\times\operatorname{Re}[\bar{G}^+_{\mathbf{k}_1+\mathbf{k}/2}(\omega_1-\omega)\bar{G}^-_{\mathbf{k}_1-\mathbf{k}/2}(\omega_1)U^j_{\mathbf{k}_1,\mathbf{k}_2}(\omega,\omega_1)\bar{G}^+_{\mathbf{k}_2+\mathbf{k}/2}(\omega_1-\omega)\bar{G}^-_{\mathbf{k}_2-\mathbf{k}/2}(\omega_1)].$$

Here $n(\omega)$ is the equilibrium Planck's function of the phonon distribution, while the diffusion vertex $U^j_{\mathbf{k}_1,\mathbf{k}_2}(\omega,\omega_1)=U^j(\mathbf{k}_1+\mathbf{k}_2;\omega,\omega_1)=U^j(\mathbf{q};\omega,\omega_1)$ is the sum of the fan-type graphs (see below). The first term in Eq. (9) describes the correction to the damping of phonons because of the standard anharmonic interaction between acoustic phonons in the presence of defects. The second term appeared because of taking into account the interaction of the acoustic mode with the two-phonon coherent states, which determine the weak-localization regime when the following conditions are satisfied:

$$ql^j\ll 1,\quad \omega\tau_i^j\ll 1, \tag{10}$$

where $l^j=v^j\tau_i^j$ is the free path of a phonon of jth polarization, limited by elastic scattering at impurities. In writing Eq. (9), we carried out the first iteration in the Bethe-Salpeter equation for a two-frequency lattice Green's function; i.e., $\operatorname{Im}\Pi^j(\mathbf{k},\omega)$ as a result of the term $\operatorname{Im}\Pi_2^j(\mathbf{k},\omega)$ includes only the first diffusion correction.

Expressions were obtained in Ref. 1 for the vertex U^j in the case of longitudinal and bending modes of the vibrations. The contributions of these modes to the vertex U^j were considered independent in the calculations. Using the results of Ref. 1, it can be shown that the expression for the vertex U (we shall omit superscript j in what follows) in the region of relatively low frequencies, where the vibrational spectrum manifests quasi-one-dimensional properties when the transverse dispersion is neglected, has the form

$$U(\mathbf{q};\omega_1,\omega)=\frac{2\omega_1^2}{\pi\tau_i^2(\omega_1)g(\omega_1)}\frac{1}{D_\perp^0 q_\perp^2-i\omega+\dfrac{1}{\tau_N(\omega_1)}} \tag{11}$$

Here $D_\perp^0=v_\perp^2(\omega_1)\tau_i(\omega_1)$, $v_\perp^2=v_\perp^{\circ 2}(1-\omega_0^2/\omega_1^2)$, and $\omega_1>\omega_0$. Term $1/\tau_N$ in Eq. (11) takes into account the delocalization role of the normal anharmonic processes. At low temperatures, phonon scattering occurs mainly at impurities: $\tau_i^{-1}(\omega_T)\gg\tau_N^{-1}(\omega_T)$ ($\omega_T=k_BT/\hbar$ is the characteristic frequency of the phonons). However, the presence of phonon-phonon scattering, as before, remains important. Taking the weak anharmonic damping into account in the diffusion vertex can radically alter the contribution of the localization corrections in the damping of sound and thermal conduction. Let us give the anharmonic interaction parameter Φ^3 in the standard approximation:

$$\Phi^3(\mathbf{k},\mathbf{k}_1,\mathbf{k}_2)=-i\tilde{\gamma}_3\omega(\mathbf{k})\omega(\mathbf{k}_1)\omega(\mathbf{k}_2),$$

$$\tilde{\gamma}_3=\frac{\gamma_3}{(\gamma_\parallel^2\gamma_\perp)^{1/2}}. \tag{12}$$

Here $\gamma_\parallel$, $\gamma_\perp(\gamma_\perp\gg\gamma_\parallel)$, and γ_3 are the effective harmonic and anharmonic force constants. Note that, in order of magnitude,

$$\frac{\tilde{\gamma}_3^2\omega_{\max}}{\gamma_\parallel^2\gamma_\perp}=\tilde{\gamma}_3^2\omega_{\max}\approx 10\frac{\langle u^2\rangle}{a^2}=10\delta_A, \tag{13}$$

where $\langle u^2\rangle$ is the mean square of the atomic displacements, $\omega_{\max}\approx\omega_{3(\perp)}$ is the maximum frequency in the acoustic spectrum, a is the characteristic interatomic distance, and δ_A is the anharmonicity parameter. Its value can be of the order of $10^{-1}-10^{-2}$, but not 10^{-3} (see, for example, Ref. 10).

The separate terms of the polarization operator that appear in Eq. (9), taking Eq. (12) into account, are determined as follows:

$$\operatorname{Im}\Pi_1(\mathbf{k},\omega)=2\tilde{\gamma}_3^2\omega^2(\mathbf{k})\frac{\omega}{T}\sum_{\mathbf{k}_1}\omega^2(\mathbf{k}_1)n(\omega(\mathbf{k}_1))$$
$$\times[n(\omega(\mathbf{k}_1))+1]\tau_i(\omega(\mathbf{k}_1)), \tag{14}$$

$$\mathrm{Im}\,\Pi_2(\mathbf{k},\omega)=\tilde{\gamma}_3^2\omega^2(\mathbf{k})\frac{\omega}{T}\int_{\omega_0}^{\omega_{\max}}\frac{d\omega_1}{2\pi}g(\omega_1)n(\omega_1)\times[n(\omega_1)+1]\sum_{\mathbf{q}}U(\mathbf{q};\omega_1,\omega). \quad (15)$$

In obtaining Eqs. (14) and (15), we neglected the small terms **k** and **q** in the arguments of the Green's function and the anharmonic vertex Φ^3. After this, the integration over $d\omega_1$ and the summation over **q** in Eq. (15) were factorized.

The sum in Eq. (14) diverges in the region of the limiting low temperatures. It becomes finite if one takes into account the weak anharmonic damping of the thermal phonons and the fact that they are scattered at the boundaries of the sample. The sound-absorption mechanism described by Eq. (14) is substantial in the intermediate temperature region, where the scattering of thermal phonons is sensitive to defects.[18] The expression for $\mathrm{Im}\,\Pi_2$ is valid in the frequency interval $\omega_0 \leqslant \omega < \omega_{\max}$, in which the dispersion law displays quasi-one-dimensional behavior.

Let us consider sound whose frequency satisfies the condition $\omega\tau_i \ll 1$. The temperature-dependent part of the sound-damping coefficient, taking into account Eq. (9) can be written as

$$\Gamma(\omega)=\Gamma_1(\omega)+\Gamma_2(\omega)=\frac{\mathrm{Im}\,\Pi_1(\omega(\mathbf{k}))+\mathrm{Im}\,\Pi_2(\omega(\mathbf{k}))}{2\omega(\mathbf{k})}, \quad (16)$$

assuming $\omega \approx \omega(\mathbf{k})$. Let us consider the situation in which the standard anharmonic interaction of the thermal phonons can be neglected in a nonideal crystal. Let us clarify under what condition this is possible. If $\mathrm{Im}\,\Pi_1$ is computed using the spatial Fourier components of the Green's functions of an ideal lattice, we get for phonon damping τ_N^{-1}, as a consequence of N processes in the zeroth approximation in the anharmonic phonon interaction,

$$\tau_N^{-1}=\tilde{\gamma}_3^2\omega_\perp\omega^2(\mathbf{k})\frac{\omega_0^2}{\omega_\perp^3}\exp(-\hbar\omega_0/k_BT)=\frac{\gamma_G^2(T)h}{M_0\omega_\perp a^2}\omega^2(\mathbf{k})\frac{\omega_0^2}{\omega_\perp^3}\exp(-\hbar\omega_0/k_BT), \quad (17)$$

$\gamma_G(T)$ is the Grüneisen constant, and M_0 is the mass of the atom. Then, using Eq. (8), the inequality $\tau_i^{-1} \gg \tau_N^{-1}$ is satisfied if

$$c\varepsilon^2 \gg \gamma_G^2(T)\frac{\hbar\omega_\perp}{M_0v^2}\frac{\omega_0^2}{\omega_\perp^2}\exp(-\hbar\omega_0/k_BT), \quad (18)$$

and v is the mean speed of sound.

We should point out that the Grüneisen constant at low temperatures for the vibrational mode under consideration depends very substantially on the temperature and increases as $\gamma_G(T)\sim T^{-2}$ as temperature decreases. It is estimated to be about 10^2 when $T=1$ K.[9,10]

A typical experiment on the absorption of sound has been carried out at frequencies in the megahertz range. Taking Eq. (17) into consideration and using the experimental data of Refs. 7–10 for the compound $(Ta_{1-x}Nb_xSe_4)_2I$ ($M_0 \approx 10^{-25}$ kg, $\omega_\perp/2\pi \approx 10^{12}$ Hz, $a \approx 10$ Å, $T=4$ K, $\gamma_G \approx 20$, $\omega_0/2\pi \approx 10^{11}$ Hz), we get

$$\frac{\tau_N^{-1}}{\omega}\approx 10^{-2}\frac{\omega}{\omega_\perp}, \quad (19)$$

i.e., $\omega\tau_N \gg 1$. This inequality demonstrates a weak dependence of the diffusion vertex of Eq. (11) on τ_N^{-1}. Let us estimate how realistic is the contribution of the weak localization effect to the sound damping. Let us compare Γ_1 and Γ_2. Omitting the intermediate computations, in the approximation of the dominant phonons from Eqs. (14) and (15), using Eqs. (11), (16), and (19), we have

$$\frac{\Gamma_2}{\Gamma_1}=\frac{1}{8}\sqrt{\frac{1}{2\tau_i\omega}}. \quad (20)$$

Let us make a numerical estimate of Eq. (20) for $T=4$ K. With $c\varepsilon^2 \approx 10^{-2}$ and $\omega/2\pi=50$ MHz, we get $\Gamma_1/\Gamma_2 \approx 0.16$. It can be concluded that the contribution of the weak localization effect of the flat-dispersion acoustic vibrational mode to the damping coefficient of sound in the low-temperature region becomes appreciable at an atomic defect concentration of $c \geqslant 5\%$. Note that the damping mechanism for Γ_2 can be experimentally identified from the frequency dependence $\Gamma_2 \sim \omega^{3/2}$.

V. TEMPERATURE DEPENDENCE OF THE SPEED OF ULTRASOUND

Another characteristic associated with the propagation of sound is its speed. Its temperature dependence is determined by the real part of the polarization operator, corresponding to the fourth-order dynamic anharmonic interion interaction (the second term in the Hamiltonian H_{int}). In first order of the anharmonic perturbation theory, taking into account impurity scattering,[20–22] the polarization operator Π^4 corresponding to four-phonon interaction processes is determined by

$$\Pi^4=-\frac{i}{4}\sum_{\mathbf{k}_1}\Phi^4_{\mathbf{k},-\mathbf{k}_1,\mathbf{k}_1,-\mathbf{k}}\int_0^\infty\frac{d\omega_1}{2\pi}\coth\frac{\omega_1}{2T}[\bar{G}^+(\mathbf{k}_1,\omega_1)-\bar{G}^-(\mathbf{k}_1,\omega_1)]. \quad (21)$$

Let us assign the anharmonic vertex Φ^4 in the standard approximation:

$$\Phi^4_{\mathbf{k},-\mathbf{k}_1,\mathbf{k}_1,-\mathbf{k}}=\tilde{\gamma}_4\omega^2(\mathbf{k})\omega^2(\mathbf{k}_1);\quad \tilde{\gamma}_4=\frac{\gamma_4}{\gamma_2^2}, \quad (22)$$

where γ_4 is the fourth-order effective anharmonic force constant. Taking into account Eqs. (7) and (22), after a number of transformations, we get from Eq. (21) that

$$\Pi^4(\omega,\mathbf{k})=\frac{\tilde{\gamma}_4}{8}\omega^2(\mathbf{k})\int_0^{\omega_{\max}}d\omega(\mathbf{k}_1)g(\omega(\mathbf{k}_1))\omega(\mathbf{k}_1)\times\coth\frac{\omega(\mathbf{k}_1)}{2T}=\omega^2(\mathbf{k})\Delta(T). \quad (23)$$

In experiment, one usually measures the temperature dependence of the relative variation of the speed of an ultrasound wave,

$$\frac{v(T)-v(T_0=0)}{v(T_0=0)}=\frac{\Delta v(T)}{v}.$$

In lowest-order perturbation theory, in terms of the anharmonic interaction Φ^4, the value of $\Delta v/v$ in terms of the model dispersion law of Eq. (2) is determined by

$$\frac{\Delta v}{v}=\frac{\Delta v_\perp}{v_\perp}=\frac{\Delta v_\parallel}{v_\parallel}=\frac{d\Delta(T)}{dT}T$$
$$=-\frac{Th}{8Mv^2}\left\{\gamma_G^2(T)C(T)-U(T)\left|\frac{\gamma_G^2(T)}{dT}\right|\right\}. \quad (24)$$

here

$$C(T)=\frac{1}{T^2}\int_0^{\omega_{\max}}d\omega g(\omega)\omega^2 n(\omega)[n(\omega)+1],$$

$$U(T)=\frac{1}{2}\int_0^{\omega_{\max}}d\omega g(\omega)\omega\coth\frac{\omega}{2T},$$

$$|\tilde{\gamma}_4(T)|\omega_{\max}\approx\frac{\gamma_G^2(T)h}{M\omega_{\max}a^2}.$$

According to Eq. (24), the total renormalization of the speed of sound is determined by two terms. In considering the low-temperature region in Eq. (24), the behavior of the second term is essential. It results in an increase $\Delta v/v$ as T increases. However, its role becomes secondary at a certain temperature [since $\gamma_G(T)\approx$const], and the variation $\Delta v/v$ will be determined chiefly by the first term in Eq. (24). The results of an experimental investigation of renormalization of the speed of sound in quasi-one-dimensional systems are reflected in Ref. 10. They are evidence that there is a maximum in the temperature dependence of $\Delta v/v$ for the $(Ta_{1-x}Nb_xSe_4)_2I$ system.

VI. LATTICE THERMAL CONDUCTION

Using the standard Kubo formula, let us determine the static thermal-conductivity tensor $\chi_{\alpha\alpha'}$ for the low-temperature interval in which the free path is dictated by the elastic scattering of phonons by defects. The case of a layered crystal is discussed in detail in Refs. 11 and 12.

In the case of a chainlike crystal, the lattice possesses axial symmetry, and the tensor $\chi_{\alpha\alpha'}$ has two principal values, which we call $\chi_\parallel$ and $\chi_\perp$. They characterize the thermal conductivity in the xy plane and along the z axis, respectively. According to Ref. 1, in the one-dimensional approximation, we have

$$\chi_{\alpha\alpha'}=\frac{1}{NT^2}\sum_{\mathbf{k}}\omega^2(\mathbf{k})n(\omega(\mathbf{k}))[n(\omega(\mathbf{k}))+1]D_{\alpha\alpha'}(\omega(\mathbf{k})) \quad (25)$$

(N is the number of lattice atoms per unit volume). In Eq. (25), $D_{\alpha\alpha'}$ denotes the diffusion-coefficient tensor, and α is the Cartesian index. The quantity $D_{\alpha\alpha'}(\omega_1)$ has the form

$$D_{\alpha\alpha'}(\omega_1)=\frac{4}{\pi g(\omega_1)}\times\sum_{\mathbf{kk}'}v_\alpha(\mathbf{k})v_{\alpha'}(\mathbf{k}')\omega(\mathbf{k})\omega(\mathbf{k}')G_2(\mathbf{k},\mathbf{k}';\omega_1). \quad (26)$$

We recall that the quantities $\omega(\mathbf{k})$ and $v=\partial\omega(\mathbf{k})/\partial\mathbf{k}$ in Eqs. (25) and (26) are the dispersion law and the group velocity of the phonon mode with quasi-momentum $\mathbf{k}$. The spatial Fourier component of the two-particle Green's function G_2 is expressed in terms of the one-particle Green's functions:

$$G_2(\mathbf{k},\mathbf{k}';\omega_1)=\lim_{\omega\to\infty}\langle G^+_{\mathbf{kk}'}(\omega)G^-_{\mathbf{kk}'}(\omega_1-\omega)\rangle_c, \quad (27)$$

where the symbol $\langle\ldots\rangle_c$ denotes averaging over the different impurity configurations. In general (see Refs. 1, 20, 23, and 24), in the momentum representation, the equation for G_2 is written in the form of the Bethe–Salpeter equation:

$$G_2(\mathbf{k},\mathbf{k}';\omega_1)=\lim_{\omega\to\infty}\left\{\tilde{G}^+_{\mathbf{k}}(\omega_1)\tilde{G}^-_{\mathbf{k}'}(\omega_1-\omega)\times\left[\delta_{\mathbf{kk}'}+\sum_{\mathbf{k}_1}U(\mathbf{k},\mathbf{k}_1;\omega_1,\omega)G_2(\mathbf{k}_1,\mathbf{k}';\omega_1,\omega)\right]\right\}. \quad (28)$$

We shall consider the role of the inverse coherent-scattering processes (certain specific interference processes that appear when phonons are scattered at fluctuations of the phonon density of states close to defects). As pointed out above, they determine the weak localization regime, implemented when inequalities (10) are satisfied. In the case of interest to us, the vertex part of U that appears in Eq. (28) is determined by Eq. (11).

Let us determine the principal value of tensor $D_\perp$ when inequalities (10) are satisfied. Using the representation for the Green's function in Eq. (7) and taking into account Eqs. (26) and (28), we have

$$D_\perp(\omega_1)=D^0_\perp(\omega_1)\left(1-\frac{\tau_i^2(\omega_1)}{2\omega_1^2}\sum_{\mathbf{q}}U(\mathbf{q};\omega_1)\right). \quad (29)$$

After substituting into Eq. (29) the expressions for the vertex, Eq. (11), in which the weak anharmonic interaction of the thermal phonons (N processes) is taken into account, we get an expression for $D_\perp$ in the form

$$D_\perp(\omega_1)=D^0_\perp(\omega_1)\left(1-\frac{1}{8\sqrt{2}}\sqrt{\frac{\tau_N}{\tau_i}}\right). \quad (30)$$

We should emphasize that the deviation of $D_\perp(\omega_1)$ from $D^0_\perp(\omega_1)$ is associated with the effect of inverse coherent scattering processes. It directly follows from a consideration of Eq. (30) that the picture of phonon transport substantially depends on the ratio of the elastic and inelastic relaxation times. The representation for $D_\perp(\omega_1)$ in the form of Eq. (30) is valid in the temperature region for which inequality (18) is satisfied, i.e., $\tau_i^{-1}\gg\tau_N^{-1}$.

Let us estimate the value of τ_N/τ_i for two temperatures. Let the disorder parameter be $c\varepsilon^2 \approx 10^{-2}$. When $T=1$ K($\gamma_G \approx 10^2$), we get $\tau_N/\tau_i \approx 8$, whereas, when $T=4.2$ K($\gamma_G \approx 20$), this quantity is about 10.

VII. CONCLUSION

This paper has analyzed how the weak localization of the low-energy acoustic vibrational mode with a large flat section affects the low-temperature lattice coefficients of thermal conductivity and ultrasound damping in a nonideal, anharmonic, strongly anisotropic, chainlike crystal lattice. It has been established that, at a low impurity concentration, the presence of a large phase volume of quasi-one-dimensional dynamic behavior produces no substantial changes in the propagation of sound and heat. According to numerical estimates, in the case of thermal conduction, this is associated with significant limitation of the elastic relaxation processes by inelastic relaxation processes: at liquid-helium temperatures and an atomic concentration of defects ($\sim 1\%$), the inequality $\tau_i \ll \tau_N$ is not rigorously satisfied.

It would be most informative to compare the experiment results with the qualitative predictions of theory—the frequency dependence of the damping coefficient of sound, $\Gamma_2 \sim \omega^{3/2}$, associated with the effect considered above. However, such a frequency dependence was not observed experimentally, apparently because of the inadequate disorder of the actually existing weakly doped samples. Samples of $(Ta_{1-x}Nb_xSe_4)_2I$ with $x \geqslant 0.2$ are suitable for observing the given frequency dependence, if the ultrasound frequency used in the experiment is $\omega/2\pi \leqslant 10$ MHz. The behavior of $\Delta v(T)/v$ can be qualitatively explained in a wide temperature region by the influence of fourth-order anharmonic processes.

The contribution of localization effects to the propagation of sound and heat in $(Ta_{1-x}Nb_xSe_4)_2I$ systems can thus be experimentally detected at atomic defect concentrations of $c \geqslant 5\%$.

This work was carried out with the partial financial support of the Russian Foundation for Basic Research (Grants 03-02-16233 and 04-02-16680).

[a)]E mail: chulkin@otf.pti.udm.ru

[1]A. P. Zhernov and E. P. Chulkin, Zh. Éksp. Teor. Fiz. **117**, 350 (2000) [JETP **90**, 308 (2000)].
[2]E. P. Chulkin, A. P. Zhernov, and T. N. Kulagina, Fiz. Nizk. Temp. **26**, 173 (2000) [Low Temp. Phys. **26**, 128 (2000)].
[3]E. P. Chulkin, Zh. Éksp. Teor. Fiz. **122**, 1022 (2002) [JETP **95**, 881 (2002)].
[4]I. M. Lifshits, Zh. Éksp. Teor. Fiz. **22**, 475 (1952).
[5]A. M. Kosevich, *Theory of the Crystal Lattice* [in Russian] (Kharkov, Vishcha Shkola, 1988).
[6]E. G. Brovman, R. Kagan, and A. Kholas, Zh. Éksp. Teor. Fiz. **61**, 2429 (1971) [Sov. Phys. JETP **34**, 1300 (1972)].
[7]J. E. Lorenzo, R. Currat, A. J. Dianoux, P. Monceau, and F. Levy, Phys. Rev. B **53**, 8316 (1996).
[8]J. E. Lorenco, R. Currat, P. Monceau, B. Hennion, H. Berger, and F. Levy, J. Phys.: Condens. Matter **10**, 5039 (1998).
[9]R. Maynard, A. Smontara, and J. C. Lasjaunias, Physica B **263–264**, 678 (1999).
[10]M. Saint-Paul, S. Holtmeier, P. Monceau, R. Currat, and F. Levy, J. Phys.: Condens. Matter **8**, 2021 (1996).
[11]A. P. Zhernov and E. P. Chulkin, Zh. Éksp. Teor. Fiz. **113**, 930 (1998) [JETP **86**, 507 (1998)].
[12]A. P. Zhernov and E. P. Chulkin, Fiz. Tverd. Tela (St. Petersburg) **40**, 132 (1998) [Phys. Solid State **40**, 118 (1998)].
[13]I. Ya. Polishchuk, A. L. Burin, and L. A. Maksimov, JETP Lett. **51**, 730 (1990).
[14]A. P. Zhernov, E. I. Salamatov, and E. P. Chulkin, Phys. Status Solidi B **165**, 355 (1991).
[15]A. P. Zhernov and E. P. Chulkin, Zh. Éksp. Teor. Fiz. **109**, 602 (1996) [JETP **82**, 321 (1996)].
[16]I. Y. Polishchuk, L. A. Maksimov, and A. L. Burin, Phys. Rep. **288**, 205 (1997).
[17]Yu. M. Kagan, *Materials of the School on the Theory of Defects in Crystals* [in Russian] (Tbilisi, 1969), vol. 2, p. 93.
[18]R. Berman, *Thermal Conduction of Solids* [in Russian] (Mir, Moscow, 1979).
[19]E. P. Chulkin, A. P. Zhernov, and T. N. Kulagina, Fiz. Nizk. Temp. **25**, 1218 (1999) [Low Temp. Phys. **25**, 912 (1999)].
[20]A. A. Maradudin and S. Califano, Phys. Rev. B **48**, 12 628 (1993).
[21]A. P. Zhernov and E. P. Chulkin, Fiz. Tverd. Tela (St. Petersburg) **36**, 2302 (1994) [Phys. Solid State **36**, 1254 (1994)].
[22]A. P. Zhernov and E. P. Chulkin, Phys. Status Solidi B **193**, 67 (1996).
[23]E. Akkermans and R. Maynard, Phys. Rev. B **32**, 7850 (1985).
[24]Qian-Jin Chu and Zhao-Qing Zhang, Phys. Rev. B **38**, 4906 (1988).

Translated by W. Manthey

LOW-TEMPERATURE PHYSICS OF PLASTICITY AND STRENGTH

The effect of low-temperature strain on the structure and the critical-current degradation of the superconducting alloy Nb–Ti

O. I. Volchok, M. B. Lazareva,[b] A. V. Mats, Ya. D. Starodubov,[a] N. A. Chernyak, and O. V. Chernyĭ

Kharkov Physicotechnical Institute National Science Center, ul. Akademicheskaya, 1, Kharkov 61108, Ukraine

(Submitted January 27, 2005; resubmitted March 21, 2005)
Fiz. Nizk. Temp. **31**, 1171–1176 (October 2005)

The structural-phase aspects of the behavior of the critical current under load in the superconductive alloy Nb–48.5 wt% Ti are studied. It is shown that the optimum preliminary strain at $T=77$ K with subsequent annealing suppresses the tendency of the β matrix of the alloy to undergo phase transformations according to martensitic kinetics under uniaxial tension at $T=4.2$ K, and this is manifested in the reduction of the critical-current degradation effect when loaded to $\sigma=0.9\sigma_{\text{fr}}$ in a transverse magnetic field of $H=5$ T. The paper discusses possible critical-current degradation mechanisms under mechanical loading in the niobium-titanium alloy, based on models of critical current flow in the β matrix reinforced with martensitic interlayers. © *2005 American Institute of Physics*. [DOI: 10.1063/1.2126947]

Superconductive materials based on niobium-titanium alloy and possessing a unique combination of electrophysical and mechanical properties are being widely used in the creation of a number of superconductive magnetic systems. The conditions that arise when superconductive magnetic systems are operated make it necessary to study the behavior of the current-carrying characteristics of conductors made from these alloys under mechanical stress. It is well known that a reduction in the critical current density J_c (critical-current degradation) is observed in niobium-titanium superconductors as a result of unidirectional tension. This phenomenon usually has a reversible character and, according to existing concepts, is a manifestation of pseudoelasticity effects, in particular, a reversible martensitic transformation.[1–4] The implementation of these structural reconstructions is sensitive to the defect concentration of the alloy and its phase composition, the specifics of the formation of which largely depend on the temperature conditions of the strain of the alloy.

In this connection, the goal of this paper was to study how the features of the structural-phase state of a Nb–Ti alloy, formed as a result of strain by drawing at 77 K, affects the value of the critical-current degradation.

THE MATERIAL AND THE EXPERIMENTAL TECHNIQUE

The starting material for the investigations was a single-core wire superconductor made from the alloy Nb–48.5 wt% Ti with a diameter of $d=1.5$ mm, subjected to preliminary multistage thermomechanical processing.[5] To obtain comparative data that reveals the role of the cryogenic strain conditions, further drawing with $d=1.5$ mm was accomplished in two regimes: in a single stage, at 300 K to the final diameter ($d_f=0.27$ mm); and in two stages, in which part of the strain to the final diameter was produced at 77 K (ε_{77} is the fraction of the strain at 77 K), with subsequent strain at 300 K to the final diameter. After deformation by drawing, the wire samples were annealed at 670 K for 70 h for the first regime and 10 h for the second regime, resulting in diffusion decay of the β solid solution in the form of precipitation of α-Ti particles, which provided the current-carrying ability of the superconductor. The temperature-time parameters of the annealing of the samples was chosen, as shown in Ref. 6, from considerations of optimizing the volume density of particles of the α-Ti phase.

Deformation by drawing at 77 K was carried out on the apparatus described in Ref. 7. The substructural state of the alloy was monitored by means of a transmission electron microscope. Measurements of J_c under uniaxial tension were made on a special apparatus[8] both under load and after the sample was unloaded in a transverse magnetic field of $H=5$ T at 4.2 K. The critical field was determined from the appearance of a potential difference of 1 μV on a sample length of 1 cm. The error of determining J_c was 1%. The quantity $\delta J_c=[(J_{c0}-J_c)/J_{c0}]\%$ was used as a parameter that characterizes the critical-current degradation effect, where J_{c0} and J_c are the critical current densities before loading and for stresses of $\sigma=0.9\sigma_{\text{fr}}$, respectively ($\sigma_{\text{fr}}$ is the fracture strength of the alloy at 4.2 K).

RESULTS AND DISCUSSION

Figure 1 shows the dependences of the reduced critical current density J_c/J_{c0} on the tensile stress for Nb–Ti alloy samples that have undergone successive mechanical-thermal processing using two regimes: in a single stage (deformation by drawing at 300 K) and in two stages (deformation by drawing at 77 K, $\varepsilon_{77}=84\%$, and then at 300 K).

It can be seen that the reduced critical current density decreases monotonically as the stress increases and is restored to its initial value when the sample is unloaded. It is noteworthy that the stress σ_0 at which the critical-current degradation begins (the conventional threshold of degrada-

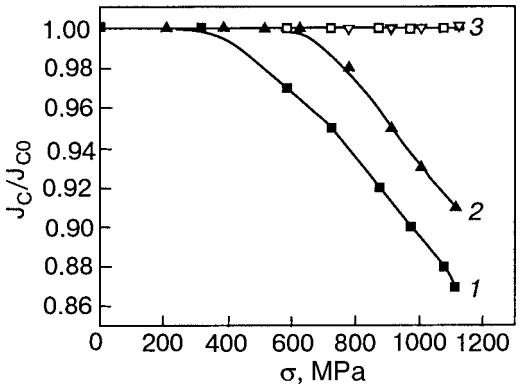

FIG. 1. Reduced critical current density of alloy Nb–48.5 wt% Ti vs tensile stress at 4.2 K in a field of 5 T: after deformation by drawing at 300 K to the final diameter (*1*); after accomplishing a fraction of the deformation by drawing in liquid nitrogen ($\varepsilon_{77}=84\%$), with subsequent drawing at 300 K to the final diameter (*2*); after unloading the samples at each loading cycle (*3*).

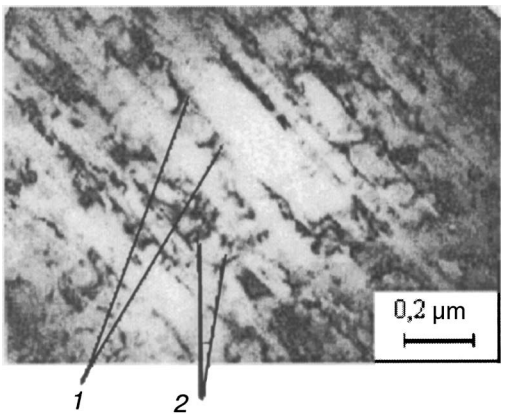

FIG. 3. Microstructure of alloy Nb–48.5 wt% Ti after drawing at 77 K ($\varepsilon_{77}=84\%$); accumulation of dislocations of the same kind (*1*) and of strain boundaries (*2*).

tion) is 600 MPa for the alloy undergoing the low-temperature stage of strain, and only 250 MPa for the alloy strained only at 300 K.

Figure 2 shows how parameter δJ_c at $\sigma=0.9\sigma_{\rm fr}$ depends on the strain at the low-temperature stage of drawing. In the interval 20–97%, the suppression effect of the critical-current degradation has a pronounced minimum in the region of $\varepsilon_{77}=84\%$ and varies from 23 to 12%. We should point out that, for samples that undergo mechanical-thermal action by single-stage strain at 300 K, the parameter δJ_c is 22% when $\sigma=0.9\sigma_{\rm fr}$.

As already pointed out, a structural factor of critical-current degradation when niobium-titanium alloys are loaded is the formation of a martensitic phase, and this is confirmed by the data of Ref. 9, where lamellar inclusions of the martensitic phase were observed at 4.2 K (*in situ*) in the electron microscope, disappearing after the load was removed. It is well known[10] that the dynamics of the implementation of the processes of forming martensite are determined by the superposition of the applied external stress and local internal stresses, depending, in particular, on the state of the boundaries of the fragments of the β matrix, which varies as the strain builds up. Consequently, it is natural to associate the nonmonotonic character of $\delta J_c(\varepsilon_{77})$ with the evolution of the structural state of the material accompanying successive mechanical-thermal processing, the main stage in which is deformation by drawing at 77 K.

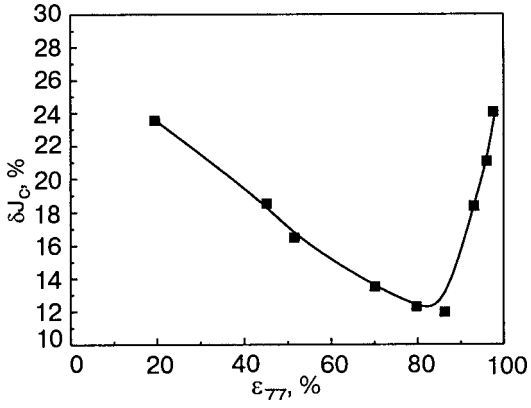

FIG. 2. Critical-current degradation parameter of alloy Nb–48.5 wt% Ti in a field of $H=5$ T vs the fraction of deformation by drawing in liquid nitrogen.

The electron-microscope studies showed that the dominant types of defect structure of the niobium-titanium alloy after drawing at 77 K are dislocation-dislocation boundaries, extending in the direction of the drawing, and dense clusters of dislocations of a single type, connecting the sections of these boundaries. These structural elements are the result of the manifestation at large plastic strains of the collective interaction of dislocations, the implementation of rotary modes of plastic strain, and the partial annihilation of dislocations. The gradual increase of the degree of cryogenic strain all the way to $\varepsilon_{77}=84\%$ substantially changes the character of the elastically stressed state of the material: The mean transverse size of the subgrains decreases to about 490 Å, and the density of clusters of dislocations of the same sign increases, causing a sharply inhomogeneous distribution of internal stresses and constituting the sites of formation of transverse strain boundaries (Fig. 3).

The microdiffraction data that determine how the azimuthal component of the disorientation angle ω_i of the subgrains depends on ε_{77} are noteworthy (Fig. 4). The microdiffraction data are evidence that a wide spectrum of disorientations has appeared. As the mean disorientation angle ω_i increases all the way to the maximum value, groups of fragments appear, some compensated and some uncompensated with respect to disorientations; i.e., the degree of disorientation of the subgrains can accumulate in the final volume. This indicates that the internal stress distribution is becoming more inhomogeneous. We should point out that the contribution of the subsequent deformation by drawing at 300 K to $d_f=0.27$ mm has an insignificant effect on the evolution of the structure of the alloy.

Annealing at 670 K after the alloy undergoes strain at $T=77$ K corresponds to the first stage of recovery (relaxation).[11] Redistribution of the dislocations both by slip (including transverse slip) and by climb is observed in this case, as well as by annihilation of part of the dislocations of opposite sign. Moreover, part of the small-angle boundaries break down without the formation of new ones. As can be seen from Fig. 5a, the distance between the boundaries of the fragments increases by a factor of 2, and the dislocations are distributed more uniformly in the body of the fragments. It is

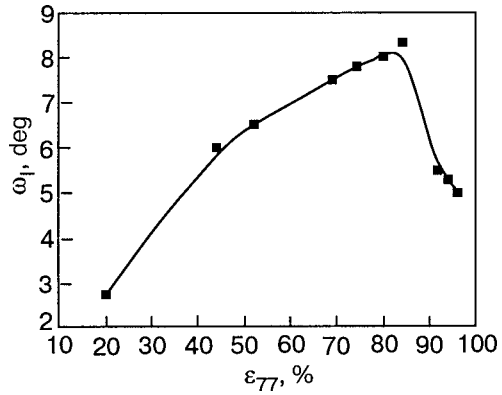

FIG. 4. Variation of disorientation angles between separate fragments of the β phase of alloy Nb–48.5 wt% Ti vs deformation by drawing in liquid nitrogen ($\varepsilon_{77}=84\%$).

well known that recovery processes occur more intensively, the higher the defect concentration in the crystal lattice. In the case under consideration, the defect concentration and the corresponding level of the elastically stressed state are maximized at a low-temperature strain of ε_{77} in the region of 84%, and this significantly increases the completeness of the thermally activated recovery processes. It should be pointed out that, besides dislocation recovery, diffusion processes are activated that implement phase transformations with precipitation of α-Ti particles (Fig. 5b and 5c). In this case, as indicated earlier,[6] the new formations are distributed fairly uniformly and have highly coherent boundaries with the matrix that do not possess long-range stresses. The decrease of the concentration of point defects and the formation of a new phase can thus be classified as the appearance of relaxation processes.

The resulting data are evidence that the mechanical-thermal processing setup used for this paper results in the state of the crystal lattice of the alloy that is closest to equilibrium and that significantly reduces the concentration of potential nucleation sites of elastic martensitic formations accompanying subsequent loading at 4.2 K.

A further increase of the degree of drawing ($\varepsilon_{77}>84\%$) at 77 K is accompanied by dynamic recovery effects: a certain increase of the transverse size of the subgrains, a transformation of the clusters of dislocations of the same kind into boundaries of various capacities, and a decrease of the free-dislocation density, with the formation of low-angle dislocation boundaries ($\omega_i=0.5-1.5°$); this, in particular, is reflected in a reduction of the mean value of ω_i (Fig. 4). In this case, as a result of annealing, the efficiency of the thermally activated relaxation processes is reduced, and microvolumes are maintained with an increased level of local internal stresses of one origin or the other and serve as the nucleation foci of martensite when the material is subsequently loaded at 4.2 K. Thus, conditions are again created for the development of martensitic transformations (the suppression effect of the critical-current degradation levels out—see Fig. 2, right-hand branch).

Let us compare the revealed structure-phase variations of the alloy with the behavior of the experimental $J_c/J_{c0}(\sigma)$ dependences. It can be seen from Fig. 1 that the critical current-density degradation threshold in samples undergoing the drawing stage at 77 K is greater than in samples deformed only at 300 K. Let us consider the main factors that can result in a shift of the σ_0 value, assuming that $\sigma_0 \sim \sigma_e$, where σ_e is the external elastic stress at which strain martensite arises in the material.[3] The stresses in the region where martensitic inclusions arise can be determined by means of

$$\sigma_0 \sim S_s + S_0 + \sigma_T, \tag{1}$$

where S_s, S_0, and σ_T are the stresses caused, respectively, by the force of surface tension, the force of dry friction, and the difference of chemical potentials of the phases.[10] We shall qualitatively estimate the value of S_s as $S_s \sim 10^{-3}G$, where G is the shear modulus. It is well known that the G values for alloys undergoing diffusion phase transformations are mainly determined by the variation of the chemical composition of the solid solution.[12] Variations of the defect structure have no substantial effect on G in this case. According to Ref. 4, the precipitation of titanium-containing phases when a β solid solution decays must be accompanied by an increase of G. It follows from the accumulated experimental data that S_0 increases as the defect concentration of the material and the fraction of internal stresses increase and, from its upper limit, we find $S_0 \sim \sigma_{0.2}$, where $\sigma_{0.2}$ is the yield strength of the material. The increase of parameters S_s and S_0 must reduce the tendency of the β phase to undergo low-temperature phase transformations. We estimate the σ_T term as[3]

$$\sigma_T = \frac{a}{b} q \frac{T - T_0}{T_0}, \tag{2}$$

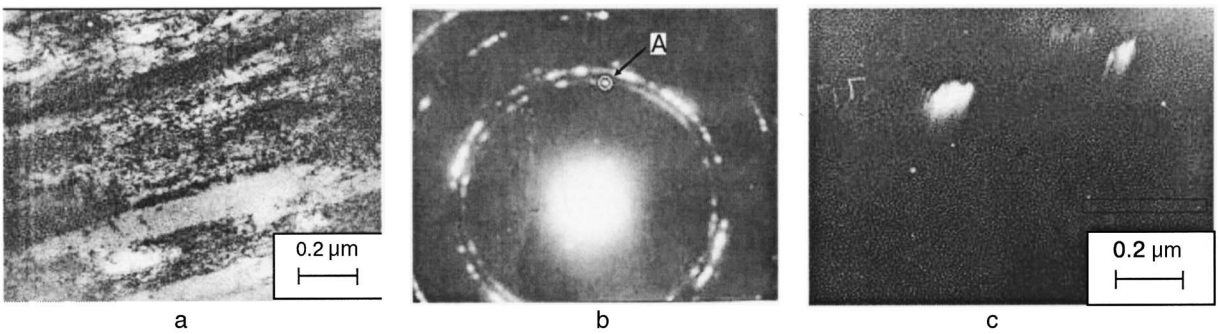

FIG. 5. Structure of alloy Nb–48.5 wt% Ti after deformation by drawing ($\varepsilon_{77}=84\%$) in liquid nitrogen and final annealing at $T=670$K for 10 h: bright-field image (*a*); microelectron-diffraction pattern (showing the diffraction spot *A* at which the dark-field image was photographed) (*b*); and dark field at the diffraction spot $\bar{g}=10\bar{1}0$ of α-Ti (*c*).

where a is the interplanar distance, b is the Burgers vector of the transformation dislocation, q is the specific heat of the phase transformation, and T_0 is the phase-equilibrium temperature, with $T_0 \sim T_m$, where T_m is the temperature at which strain martensite appears, while T is the temperature of the experiment (4.2 K). Since increasing the niobium concentration in the β phase displaces the temperature region of the martensitic reaction toward lower temperatures, the nucleation process of martensite in the structure, obtained by cryogenic drawing, is suppressed. Consequently, the β phase becomes more stable against martensitic transformations at low temperatures as the decay of the β solid solution with precipitation of the α phase becomes more intense.[13] Our analysis of Eq. (1) qualitatively explains the experimental fact that the degradation threshold σ_0 is displaced toward larger values if the alloy is preprocessed at 77 K (Fig. 1).

As is well known, in optimized Nb–Ti conductors, good correlation is established between the substructure of the alloy, a high level of J_c, and the magnetic-flux pinning mechanism. In this case, the pinning caused by magnetic interaction of vortex filaments with ribbonlike precipitates of the α-Ti phase can be considered dominant.[13,14] The appearance of strain martensite in the form of various oriented flat interlayers introduces significant changes into the effective structure of the pinning centers. The absence of systematic literature data on the parameters of the martensitic phase in niobium-titanium alloys at the instant of loading makes it hard to treat the experimental results in terms of critical-current degradation.

Let us regard the interface of the martensitic phase as a successive alternation of the sections of coherence that separate the growth steps (regions of noncorrespondence) and generate long-range elastic fields.[15] Because of their morphology, the phase interfaces represent strong obstacles for transverse motion of the vortices. If the phase interface is oriented parallel to a moving Lorenz force, the part of the vortices fixed to its pinning potential acquire the possibility of being displaced along this boundary. One cause that initiates dissipative motion of the localized vortices when $J_c < J_{c0}$ can be that the elementary pinning force is reduced because of the longitudinal lengthening of the core of the vortex filament in the plane of a coherent boundary segment.[16,17] In this connection, the behavior of the $J_c(\sigma)$ dependence will be determined by the development of a network of favorably oriented martensitic boundaries, playing the role of channels of preferred motion of the vortices. Moreover, such interphase boundaries possess elevated fluctuational mobility, caused by the local stress concentration.[18] Consequently, thermally activated depinning of the vortices can be the mechanism that controls the variation of $J_c(\sigma)$. It can thus be assumed that the preliminary mechanical-thermal action used here, which reduces the mobility of the transformation dislocations, must suppress the critical-current degradation process under the action of tensile stress.

CONCLUSIONS

1. The regime of drawing a conductor made from the alloy Nb–48.5 wt% at 77 K has been optimized in the level of strain (ε_{77}), reducing the degradation effect of critical current J_c under mechanical loading by a factor of 2 and increasing the stress at which degradation begins by a factor of 2.5. It has been established that the optimum value of deformation by drawing at 77 K($\varepsilon_{77}=84\%$) corresponds to the active development of the rotational mode of plastic strain in the alloy, and this manifests itself in the maximization of the azimuthal component of the disorientation angle ω_i of the subgrains ($\omega_{i\,\max} \approx 8°$).

2. On the basis of the structural differences in the alloy Nb–48.5 wt% after deformation by drawing at 77 K with various values of ε_{77} explained here, concepts have been developed concerning how thermal relaxation processes affect the completeness of the martensitic transformation with subsequent stretching of the alloy at 4.2 K.

3. Possible critical-current degradation mechanisms have been discussed, according to which the reduction of J_c can be determined both by the dissipative motion of vortices more weakly attached to coherent sections of the martensitic phase boundaries and by the elevated fluctuational mobility of the transformation dislocations, leading to thermally activated depinning of the vortices.

[a)]Deceased
[b)]Email: mlazarev@kipt.kharkov.ua

[1]J. W. Ekin, F. R. Fickett, and A. F. Clark, Adv. Cryog. Eng. **22**, 449 (1977).
[2]J. W. Ekin, IEEE Trans. Magn. **13**, 127 (1977).
[3]V. S. Boĭko, M. B. Lazareva, Ya. D. Starodubov, O. V. Chernyĭ, and V. M. Gorbatenko, Fiz. Nizk. Temp. **18**, 121 (1992) [Sov. J. Low Temp. Phys. **18**, 83 (1992)].
[4]C. C. Koch and D. S. Easton, Cryogenics **17**, 391 (1977).
[5]O. V. Chernyi, L. G. Udov, G. E. Storozhilov, M. B. Lazareva, N. F. Andrievskaya, L. A. Kornienko, V. V. Slezov, V. V. Sagalovich, Ya. D. Starodubov, and T. Yu. Rudycheva, Cryogenics, ICMC Suppl. **32**, 597 (1992).
[6]V. K. Aksenov, O. I. Volchok, V. M. Gorbatenko, V. A. Emlyaninov, M. B. Lazareva, A. V. Mats, V. S. Okovit, Ya. D. Starodubov, O. V. Chernyĭ, and L. A. Chirkina, Fiz. Nizk. Temp. **20**, 595 (1994) [Low Temp. Phys. **20**, 471 (1994)].
[7]O. I. Volchok, I. M. Nekluidov, Ya. D. Starodubov, and B. P. Chornyi, Cryogenics ICMC Suppl. **32**, 114 (1992).
[8]M. B. Lazareva, Ya. D. Starodubov, and M. P. Starolat, Voprosy Atomnoĭ Nauki i Tekhniki, ser. Fund. Prik. Sverkhprovodimost' No. **1**(15), 23 (1977).
[9]B. Obst and D. Pattanayak, J. Low Temp. Phys. **41**, 595 (1980).
[10]V. S. Boĭko, R. I. Garber, and A. M. Kosevich, *Reversible Plasticity of Crystals* [in Russian] (Nauka, Moscow, 1991).
[11]S. S. Gorelik, *Recrystallization of Metals and Alloys* [in Russian] (Metallurgiya, Moscow, 1967).
[12]M. L. Bernshteĭn and V. A. Zaĭmovskiĭ, *Structure and Technical Properties of Metals* [in Russian] (Metallurgiya, Moscow, 1970).
[13]L. D. Cooley, P. J. Lee, and D. C. Larbalestier, Phys. Rev. B **53**, 6638 (1996).
[14]V. V. Slezov and O. V. Chernyĭ, Voprosy Atomnoĭ Nauki i Tekhniki, ser. Vakuum, Chistye Materialy, Sverkhprovodimost' No. **12**(1), 80 (2002).
[15]J. W. Cristian, Metall. Trans. A **13**, 509 (1982).
[16]A. Gurevich, Phys. Rev. B **48**, 12 857 (1993).
[17]A. Gurevich and L. D. Cooley, Phys. Rev. B **50**, 13 563 (1994).
[18]*Shape-Memory Effects in Alloys* [in Russian] (Metallurgiya, Moscow, 1979), p. 60.

Translated by W. Manthey

A low-temperature plasticity anomaly of concentrated fcc solid solutions: the Pb–In system

N. V. Isaev,[a] V. D. Natsik, V. V. Pustovalov, V. S. Fomenko, and S. É. Shumilin

B. I. Verkin Physicotechnical Institute of Low Temperatures, National Academy of Sciences of Ukraine, pr. Lenina, 47, Kharkov 61103, Ukraine

(Submitted December 27, 2004; resubmitted February 25, 2005)
Fiz. Nizk. Temp. **31**, 1177–1189 (October 2005)

This paper discusses the regularities of the plastic strain of single crystals of solid solutions of the Pb–In system at low and very low temperatures, 0.5 K$<T<$30 K. For Pb alloys with 5, 10, and 20 at. % In, the temperature dependences of the yield strength, $\tau_0(T)$, and of the increment of the deforming stress, $\Delta\tau(T)$, are measured after a tenfold increase of the strain rate. Specific features (anomalies) of these dependences are detected that do not correspond to concepts of thermally activated motion of dislocations through impurity barriers. It is established that the character of the anomalies substantially changes as the indium concentration varies from moderate values (5 and 10 at. %) to high values (20 at. %). The low-temperature plasticity anomaly of moderately concentrated alloys is interpreted on the basis of the concepts of thermal-inertial and quantum-inertial motion of dislocations through a system of single impurity atoms. In the case of the highly concentrated alloy, the anomaly is interpreted in terms of a model of an inhomogeneous impurity distribution—the presence in the alloy of small clusters that create stronger barriers for the motion of dislocations than do single impurity atoms. The high level of efficient deforming stresses under conditions of deep cooling results in a dynamic regime of dislocation motion through the system of clusters and single impurities, with the yield strength τ_0 of the alloy being determined by impurity inhibition of dry-friction type, while the rate sensitivity $\Delta\tau$ of the deforming stress is determined by viscous inhibition by electrons and phonons. The athermal character of impurity dry friction and the sharp decrease of viscous friction upon cooling determine the character of the anomaly in this case. © *2005 American Institute of Physics*.
[DOI: 10.1063/1.2126948]

I. INTRODUCTION

In the temperature region $T\leqslant 10$ K, the plasticity of metals and alloys has features that do not correspond to classical concepts of plastic strain as a process of thermally activated motion of dislocations.[1,2] Such features have become known in the literature as low-temperature plasticity anomalies. They include, for example, the nonmonotonic character of the temperature dependence of the yield strength: the transition from a monotonic increase to a decrease when the sample is cooled below a certain threshold temperature. A second feature of this type is the loss of sensitivity of the plasticity characteristics to temperature variation in the region of fairly low temperatures (athermal plasticity). The plastification effect of metallic superconductors when they make the transition from the normal to the superconducting state is also regarded as a distinctive low-temperature anomaly. Such anomalies are inherent to crystalline metals and alloys with various types of lattice structure and are recorded in experiments involving various forms of mechanical tests: active strain, relaxation of the deforming stress, climb.

The main cause of the appearance of the indicated anomalies is the change of the physical mechanisms that determine the dynamic friction of the dislocations and their motion through different types of barriers when the sample enters the low-temperature region: Peierls lattice distortion, impurity barriers, barriers created by dislocations of other slip systems (the forest dislocation effect), etc. Under the conditions of low-temperature strain, the dislocation-inhibition forces and the character of their temperature dependence are determined by the combined action and comparative efficiency of the electronic and phonon viscosities,[3,4] thermal and quantum fluctuations,[5–8] and inertial effects.[9,10]

In metals and alloys with an fcc lattice, plastic flow is determined by the interaction of dislocations with local obstacles, and therefore the character of the low-temperature anomalies substantially depends on the purity of the metal and the concentration of the dopant element in the alloy. In connection with forest dislocation effects, preliminary strain and orientation of the crystal also play an important role. An analysis of the accumulated experimental material led to the conclusion that the main cause of low-temperature anomalies in fcc metals is that the mechanism of fluctuational unpinning of dislocations from local impurity barriers changes when the sample is cooled. According to one of the models proposed in Ref. 9 and developed in Refs. 10, a dislocation string pinned by point barriers can carry out damping vibrations, whose character is determined by the value of the viscous friction. When the crystal's temperature is reduced, the viscous friction of the dislocations decreases because of the temperature dependence of the phonon component. Below a certain threshold temperature T_i, for a definite relationship of the friction coefficient, the self-mass of the dislocation string, and the effective length of the dislocation segment,

which depends on the concentration of local barriers, the dislocation segments make a transition to the undamped state. After thermal-fluctuation unpinning under the action of external loading, such segments are capable of overcoming part of the local barriers because of their inertial properties without the help of thermal fluctuations; i.e., the dislocations make a transition to the regime of fluctuational-inertial motion. When a sample is strained at a given rate, this is accompanied by an increase of the activation area swept by a segment after it is unpinned from a barrier, and this reduces the stress of the plastic flow of the strained sample. According to the theoretical model, as the impurity concentration in the alloy increases, i.e., as the mean length of the dislocation segments decreases, the conditions for them to make a transition to the undamped state are satisfied at higher values of the threshold temperature T_i. Below T_i, the phonon component of the viscous friction rapidly decreases; however, the inertial properties of the dislocations can become stronger because of the variation of the electron component, and this is one of the reasons that the yield stress of an alloy decreases when it goes to the superconducting state.[10]

The theory of thermal-inertial motion is based on the string model of a dislocation that interacts with a system of local (point) barriers of the same type randomly distributed in a glide plane. In practice, this model is implemented in a number of dilute solid solutions, for example, those based on lead.[11–13] An analysis of the experimental data for lead alloys carried out in the indicated papers showed that, at moderately low temperatures and impurity concentrations of several atomic percent, the plasticity has a purely activation character and is determined by the thermal-fluctuation unpinning of dislocations from single impurity atoms. The threshold temperature T_i below which the thermal-fluctuation regularities of plastic flow break down increases as the impurity concentration increases, and this qualitatively corresponds to the model of thermal-inertial motion of dislocations. The experimental $T_i(c)$ dependences, where c is the atomic impurity concentration, allowed us to correctly calculate the phonon and electron frictional coefficients of the dislocations, i.e., to qualitatively confirm the hypothesis of the role of inertial properties of the dislocations.[14,15]

At the same time, to further understand the physical mechanisms of low-temperature plasticity and to determine the limits of applicability of the theoretical models mentioned above, it is of interest to study the regularities of the motion of dislocations in concentrated solid solutions, taking into account the features of their fine structure. It is well known that, for a favorable relationship of the valences and concentrations of the components of a solid solution, the negative electronic potential around the atoms of the dopant element causes an inhomogeneous distribution of the impurity atoms.[16] Segregations are formed in the metal—regions with local atomic order that are stronger barriers for mobile dislocations than are single randomly distributed impurity atoms in an ideal solution. For sufficiently high impurity concentrations, it should be expected that local order has a substantial effect on the character of the thermal fluctuational motion and the inertial properties of the dislocations, and hence on the macroscopic plasticity of the alloy. It is extremely convenient to use the Pb–In system, with a wide region of solubility of indium in lead, to study effects of this type. Studies using the diffuse scattering of x rays, carried out in Ref. 17, showed that the local order coefficient takes positive values for an indium concentration above 20 at. %, and this corresponds to the formation of small impurity clusters in the solution. It was shown in Ref. 15 that, in the alloy Pb–20 at. % In, a change of the form of the temperature dependence of the yield strength is observed in the low-temperature region, by comparison with less concentrated lead alloys. A thermal-activation analysis of the experimental dependences made it possible to establish that the high activation enthalpy of the process of strain and the high threshold shear stress characteristic of the alloy Pb–20 at. % In are not explained by a simple increase of the atomic concentration, if it is assumed that the alloy is an ideal (disordered) solid solution. Moreover, the threshold temperature T_i of the low-temperature plasticity anomaly begins to decrease for strong doping, and this contradicts the conclusions of the theory of thermal-inertial motion of dislocations, developed for the case of local barriers of the same type.

For this paper, comparative experimental studies of the plasticity of moderately concentrated (disordered) and concentrated (heterogeneous) solid solutions of Pb–In have been carried out to study the indicated features in the low- and superlow-temperature region.

II. EXPERIMENTAL TECHNIQUE

Single crystals of the alloys Pb–5, 10, and 20 at. % In were investigated for this paper. The purity of the starting materials for preparing the alloys was 99.999% for Pb and 99.997% for In. The Bridgman method was used in a dismountable graphite mold to grow from a single seed crystal two series of ten single crystals of each alloy, with the orientation of the stretching axis favorable for singlet slip; the size of the working part of the sample was $15\times3\times1$ mm. The process for preparing the samples is described in Ref. 18.

The samples were deformed by stretching at a constant rate at temperatures of $4.2\ \mathrm{K}<T<30\ \mathrm{K}$ on a strain machine with a ^{4}He cryostat, and at $0.53\ \mathrm{K}<T<4.5\ \mathrm{K}$ on a strain machine with the ^{4}He and ^{3}He cryostats whose designs are described in detail in Ref. 19. The temperature of the sample in the 4.2–30-K interval was measured from the readings of three resistance thermometers, located at different points of its working part. The temperature of the sample was determined in the 0.53–4.5-K interval from the readings of one resistance thermometer at the center of the working part of the sample. In both cases, the relative temperature-measurement error did not exceed 10^{-2}.

Complete load-time diagrams were recorded by means of a printer and were then recalculated in shearing-stress τ-shearing-strain ε coordinates. The amplified signal of resistance strain gages made it possible to record the deforming stress to within at least ±10 kPa, while movable rods provided a constant strain rate of $\dot{\varepsilon}=1.1\times10^{-4}\ \mathrm{sec}^{-1}$. The identity of the initial samples was evaluated from the characteristic parameters of the $\tau(\varepsilon)$ curve: the critical shear stress τ_0, the strain-hardening coefficient $\Delta\tau_1/\Delta\varepsilon_1$ at stage I of easy slip, and the elongation ε_1 of this stage. For two samples of the same series, tested on different strain ma-

chines at 4.2 K, the relative scatter of the indicated parameters did not exceed 15%. At $T=0.5$ K, for all the test samples, the values of $\Delta\tau_1/\Delta\varepsilon_1$ were 3–6 MPa, and the elongation of the stage was $\varepsilon_1=1.1-1.3$.

Because of the relatively low values of $\Delta\tau_1/\Delta\varepsilon_1$ and the large ε_1, it became possible to record the value of τ_0 by loading and unloading the sample at three or four temperatures. Stress τ_0 at each loading was calculated with a correction on the strengthening from the previous loading. The correctness of such a technique for calculating the $\tau_0(T)$ dependence was verified earlier.[11–13,15]

Besides strain with a constant rate $\dot{\varepsilon}$, intermittent cyclic variation of $\dot{\varepsilon}$ was carried out between 1.1×10^{-5} and 1.1×10^{-4} sec^{-1} (by making changes in the strain machine's gear drive). The load increment during cycling was recorded after additional amplification of the strain-gage signal. The total signal gain made it possible to estimate the corresponding shear-stress jump $\Delta\tau$ to within ±1 kPa. One sample was tested at three or four temperatures.

The $\tau_0(T)$ and $\Delta\tau(T)$ dependences at temperatures below the superconducting transition temperature T_c were measured in the superconductive state (T_c is 6.90–7.12 K for different indium concentrations). It was difficult in our experiments to measure these values in the normal state (by means of the corresponding magnetic field). The reasons for this are, first, that the thermal and geometrical characteristics of the apparatus with the ^{3}He-evaporation cryostat makes it impossible to use a strong enough superconducting solenoid to break down the superconductivity in all the test alloys; second, an experiment carried out on the example of alloy Pb–5 at. % In, in which superconductivity breaks down at $T=4.2$ K, showed that the sensitivity of the apparatus is inadequate to reliably record how the electronic state of the sample affects $\Delta\tau$.

III. EXPERIMENTAL RESULTS

A. Critical shear stress $\tau_0(T)$

The experimental temperature dependences of the critical shear stress (CSS) τ_0 in the 0.5–30-K interval are shown in Fig. 1. The mean critical superconducting-transition temperature T_c is noted by a vertical dashed line. The solid curves in Fig. 1 correspond to the theoretical dependences for the case of simple thermal-fluctuation unpinning of the dislocations from the impurity atoms, if the metal is in the normal state. The empirical parameters of this mechanism are calculated from the experimental data in Ref. 15. The calculations showed that the thermal-fluctuation model gives a good description of the experimental $\tau_0(T)$ dependences of the test alloys at temperatures above the threshold temperature T_i (its value for each alloy is noted by an arrow). However, as can be seen from Fig. 1, the experimental values of the CSS in the interval $T<T_i$ become lower than the theoretical values, which correspond to a purely thermal-activation process. In this case, the $\tau_0(T)$ dependences for alloys with small and large dopant-element concentration c are qualitatively different in the $T<T_i$ region: For $c=5$ and 10 at. %, the $\tau_0(T)$ dependence has a weakly expressed maximum, whereas, for $c=20$ at. %, τ_0 becomes virtually constant below T_i. It can also be seen that, for $c=5$ and 10 at. %, an additional falloff of τ_0 occurs in the region $T<T_c$, and this can be interpreted as a plastification effect accompanying the superconducting transition.[1,2] A falloff of the stress of about the same magnitude was observed earlier when polycrystalline samples of these alloys were studied.[20]

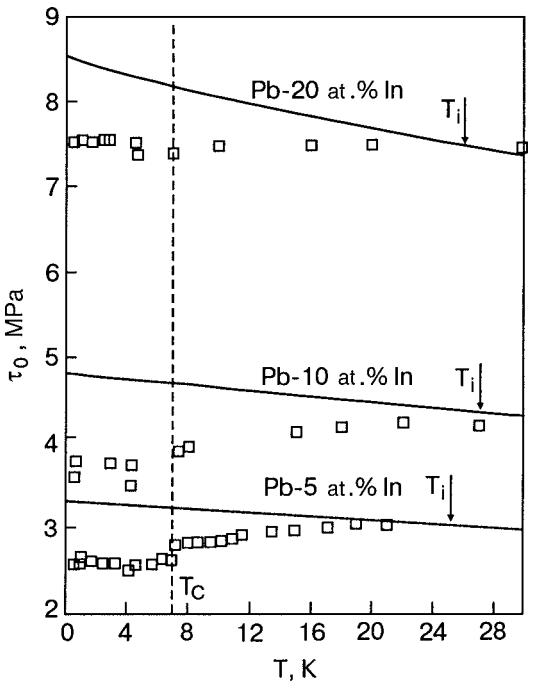

FIG. 1. Temperature dependences of the critical shear stress $\tau_0(T)$ of Pb–In single crystals with various concentrations of indium, obtained at $\dot{\varepsilon}=1.1\times10^{-4}$ sec^{-1}. The vertical dashed line separates the regions of normal ($T>T_c$) and superconducting ($T<T_c$) states. The solid curves correspond to the regime of thermally activated plasticity with optimum values of the parameters calculated in Ref. 15 and listed in Table I. The limiting temperature T_i for this regime is shown by arrows.

At temperatures below $0.6T_c$, the stress τ_0 is independent of temperature for all three alloys. It is essential for the subsequent discussion that, for $c=5$ and 10 at. %, when $T<0.6\,T_c$, the limiting values of τ_0 are less than the stress $\tau_0(T_i)$, whereas, in the case $c=20$ at. %, the indicated values are at least equal. It is also easy to see that an increase occurs in the threshold temperature T_i as the indium concentration increases from 5 to 10 at. %, but that this tendency breaks down for $c=20$ at. %.

B. Rate sensitivity of the stress, $\Delta\tau(T)$

Typical segments of the load-time stretching diagrams are shown in Fig. 2. The times at which the speed of the strain machine's rod changes are indicated by arrows. The random vibrations of the load can be associated with the external conditions of the experiment, in particular with vibration and friction in the movable couplings of the strain machine. The amplitude of the random oscillations illustrates the actual noise-to-signal ratio.

For the Pb–5 at. % In single crystals, discontinuities in the loading when there is a tenfold change of the stretching rate are recorded in the entire interval of temperatures studied here all the way to $T=0.53$ K. At the instant that the rod comes to a complete stop, characteristic signs of load relaxation were observed. The diagrams for Pb–10 at. % In had a similar form. However, for the Pb–20 at. % In single crystals, the rate sensitivity of the loading could be reliably re-

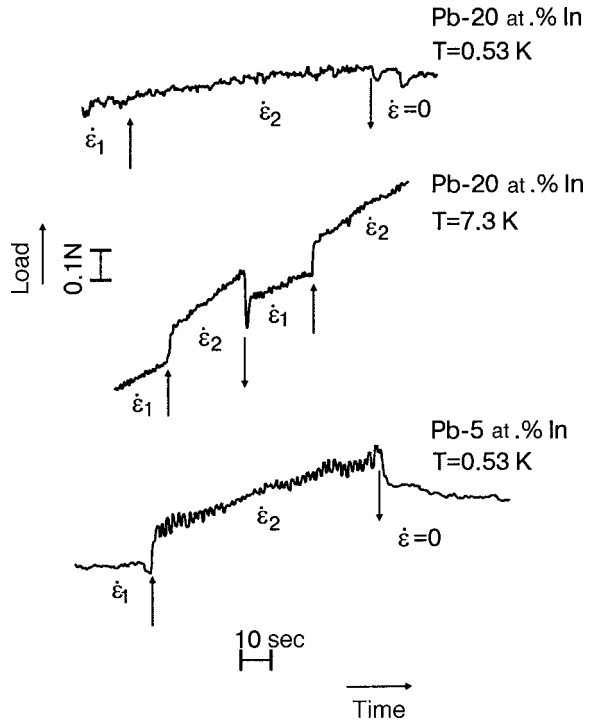

FIG. 2. Segments of patterns showing stretching at various rates in load-time coordinates. The arrows show the times at which the speed of the strain-machine rod changes (stops). The corresponding rates of plastic strain are $\dot{\varepsilon}_1 = 1.1 \times 10^{-5}$ sec^{-1} and $\dot{\varepsilon}_2 = 1.1 \times 10^{-4}$ sec^{-1}.

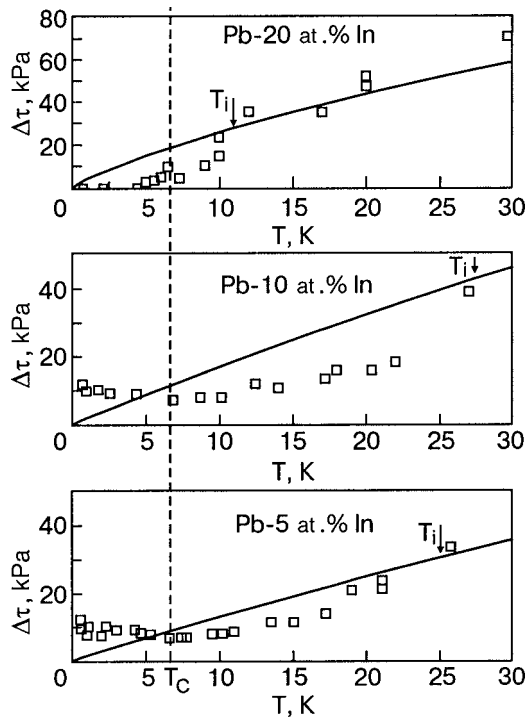

FIG. 3. Temperature dependences of the yield-stress sensitivity $\Delta\tau(T)$ to a change of the strain rate from $\dot{\varepsilon}_1 = 1.1 \times 10^{-5}$ sec^{-1} to $\dot{\varepsilon}_2 = 1.1 \times 10^{-4}$ sec^{-1}. The solid curves correspond to the thermally activated plasticity regime at the optimum values of the parameters calculated in Ref. 15 and shown in Table I. The limiting temperatures T_i for this regime are shown by arrows.

corded to temperatures of 4–7 K. As the temperature was reduced to 0.53 K, the useful signal amplitude, corresponding to a jump in the load, did not exceed the noise level, and no signs of load relaxation were observed.

The load-time diagrams are used to estimate the rate sensitivity of the yield stress $\Delta\tau$, taking into account the variation of the cross section and the crystallographic orientation of the single crystals. The $\Delta\tau(T)$ dependences for samples strained at the stage of easy slip are shown in Fig. 3. The solid curves show the dependences calculated for the case of simple thermal-fluctuation unpinning of the dislocations from the local impurity barriers in the normal state of the metal.[15] It can be seen that, for all the alloys studied here, at temperatures below a certain threshold T_i, the experimental values of $\Delta\tau$ become less than predicted by the theory of thermally activated plasticity. The threshold temperature T_i in this case turns out to be greater for Pb–5 and 10 at. % In alloys than for Pb–20 at. % In. Qualitatively, the $\Delta\tau(T)$ dependence is distinguished by the fact that $\Delta\tau$ for the first two alloys tends a constant finite value as the temperature decreases, whereas, for Pb–20 at. % In, it tends to zero at temperatures below 4 K.

Thus, the experimental $\tau_0(T)$ and $\Delta\tau(T)$ dependences in the temperature interval 0.5–30 K deviate from the regularities of purely thermally activated plasticity for all three alloys, but these deviations have additional specific features for the alloy with the maximum impurity concentration.

IV. DISCUSSION OF THE RESULTS

Let us consider the results of the experimental study of the plasticity of the alloys Pb–5, 10, 20 at. % In in the temperature interval 0.5–30 K, along with the results of Ref. 15, in which these alloys are studied at higher temperatures. Moreover, let us compare these data with the data on the low-temperature plasticity of less concentrated alloys of Pb with Sn, Sb, and Bi.[11–14] Such a comparison makes it possible to point out several important features and to formulate certain conclusions.

A. Regularities and mechanisms of the plastic strain of Pb–In alloys in the interval of moderately low temperatures $T > T_i$

First feature: For all the alloys mentioned here, there is a characteristic temperature T_i above which their plastic strain close to the yield strength τ_0 is determined by the thermally activated motion of dislocations through local potential barriers of impurity origin. This process is described by the kinetic equation of Arrhenius,

$$\dot{\varepsilon} = \dot{\varepsilon}_0 \exp\left[-\frac{H(\tau^*)}{kT}\right], \tag{1}$$

which establishes a connection between the rate of plastic shear strain $\dot{\varepsilon}$, the deforming shear stress τ, and the temperature T.[5] Here $\tau^* = \tau - \tau_i$ is the effective stress, which is the difference between the deforming stress τ and the long-range (internal) stress τ_i; $H(\tau^*)$ is the effective activation energy (enthalpy), the specific form of which depends on the force law of interaction of a dislocation with a pinning center and the distribution statistics of these centers along a dislocation line. The pre-exponential factor $\dot{\varepsilon}_0$ includes the density of mobile dislocations, the mean area swept by a segment as a result of a favorable thermal fluctuation, and also the frequency of the attempts to overcome the barrier. At $T > T_i$, the weak dependence of $\dot{\varepsilon}_0$ on temperature and stress can be

TABLE I. Empirical estimates of the threshold temperature T_i and the main parameters in Eqs. (1) and (2) for lead-based solid solutions.

Alloy	c, at.%	H_0, eV	τ_c, MPa	T_i, K	K, MPa	m	Refs.
Pb–Sn	1.0	0.24	0.89	22	12	2/3; 1/2	[11,14]
	3.0	0.24	1.50	25			
Pb–Sb	0.4	0.33	1.62	18	16	2/3; 1/2	[12,14]
	1.5	0.33	2.50	–			
Pb–Bi	0.1	0.25	0.30	12	5	1/2	[13,14]
	0.5	0.25	0.37	15			
	1.0	0.25	0.57	17			
	3.0	0.25	0.99	22			
	6.0	0.27	1.35	25			
Pb–In	1.0	0.22	0.60	14	4	1/2	[16]
	5.0	0.25	1.00	25			
	10.0	0.26	1.40	27			
	20.0	0.50	3.45	26	–	–	

neglected, and the stress dependence of the activation enthalpy can be approximated by[5,8]

$$H(\tau^*) = H_0\left[1 - \left(\frac{\tau^*}{\tau_c}\right)^p\right]^q, \tag{2}$$

where H_0 is the energy parameter of the dislocation-impurity interaction, while τ_c is the critical stress of nonactivation (force) penetration of the impurity barriers by dislocations. Exponents p and q are numerical parameters of the order of unity, whose values depend on the shape of the barrier and the distribution statistics of the barriers along the dislocation line. Empirical estimates of the threshold temperature T_i and of the main parameters in Eqs. (1) and (2) for a number of lead-based solid solutions are shown in Table I.

Second feature: For all the lead alloys, with the exception of that with the maximum concentration of indium, parameter H_0 has approximately equal values for each specific type of dopant element, regardless of its concentration; the critical stress τ_c substantially depends on the atomic concentration c of the dopant element, and this dependence is described by an empirical formula of the form

$$\tau_c \approx K c^m, \tag{3}$$

where $1/2 < m < 2/3$, and the value of K correlates with the dimensional and modular mismatch parameters of the single impurity atoms in the lead lattice (see Table I).

Third feature: For all the lead alloys except for Pb–20 at. % In, the threshold temperatures T_i monotonically increase with increasing concentration of the dopant element (see Table I); in the neighborhood of T_i, the derivative $\partial\tau_0/\partial T$ changes sign, while the rate sensitivity $\Delta\tau$ sharply decreases with decreasing temperature.[11–14]

The features described above make it possible to formulate the following conclusions:

- The plasticity of the lead alloys with impurity concentration to 10 at. % in the temperature region $T > T_i$ is determined by thermally activated motion of dislocations through barriers created by single impurity atoms, which are randomly distributed in the glide planes.
- Processes of inertial unzipping of the dislocation segments begin in the neighborhood of temperature T_i.[14,15]

B. A low-temperature plasticity anomaly of moderately concentrated alloys

Let us discuss the features of the plasticity of the lead alloys with concentrations of the dopant element up to 10 at. % under conditions of deep cooling (at $T < T_i$). The kinetics of plastic flow undergo substantial changes in this temperature region because of two circumstances. First, a sharp decrease of the phonon component of the dynamic friction of the dislocations gives rise to the phenomenon of unzipping along the dislocation line pinned by impurity atoms and to a sharp increase of the area swept by this line after it is unpinned from an individual attachment point.[9,10] This effect results in a substantial change of the preexponential factor in Eq. (1):[11,12]

$$\dot{\varepsilon}_0 \to \dot{\varepsilon}_0 I[\tau^*, B(T)]. \tag{4}$$

Here $I[\tau^*, B(T)]$ is a function of the effective stress τ^* and the dynamic friction coefficient $B(T)$, which exponentially increases as B decreases and τ^* increases. Although the analytical form of this function is not known, a numerical analysis shows that, because of competition of $I[\tau^*, B(T)]$ and $\exp[-H(\tau^*)/kT]$, a maximum appears on the $\tau_0(T)$ dependences.[10]

The second circumstance that must be taken into account when describing the motion of dislocations through impurity barriers under conditions of deep cooling is the sharp decrease of the intensity of the thermal fluctuations and the increasing role of quantum effects in this process.[8,11,12] Taking quantum effects into account qualitatively reduces to replacing temperature T in Eq. (1) by the "effective" temperature $T^*(T)$:

$$T^*(T) = \begin{cases} T, & T > \theta \\ \dfrac{\theta}{2}\left(1 + \dfrac{T^2}{\theta^2}\right), & T < \theta. \end{cases} \tag{5}$$

Here θ is a characteristic limiting temperature, below which quantum effects become determining.

In the final analysis, simultaneously taking inertial unzipping, quantum fluctuations, and thermal fluctuations into account makes it necessary to replace the classical Arrhenius equation of Eq. (1) with a more complex equation of the form

$$\dot{\varepsilon} = \dot{\varepsilon}_0 I[\tau^*, B(T)] \exp\left[-\frac{H(\tau^*)}{kT^*(T)}\right]. \tag{6}$$

This equation makes it possible to describe all the main features of the kinetics of low-temperature plastic strain of weakly and moderately doped fcc solid solutions both in the region $T > T_i$ and in the region $T < T_i$.

The $\tau_0(T)$ and $\Delta\tau(T)$ dependences shown in Figs. 1 and 3 for alloys Pb–5 and 10 at. % In are similar to the corre-

sponding dependences given in Refs. 11–13 for other lead alloys: In the neighborhood of temperature T_i, the derivative $\partial\tau_0/\partial T$ changes sign, while the value of $\Delta\tau$ sharply drops off with decreasing temperature. The low-temperature plasticity anomalies of the Pb–In alloys with concentrations to 10 at. % are determined by the same physical mechanisms as were invoked to explain the plasticity anomalies of Pb–Sn, Pb–Sb, and Pb–Bi alloys, in particular inertial unzipping of dislocations from local impurity barriers formed by single atoms.

In the region of very low temperatures, the experimental values of τ_0 and $\Delta\tau$ for Pb–5 and 10 at. % In tend to finite values that are independent of temperature (see Figs. 1 and 3). As shown by the numerical estimates of Refs. 11 and 12 the conditions of inertial unzipping in this case, as before, are satisfied; however, the displacement of a dislocation by several interimpurity distances precedes the unpinning of a dislocation line from an individual impurity atom as a result of a quantum fluctuation. Moreover, the phonon friction of the dislocations is small in this temperature region, and coefficient B is mainly determined by the electronic component B_e, which in the normal state of the metal is independent of temperature: $B(T)\approx B_{eN}$=const. According to Refs. 11 and 12 the $\tau_0(T)$ and $\Delta\tau(T)$ dependences are determined in this case only by the $T^*(T)$ dependence. Taking Eqs. (5) and (6) into account, for comparison with experiment, it is convenient to use the relationship

$$\frac{\tau_c \Delta \ln \dot{\varepsilon}}{\Delta\tau} = \frac{\tau_c}{\tau_1} + \frac{T_1}{T^*(T)}, \tag{7}$$

where

$$\tau_1^{-1} = \frac{\partial}{\partial\tau^*} \ln I(\tau^*, B_e)|_{\tau^*=\tau_0^*};$$

$$T_1 = \frac{pqH_0}{k}\left(\frac{\tau^*}{\tau_c}\right)^{p-1}\left[1-\left(\frac{\tau^*}{\tau_c}\right)^p\right]^{q-1}. \tag{8}$$

The values of parameter T_1 can be computed by using the empirical values of the plasticity parameters obtained in Ref. 15. Two parameters remain unknown: the characteristic quantum temperature θ and parameter τ_1, which characterizes the influence of the inertial properties of the dislocations. By varying parameters θ and τ_1, it is possible to compare the $\Delta\tau(T)$ dependences obtained by means of Eq. (7) with the experimental $\Delta\tau(T)$ dependences for the Pb–In system. The maximum correlation with Eq. (7) can be achieved (see Fig. 4) for the values of the desired parameters shown in Table II. For comparison, this also shows the values of the analogous parameters for other alloys. As can be seen from the table, the resulting value of θ=10 K is the same for all the alloys, while the optimum values of T_1 and τ_1 depend on the type and concentration of the impurities.

The plasticity anomalies observed in the region of low and superlow temperatures on the temperature dependences $\tau_0(T)$ and $\Delta\tau(T)$ for alloys Pb–5 and 10 at. % In can thus be explained by the successive transition in the neighborhood of T_i from a thermal activation mechanism to a thermal-inertial mechanism of motion of dislocations through single impurity atoms, and in the region $T<10$ K to a quantum-inertial mechanism of motion of dislocations.

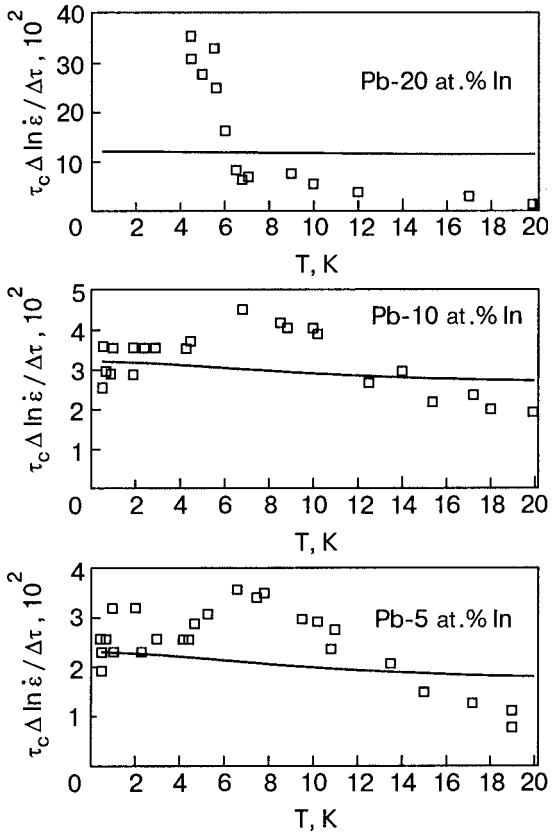

FIG. 4. Comparison of experimental $\Delta\tau(T)$ dependences with the theoretical dependence given by Eq. (7) (solid lines) for Pb–In alloys for the values of the parameters shown in Tables I and II.

C. Low-temperature plasticity anomaly of the concentrated alloy

Let us now proceed to a discussion of the low-temperature plasticity anomaly of the concentrated alloy Pb–20 at. % In. In this case, to within the scatter of the data, there is no maximum on the $\tau_0(T)$ dependence (see Fig. 1), while the value of $\Delta\tau$ tends to zero with decreasing temperature (see Figs. 2 and 3). If Eqs. (6) and (7) are used in analyzing the experimental data, the empirical values of the parameters of the theory will very significantly differ from the values for the other alloys (see Table I). The value of parameter H_0 does not correspond to fluctuation unpinning of dislocations from single impurity atoms at $T>T_i$. The concepts that a transition occurs to the thermal-inertial and

TABLE II. Empirical estimates of the optimum values of the parameters in Eq. (7), for lead-based solid solutions.

Alloy	c, at.%	T_1, K	τ_1, kPa	θ, K	Ref.
Pb–Sn	1.0	170	2.3	10	[12]
	3.0	220	3.6	10	
Pb–Sb	0.4	190	3.7	10	
	1.5	260	2.7	10	
Pb–In	5.0	310	5.0	10	This paper
	10.0	300	4.8	10	
	20.0	390	< 0.5	10	

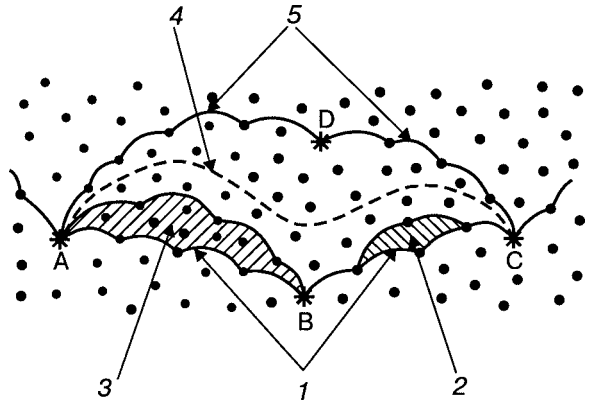

FIG. 5. Sequence of configurations of a dislocation line when a dislocation moves in a heterogeneous solid solution: *1*—initial configuration of a dislocation segment pinned by impurity clusters at points A, B, C (*) and by a certain number of single impurity atoms (●); *2*—elementary event of plastic strain in the fluctuation regime of motion of a dislocation through a collection of single impurity atoms in a region of a homogeneous solid solution; *3*—elementary event of plastic strain for fluctuation-inertial motion of a dislocation through a collection of single impurity atoms in a region of a homogeneous solid solution; *4*—intermediate configuration of a dislocation segment after it is unpinned from cluster *B* in the process of being displaced to cluster *D*; *5*—final configuration of a dislocation segment pinned by clusters A, D, C and by a set of single impurity atoms.

quantum-inertial mechanisms of dislocation motion are also not confirmed when $T < T_i$. The latter circumstance is illustrated in Fig. 4, in which the experimental data in the corresponding coordinates are compared with Eq. (7) with the numerical values of the parameters from Table II substituted in it. It can be seen that the experimental points for the alloy Pb–20 at. % In do not even approximately match the graph of the dependence given by Eq. (7).

Reference 15 explained the features of the plasticity of the concentrated solid solution Pb–20 at. % In, observed at $T > T_i$, by a substantially inhomogeneous distribution of impurity atoms, namely, by the appearance of small impurity clusters, which form stronger barriers for mobile dislocations than do single impurity atoms. The presence of such clusters in Pb–In solid solutions was detected earlier in Ref. 17. It is natural to assume that the anomalous plasticity of the alloy Pb–20 at. % In in the interval $T < T_i$ is also a reflection of the conditions of dislocation motion in a solid solution with clusters. A possible diagram of such motion is shown in Fig. 5.

We assume that the concentrated solid solution has a heterogeneous impurity distribution; i.e., it consists of randomly arranged single impurity atoms and approximately identical clusters, consisting of several (two or three) impurity atoms, the distance between which is of the order of the lattice parameter. As single atoms, such clusters are local potential barriers for mobile dislocations. Under the action of relatively small stresses, the dislocations can overcome both types of barriers because of thermal or quantum fluctuations and, at sufficiently high stresses, by purely mechanical means. Of course, the height of a cluster barrier significantly exceeds the height of a barrier formed by a single atom. This explains the relatively large value of H_0 for the alloy Pb–20 at. % In (see Table I).

Dislocations can be displaced in the region of an ideal solid solution under the action of relatively small effective stresses by several elementary processes (Fig. 5). Let us consider dislocation segment *ABC*, pinned at three clusters (at points *A*, *B*, and *C*) and by a certain number of single impurity atoms (configuration *1*). Under the action of a small effective stress, the unpinning of the segment from cluster *B* and the displacement in the direction of the nearest cluster *D* precedes the fluctuational overcoming by segments *AB* and *BC* of single impurity atoms. Two regimes of motion are possible in this case: purely fluctuational, and fluctuational-inertial. In the former case, the elementary event of plastic strain is schematically shown in Fig. 5 by hatched segment *2*: As a consequence of thermal or quantum fluctuation, the dislocation line overcomes an individual impurity atom and collapses to the nearest impurity atom in the course of the motion. The second regime of motion corresponds to the elementary event conventionally shown in Fig. 5 by hatched segment *3*: The fluctuational overcoming of the one impurity atom is accompanied by inertial unzipping, i.e., by unactivated overcoming of several impurity atoms in the course of the motion. As a result of the unpinning from single atoms, it becomes possible to unpin the dislocation line from cluster *B* and to implement intermediate configuration *4*, shown by a dashed line. At this stage of the dislocation motion, the forces of tension in the central part of segment *AC* substantially increase the effective stress, which acts on the small elements of the segment and displaces the segment in the direction of cluster *D*. Because of this, the transition from initial configuration *1* (*ABC*) to final configuration *5* (*ADC*) occurs in the quasi-dynamic regime, and the inhibiting action of the impurity barriers in region *ABCD* at fairly low temperatures is equivalent to dry friction.

The successive implementation of the elementary events of displacement of the dislocation line shown in Fig. 5 by segments *1* and *2* (first-order elementary events) thus promotes the implementation of a more complex process (a second-order elementary event), which enables the dislocations to move through a system of clusters by making a transition from initial configuration *ABC* to final configuration *ADC*.

To better understand the proposed model, let us explain it in more detail. In describing the motion of a dislocation in a highly concentrated solid solution in which a small part of the impurity atoms have formed clusters, the regions between the clusters can be regarded as an effective homogeneous medium, while the resistance to the motion of a dislocation segment in such a system at low temperatures can be replaced by dry friction. The correctness of this replacement follows naturally from the limiting transition from thermally activated motion of the dislocations through impurity barriers to a purely mechanical "cutting off" of the barriers, which is possible if the stress acting on a dislocation exceeds critical value τ_c. In accordance with this, the dry-friction stress τ_{sf} can be estimated from Eq. (3) by extrapolating it to the region of high impurity concentrations.

We should point out one important circumstance because of which fluctuational motion in a heterogeneous solid solution substantially differs from motion in a homogeneous solid solution. In the case of a homogeneous solid solution, for a definite relationship between the concentration of impurity barriers, the viscous friction of a dislocation, and the effective stress, it is possible to have the unzipping effect and

the regime of fluctuational-inertial motion of a dislocation. In the case of a heterogeneous solid solution, the unzipping effect is possible only when a dislocation line moves in the intervals between clusters. When fluctuational unpinning of a dislocation line from a cluster occurs and it collides with the adjacent cluster in the course of displacement (the series of configurations *1–5* in Fig. 5), the inertial effect is absent because of the inhibiting action (dry friction) created by single impurity atoms on the sections of the glide plane between clusters. On a background of dry friction, the decrease of the phonon component of viscous friction upon cooling does not cause the manifestation of inertial properties of the dislocations, which serve as the cause of the appearance of a maximum on the temperature dependence of the CSS. As can be seen in Fig. 1, to within the scatter of the data, the low-temperature values of the CSS are independent of temperature in the case of Pb–20 at. % In.

We should point out that reduction of the deforming stress when the superconductive transition occurs ($T<T_c$) also is not observed in a solid solution with clusters (Fig. 1), even though the high concentration of impurities has no substantial effect on the strength of the electron inhibition of the dislocations.[15]

The temperature dependence of the rate sensitivity of the stress, $\Delta\tau(T)$, for the alloy Pb–20 at. % In does not contradict models of thermally activated motion of dislocations all the way to temperatures of the order of 10 K (solid curve in Fig. 3). However, with further cooling to $T<T_c$, the value of $\Delta\tau$ tends to zero (for the given measurement sensitivity of the order of 1 kPa).

Let us show that the specific character of the low-temperature plasticity anomaly of the alloy Pb–20 at. % In can be explained by assuming that a dynamic regime of dislocation motion is implemented in this alloy at $T<T_i$, in which all the impurity barriers are overcome by dislocations of nonactivation type. In such a regime of dislocation-flux motion, the deformation equation acquires the form

$$\dot{\varepsilon} = b\rho_d V_d(\tau^*, B_c), \tag{9}$$

where ρ_d is the density of moving dislocations, while V_d is the mean dynamic velocity, which is determined by a balance of the force $b\tau$ acting on the dislocation from the side of deforming stress τ and the total inhibition force that results from the action of internal stresses τ_i, of impurities (dry friction τ_{sf}), of phonons, and of conduction electrons (viscous friction with coefficient B). If all the forces are per unit length of the dislocation line, the balance of forces reduces to the equation

$$b\tau = b(\tau_i + \tau_{sf}) + BV_d. \tag{10}$$

By using Eqs. (9) and (10), it is easy to obtain an explicit expression for the deforming stress (CSS) $\tau_0(\dot{\varepsilon},T)$ that corresponds to the dynamic regime of motion of the dislocations:

$$\tau_0(\dot{\varepsilon},T) = \tau_i + \tau_{sf} + B(T)\dot{\varepsilon}/b^2\rho_d. \tag{11}$$

In this case, the CSS linearly depends on the strain rate $\dot{\varepsilon}$, while its temperature dependence is determined by the coefficient of dynamic inhibition of dislocations, $B(T)$.

For the rate sensitivity $\Delta\tau(T)$ of the deforming stress, we get

$$\Delta\tau = B(T)\Delta\dot{\varepsilon}/b^2\rho_d. \tag{12}$$

It is established in Ref. 15 that, for the alloy under consideration, coefficient $B(T)$ is described by

$$B(T) = B_e + \eta(T/\theta_D)^3. \tag{13}$$

Here B_e is the electronic contribution, which in the normal state is independent of temperature and has a value of $B_e = B_{eN} \approx 2\times10^{-5}$ Pa·sec; the second term in Eq. (13) describes the phonon contribution, with $\eta = 7\times10^{-3}$ Pa·sec, while $\theta_D \approx 96$ K.

Let us check whether Eqs. (11)–(13) can be used to describe the low-temperature plasticity anomaly of the alloy considered here by comparing the values obtained by using these equations with the results of measurements of $\Delta\tau$, which were determined to within $\delta\tau \approx 10^3$ Pa (Fig. 3). Equation (12) satisfactorily describes the temperature dependence $\Delta\tau(T)$ close to T_i, as well as at lower temperatures. Since the alloy transforms into the superconducting state below $T_c \approx 7$ K, the coefficient of electron friction B_e sharply decreases at $T<T_c$:[3]

$$B(T) = 2B_{eN}[1+\exp(\Delta/kT)]^{-1} + \eta(T/\theta_D)^3, \quad T<T_c. \tag{14}$$

Substituting Eq. (14) into Eq. (12) results in a formula for $\Delta\tau(T)$ that reflects all the other features of this dependence observed in experiment in the region $T<T_i$—in particular, it shows that $\Delta\tau$ sharply decreases and goes to zero in the superconducting state (Fig. 3).

This conclusion makes it possible to obtain an empirical estimate for the dislocation density ρ_d responsible for plastic strain under these conditions. The experimental points in Fig. 3 are obtained for values of the strain-rate discontinuity of $\Delta\dot{\varepsilon} = (1.1\times10^{-4} - 1.1\times10^{-5})$ sec$^{-1} \approx 10^{-4}$ sec^{-1}. According to Eq. (13), at $T=10$ K, we get $B \approx 3\times10^{-5}$ Pa·sec. Since $\Delta\tau \approx 2.5\times10^4$ Pa at this temperature, by using Eq. (12), we get the estimate $\rho_d \approx 10^6$ m^{-2}.

Let us now discuss the temperature dependence of the CSS of the alloy under consideration. Formally, Eq. (11) contains a term that is proportional to $B(T)$ and decreases upon cooling. However, for the given strain rates of $\dot{\varepsilon} = (10^{-4} - 10^{-5})$ sec^{-1} and the value obtained above for the dislocation density of $\rho_d \approx 10^6$ m^{-2}, the value of this term is less than 10^5 Pa; i.e., it does not exceed the scatter of the points in Fig. 1 for Pb–20 at. % In. This estimate explains why the CSS of the alloy is virtually independent of temperature. It may be that more accurate measurements of $\tau_0(T)$ on one sample in the temperature region $T<10$ K will make it possible to observe a reduction of the value of τ_0 upon cooling, caused by the last term in Eq. (11), in particular a reduction of τ_0 when the sample makes a transition to the superconducting state. We should point out that, in experiments on polycrystalline samples of the alloy Pb–20 at. % In, a reduction of the yield strength by $\Delta\sigma \approx 5\times10^5$ Pa when the sample made a transition to the superconducting state was observed in Ref. 20.

The above analysis thus shows that the assumption that the motion of the dislocations upon plastic strain of the alloy Pb–20 at. % In occurs in the dynamic regime in the temperature region $T<T_i$ qualitatively agrees with the experimental observations.

V. CONCLUSION

This paper has explained the results of a study of the low-temperature plasticity of solid solutions of the Pb–In system with indium concentrations of $c=5$ and 10 at. % (moderately concentrated alloys) and $c=20$ at. % (highly concentrated alloy). The experiments involved recording the temperature dependences of the yield strength $\tau_0(T)$ when a single crystal was stretched at a constant rate and the increment of the deforming stress $\Delta\tau(T)$ when the stretching rate was increased by a factor of 10. Features (anomalies) of these dependences are detected in the temperature region $T<30$ K that do no correspond to the concepts of plastic flow as a process of thermally activated motion of dislocations through barriers created by single impurity atoms.

For the alloys with $c=5$ and 10 at. %, these anomalies are similar to what was observed earlier when studying other moderately doped substituted solid solutions based on fcc metals:[11–14] When the samples were cooled, the $\tau_0(T)$ dependence passes through a maximum and goes to a constant value in the region $T<10$ K (athermal plasticity), while $\Delta\tau(T)$ monotonically decreases, and τ_0 also reaches a finite constant value in the region of athermality.

An increase of the indium concentration to $c=20$ at. % results in a substantial transformation of the low-temperature anomaly: The maximum on the $\tau_0(T)$ dependence virtually disappears, and the region of athermality broadens to the limit of the anomaly, whereas $\Delta\tau$ sharply decreases upon cooling and goes to zero below 4 K.

An analysis of the experimental results using the data obtained earlier on the plasticity of these alloys at higher temperatures,[15] as well as data on the low-temperature plasticity of other moderately concentrated alloys of lead with Sn, Sb, and Bi, makes it possible to formulate the following conclusions:

1. The low-temperature plasticity anomalies, observed on the temperature dependences $\tau_0(T)$ and $\Delta\tau(T)$ for Pb–In solid solutions with $c=5$ and 10 at. %, are determined by the same physical mechanisms as were invoked to explain the anomalies of the plasticity of solid solutions of Pb–Sn, Pb–Sb, and Pb–Bi, namely, a successive transition in the 25–30-K region from a thermal-activation mechanism to a thermal-inertial mechanism, and, in the $T<10$ K region, to a quantum-inertial mechanism of motion of the dislocations through single impurity atoms. Inertial effects are the cause of the appearance of a maximum on the $\tau_0(T)$ dependence, while quantum mechanisms of overcoming the impurity barriers lead to athermality of the plastic flow.

2. The additional features of the low-temperature plasticity of alloyPb–20 at. % In reflect the specifics of the motion of dislocations through two types of potential barriers: single impurity atoms and segrations composed of two or three atoms (impurity clusters), which arise as a close-order element in the concentrated alloy.[17] Under the action of relatively small effective stresses (high temperatures), the dislocations overcome both types of barriers because of thermal fluctuations and, at fairly high stresses (low temperatures), move in a dynamic regime. Such a regime implies that a dislocation is acted on by the effective stress, the forces of viscous phonon and electron frictions, and the forces of inhibition on single impurity atoms of the type of dry friction. Dry friction quenches the inertial effects after the dislocation segments are unpinned from the clusters, and this eliminates the cause of the appearance of a maximum on the $\tau_0(T)$ dependence. The value of $\Delta\tau$ when plastic flow has a dynamic character is proportional to the coefficient of viscous friction, which decreases sharply when the alloy makes a transition to the superconducting state (when $T<T_c\approx 7$ K), and this explains the vanishing of $\Delta\tau(T)$ observed experimentally.

The authors are grateful to Yu. G. Kazarov for preparing the single crystals and to S. V. Lubents for useful discussions.

[a)]Email: isaev@ilt.kharkov.ua

[1]V. I. Startsev, V. Ya. Il'ichev, and V. V. Pustovalov, *Plasticity and Strength of Metals and Alloys at Low Temperatures* [in Russian] (Metallurgiya, Moscow, 1975).
[2]V. I. Startsev, in Dislocations in Solids, F. R. N. Nabarro, ed., (Elsevier, Amsterdam, 1983), vol. 6, p. 143.
[3]M. I. Kaganov, V. Ya. Kravchenko, and V. D. Natsik, Usp. Fiz. Nauk **111**, 655 (1973) [Sov. Phys. Usp. **16**, 878 (1974)].
[4]V. I. Al'shits, V. L. Indenbom, Usp. Fiz. Nauk **115**, 3 (1975) [Sov. Phys. Usp. **18**, 1 (1975)].
[5]U. F. Kocks, A. S. Argon, and M. F. Ashby, Prog. Mater. Sci. **19**, 288 (1975).
[6]A. Seeger, Zs. Metallkunde B **72**, 369 (1981).
[7]B. V. Petukhov and I. N. Pokrovskiĭ, Zh. Eksp. Teor. Fiz. **63**, 634 (1972) [Sov. Phys. JETP **36**, 336 (1973)].
[8]V. D. Natsik and H.-J. Kaufmann, Phys. Status Solidi A **65**, 571 (1981).
[9]A. V. Granato, Phys. Rev. B **4**, 2196 (1971).
[10]A. I. Landau, Phys. Status Solidi A **61**, 555 (1980); **65**, 119 (1981).
[11]I. A. Shepel', L. N. Zagoruĭko, V. D. Natsik, V. V. Pustovalov, and V. P. Soldatov, Fiz. Nizk. Temp. **17**, 390 (1991) [Sov. J. Low Temp. Phys. **17**, 202 (1991)].
[12]N. V. Isaev, V. D. Natsik, V. V. Pustovalov, I. A. Shepel', and S. É. Shumilin, Fiz. Nizk. Temp. **18**, 911 (1992) [Sov. J. Low Temp. Phys. **18**, 641 (1992)].
[13]N. V. Isaev, V. D. Natsik, V. V. Pustovalov, V. S. Fomenko, and S. É. Shumilin, Fiz. Nizk. Temp. **24**, 786 (1998) [Low Temp. Phys. **24**, 593 (1998)].
[14]N. V. Isaev, V. D. Natsik, and V. S. Fomenko, Fiz. Nizk. Temp. **25**, 987 (1999) [Low Temp. Phys. **25**, 740 (1999)].
[15]N. V. Isaev, V. S. Fomenko, V. V. Pustovalov, and I. S. Braude, Fiz. Nizk. Temp. **28**, 522 (2002) [Low Temp. Phys. **28**, 369 (2002)].
[16]J. S. Langer and S. H. Vosko, J. Phys. Chem. Solids **12**, 196 (1959).
[17]Y. Koike and J. M. Sivertsen, J. Phys. Soc. Jpn. **29**, 1235 (1970).
[18]G. Yu. Kazarov, Fizika Kond. Sost. Khar'kov No. 11, 100 (1973).
[19]I. N. Kuz'menko, V. V. Pustovalov, and S. É. Shumilin, Prib. Tekh. Eksp. **1**, 196 (1988).
[20]V. S. Fomenko and V. A. Sirenko, Phys. Status Solidi A **74**, 459 (1982).

Translated by W. Manthey

The role of Peierls relief in the low-temperature plasticity of pure α-Ti

V. A. Moskalenko,[a] V. D. Natsik, and V. N. Kovaleva

B. I. Verkin Physicotechnical Institute of Low Temperatures, National Academy of Sciences of Ukraine, pr. Lenina, 47, Kharkov 310103, Ukraine

(Submitted February 9, 2005; resubmitted February 23, 2005)
Fiz. Nizk. Temp. **31**, 1190–1200 (October 2005)

A detailed investigation of the low-temperature plasticity of high-purity polycrystalline α-Ti (interstitial impurities O+N=0.06 at. %) is carried out. The temperature dependences of the yield strength, effective stress, rate sensitivity of the deforming stress, and activation volume are obtained in the temperature interval 0.5–450 K. A thermal-activation analysis of the experimental data is carried out in terms of a model of activated motion of a dislocation string in Peierls relief. It is shown that the plastic flow of pure α-Ti in the region of moderately low temperatures ($7\ \mathrm{K} < T < 150\ \mathrm{K}$) results from thermally activated overcoming of Peierls barriers by the mechanism of generation, expansion, and annihilation of paired kinks. Empirical values are obtained for the parameters of the theory for $\{10\bar{1}0\}\langle 11\bar{2}0\rangle$ prismatic slip in α-Ti at low temperatures: the Peierls stress $\tau_P = 72$ MPa and the characteristic energy of a critical paired kink, $H_c = 1.5 \times 10^{-19}$ J=0.96 eV. At $T < 7$ K, the plasticity of pure α-Ti has a pronounced anomaly, which may be caused by a transition as the temperature is reduced, from a thermally activated regime of dislocation motion to a dynamic (over-barrier) regime. At elevated temperatures ($T > 150$ K), the plasticity of pure α-Ti qualitatively maintains characteristic features that correspond to the mechanism of thermally activated dislocation motion in the Peierls relief for low values of the effective stresses. © *2005 American Institute of Physics*. [DOI: 10.1063/1.2126949]

I. INTRODUCTION

One of the central problems in the physics of the plasticity of crystallographic materials is to elucidate the relative influence of Peierls relief and impurity barriers on the mobility of dislocations in easy-slip systems, which act under conditions of low-temperature strain. In solving this problem, the maximum clarity is achieved for metals with bcc and fcc structures. It is established that the kinetics of low-temperature strain of pure bcc metals at the easy-slip stage are determined by the motion of dislocations in {110} planes, which overcome the Peierls barriers by generating paired kinks as a result of the action of thermal or quantum fluctuations. Such a mechanism corresponds to a large yield strength of $\tau_0 \sim 10^{-3}G$ (G is the shear modulus), a sharp increase of τ_0 as temperature decreases, and the presence in the $\tau_0(T)$ dependence of characteristic features that are associated with a change of the interaction law of kinks on a dislocation as one goes from small to large values of the effective stress.[1,2] Similar regularities are found for pure β-Sn (bct structure) accompanying deformation according to the $\{100\}\ \langle 010\rangle$ slip system.[3,4] It is observed that impurities have an appreciable effect on the value and temperature dependence of the yield strength of both bcc metals and of β-Sn at concentrations of the order of 0.1 at. % and above.

In the case of fcc metals and alloys, Peierls barriers in the {111} easy-slip planes are negligible, and the main obstacles for dislocation motion are substitutional impurities, beginning with the lowest concentrations. Only far from the yield strength, with fairly large degrees of strain, is the influence of impurities able to mask the mutual inhibition of propagating dislocations (the forest-dislocation effect). Dislocation motion through local impurity barriers and the intersection of forest dislocations is also ensured by the action of thermal or quantum fluctuations.

Substitutional impurities in fcc metals have atomic radii close to the radii of the matrix atoms and are relatively weak obstacles for dislocation motion; therefore this mechanism corresponds to a less sharp increase of the yield strength $\tau_0(T)$ as the temperature decreases than in the case of pure bcc metals. For high impurity concentrations, of the order of 1 at. % and higher, the yield strengths of fcc metals acquire a characteristic low-temperature anomaly—a maximum on the temperature dependence of the yield strength that results from a transition from purely fluctuational to fluctuation-inertial motion of the dislocations through the impurity barriers.[5,6]

In studying the relative role of Peierls barriers and impurity barriers in the kinetics of plastic flow of metals, the most contradictory results are obtained in the case of metals with hcp structure. These metals can be divided into two groups. The first of them is a collection of simple divalent hcp metals (Be, Mg, Zn, Cd) with clearly expressed slip in the base plane (0001), in which Peierls barriers are also negligible, and the main obstacles to dislocation motion are forest dislocations or impurities. The regularities of the low-temperature plasticity of these metals are similar to those for fcc metals: at low impurity concentrations, they have small and weakly temperature-dependent yield strengths ($\tau_0 \sim 10^{-4}-10^{-5}G$); as the concentration increases, a characteristic fluctuational-inertial anomaly appears on the $\tau_0(T)$ dependences (see, for example, Ref. 7). In those few cases in which it is possible in the pure metals of this group to implement slip of the dislocations in $\{11\bar{2}2\}$ pyramidal planes, which possess high Peierls barriers, their mobility at low

temperatures is completely controlled by thermally activated generation of paired kinks.[8,9]

The behavior is quite different in the transition metals of group IV-A of Mendeleev's periodic table (Ti, Zr, Hf), in which easy slip occurs along the $\{10\bar{1}0\}$ prism planes in the $\langle 11\bar{2}0\rangle$ direction. Even at low impurity concentrations (especially of interstitial atoms—oxygen and nitrogen), they have rather high yield strengths $\tau_0 \sim 10^{-3}-10^{-4}G$ and a strong increase of $\tau_0(T)$ as temperature decreases;[10] this makes them similar to bcc metals. In this group, α-titanium has received the most detailed study: Even when it is fairly pure, it has a high yield strength, which increases strongly with decreasing temperature, especially as the impurity concentration increases,[11–18] when, at the same time, the plasticity of the titanium acquires additional features.[19] However, the conclusions concerning dislocation mechanisms, which control the plastic strain of pure titanium, are in conflict, and there currently is no unambiguous opinion, for example, relative to whether Peierls barriers have a significant influence on its plasticity. When the experimental results are analyzed, the high sensitivity to interstitial impurities makes it hard to separate the influence of Peierls barriers and impurity barriers on dislocation motion in easy-slip planes of type $\{10\bar{1}0\}$.

On the basis of the large volume of experimental results obtained when investigating titanium with various concentrations of interstitial impurities, it was asserted in Refs. 12–16 that the controlling mechanism of plastic strain in titanium involves thermally activated dislocations overcoming the obstacles created by impurity atoms. At the same time, the results of an investigation of the strain kinetics of high-purity titanium allowed the authors of Refs. 11 and 18 to conclude that lattice friction (Peierls relief) plays the controlling role. A theoretical analysis of the electronic structure of the dislocation cores in α-titanium also leads to the conclusion that the Peierls barriers are rather large in the prism plane.[20,21]

A significant step in the study of the question under discussion was achieved in our previous papers,[22,23] where the plasticity of a polycrystalline solid interstitial solution of Ti–O was studied in detail in a very wide temperature interval (0.5–550 K), with the oxygen concentration varying in the range 0.06–1.6 at. %. Using the modern rigorous procedure of thermal-activation analysis of the experimental data, we were able to show that, at oxygen concentrations of about 0.2 at. % and above, the plastic-flow kinetics of α-titanium are controlled by thermally activated or thermal-inertial motion of the dislocations through the impurity barriers. However, the regularities of plastic flow of purer α-Ti (0.06 at. % of interstitial impurities) do not agree with the impurity model of dislocation retardation, and this allowed us to assume that a Peierls barrier may play a controlling role in this case.[22] This paper reports a more detailed experimental investigation of the low-temperature plasticity of α-titanium of the given purity. Taking the results given in Ref. 22 into account, in particular for temperatures $T<2$ K, temperature dependences were obtained for the yield strength, the effective stress, the rate sensitivity of the deforming stress, and the activation volume of the deformation process. A thermal-activation analysis of the experimental data was carried out in terms of the model of activated motion of a dislocation string in Peierls relief, theoretically studied in Refs. 1, 2, and 24. It was shown that the experimental data are in good agreement with this model in a fairly wide interval of moderately low temperatures (7–150 K), and empirical estimates are obtained for its parameters.

II. EXPERIMENTAL TECHNIQUE AND RESULTS

The starting raw material for obtaining the ingots is titanium iodide. The melting was carried out in an arc furnace with a nonconsumable tungsten electrode in an atmosphere of purified argon (passed through molten lithium and a premelted getter) at a gas pressure somewhat below atmospheric. The initial concentration of interstitial impurities (oxygen, nitrogen, carbon, and hydrogen) did not exceed 0.05 at. %. The ingots produced by this process, with a diameter of 18 mm, were converted by rolling in vacuum at a temperature of 1073 K into strips 2 mm thick, from which samples for tensile strain were cut off in the direction of the rolling. After annealing in a vacuum no worse than 7×10^{-3} Pa for an hour at a temperature of 973 K, the mean grain diameter in the samples was about 35–50 μm; their recrystallization texture produced an angle between the stretching axis and the $\langle 10\bar{1}0\rangle$ direction of about 20°. Such conditions maximized the shear stress at the initial instant of strain, and consequently the predominant slip occurred in one of the family of $\{10\bar{1}0\}\langle 11\bar{2}0\rangle$ prism planes, which are the predominant planes (and, below $T\approx200$ K, the only ones) for slip in the temperature region investigated here.

The temperature dependences of the yield strength $\tau_0(T)$ for the $\{10\bar{1}0\}\langle 11\bar{2}0\rangle$ slip system were determined by active strain with a base rate of $\dot{\varepsilon}=2.7\times10^{-4}$ sec^{-1} in the temperature interval 0.5–450 K. The dependence of the tensile stress $\sigma(\varepsilon)$ on the plastic strain ε was recorded in the experiments, and the stress $\tau_0=0.5\sigma_{0.2}$ corresponding to the relative value of tensile plastic strain of $\varepsilon_0=0.2\%$ was chosen as the yield strength. We should point out that, in α-Ti, besides prism slip, another strain mode of is twinning, which is activated with decreasing temperature and increasing strain. Naturally, this will affect the values of the parameters of the strain curve—most notably the strain-hardening rate, the yield strength, and the plasticity. At the same time, optical and electron-microscope studies[25] show that, for a plastic strain corresponding to the conventional yield strength of $\sigma_{0.2}$ ($\varepsilon_0=0.2\%$), the density of twins, and consequently their contribution to the overall plastic strain of the sample, is negligible, and therefore the influence of twinning on the yield strength can be ignored.

The rate sensitivity of the deforming stress, $\beta=(\Delta\tau/\Delta\ln\dot{\varepsilon})_T$, was determined by two methods: in experiments in which the strain rate was changed by a factor of 10 (and in certain cases by a factor of 100) with respect to the base value, and in experiments in which the stress relaxation was studied as $\Delta\tau/\Delta\ln(-\dot{\tau})$, where $\dot{\tau}$ is the rate of change of the stress on a sample when it relaxes. Both methods gave virtually identical results in all the measurements. This value was measured along the strain curves until the samples broke down, and special attention was paid to its values close to the yield strength. Here, as in the case of the yield strength, the influence of twinning can be neglected, and it can be assumed that the process of plastic strain in experiments of the

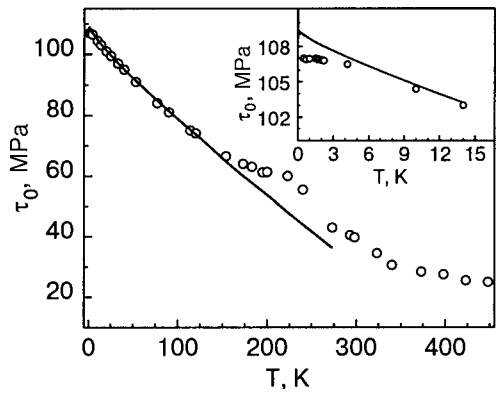

FIG. 1. Temperature dependence of the yield strength $\tau_0=0.5\ \sigma_{0.2}$ of high-purity polycrystalline titanium (concentration of O+N=0.06 at.%). The symbols show the experimental results, and the solid curve shows the theoretical dependence of Eq. (5) for the given parameters, shown in Table I. The inset shows the character of the dependence in the region of very low temperatures.

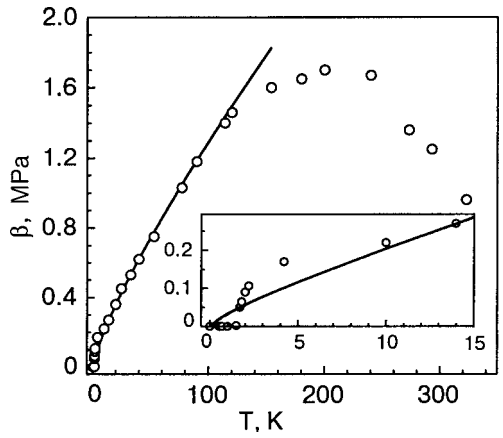

FIG. 2. Temperature dependence of the rate sensitivity of the yield strength $\beta=(\Delta\tau/\Delta\ln\dot{\varepsilon})_T$ of high-purity polycrystalline titanium. The solid curve shows the theoretical dependence of Eq. (6) for the given parameters, shown in Table I. The inset shows the character of the dependence in the region of very low temperatures.

given type occurs because of the motion of complete dislocations in the $\{10\bar{1}0\}\langle 11\bar{2}0\rangle$ system. The basis for this is that new twins are not likely to appear when the stress level is reduced in experiments on stress relaxation (or with a change of strain rate $\dot{\varepsilon}$ from higher to lower). The fact that different methods of measuring the activation volume yield the same values confirms the correctness of our considerations.

Figure 1 shows the temperature dependence of the yield strength $\tau_0(T)=0.5\ \sigma_{0.2}(T)$ of the titanium studied in the interval 0.5–450 K. Several sections can be distinguished on the $\tau_0(T)$ curve that differ in the degree of sensitivity of τ_0 to a temperature change. At temperatures above and of the order of room temperature, as well as in a wide region of moderately low temperatures, two sections are observed with a monotonic increase of the yield strength as the samples are cooled, characteristic of thermally activated plasticity; these sections are separated by a feature of the type of a smeared bend in the neighborhood of 200 K. This dependence is qualitatively similar to the temperature dependences of the yield strengths of pure single crystals of α-Fe (Ref. 2) and β-Sn.[3] Deep cooling ($T\leqslant 7$ K) significantly weakens the temperature dependence $\tau_0(T)$, and the plasticity below 2 K becomes virtually athermal (inset in Fig. 1). Such behavior of $\tau_0(T)$ is anomalous from the viewpoint of concepts concerning thermally activated strain. Similar low-temperature anomalies were observed earlier when studying pure β-Sn,[4] as well as weakly concentrated solid solutions based on Zn (Ref. 7) and fcc metals.[6]

The temperature dependence of the rate sensitivity of the deforming stress $(\Delta\tau/\Delta\ln\dot{\varepsilon})_T$ close to the yield strength (Fig. 2) also has features that correlate with the features of $\tau_0(T)$. This quantity has a dome shape on the main part of the temperature interval studied here, with a maximum close to 200 K, where a bend is recorded on the $\tau_0(T)$ dependence. The rate sensitivity sharply decreases below 7 K and virtually disappears in the interval (2–0.5 K) (inset in Fig. 2), and this correlates with the weakening of the $\tau_0(T)$ dependence in the same interval and the transition to athermal plasticity. It should be pointed out that this anomaly substantially differs from the behavior of the rate sensitivity $(\Delta\tau/\Delta\ln\dot{\varepsilon})_T$ of β-Sn,[4] Zn,[7] and fcc metals,[6] for which it maintains a finite value in the region of athermal plasticity.

In identifying the microscopic mechanisms that control the plastic flow of crystals, special attention is usually paid to measuring and analyzing the activation volume of the process of plastic flow,

$$V^* = kT(\Delta\ln\dot{\varepsilon}/\Delta\tau)_T = kT/\beta. \tag{1}$$

Not only the characteristic values of this parameter but also its dependence on temperature, the value of the total plastic strain, and the values of the deforming and effective stresses are extremely informative. In this paper, values of the activation volume for pure α-Ti were obtained on the basis of measurements of the rate sensitivity of the deforming stress, $kT(\Delta\tau/\Delta\ln\dot{\varepsilon})_T$, when the strain rate or the value of $[\Delta\tau/\Delta\ln(-\dot{\tau})]_T$ was changed in experiments on stress relaxation along the strain curves $\tau(\varepsilon)_T$ recorded at fixed temperatures. Figure 3 shows the $V^*(\varepsilon)$ dependences for values of the activation volume in units of b^3, where $b=2.95\times10^{-10}$ m is the magnitude of the Burgers vector for the slip system $\{10\bar{1}0\}\langle 11\bar{2}0\rangle$ in α-titanium. It can be seen from Fig. 3 that, in the region of very low and moderately low temperatures, the activation volume is independent of the strain and has a value of $V^*/b^3\lesssim 50$. According to the concepts usually adopted in the physics of plasticity, these attributes

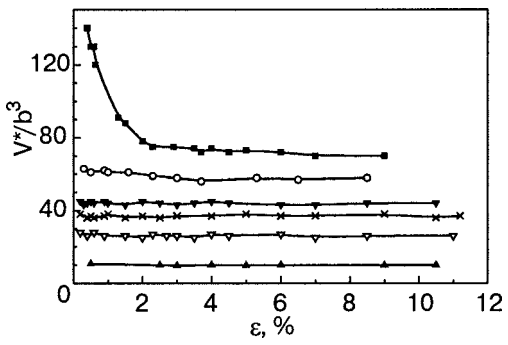

FIG. 3. Activation volume $V^*=kT/\beta$ vs plastic deformation ε at various temperatures, K: 293 (■), 200 (○), 77 (▼), 53 (×), 25 (△), 4.2 (▲). The values of V^* are shown in units of b^3 ($b=2.95\times10^{-10}$ m is the magnitude of the Burger's vector for the slip system $\{10\bar{1}0\}\langle 11\bar{2}0\rangle$).

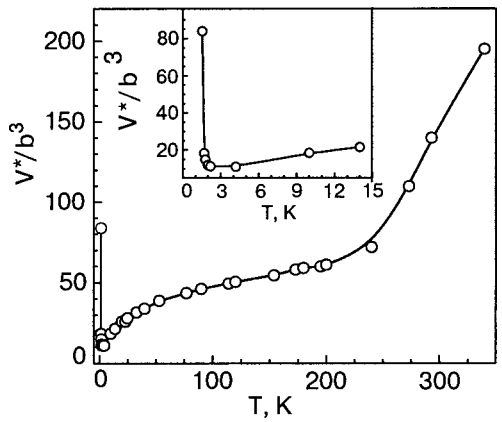

FIG. 4. Temperature dependence of the activation volume V^*/b^3. The inset shows the character of the dependence in the region of very low temperatures.

are proof that Peierls relief has the determining influence on the mobility of dislocations responsible for plastic strain. At $T>200$ K, a certain strain dependence of the activation volume appears at the initial stage of the strain, and this is apparently evidence that processes of dislocation multiplication play a significant role under these conditions.

Figure 4 shows the temperature dependence of the activation volume $V^*(T)$, which is determined for a tensile plastic strain of $\varepsilon_0 \simeq 0.2$ at. %, i.e., close to the conventional yield strength τ_0. The graph of the $V^*(T)$ dependence changes the sign of its curvature in the neighborhood of 200 K; this feature corresponds to the maximum on the temperature dependence of the rate sensitivity (Fig. 2) and correlates with the bend on the $\tau_0(T)$ dependence (Fig. 1). The plasticity anomaly observed under conditions of deep cooling at $T<7$ K shows up on the $V^*(T)$ dependence as a change of the very weak decrease to a very sharp increase ($T<2$ K) of this value (see inset in Fig. 4).

III. DISCUSSION OF THE EXPERIMENTAL RESULTS

The experimental temperature dependences of the yield strength $\tau_0(T)$ (Fig. 1) and its rate sensitivity $\beta(T) = (\Delta\tau/\Delta \ln \dot{\varepsilon})_T$ (Fig. 2) for pure polycrystalline α-Ti in a wide temperature region (450–7 K) qualitatively correspond to concepts concerning dislocation-type thermally activated plasticity of this material. The reaction of the plasticity parameters of α-Ti to temperature variation is anomalous from the viewpoint of these concepts only under conditions of deep cooling (7–0.5 K).

It is customary to describe the kinetics of thermally activated plastic flow in crystalline materials by the well known Arrhenius equation:

$$\dot{\varepsilon} = \dot{\varepsilon}_0 \exp[-H(\tau^*)/kT]. \tag{2}$$

This equation connects the variation of the plastic strain ε and its rate $\dot{\varepsilon}$ with the variation of the effective stress $\tau^* = \tau - \tau_i(\varepsilon)$ that acts on the dislocations in the slip system under consideration [τ is the deforming stress, and $\tau_i(\varepsilon)$ is the characteristic value of the internal long-range stresses that inhibit the motion of the dislocations]. The pre-exponential factor $\dot{\varepsilon}_0$ is proportional to the density of mobile dislocations, and its dependence on τ^* and temperature T is considered unimportant if Eq. (1) is used to describe thermally activated plasticity in pure form (neglecting dynamic dislocation-inertial effects, etc). In this approximation, the main features of plastic flow are associated with the specific form of the dependence of the activation energy (enthalpy) $H(\tau^*)$ on the effective stress τ^*. The analytical form of function $H(\tau^*)$ and the values of the parameters included in it substantially depend on the type and characteristics of the short-range barriers (impurity centers, forest dislocations, Peierls relief, etc.) that inhibit the motion of the dislocations, along with the internal stress τ_i. The main goal of thermal-activation analysis is to determine the type of barriers and to obtain empirical estimates for their characteristics. This goal is achieved by comparing the consequences that follow from Eq. (2) with the results of an experimental study of the regularities of the plastic strain of the material of interest to us under some conditions or other.

We shall discuss the results of the experimental study of the plasticity of pure α-Ti described in the preceding section, assuming that the main cause of the inhibition of plastic flow is Peierls barriers for dislocations in the $\{10\bar{1}0\}\langle 11\bar{2}0\rangle$ slip system. This assumption is based on the results of our earlier paper,[22] in which it was shown that impurity barriers determine the kinetics of the plastic strain of polycrystalline α-Ti only for concentrations of interstitial impurities (oxygen) of the order of 0.2 at. % and above, while the regularities of the plastic flow of purer α-Ti do not match the impurity mechanism of retardation of the dislocations.

There are also no serious bases for adopting the assumption, expressed in Ref. 15, that the intersection of sliding dislocations with forest dislocations has a substantial effect on the inhibition of the former, especially for low-temperature strain of pure α-Ti. This assumption is contradicted by the results of the measurements shown in Fig. 3: first, the fact that the activation volume of the plastic-flow process is independent of the strain at $T<200$ K, whereas forest dislocations arise and propagate in the process of deformation; second, the fact that the activation volume ($V^* \lesssim 50b^3$) has a comparatively low value, which must correspond to an unreasonably large density of forest dislocations ($\rho \gtrsim 5\times 10^{11}$ cm^{-2}) if they are the main barriers for sliding. In the higher-temperature region $T>200$ K, a certain strain dependence of the activation volume appears at an early stage of the strain. This circumstance means that the controlling role of Peierls under these conditions is somewhat disturbed by some additional factor, most likely the intense propagation of mobile dislocations in the active slip system.

In this paper, we restrict ourselves to a thermal-activation analysis of the experimental results obtained in the region of moderately low temperatures 7 K $<T<$ 200 K. It is anticipated that the low-temperature anomaly at $T<7$ K and the feature associated with the strain dependence of the activation volume at $T>200$ K will be discussed in detail in a separate publication.

A. The main relationships of the theory of low-temperature plasticity in the Peierls model

In considering the plastic flow of a crystal that is fairly free from interstitial impurities, which occurs at low temperatures and is controlled by the thermally activated motion

of dislocations through Peierls barriers, two circumstances must be kept in mind. First, at fairly low temperatures, the effective stress τ^* that acts on dislocations in an active slip system will be comparable in magnitude with the critical stress τ_P of nonactivation motion. Second, when $\tau^* < \tau_P$, the displacement of a dislocation by large distances occurs by thermally activated generation of critical paired kinks on a dislocation line, after which these kinks expand and are annihilated. In this regime of dislocation motion, the role of activation enthalpy $H(\tau^*)$ in kinetic Eq. (2) is played by half the energy of a critical paired kink and, when $\tau^* - \tau_P \ll \tau_P$, we get[3,4,24]

$$H(\tau^*) = 0.5H_c(1 - \tau^*/\tau_P)^{5/4}. \tag{3}$$

Energy parameter $0.5H_c$ is of the order of the energy of a single dislocation kink. The precise value of this parameter depends on the magnitude b of the Burgers vector and the intrinsic linear energy C (the energy of linear tension) of a dislocation, as well as on the differential characteristics of the Peierls relief $U_P(y)$ (y is the coordinate in the direction of motion of the dislocation) at the inflection point y_0 for function $U_P(y)$:

$$H_c = (24/5)C^{1/2}(2b\tau_P)^{5/4}|U_P'''|^{-3/4};$$

$$b\tau_P = [\partial U_P(y)/\partial y]_{y=y_0}, \quad U_P''' = [d^3U_P(y)/dy^3]_{y=y_0}. \tag{4}$$

Here y_0 is the value of the argument of function $U_P(y)$ at which its first derivative reaches a maximum, while the second derivative equals zero. Thus, in this treatment, the Peierls relief is characterized by three parameters: period a of potential $U_P(y)=U_P(y+a)$ in the direction of motion of the dislocation, the Peierls stress τ_P, and the quantity U_P'''.

We should point out that situations are also possible in which a dislocation has a limited length, and its displacement occurs by the expansion of one paired kink to the end of the dislocation line without annihilation with things similar to itself. In this case, the role of the activation enthalpy in Eq. (2) will be played by the energy of the paired critical kink, while the pre-exponential factor acquires a dependence on the length of the dislocation line. This question was discussed in more detail in Refs. 2 and 4.

Substituting Eq. (3) into Eq. (2) gives the following expression for the yield strength and its rate dependence:

$$\tau_0(T,\dot\varepsilon) = \tau_{i0} + \tau_P[1 - (T/T_0)^{4/5}], \tag{5}$$

$$(\Delta\tau/\Delta \ln \dot\varepsilon)_T = (4\tau_P/5A)(T/T_0)^{4/5}, \tag{6}$$

$$A = \ln(\dot\varepsilon_0/\dot\varepsilon), \quad T_0 = H_c/2kA. \tag{7}$$

Here $\tau_{i0}(T)$ is the value of the internal stresses close to the yield strength.

B. Analysis of the temperature dependences of the plasticity characteristics

The correspondence of the experimental data shown in Figs. 1 and 2 to Eqs. (5) and (6) in the region of moderately low temperatures can be checked if a simple computer program is used to approximate these data by functions of the form

$$\tau_0(T) = \tau_{i0}(T) + a_1 - a_2T^{4/5}, \tag{8}$$

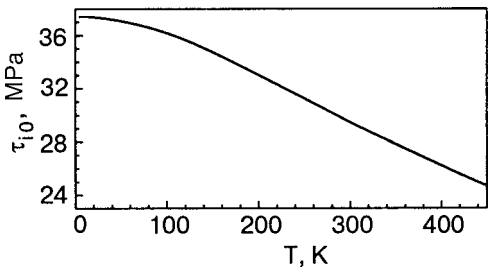

FIG. 5. Temperature dependence of the internal stresses τ_{i0} close to the yield strength ($\varepsilon \approx 0.2\%$) for polycrystalline samples of pure α-Ti constructed according to Eq. (10) on the basis of measurements of $C_{66}(T)$ in Ref. 27.

$$(\Delta\tau/\Delta \ln \dot\varepsilon)_T = a_3T^{4/5}. \tag{9}$$

The temperature dependences in these approximations are derived in explicit form, while coefficients a_1, a_2, and a_3 are certain implicit functions of the strain rate $\dot\varepsilon$.

In general, fundamental difficulties in this procedure can arise in connection with the need to correctly allow for the temperature dependence of the internal stresses, $\tau_{i0}(T)$, since there are no reliable direct experimental methods to determine them at low temperatures.[26] A method is therefore proposed in Ref. 22 to indirectly determine the empirical values of function $\tau_{i0}(T)$ by thermal-activation analysis of the flow strength, the rate sensitivity, and their derivatives with respect to temperature. The use of this method led to the conclusion that the $\tau_{i0}(T)$ dependence for pure α-Ti is rather weak and is associated only with the temperature dependence of the shear modulus $G(T)$. For the $\{10\bar10\}\langle11\bar20\rangle$ slip system, it is determined by the dependence of the shear modulus $C_{66}(T)$, which is obtained by means of high-frequency acoustic measurements in Ref. 27. When the measured and computed values of τ_{i0} were compared for high-purity α-Ti (0.06 at. % interstitial impurities), it was established that, to within the accuracy used here, the effective stress $\tau^* \to 0$ when $T \approx 423$ K; i.e., $\tau_{i0}(423\text{ K}) \cong \tau_0(423\text{ K})$. This circumstance makes it possible to describe the $\tau_{i0}(T)$ dependence by an approximation of the form

$$\tau_{i0}(T) = \tau_0(423\text{ K})[C_{66}(T)/C_{66}(423\text{ K})]. \tag{10}$$

Using the values $\tau_{i0}(423\text{ K}) = 25.5$ MPa (Fig. 1) and the results of measurements of $C_{66}(T)$ in Ref. 27, we get the values of $\tau_{i0}(T)$ shown in Fig. 5.

Coefficients a_1, a_2, and a_3 in Eqs. (8) and (9) depend, generally speaking, on strain rate $\dot\varepsilon$ and, for each fixed value of $\dot\varepsilon$, are chosen so that the graphs of the functions in Eqs. (8) and (9) have the minimum rms deviation from the experimental points in the widest possible temperature interval. Figures 6 and 7 show the results of an approximation by the functions in Eqs. (8) and (9) of the experimental data on the temperature dependence of the effective stresses $\tau^*(T) = \tau_0(T) - \tau_{i0}(T)$ (found by the method indicated above, using Figs. 1 and 5) and of the rate sensitivity $\beta(T) = (\Delta\tau/\Delta \ln \dot\varepsilon)_T$ for values of the coefficients

$$a_1 = 72\text{ MPa}, \quad a_2 = 0.74\text{ MPa/K}^{4/5},$$

$$a_3 = 0.0325\text{ MPa/K}^{4/5}. \tag{11}$$

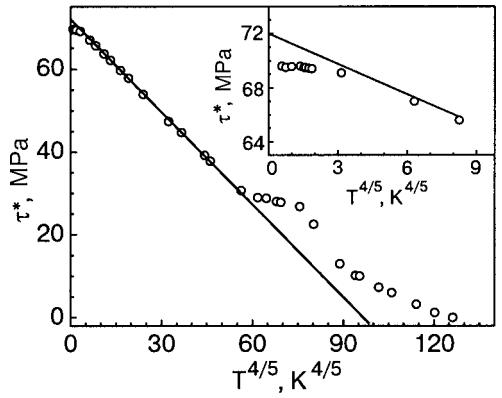

FIG. 6. Temperature dependence of the effective stress $\tau^* = \tau_0 - \tau_{i0}$ in coordinates corresponding to Eq. (5). The solid line is the function $\tau^* = 72 - 0.74T^{4/5}$.

TABLE I. Empirical values of the parameters of the theory of thermally activated dislocation motion in Peierls relief for $\{10\bar{1}0\}\langle 11\bar{2}0\rangle$ prismatic slip in α-titanium at low temperatures.

Parameters	Numerical values
b	$2.95\cdot10^{-10}$ m
τ_P	72 MPa
T_0	308 K
A	18
H_c	$1.5\cdot10^{-19}$ J
$\dot{\varepsilon}$	$1.8\cdot10^{4}$ c^{-1}

It can be seen that both graphs have fairly extensive sections on which the experimental data in the temperature interval from approximately 7 to 150 K are described well by linear functions of $T^{4/5}$.

The analysis carried out above shows that the temperature dependences recorded in experiments on the plasticity characteristics of pure titanium in the temperature interval 7–150 K agree well with the assumption that the thermally activated motion of the dislocations through the Peierls barriers involves the mechanism of generation and annihilation of paired kinks, while the enthalpy of this process is described by Eqs. (3). A comparison of Eqs. (5) and (6) with the approximations given by Eqs. (8)–(10) and using the values of the coefficients in Eqs. (11) makes it possible to obtain empirical estimates for several parameters of the theory: τ_P, T_0, A, H_c, $\dot{\varepsilon}_0$ (see Table I). The degree to which the theory agrees with the experimental data is illustrated by the solid curves in Figs. 1 and 2, which are graphs of Eqs. (5) and (6) constructed using these estimates.

We should point out that the value of $0.5H_c = 0.75 \times 10^{-19}$ J $= 0.48$ eV that we found is close to the energy of a single kink $U_k = 0.56 \times 10^{-19}$ J, obtained in Ref. 11 by analyzing the experimental data on the low-temperature plasticity of higher-purity α-Ti (0.03 at. % interstitial impurities).

It is possible to propose one more illustration of the validity of the assumption concerning the inhibition of low-temperature plastic flow by Peierls barriers in the case of pure titanium and the transition to impurity inhibition when it is doped with interstitial impurities. Figure 7, which shows the temperature dependences of the rate sensitivity $(\Delta\tau/\Delta \ln \dot{\varepsilon})_T$ for pure titanium in coordinates corresponding to Eq. (6), also shows similar data for titanium containing 0.3 at. % oxygen. It was established earlier[22] that, in titanium with an oxygen concentration greater than 0.2 at. %, the controlling mechanism at moderately low temperatures involves thermally activated dislocations overcoming impurity interstitial atoms. It is clear in this figure that a dependence of the form of Eq. (6) agrees very well with the experimental data at $7\ \text{K} < T < 150$ K for pure samples and deviates from it very much for oxygen-doped samples.

The Peierls mechanism of inhibition of the dislocation flux corresponds fully to a definite dependence of the activation volume $V^*(\tau^*)$ on the effective stress τ^* that acts on the dislocation. In the region of high τ^* values of interest to us, this dependence, according to Eqs. (1)–(3), has the form

$$V^*(\tau^*) = -dH(\tau^*)/d\tau^* = V^*(0)[1 - \tau^*/\tau_P]^{1/4}, \tag{12}$$

$$V^*(0) = 5H_c/8\tau_P = 3(\tau_P)^{1/2}C^{1/2}(2b)^{5/4}|U_P'''|^{-3/4}. \tag{13}$$

Figure 8 shows experimental data on the $V^*(\tau^*)$ dependence obtained by means of Figs. 4 and 6 in coordinates corresponding to Eq. (12). This figure also illustrates good agreement of the experimental values of the activation vol-

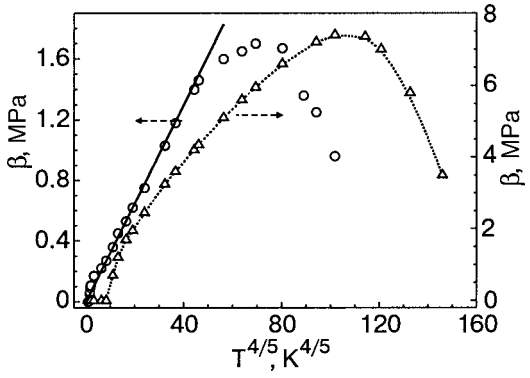

FIG. 7. Temperature dependence of the rate sensitivity of the yield strength, in coordinates corresponding to Eq. (6) for titanium with various concentrations of interstitial impurities: ○ 0.06 at.% O+N; Δ 0.3 at.% O. The solid line is the function $\beta = 0.0325\ T^{4/5}$.

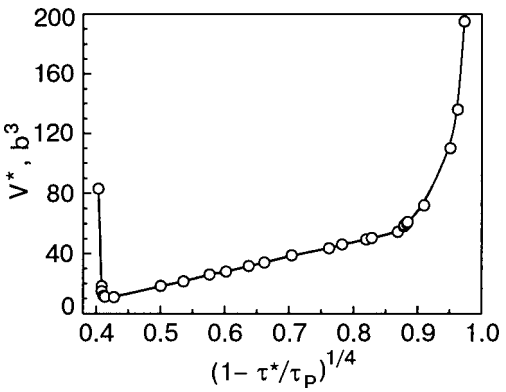

FIG. 8. Activation volume V^* vs effective stress τ^* in coordinates corresponding to Eq. (12).

ume with the dependence in Eq. (12) in the interval 32 MPa $< \tau^* <$ 68.5 MPa, which corresponds to the temperature interval 7–150 K.

In concluding this section, let us discuss the possible causes of deviations of the experimentally measured plasticity characteristics of pure α-Ti from the theoretical dependences of Eqs. (5) and (6) outside the temperature interval 7–150 K. When the samples are strained under deep cooling at $T < 7$K, the effective stress level of τ^* approaches the threshold value τ_P of nonactivation motion of the dislocations. For example, it can be seen from Fig. 8 that a low-temperature anomaly arises when $(1-\tau^*/\tau_P)^{1/4} \approx 0.41$, which corresponds to $\tau^* \approx 0.97\tau_P$. It is thus natural to assume that the appearance of the anomaly at $T < 7$K is associated with a transition from thermal-activation motion of dislocations through Peierls barriers to purely dynamic (above-barrier) motion at high rates. It is planned to carry out a more detailed analysis of the anomaly and the basis of this assumption in a separate publication. We only point out that the question of the possible role of dynamic effects and of the competition of the fluctuation and dynamic regimes of dislocation motion arises and becomes acute when the plastic strain of many crystalline materials under conditions of deep cooling is analyzed. This circumstance was established earlier when studying a low-temperature plasticity anomaly of pure β-Sn (Ref. 28) and of highly concentrated solid solution of Pb–In.[29] The main reason that the role of the dynamic effects is increased in plastic strain processes at very low temperatures is the anomalously small values of the effective barrier potentials that inhibit the motion of dislocations under these conditions. For the pure α-Ti discussed here, a low-temperature anomaly arises when the effective stress reaches $\tau^* \approx 0.97\tau_P$, which corresponds to an activation enthalpy of about

$$H(\tau^* = 0.97\tau_P) \approx 1.13 \times 10^{-21} \text{ J} \approx 0.01 \text{ eV}. \qquad (14)$$

An alternative interpretation of the low-temperature plasticity anomaly has been discussed many times, based on concepts of the quantum mechanics of the dislocation motion through Peierls barriers[4] and impurity barriers.[6] The quantum regime of dislocation motion is also the result of a lowering of the barriers at high values of the effective stress. Quantum plasticity is characterized by athermal behavior of the yield strength τ_0 and its rate sensitivity $(\Delta\tau/\Delta \ln \dot{\varepsilon})_T$, but the rate sensitivity maintains a finite value in this case. The vanishing of the rate sensitivity for pure α-Ti in the temperature region $T < 2$K does not make it possible to use a quantum interpretation of the anomaly in this case.

In the temperature region $T > 150$ K, Eqs. (5) and (6) are also in contradiction with the experimental data for pure α-Ti. However, in interpreting these data, there are no bases for rejecting the concepts of thermally activated plasticity and describing it in terms of the Peierls model. There is a simpler reason why theory and experiment are in conflict: As one goes into this temperature region, a decrease of the effective stress τ^* by a factor of more than 2 (Fig. 6) breaks down the applicability of Eq. (3) for the activation enthalpy $H(\tau^*)$, which is valid only when $\tau_P - \tau^* \ll \tau_P$.[4,24] A preliminary analysis showed that the use of another analytical approximation for function $H(\tau^*)$, obtained in Refs. [2,24] for values of $\tau^* \lesssim 0.5\tau_P$, makes it possible to satisfactorily match the experimental data with the theory even at a certain temperature interval in the region $T > 150$ K. It can be asserted that the plasticity of pure α-Ti in a wide region of moderately low temperatures has the same characteristics as were detected earlier when studying α-Fe (Ref. 2) and β-Sn.[3] These features are associated with a change of the interaction law of the kinks on dislocations when a transition is made from large to small values of effective stress τ^* as the temperature of strain increases.

In the temperature region of the order of room temperature and higher, the plasticity of pure polycrystalline α-Ti has an additional feature, one manifestation of which is that the activation volume strongly depends on the strain at the initial stage of deformation (Fig. 3). A detailed analysis and interpretation of all the features of the plasticity of α-Ti in the temperature region $T > 150$ K will be carried out later. It is assumed that comparing the plasticity features that characterize various temperature intervals makes it possible to obtain empirical estimates for most of the parameters of the theory of thermally activated dislocation motion in the Peierls model, as well as to establish the shape of the Peierls relief $U_P(y)$ in the test material.

IV. CONCLUSION

The experimental data obtained in this paper concerning the regularities of plastic strain of pure polycrystalline α-Ti in a wide temperature region (0.5–450 K) has shown that the main physical factor that determines the plasticity of this material is retardation of the dislocations by Peierls barriers.

An analysis of the experimental temperature dependences of the yield strength $\tau_0(T)$ and the rate sensitivities of the deforming stress $(\Delta\tau/\Delta \ln \dot{\varepsilon})_T$ showed that the entire temperature interval studied here can be divided into three narrower intervals in each of which the motion of the dislocations in the Peierls relief has its own specific features: the interval of very low temperatures $T < 7$ K, the interval of moderately low temperatures 7 K $< T <$ 150 K, and the interval of elevated temperatures 150 K $< T <$ 420 K.

A detailed thermal-activation analysis of the experimental results has been carried out in this paper for the interval of moderately low temperatures 7 K $< T <$ 150 K. It was shown that plastic flow of pure α-Ti occurs under these conditions because thermally activated dislocations of the $\{10\bar{1}0\} \times \langle 11\bar{2}0\rangle$ system overcome Peierls barriers by the mechanism of generation, expansion, and annihilation of paired kinks. The role of effective activation energy in this case is played by half the energy of a paired kink, and its dependence on the effective stress corresponds to the analytical approximation obtained in Ref. 24 for stresses close to the Peierls critical stress. Empirical estimates are obtained for the Peierls stress $\tau_P = 72$ MPa and the characteristic energy of the critical paired kink, $H_c = 1.5 \times 10^{-19} J = 0.96$ eV.

In the region of very low temperatures, the plasticity of pure α-Ti has a clearly expressed anomaly: the yield strength does not vary as temperature is reduced (athermal plasticity), and the rate sensitivity of the deforming stress goes to zero (to within the sensitivity limits of the measurement apparatus). The transition at low temperature from the regime of

thermally activated motion of dislocations through Peierls barriers to the dynamic (above-barrier) regime is discussed as a possible cause of this anomaly.

When a transition is made into the region of elevated temperatures $T>150$ K, the plasticity of pure α-Ti qualitatively maintains the characteristics corresponding to the mechanism of thermally activated motion of dislocations in Peierls relief. However, at the inital stage of strain (close to the yield strength), the activation volume of the strain process substantially depends on the amount of strain, and this makes it hard to quantitatively interpret the experimental data by using only the Peierls model, without invoking other mechanisms.

This work was carried out as part of a special program of the Physics and Astronomy Section of the National Academy of Sciences of Ukraine, Topic 1.4.10.1.8.

[a)]Email: Moskalenko@ilt.kharkov.ua

[1]P. Guyot and J. E. Dorn, Can. J. Phys. **45**, 983 (1967).
[2]A. Seeger, Zs. Metallkunde B **72**, 369 (1981).
[3]G. I. Kirichenko, V. D. Natsik, and V. P. Soldatov, Fiz. Met. Metalloved. **63**, 386 (1987).
[4]V. D. Natsik, G. I. Kirichenko, V. V. Pustovalov, V. P. Soldatov, and S. É. Shumilin, Fiz. Nizk. Temp. **22**, 965 (1996) [Low Temp. Phys. **22**, 740 (1996)].
[5]R. B. Schwarz, R. D. Isaac, and A. V. Granato, Phys. Rev. Lett. **38**, 554 (1997).
[6]N. V. Isaev, V. D. Natsik, V. V. Pustovalov, V. S. Fomenko, and S. É. Shumilin, Fiz. Nizk. Temp. **18**, 911 (1992) [Sov. J. Low Temp. Phys. **18**, 641 (1992)].
[7]L. N. Zagoruĭko, V. D. Natsik, and V. P. Soldatov, Fiz. Nizk. Temp. **12**, 1073 (1986) [Sov. J. Low Temp. Phys. **12**, 605 (1986)].
[8]I. V. Gektina, F. F. Lavrent'ev, and V. D. Natsik, Zh. Eksp. Teor. Fiz. **79**, 1927 (1980) [Sov. Phys. JETP **52**, 973 (1980)].
[9]I. V. Gektina, F. F. Lavrent'ev, and V. D. Natsik, Fiz. Met. Metalloved. **67**, 676 (1989).
[10]W. R. Tyson, Chem. Eng. J. **6**, 301 (1967).
[11]E. D. Levine, Trans. Metall. Soc. AIME **236**, 1558 (1966).
[12]H. Conrad, Can. J. Phys. **45**, 581 (1967).
[13]V. A. Moskalenko and V. N. Puptsova, Fiz. Met. Metalloved. **34**, 1264 (1972).
[14]V. A. Moskalenko and V. N. Puptsova, Mater. Sci. Eng. **16**, 269 (1974).
[15]G. Baur and P. Lehr, J. Less-Common Met. **69**, 203 (1980).
[16]H. Conrad, Cryogenics **24**, 293 (1984).
[17]S. Naka, A. Lasalmonie, P. Costa, and L. P. Kubin, Philos. Mag. A **57**, 717 (1988).
[18]P. Biget and G. Saada, Philos. Mag. A **59**, 747 (1989).
[19]V. A. Moskalenko, V. I. Startsev, and V. N. Kovaleva, Cryogenics **20**, 507 (1980).
[20]A. Girshick, D. G. Pettifor, and V. Vitek, Philos. Mag. A **77**, 999 (1998).
[21]B. Legrand, Philos. Mag. A **52**, 83 (1985).
[22]V. N. Kovaleva, V. A. Moskalenko, and V. D. Natsik, Philos. Mag. A **70**, 423 (1994).
[23]V. A. Moskalenko, V. N. Kovaleva, V. D. Natsik, V. V. Pustovalov, and S. É. Shumilin, Fiz. Nizk. Temp. **22**, 1459 (1996) [Low Temp. Phys. **22**, 1108 (1996)].
[24]B. V. Petukhov and V. L. Pokrovskiĭ, Zh. Eksp. Teor. Fiz. **63**, 634 (1972) [Sov. Phys. JETP **36**, 336 (1973)].
[25]V. A. Moskalenko, A. R. Smirnov, V. N. Kovaleva, and V. D. Natsik, Fiz. Nizk. Temp. **28**, 1310 (2002) [Low Temp. Phys. **28**, 935 (2002)].
[26]V. I. Dotsenko, Phys. Status Solidi B **54**, 99 (1979).
[27]E. S. Fisher and C. J. Renken, Phys. Rev. A **135**, 482 (1964).
[28]V. D. Natsik, V. P. Soldatov, G. I. Kirichenko, and L. G. Ivanchenko, Fiz. Nizk. Temp. **29**, 451 (2003) [Low Temp. Phys. **29**, 340 (2003)].
[29]N. V. Isaev, V. D. Natsik, V. V. Pustovalov, S. É. Shumilin, and V. S. Fomenko, Fiz. Nizk. Temp. **31**, 1177 (2005) [Low Temp. Phys. **31**, 898 (2005)].

Translated by W. Manthey

LETTER TO THE EDITOR

Electric activity of vortices in superfluid ^{4}He

V. D. Natsik[a)]

B. I. Verkin Physicotechnical Institute of Low Temperatures, National Academy of Sciences of Ukraine, pr. Lenina, 47, Kharkov 61103, Ukraine

(Submitted July 15, 2005)
Fiz. Nizk. Temp. **31**, 1201–1203 (October 2005)

The vortical motion of atoms in a quantum liquid is accompanied by their weak polarization under the action of centrifugal forces. Theoretical estimates of the effect give an electric field close to the axis of the vortex of about 300 $V \cdot cm^{-1}$ and a linear density of the bound charge in the core of about $(3e)cm^{-1}$ (e is the charge of an electron). © *2005 American Institute of Physics*.
[DOI: 10.1063/1.2126950]

1. Recent experimental investigations[1,2] revealed a weak but reliably recordable electric activity of liquid ^{4}He in the superfluid state (the He II phase). It was established that the excitation of macroscopic fluxes (flows) in He II by two different methods is accompanied by the appearance of electric displacement in the volume of the helium-filled cell. Relative motion of the superfluid and normal components was excited in experiments in He II: In Ref. 1, the counterflows of the components were created by temperature vibrations on the cell wall (a standing wave of second sound was excited). In Ref. 2, such counterflows appeared in a helium film on the surface of a cylindrical vessel when it underwent forced rotational vibrations. In both experiments, vibrations of the electric potential of about 10^{-7} V were recorded on the cell, and this, converted to the volume density of the effective charge, corresponded to about $10^4 e/cm^3$ (e is the absolute magnitude of the electronic charge).

Two attempts at a theoretical description of the results of these experiments are currently known.[3,4] In Ref. 3, it is proposed that the electric activity of He II can be described on the basis of a phenomenological assumption of the specific ordering of the isotropic quadrupole moment of the atoms in the superfluid state, which shows no electric activity in an equilibrium liquid but is polarized by the inhomogeneous distribution of the superfluid flux. No microscopic model of such ordering was proposed in this case, and this approach left open the question of the physical nature of the observed effects. Reference 4 directed attention to the possibility in principle of spontaneous polarization of any dielectric medium when its elements undergo nonequilibrium motion: Under these conditions, polarization appears in the individual atoms because of the difference of the inertial forces acting on the nucleus and the electron shell, whose masses differ by several orders of magnitude. In the experiments under discussion, macroscopic fluxes were actually excited in He II by dynamic actions of variable sign, and the resulting electric displacement can be the consequence of inertial polarization of the helium atoms. However, if one uses values of the acceleration of the macroscopic elements of the liquid that are characteristic of the experiments when one estimates the magnitude of the effect, the result is smaller than the experimental data by several orders of magnitude.

2. In this note, we discuss one more possibility of using the inertial-polarization-of-atoms effect to describe the electric activity of He II, associated with taking its specific properties as a quantum superfluid into account. Only the inherent steady-state vortical motion—quantum vortices—exists in such a liquid.[5,6] The specific attribute of the vortical motion that is important to us is the fact that, even when such motion has a steady-state character (constant angular velocity), inertial centrifugal forces act on the atoms in the liquid flux, and the polarization of the atoms caused by these forces appears. Vortical motion in a superfluid is nondissipative, and a quantum vortex is a stable nonlinear excitation with conservative distribution of the flow velocities and centrifugal accelerations with respect to the axis of the vortex. Consequently, a spontaneous inhomogeneous polarization and the corresponding (bound) polarization charge, whose distribution with respect to the axis of the vortex is also independent of time, must exist around the axis of an individual quantum vortex.[1)] Three additional circumstances should be pointed out: First, in a quantum vortex, the atoms participating in collective motion close to the axis of the vortex have an extremely large linear velocity (of the order of the velocity of sound in the liquid), and therefore the corresponding centrifugal forces and the resulting dipole moments of the atoms must have be quite large. Second, the direction of the centrifugal forces is independent of the sign of the vortex (the direction of rotation); therefore, all the vortices must have effective charges of the same sign, and their electric activity increases proportionally to the increase of the number of vortices. Finally, in a macroscopic volume of superfluid, it is possible to excite a macroscopically large number of quantum vortices, and therefore their total electric activity can also be macroscopically significant.

3. It is easy to construct a description of the spontaneous electric polarization of a quantum vortex by using the well-known results of the hydrodynamics of a superfluid.[5,6] The two-dimensional velocity field around the axis of a straight vortex is described by

$$V_s(\mathbf{r}) = \frac{\hbar}{mr}, \tag{1}$$

where m is the mass of an atom of the liquid, and $\mathbf{r}$ is the radius vector measured from the axis of the vortex. The mass of an atom that participates in collective vortical motion and whose mass can also be considered equal to m is subject to the action of the centrifugal force

$$F(\mathbf{r}) = \left(\frac{\hbar^2}{m}\right)\frac{\mathbf{r}}{r^4}. \tag{2}$$

If the coefficient of elastic flexibility η is introduced for the nucleus-electron-shell bond, and if the inertia of the electrons is neglected, we get for the displacement of the nucleus with respect to the center of the atom under the action of the force in Eq. (2)

$$\boldsymbol{\delta}_F = \eta\mathbf{F}(\mathbf{r}) = \eta\left(\frac{\hbar^2}{m}\right)\frac{\mathbf{r}}{r^4}. \tag{3}$$

Coefficient η is unambiguously associated with the electric polarization factor α of the atom:[4] On one hand, in a homogeneous electric field $\mathbf{E}$, dipole moment $\mathbf{d}=\alpha\mathbf{E}$ appears on a spherically symmetric atom; on the other hand, the modulus of this moment can be determined as $d=Ze\delta_E$, while $\delta_E = \eta(2ZeE)$, where Z is the number of electrons in the shell; we thus get the equation

$$\eta = \frac{\alpha}{2(Ze)^2}. \tag{4}$$

For a dipole moment of the atom of $\mathbf{d}=-Ze\boldsymbol{\delta}_F$, caused by the action of the centrifugal force, according to Eqs. (3) and (4), we get

$$\mathbf{d} = -\left(\frac{\alpha\hbar^2}{2Zem}\right)\frac{\mathbf{r}}{r^4}; \tag{5}$$

the dipole-moment vector by definition is directed from positive to negative charges: Close to the axis of the vortex, there is an excess of negative electronic charge, while the positive charges are somewhat displaced by centrifugal force toward the periphery.

If $n(r)$ is the density distribution of atoms in a vortex, the dipole moments in Eq. (5) correspond to the polarization fields $\mathbf{P}(\mathbf{r})=n(r)\mathbf{d}(\mathbf{r})$ and the volume bound-charge density $\rho_V^*(\mathbf{r})=-\mathrm{div}\mathbf{P}(\mathbf{r})$:

$$\mathbf{P}(\mathbf{r}) = -\left(\frac{\hbar^2\alpha}{2Zem}\right)\frac{n(r)\mathbf{r}}{r^4}; \tag{6}$$

$$\rho_V^*(r) = -\frac{\hbar^2\alpha n(r)}{Zemr^4}\left[1 - \frac{r}{2}\frac{d}{dr}\ln n(r)\right]. \tag{7}$$

We should point out that the description of the spontaneous inertial polarization of a vortex is obtained in the hydrodynamic approximation on the basis of Eq. (1), and therefore Eqs. (5)–(7) have singularities on the axis of the vortex ($r\to 0$) that are natural for this approximation and remain physically correct only in the region $r>r_0\simeq a$, where a is the interatomic distance in a homogeneous equilibrium liquid. The equivalent electric field $E^*=\alpha^{-1}d$ needed to create the inertial dipole moment can serve as an estimate of the effect at microdistances;

$$\max|E^*| \approx \frac{\hbar^2}{2Zemr_0^3}. \tag{8}$$

The electrical activity of the core of the vortex can also be characterized by the linear density ρ_L^* of the bound charge, which is computed by integrating Eq. (7) over a plane perpendicular to the axis of the vortex. This quantity can be estimated by neglecting the weak inhomogeneity of the density of the liquid close to the axis of the vortex ($n=\mathrm{const}$)[2)] and by excluding from the region of integration a tube of radius r_0. As a result, we get

$$\rho_L^* = -\frac{\pi\hbar^2\alpha n}{Zemr_0^2}. \tag{9}$$

It is easy to show that a vortex in the form of a ring with macroscopic radius R creates polarization that corresponds to the bound charge $Q^*=2\pi R\rho_L^*$.

When He II rotates with angular velocity Ω in a cylindrical vessel with radius R, an equilibrium number N of vortices arises in the helium, and the linear density of bound charge that they cause (per unit length of the vessel) is $Q_L^* = N\rho_L^*$:

$$N = \frac{m\Omega R^2}{\hbar}, \quad Q_L^* = -\frac{\pi\hbar\alpha n\Omega R^2}{Zer_0^2}. \tag{10}$$

The values of the parameters of helium: $Z=2$, $m=7\times10^{-24}$ g, $\alpha=2\times10^{-25}$ cm^3, $n=2\times10^{22}$ cm^{-3}, $r_0\simeq n^{-1/3}=3.7\times10^{-8}$ cm, correspond to the linear density of the bound charge per unit vortex $\rho_L^*\simeq-(3e)\mathrm{cm}^{-1}$. The rotation of helium in a vessel with dimensions $R^2L=1$ cm^3 and frequency $\Omega=1$ rad/sec creates in it a bound charge of $Q^*\simeq 2\times10^4 e$. For the maximum electric field close to the vortex line, according to Eq. (8), we get the estimate $\max|E^*|\approx 300\ \mathrm{V\cdot cm^{-1}}$.

4. In conclusion, it should be pointed out that the interpretation and quantitative processing of the results of specific experiments in terms of the spontaneous polarization of quantum vortices of course requires the formulation and analysis of a model of the dynamic behavior of the vortex system that is adequate for the experimental conditions. Such a model must take into account the processes of generation and annihilation of the vortices, their shape, and the individual and collective vibrations, allowing for inertial polarization and the entrainment of the vortices by the electric field, by temperature gradients, by the vessel walls, etc. Rough estimates show that the electric activity of He II observed in experiment can provide an output of 10^{10}–10^{11} ends of vortex lines per 1 cm^2 of metallic surface.

The authors are sincerely grateful to A. M. Kosevich, A. S. Rybalko, S. I. Shevchenko, I. V. Kriv, and Yu. Z. Kovdr for interest in the work and for numerous stimulating discussions.

[a)]Email: Natsik@ilt.kharkov.ua

[1)]Quantum vortices in superfluid ^{3}He also have spontaneous electric polarization,[7] but its physical nature and the character of the distribution with respect to the axis of the vortex is quite different.

[2)]A more accurate description can be obtained for a quantum vortex in an almost ideal Bose gas.[5]

[1]A. S. Rybalko, Fiz. Nizk. Temp. **30**, 1321 (2004) [Low Temp. Phys. **30**, 994 (2004)].

[2]A. S. Rybalko and S. P. Rubets, Fiz. Nizk. Temp. **31**, 820 (2005) [Low Temp. Phys. **31**, 623 (2005)].

[3]A. M. Kosevich, Fiz. Nizk. Temp. **31**, 50 (2005) [Low Temp. Phys. **31**, 37 (2005)].

[4]L. A. Melnikovsky, http://www.arxiv:cond-mat/0505102 (v.1, May (2005)).

[5]E. M. Lifshitz and L. P. Pitayevsky, *Physical Kinetics* (Nauka, Moscow, 1978; Pergamon Press, Oxford, 1981).

[6]R. P. Feynman, *Statistical Mechanics; Notes taken by R. Kikuchi and H. A. Feiveson*, ed. J. Shaham (W. A. Benjamin, Reading, Mass; 1972; Mir, Moscow, 1978).

[7]G. E. Volovik, JETP Lett. **39**, 200 (1984).

Translated by W. Manthey

COMMENTARY

Comments on the article "New type of topological electronic transition in metals with a change in the Fermi energy," by V. I. Makarov, D. V. Bolotov, V. A. Gor'kavyĭ, and A. A. Yatsenko [Fiz. Nizk. Temp. 31, 422 (2005)]

M. I. Kaganov[a)]

7 Agassiz Ave., Apt. 1, Belmont MA 02478, USA
(Submitted May 30, 2005)
Fiz. Nizk. Temp. **31**, 1204–1205 (October 2005)

[DOI: 10.1063/1.2126951]

In a recent paper,[1] I was surprised that the authors did not cite papers in which I participated as a coauthor with Nurmagambetov,[2] as well as with Kamshilin and Nurmagambetov.[3] Reference 2 was most likely the *first* to point out that a qualitative change of the local geometry of the Fermi surface, even if the connectivity of the Fermi surface does not change, can result in a *generalized topological transition*. As far as I know, it was in that article that the term *generalized topological transition* was introduced.

The role of local geometry in the properties of metals has been repeatedly discussed. One can familiarize oneself with the papers on this topic from the reviews in Ref. 4 (with 41 citations in the reference list), Ref. 5 (305 citations, some annotated in a special section devoted to a bibliography), and Ref. 6 (60 citations). The monograph by Zimbovskaya should also be mentioned.[7]

The reviews and Zimbovskaya's monograph mainly deal not with the influence of external actions on the local geometry of the Fermi surface (on its differential-geometry characteristics in Makarov's terminology, etc.), but with changes of the experimental conditions that alter the topology of the geometrical shapes by means of which the metal's properties of interest are described. Examples of this are the changes of the topology of the extremal planar cross sections of the Fermi surface as the direction of magnetic field $\mathbf{H}$ varies or changes of the structure of the $\mathbf{k}\cdot\mathbf{v}=0$ zones on the Fermi surface because of variation of the direction of the wave vector $\mathbf{k}$ of sound.

In the paper by Makarov *et al.*, it is proposed to describe a new type of electronic topological transition by a change of the spherical shape of the Fermi surface. When a transition occurs abruptly, the number of pre-images of a point with spherical mapping varies. It is not very clear why there is a transition from the actual surface to its mapping onto a sphere. It seems natural to us to use a configuration of curves of parabolic points, the variation of whose topology is a *generalized topological transition-a new type of topological electronic transition*. Such an approach is described in my article with Nurmagambetov and in the tenth section of the cited review[4] (page 924). The choice of the method used in the description is up to the authors, but, in my opinion, it is not worthwhile to complicate a simple picture with mathematical devices.

A change of the topology of the Fermi surface not only results in anomalies of the thermodynamic characteristics of the metal. It manifests itself in anomalies in the other properties, if, along with the change of the topology of the Fermi surface, the geometrical patterns that determine these properties also change. Examples of such anomalies are given in the pioneering work of Lifshitz, in which a topological transition was described for the first time.[8] It should be mentioned that the discovery of a topological transition in practice is the result of the observation not of the thermodynamic features at the point of an electronic transition, but of the phenomena that accompany it.

The topological transition of I. M. Lifshitz is necessarily associated with a generalized topological transition (see the review in Ref. 4, section 9, page 921, and Fig. 14, page 922).

When a generalized topological transition occurs, i.e., when the connectivity of curves of parabolic points changes, the density of electronic energy states has no anomalies. There are thus no anomalies in the thermodynamic characteristics of the metal (the heat capacity, the thermal expansion coefficient). It is shown in the paper by Nurmagambetov and me that the surface density of states *may* have a radical singularity when there is a change of the local geometry of the Fermi surface. True, for this to happen, the crystal faces must be chosen appropriately. In this case, a *surface* phase transition of order 2 1/2 must be observed. It is this that seemed to us to be our main result. Lifshitz, whom we were able to acquaint with our work, agreed with this.

In order to be convinced of the necessity of citing my article and the reviews enumerated above in the article by Makarov *et al.*, there is no need even to read them; the figures in the article can be compared with the figures in the reviews (especially in Ref. 4).

A dumbbell-shaped Fermi surface, used as an example in the paper discussed here for numerical calculations, along with a hat-shaped Fermi surface, has long served as a convenient object for demonstrating the role of the local geometry in the properties of normal metals (see Ref. 4, Figs. 10 and 11, p. 917).

[a)]Email: mkaganov@compuserve.com

[1]V. I. Makarov, D. V. Bolotov, V. A. Gor'kavyĭ, and A. A. Yatsenko, Fiz. Nizk. Temp. **31**, 422 (2005) [Low Temp. Phys. **31**, 321 (2005)].
[2]M. I. Kaganov and A. A. Nurmagambetov, Zh. Eksp. Teor. Fiz. **83**, 2296 (1982) [Sov. Phys. JETP **56**, 1331 (1982)].
[3]M. I. Kaganov, D. V. Kamshilin, and A. A. Nurmagambetov, Fiz. Nizk. Temp. **15**, 289 (1989) [Sov. J. Low Temp. Phys. **15**, 162 (1989)].
[4]M. I. Kaganov and Yu. V. Gribkova, Fiz. Nizk. Temp. **17**, 907 (1991) [Sov. J. Low Temp. Phys. **17**, 473 (1991)].
[5]Ya. M. Blanter, M. I. Kaganov, A. V. Pontsulaya, and A. A. Varlamov, Phys. Rep. 245, No. 4 (1994).
[6]A. M. Kosevich, Fiz. Nizk. Temp. **30**, 135 (2004) [Low Temp. Phys. **30**, 97 (2004)].
[7]N. A. Zimbovskaya, *Local Geometry of the Fermi Surface and High-Frequency Phenomena in Metals* (Ekaterinburg, 1996; Springer, New York, 2001).
[8]I. M. Lifshitz, Zh. Eksp. Teor. Fiz. **38**, 1569 (1960) [Sov. Phys. JETP **11**, 1130 (1960)].

Translated by W. Manthey